Rheology of Branched Polybutadiene – Modeling Polydispersity

Si Wan Li

Degree of Doctor of Philosophy

Department of Chemical Engineering
McGill University
Montreal, Quebec, Canada
Nov. 11, 2009

A thesis submitted to the Faculty of Graduate Studies in partial fulfillment of the requirement of the degree of Doctor of Philosophy

Dedicated to my parents and Ping Gao

獻給我的父母親

李國華　嚴鳳妍

及

高平教授

ACKNOWLEDGMENTS

I would like to express my sincere gratitude to my two excellent supervisors, John M. Dealy and Milan Maric for their guidance and ceaseless support throughout my study. Their enthusiasm and insights in research have had a great influence on me. Without their patience, encouragement and belief in me over the years, this project would not have been completed.

My special thanks go to Hee Eon Park, my colleague and also my thesis advisory committee member, for his constant support, encouragement and detailed advice. I shall never forget his many attempts to drag me out of my comfort zone and help me to build up my confidence and skill.

A sincere Thank You to Ronald G. Larson and his research team members, especially Zouwei Wang and Xue Chen, for their valuable discussions in molecular modeling and their warmest hospitality during my stay in University of Michigan.

Special appreciation goes to Jimmy Mays and M. Shahinur Rahman, who prepared the valuable materials for this research and share with me their knowledge about anionic polymerization. I also extend my thanks to Mrs. Mays who take very good care of me during my stay at The University of Tennessee.

I gratefully acknowledge Taihyun Chang and his research team members, Kyuhyun Im and Heungyeal Choi at The Pohang University of Science and Technology for generously providing the temperature gradient interaction chromatography data of our samples. I am also grateful to Willem deGroot, Ray Brown and Tianzi Huang at The Dow Chemical Company, for sending me valuable data on the chromatography of our samples.

Thanks should be addressed to Chimay Das for valuable discussion in molecular modeling. I also sincerely thank Jacques Roovers for his kind lecture in anionic polymerization; Frederick Morin and Zhicheng Xia in the Chemistry Department for their help in NMR experiment; Alain Gagnon and Frank Caporuscio for their prompt technical service and advice.

Warmest thanks go to Stephane Costeux for the French translation of the abstract, and my colleagues Jen Tiang and Andres Graffe for their friendly support. Special thanks must be given to Chunwing Cheng for his tolerance and patience. I also thank my friends in Hong Kong; Olive Ma, Agnes Lam, Joyce Yeung, Michelle Lin, Martin Kwok, Kelvin Yip, Ron Lee, Youhong Tang and George Ho, who continuously gave me encouragement and love across the ocean.

Finally, I would like to thank my parents for their unconditional love and caring.

TABLE OF CONTENTS

LIST OF TABLES

Chapter 1 Introduction

Chapter 2 Living Anionic Polymerization of Model Polymers

Chapter 3 Materials Used in This Project

Chapter 4 Rheological Characterization of Linear and H-shaped Polybutadienes in LVE region Part I: Procedures

Chapter 5 Rheological Characterization of Linear and H-shaped Polybutadienes Part II: Results and Discussion

Chapter 6 Evaluation of Molecular Models

Appendix

LIST OF FIGURES

Chapter 1 Introduction

Chapter 2 Living Anionic Polymerization of Model Polymers

Chapter 3 Materials Used in This Project

Chapter 4 Rheological Characterization of Linear and H-shaped Polybutadienes in LVE region Part I: Procedures

Chapter 5 Rheological Characterization of Linear and H-shaped Polybutadienes Part II: Results and Discussion

Chapter 6 Evaluation of Molecular Models

Appendix

ABSTRACT

A series of linear and H-shaped polybutadienes (PBDs) were prepared by living anionic polymerization. These polymers were prepared in a novel way using a DPE derivative instead of a difunctional initiator to prepare the cross-bar. This new synthesis strategy was designed to reduce the presence of intermediate species and undesired by-products in the final samples. Details of the structures were revealed using temperature gradient interaction chromatography (TGIC) and the results were compared with those indicated by size exclusion chromatography (SEC) data from reputable researchers at three laboratories. Discrepancies in molecular weights and molecular weight distributions were observed amongst the three sets of SEC data. Furthermore, TGIC, which is believed to have a higher resolution than SEC, revealed that the H-shaped PBDs were actually mixtures of components having several molecular structures. Rheological characterizations were carried out over a broad frequency range by combining small amplitude oscillatory shear (SAOS) and creep (and recovery in some cases) data. Time-temperature superposition was found to work well at temperatures ranging from -75°C to 25°C, and dynamic moduli inferred from creep (or creep/recovery) data agreed well with the SAOS data at the reference temperature T_{ref} =25°C. Material constants including the zero shear viscosity η_0, plateau modulus G_{N}^0 and steady state compliance J_{S}^0 were extracted from experimental data. The effects of long-chain branching and polydispersity of arms and cross-bars on rheological behavior were studied. Two tube-based models: The Hierarchical-3.0 model developed by Larson *et al*. and the branch-on-branch (BoB) model of Das *et al*. were evaluated and compared quantitatively. The evaluation consisted of a summary of peer reviews, sensitivity and uncertainty analyses and comparison of simulations with experimental data. Hierarchical-3.0 gave the most accurate predictions for the H-shaped polymers when polydispersity in the structure was taken into account.

ABRÉGÉ

Des polybutadiènes linéaires et à structure branchée en « H » (avec deux points de branchement) ont été synthétisés par polymérisation anionique en utilisant un dérivé du diphényle-éthylène à la place d'un amorceur bi-fonctionnel pour synthétiser le segment connectant les deux points de branchement. Cette nouvelle approche a permis de réduire le nombre de produits intermédiaires et de structure moléculaires indésirables dans les échantillons produits. Une comparaison de la structure moléculaire déterminée par une méthode chromatographique à gradient de température (TGIC) avec les résultats de trois études indépendantes par chromatographie d'exclusion (SEC) réalisées par des experts en la matière a révélé des différences, en particulier parmi les résultats de SEC. La méthode TGIC, jugée plus précise et sensible, a établi que les échantillons de polybutadiène « H » étaient un mélange de structures diverses. Le comportement rhéologique sur une large gamme de fréquences a été déterminé en combinant des données dynamiques à faible amplitudes avec des donnés de fluage. Le principe de superposition temps-température a été validé entre -75°C et 25°C, et le module complexe déduit des données de fluage-recouvrance est en bon accord avec le module directement mesuré dans le mode oscillatoire à la température de référence (25°C), ce qui a permis la détermination de la viscosité au plateau Newtonien η_0, du module G_N^0 et de la complaisance à l'équilibre J_S^0. L'influence de la présence de longues branches et de la polydispersité des branches et du segment entre les points de branchement a été étudiée, et les données rhéologiques ont été utilisées pour évaluer deux modèles théoriques basés sur la théorie de la reptation. Le modèle hiérarchique « Hierarchical-3.0 » développé par Larson *et al.*, et le modèle BoB (« branch-on-branch ») proposé par Das *et al.* ont été comparés sur la base des évaluations trouvées dans la littérature, d'analyse quantitative de sensibilité et d'erreur, et de l'accord des prédictions de simulation vis-à-vis des données expérimentales. Au bilan, c'est le modèle hiérarchique qui prédit le mieux le comportement rhéologique des polymères en « H » lorsque le caractère polydisperse de la structure moléculaire est pris en compte.

Chapter 1 Introduction

Recent advances in the development of molecular models for predicting the rheological behavior of molten polymers now make it possible to simulate the behavior of branched polydisperse materials. This opens the door to their use in predicting the processing behavior of many commercial polymers. However, there has not yet been a thorough evaluation of the reliability of these predictions based on the use of well-characterized samples and very precise rheological measurements. The objective of this work described here was to meet this need.

In this chapter, a brief introduction of commercial importance of branched polymers is given, followed by a presentation of model branched polymers and the rheological properties of interested. Then, the effects of long chain branching on these rheological properties and the developments of molecular models are summarized. Finally, the specific objectives of this project and the structure of this thesis are presented.

1.1 Commercial importance of branched polymers

Based on annual production volume, polyolefins (particularly polyethylene, polypropylene, and copolymers of ethene with an alpha-olefin) are by far the most important commercial class of synthetic polymers. By 2010, annual production of polyolefins will exceed 120 million tons [1]. Due to their versatile physical and mechanical properties, non-toxicity, cheap and readily available raw materials, cost-effective production, the polyolefins market has been growing at a steady rate of 5-6% per year. Applications of polyolefins range from short-term consumables such as packaging films and rigid food containers to durable products like plastic pipes and storage containers that must withstand a relatively long service life.

Due to the increasing demand for new materials with special properties, much progress has been made on catalyst tailoring and optimization of polymerization processes. For over three decades, the production of polyolefins was based mainly on heterogeneous catalysts such as the Ziegler-Natta type; these catalysts produce non-homogeneous materials that can have complex molecular structures. It was only in the early nineties that a major breakthrough in catalyst technology led to the use of metallocene catalysts. This homogeneous or single-site catalyst gives a much more structurally uniform product [2], making it possible to produce polyolefins having well-defined structures and properties not achievable using conventional catalysts.

The processing behavior and rheological properties of a polymer are governed by its molecular structure. For example, a highly branched polymer with a polyolefin backbone can act as a minor additive to linear polyolefins for improved processability in an extrusion processes. The branches delay the onset of melt fracture and increase melt throughput rates while they maintain the mechanical properties of the original polyolefins [3]. In particular, long chain branching (LCB) has the most prominent effect on the processing behavior. There are several reports on how long an arm should be before it is considered as a long branch; Jordan *et al*. [4] and Gell *et al*. [5] examined asymmetric 3-arm star deuterated polybutadienes and a poly(ethylene-alt-propylene). Both groups concluded that branches with 2-3 entanglements are long enough to affect rheological behavior, i.e., when the arm weight is at least 2.5 times the molecular weight between entanglements.

However, the experimental determination of branching structure remains a major challenge. Ziegler-Natta catalysts usually produce polymers with broad molecular weight and composition distributions due to their multiple reactive sites. Although metallocene catalysts allow much better control of polymer structure, there is still a distribution of structures and molecular weights. As an example we can consider low-density polyethylene (LDPE) conventionally prepared under high pressure via free radical polymerization or metallocene catalysts. It is a complicated mixture of highly branched polymers with both short and long chains with a very broad molecular weight distribution, and these factors together with the existence of branches on branches make the structure impossible to characterize in any precise way [6]. The level of LCB in a polymer may be far below the detection threshold of standard analytical techniques such as nuclear magnetic resonance (NMR), infra-red scattering, or chromatographic techniques [7] but may still have a significant effect on viscosity. In a typical case, the zero shear viscosity can increase by two orders of magnitude, even when an undetectably low degree (about one side branch per 10,000 carbon atoms in the backbone) of long chain branching is introduced [8]. In such a case, rheological characterization is the only method able to detect such subtle but important structural features.

In an industrial process, it is crucial to obtain the right combination of molecular weight and structure to maintain uniform and stable melt flow behavior during processing so that the final product will have the desired appearance and mechanical and physical properties. However, due to the difficulty in characterizing branching structure, the product designer must rely on empirical models and a trial and error approach. Such a method is inefficient, time-consuming and capital intensive, and generally does not lead to an optimal formulation. If it were possible to predict the effects of the length, location and density of branches on rheological behavior, the polymer chemist would know what kind of structure to target for a specific application. Because processing behavior is so sensitive to LCB structure, there has been a major effort in recent years to develop molecular models able to predict the rheological properties of melts, and these are described in this thesis.

1.2 Model polymers

Due to the strong influence of LCB on rheological properties, much work has been done to investigate its effects on commercial polyolefins [9] such as polyethylene [10-12], polypropylene [13] and polystyrene [14]. However, it is difficult to make quantitative comparisons between data and model predictions due to irregularities in topological features in commercial polymers, such as branch length, branch point location and the number of branches. As an example, for two materials having the same total molecular weight but different topological features, the effect of these differences on zero shear viscosity is dramatic. For this reason, modeling LCB polymers with well-defined structures (*e.g.* branched polymers with precisely known molecular architectures, segmental microstructures, and molecular weight distributions approaching monodisperse) is essential to the development of quantitative relationships between molecular structure and rheological behavior.

Anionic polymerization [15], described in Chapter 2, is a powerful tool for preparing model polymers having well-defined structures. By means of the strictest possible control of impurities, it is possible to synthesize a nearly monodisperse polymer, *i.e.* one having a polydispersity index (PDI ≡ M_w/M_n where M_w is the weight average molecular weight while M_n is the number average molecular weight) less than 1.01. Although the synthesis of model polymers has traditionally involved anionic living polymerization, controlled/living radical polymerizations are also now used to prepare polymers with well-defined and complicated structure [16]. This type of polymerization utilizes a dynamic equilibrium between active and dormant species to maintain a constant but relatively low concentration of free radicals compared to that found in conventional free-radical processes. Thus, molecular weight is controlled by the low probability of termination reactions and a constant number of propagating polymer chains. The most important benefit of controlled polymerizations is the great flexibility in preparing new macromolecules having novel topologies without the exhaustive purification techniques required by anionic polymerization [17]. However, the resulting PDI is generally higher than that arising from an anionic polymerization.

Recently, there have been many studies of the linear viscoelastic behavior of model branched polymers that were prepared by anionic polymerization, including stars polymers [5,18,19], comb polymers of several types such as “H-polymers” [20-23], “pom-pom” polymers [14,24-26] and multi-armed comb [27-34], and other more complicated structure such as Cayley-tree polymer [35]. A schematic representation of these polymers’ topologies is shown in Fig. 1.1. The H-shaped polymer is attractive for basic studies, because it is the simplest species containing two branch points, and its use was first suggested by Marrucci [36]. Due to its special structure, the H-shaped polymer exhibits interesting rheological properties in entangled melts and solutions [20,21], and data contain features that resemble those of LDPE and other long-chain branched, commercial polymers. The most extensively studied model branched polymers are polyisoprene [19,21,23,27,37], polystyrene [20,31,34,38] and polybutadiene [19,26,33,39,40], although little has been published on H-shaped polybutadienes [41].

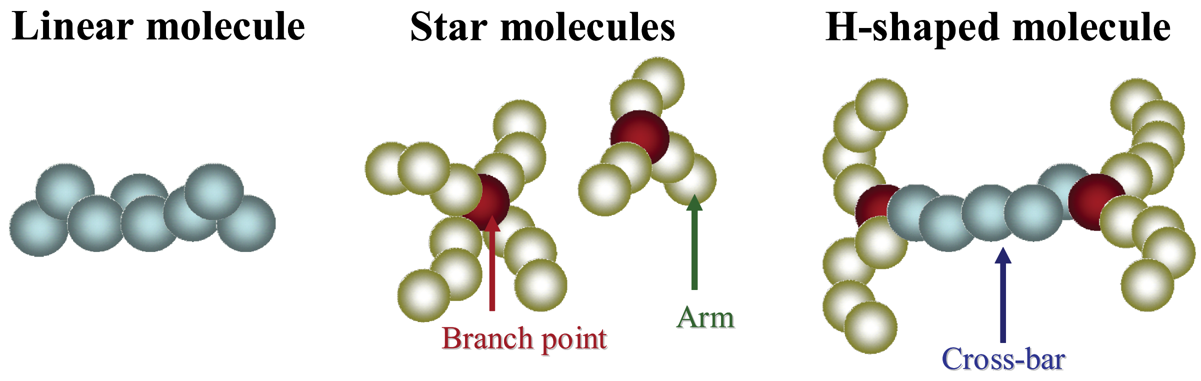

Figure 1.1 Schematic representation of polymer topology

It is possible to compare behavior of various polymers due to the power of *universality*, or the independence of physical phenomena on local, small-scale details, and this is a feature of the melt rheology of flexible polymers. Universality is achieved by expressing all molecular weights in terms of the entanglement molecular weight (M_e), which depends only on temperature and the chemical nature of the polymer. Its value for several polymers that can be prepared by anionic polymerization (PBD, PI and PS) as well as those widely used polymers (PE and PP) but cannot be synthesized by anionic polymerization is shown in Table 1.1.

Table 1.1 Molecular weight of entanglement of various polymers at 25°C [42]

Polymer	Entanglement molecular weight M_e (g/mol)
1,4 PBD	2,000
1,4 Polyisoprene (PI)	5,000
Polystyrene (PS)	18,000
Polyethylene (PE)	1,200
Atactic Polypropylene (PP)	4,390

1.3 Introduction of linear viscoelastic (LVE) properties of interest

Linear viscoelastic properties can be classified into two main categories: transient properties which are expressed as functions of time, and dynamic properties which are expressed as functions of frequency. Various important LVE properties, such as zero shear viscosity η_0 , creep compliance $J(t)$, recoverable creep compliance $J_r(t)$, steady state compliance J_s^0 and plateau modulus G_N^0, that are sensitive to molecular weight, molecular weight distribution and branching structure are introduced below.

1.3.1 Zero shear viscosity η_0

Zero shear viscosity η_0, which is the low-shear rate limiting viscosity exhibited in the regime of LVE, is a material constant that has a strong dependency on molecular weight especially on linear polymers and molecular structure, but has little dependency on molecular weight distribution. At long time, sample is shearing at a very low steady rate $\dot{\gamma}$ and by assuming that sample is at a stress-free state at $t = 0$, η_0 can be found by Eq. 1.1:

$$\eta_0 = \lim_{t \to \infty} \frac{\sigma(t)}{\dot{\gamma}} \qquad \text{Eq. 1.1}$$

In dynamic measurement, the magnitude of the complex viscosity as frequency approaches zero is equal to the zero shear viscosity.

$$\eta_0 = \lim_{\omega \to 0} | \eta^* | \qquad \text{Eq. 1.2}$$

where

$$\eta^* = \eta' - i\,\eta'' \qquad \text{Eq. 1.3}$$

and the absolute value (magnitude) of the complex viscosity is expressed as:

$$| \eta^* | = \sqrt{(\eta')^2 + (\eta'')^2} \qquad \text{Eq. 1.4}$$

1.3.2 Creep compliance *J*(t)

A complimentary test to step-strain experiment is the creep experiment, in which sample is subjected to a sudden stress with magnitude σ_0 at $t = 0$. The resulting $\gamma(t)$ is measured as a function of time and the creep compliance $J(t)$, which is independent of the applied stress, is defined as Eq. 1.5

$$J(t) \equiv \frac{\gamma(t)}{\sigma_0} \qquad \text{Eq. 1.5}$$

To ensure that rheological measurement is within the LVE region, the applied stress in a creep experiment must be sufficiently small such that the deviation of polymer chains from the equilibrium state is negligible and the Boltzmann's superposition principle is still valid. Working with a very small stress is not always possible due to instrument limitations that may result in noisy signals. On the other hand, linearity response of creep compliance cannot be guaranteed when working with a reasonable stress at long time: since the strain is accumulating, at long time it may enter the non-linear region before reaching a steady shear rate. To solve this problem, we can use a technique called creep/recovery experiment [43-45], which will be described in Chapter 4.

1.3.3 Recovery creep compliance J_r(t)

In a creep/recovery experiment, stress is applied for a short period of time only (e.g. $t = t_1$) and then removed suddenly. The recoil or recovered strain γ_r as defined by Eq. 1.6 is measured as a function of time. Fig. 1.2 is a sketch of the stress, strain and creep compliance profile in a creep/recovery experiment.

$$\gamma_r(t - t_1, t_1) \equiv \gamma(t_1) - \gamma(t) \qquad \text{Eq. 1.6}$$

Recoverable creep compliance is then defined as:

$$J_r(t) = \frac{\gamma_r(t - t_1, t_1)}{\sigma_0} \qquad \text{Eq. 1.7}$$

Creep compliance at $t > t_1$ can be extended by using the recovery information and constructing a composite creep compliance $J(t)$ over the entire experimental time [44], which is equivalent to the creep compliance for a complete creep test up to the same experimental time as long as the material response remains in the LVE region. The creep compliance can be calculated by the following two equations.

$$J(t) = \frac{\gamma(t)}{\sigma_0} \quad \text{for } (0 < t < t_1) \qquad \text{Eq. 1.8}$$

$$J(t) = \frac{\gamma(t)}{\sigma_0} + J(t - t_1) \quad \text{for } (t > t_1) \qquad \text{Eq.1.9}$$

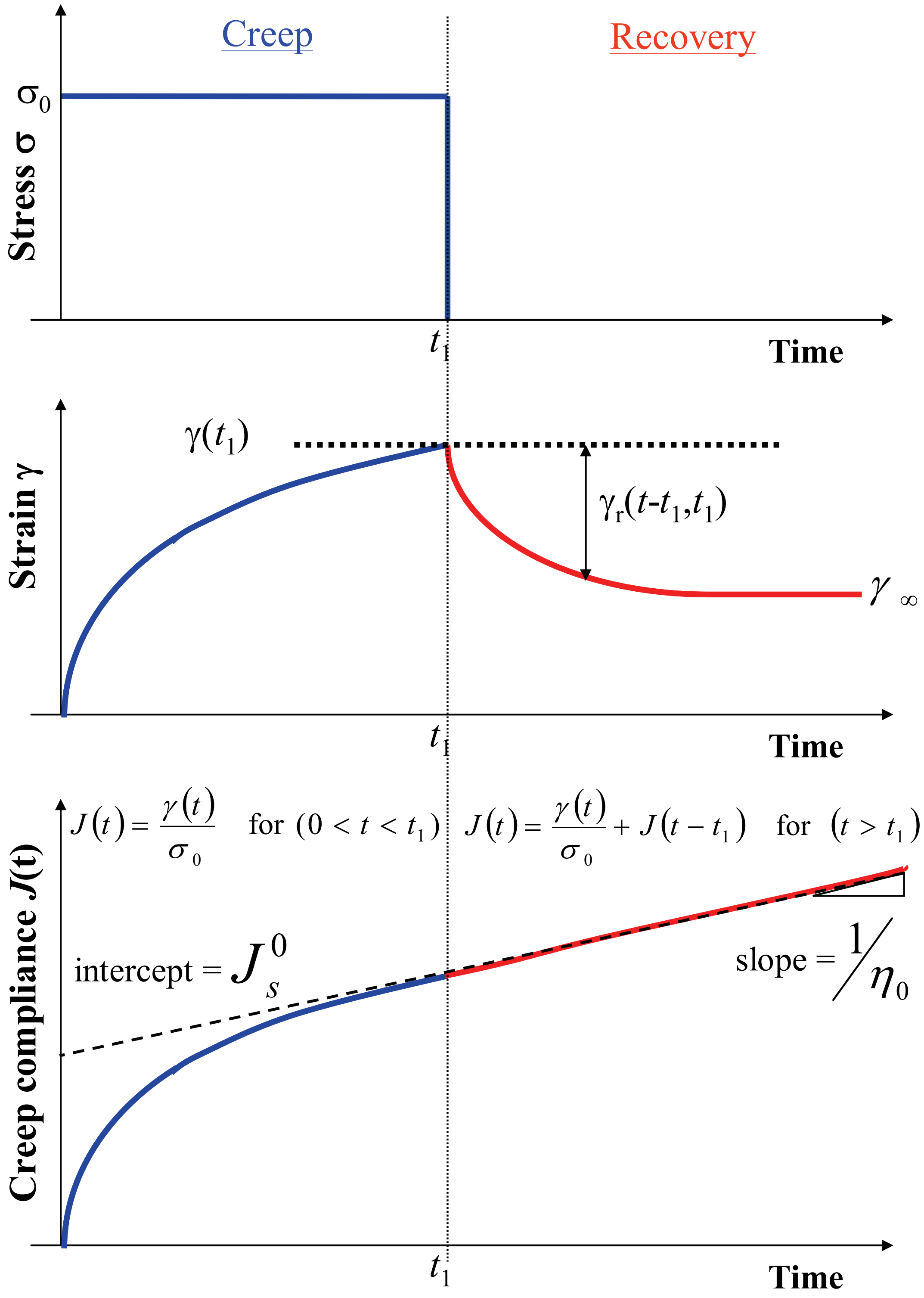

Figure 1.2 Sketch of stress, strain and creep compliance profiles with time in creep/recovery experiment for an uncross-linked polymer

1.3.4 Steady-state compliance J_s^0

For a typical creep compliance curve of a viscoelastic melt as shown in Fig. 1.2, the creep compliance becomes linear with time at long time and shear rate approaches a steady value which is considered as steady-state. To ensure that the rheological behavior is within LVE regime, the applied stress must be sufficiently small such that the strain stays within the linear range until steady-state is reached. When the creep compliance reached steady-state, based on Eq. 4.10, the linear portion of the data at long time can be extrapolated to t = 0 to determine the steady state compliance J_s^0 with the slope of the straight line equal to the reciprocal of the zero-shear viscosity.

$$J(t) = J_s^0 + \frac{t}{\eta_0} \qquad \text{Eq. 1.10}$$

1.3.5 Plateau modulus G_N^0

Plateau modulus of an entangled polymer melt is proportional to the density of entanglements. It defines the molecular weights of entanglement M_e as shown in Eq. 1.11 since M_e cannot be measured directly and must be inferred from G_N^0.

$$G_N^0 = \frac{4}{5}\frac{\rho RT}{M_e} \qquad \text{Eq. 1.11}$$

It is a characteristic constant of the chemical structure of the polymer and is independent of the molecular weight and molecular weight distribution [46].

1.4 Effect of long chain branching and entanglements on rheological properties

The most obvious effect of entanglements on the rheology of linear polymers is the strong dependence of zero-shear viscosity η_0 on weight-average molecular weight (M_w). Zero-shear viscosity is the value when the polymer is very close to its rest state; it depends on the chemical identity and structure of the polymer and temperature. In general, as η_0 decreases, the melt flows more readily at low shear rates, which is advantageous for some melt processing operations. On the other hand, a very low η_0 can cause problems in blow molding or rotational molding [47].

In linear polymers with M_w higher than a critical molecular weight for entanglement M_c, a molecule has great difficulty escaping from its topological constraints (*i.e.* entanglements) imposed by neighboring molecules; this leads to a strong increase in η_0 with M_w, with η_0 proportional to $M_w{}^a$ with a in the range of 3.4 to 3.6. When M_w is less than M_c, on the other hand, Rouse/Bueche theory is obeyed, and η_0 has a much weaker, linear dependence on M_w. A typical curve of η_0 versus M_w using log-log scales for a linear polymer is shown in Fig. 1.3.

For a star polymer, η_0 depends exponentially on the arm length [18,19] but not on the number of arms for functionalities up to at least 33 [14,48]. It has been reported that η_0 of a multi-arm star polystyrene is less than that of a linear polymer of the same molecular weight when $M_w < 10^6$ g/mol [14]. In contrast, the viscosity of a high molecular weight star is many times larger than that of its linear counterpart. As observed by Roovers a maximum in the loss modulus occurs in the plateau zone which is due to arm relaxation with a characteristic time equal to the inverse of the frequency at which this maximum occurs. In the case of symmetric stars, (*i.e.* in which all arms have the same molecular weight), this characteristic time is independent of the number of arms [49].

For low molecular weight H-shaped polymers, η_0 is the same as for linear polymers of the same molecular weight, but high molecular weight H-polymers exhibit enhanced viscosities. For the same molecular weight, H-shaped polymers show a higher degree of viscosity enhancement compared to three-and four-arm stars. Again, as observed by Roovers for H-shaped polystyrene, the maximum loss modulus that occurs in the plateau region is related to the relaxation of arms with a characteristic time that depends on the molecular weight of the arm [20]. The dynamic moduli of H-shaped polymers are qualitatively similar to those of stars, in that LCB broadens the relaxation spectrum by the addition of long-time relaxation processes that are not present for linear materials. The loss modulus has features at various time scales that can be identified with the relaxation of the arms (fast) and the cross-bars (slow). In their study of H-shaped polyisoprenes, McLeish *et al.* [21] pointed out that the presence of a small degree of polydispersity arising from anionic polymerization is enough to shift the terminal region of the retracting arms to longer times than for a truly monodisperse sample having the same M_w. This is one of the important differences between H polymers and monodisperse star melts, which do not show such behavior.

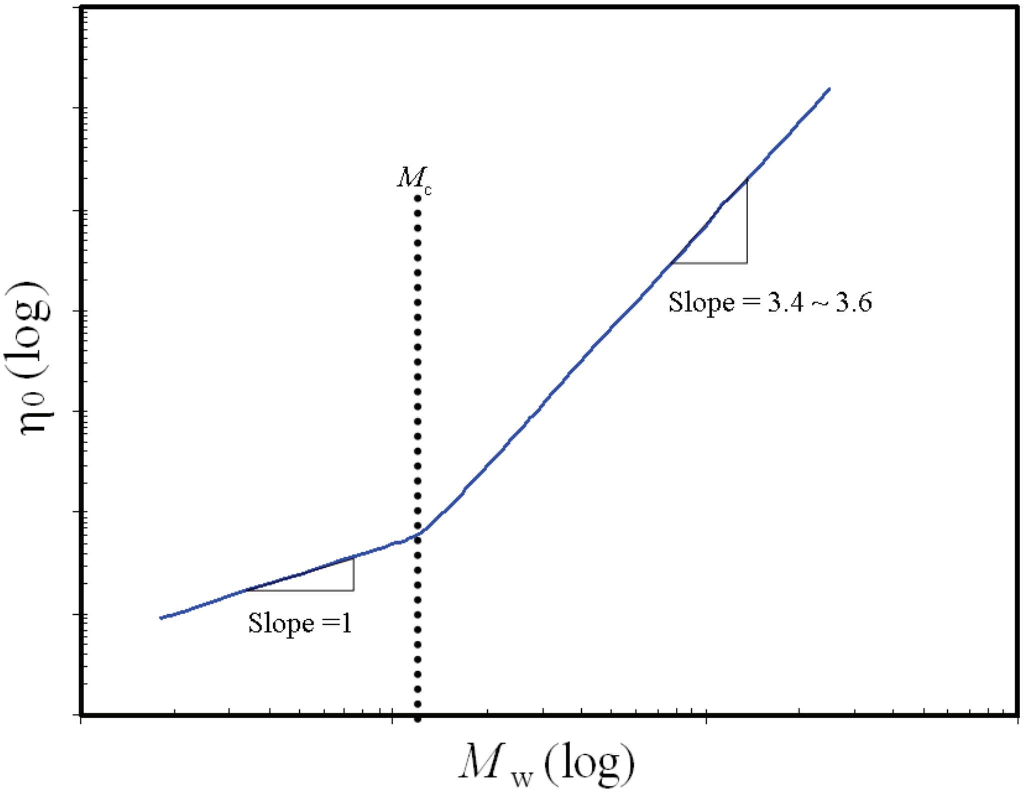

Figure 1.3 Molecular weight dependence of η_0 for linear polymer in log-log scale

For entangled, linear melts, the temperature dependence of viscoelastic functions is fairly simple. Time-temperature superposition works well, *i.e.*, the melts are thermorheologically simple. The variation of η_0 with temperature is generally not sensitive to branching, except, curiously, in commercial and model polyethylenes [19,48]. Carella *et al.* [19] studied the temperature dependence of viscosity of star-branched and linear polymers having the same microstructure. Departures from time-temperature superposition and increased temperature coefficients of viscosity relative to linear chains were observed for some of the branched systems. They concluded that the deviations were due to different relaxation mechanisms for branched and linear chains in an entangled environment. Linear viscoelasticity is important not only for characterizing processing behavior but can also provide information about molecular weight distribution as well as the structure of branched polymers; this characterization technique is called "analytical rheology".

1.5 Overview of tube-based models of entangled systems

To investigate structure-property relations in highly entangled systems with complex architectures, one needs a quantitative molecular model that can describe linear viscoelasticity (LVE) well. Although there is no general theory that can reliably predict the LVE of a branched polymer of arbitrary structure, there have been some promising advances in molecular modeling of well-defined structures [50].

At present, the most useful molecular theories for entangled polymers are based on the tube concept that was first developed by Edwards to deal with the trapped entanglements in a rubber network [51]. Base on this tube concept, de Gennes [52] proposed a relaxation mechanism that he coined the term "reptation" for a free chain in a network which later adapted to entangled melt for monodisperse linear chains by Doi and Edwards [53-56]. Prediction of LVE based on tube-based models on linear polymers is now quantitatively accurate [57-61], that the tube model is able to explain the strong dependence of the viscosity and diffusion constant on molecular weight [62]. However, the relaxation of commercial polymers, which have broad molecular weight distributions and often contain long-chain branches, is not well described by reptation alone, and this implies that these polymers have additional relaxation mechanisms besides reptation. Tube-based models such as the "Hierarchical" model developed by Larson *et al*. [60,61,63], the "BoB" model developed by Das *et al*. [59] and the "time-marching" model developed by van Ruymbeke *et al*. [64,65] share the same goal to predict LVE of arbitrary mixtures of branched polymer despite different algorithm is used to simulate the relaxation process. Details regarding the "Hierarchical" model and "BoB" model are presented in Chapter 6.

1.6 Scope and objectives

The above introduction reveals that although much work has been done to relate molecular structures to rheological behavior, this has been limited mainly to simple structures such as linear polymers and stars. To make possible the use of the latest molecular theories relating structure and flow behavior to design commercial polymers, two structural complexities must be dealt with; polydispersity and long-chain branching with more than one branch point per molecule. The simplest system containing both of these features is an H-polymer with polydisperse arms and/or backbones. Although much works have been done on multi-armed comb [27-34] polymers, there remains a challenge to measure the actual distribution of arm number and placement [34]. Despite the advantage of working with polybutadiene due to its low entanglement molecular weight, little work has been done on H-shaped polybutadiene because of difficulties in synthesis.. The overall objective of the present work was to carry out very precise measurements of the viscoelastic properties of H-polybutadienes having known arm length polydispersities and to use the resulting data to evaluate two advanced molecular models that have been developed to describe the behavior of polydisperse, branched polymers. The specific objectives are:

1. To arrange for the synthesis of H-shaped PBDs having prescribed molecular weights and branch lengths and to verify the molecular structures of the resulting samples.
2. To carry out a thorough and precise rheological characterization of the model H-shaped polymers in the linear viscoelastic region over the broadest possible frequency range.
3. To study the effect of polydispersity by blending two model H-shaped polymers with different molecular weights.
4. To use the LVE data to evaluate two recently proposed molecular models.

1.7 Overview of thesis

Chapter 2 describes the procedures used to synthesize nearly monodisperse linear polystyrenes and polybutadienes by anionic polymerization and describes efforts to develop a suitable synthesis procedure for the branched samples.

Chapter 3 describes the procedure used to establish optimum structures (*i.e.* H-shaped) of the materials to be used in the project. Molecular weight and structure characterization of the samples are presented.

Chapter 4 describes several critical experimental issues for precise and reproducible rheological data and experimental procedures used to perform linear viscoelastic measurements on all the materials studied.

Chapter 5 presents the rheological data and investigates the effect of structures, molecular weight and polydispersity of arms/cross-bar on rheological properties, particularly the zero-shear viscosity, plateau modulus and steady state creep compliance.

Chapter 6 evaluates two molecular models, namely the Hierarchical model of Larson *et al.* [60,61,63,66] and the BoB model of Das *et al.* [59] by means of peer review, sensitivity analysis, uncertainty analysis and corroboration.

Finally, conclusions and original contribution to knowledge are presented in Chapters 7 and 8.

Chapter 2 Living Anionic Polymerization of Model Polymers

2.1 Introduction

With the discovery of the living anionic polymerization of styrene in 1956 [67,68] and subsequently other controlled/living systems [69], researchers found a way to prepare polymers with precisely designed molecular architectures, making possible major developments in synthetic polymer chemistry and polymer physics. Over the past few decades, polymer chemists have discovered conditions for the living polymerization of a variety of monomers, including those that cannot be initially be polymerized anionically; and for materials with complex architectures such as asymmetric stars, comb-shaped polymers, cyclic polymers and dendritic polymers, which have a rich variety of applications [70,71]. Techniques based on anionic polymerization have proven to be best suited for synthesizing model polymers when carried out in aprotic solvents that do not exchange protons when a substance dissolves in them [72]. Living anionic polymerization also occupies a key position in the industrial production of polydiene rubbers, solution styrene/butadiene rubbers (SBR), thermoplastic elastomers of the styrenic type.

In this chapter we describe techniques for the anionic polymerization of essentially monodisperse polymers as well as the author's experiences in the use of one of these to make polystyrenes and polybutadienes (PBDs). The following chapter describes the preparation of the branched PBDs used in this project.

2.2 General aspects of living anionic polymerization

2.2.1 Definition

Living polymerization is an addition polymerization that involves successive additions of monomer to a growing chain that is initiated by some reactive species in the absence of chain termination or chain transfer [67,68,73]. More specifically, in anionic polymerization, it is the unsaturated monomer molecules that are added to a growing polymer chain one at a time to the growing chain end carrying a negative charge. Chain transfer is a reaction that involves the transfer of the reactive site of a growing chain to another molecule; the growth of the polymer chain is thereby terminated and a new reactive intermediate capable of chain propagation is generated. Therefore, chain transfer reactions generally reduce the average molecular weight of the final polymer.

A checklist of criteria has been proposed to determine whether a specific polymerization system is living or not, and critical evaluations on each criterion have been done [15,74]. Most of these criteria are closely related to the special features of living anionic polymerization that are presented in section 2.1.3. As pointed out by those who have examined these criteria, meeting a single criterion is not enough for a polymerization system to qualify as a living polymerization, since chain transfer and chain termination can have different consequences in various systems, giving rise to different sensitivities to these criteria among these systems. Therefore, Szwarc recently redefined living polymerization as a process that yields living polymers that retain the ability to propagate for a long time and grow to a desired maximum size while the degree of termination or chain transfer is negligible [75]; from this point of view, narrow molecular weight distribution should not be included in the definition of living polymerization [76].

Mechanism

Living anionic polymerization takes place in three distinct steps: chain initiation, chain propagation and chain termination.

Initiation is the process wherein a reactive intermediate is generated and then participates in a chain reaction as shown in Eq. 2.1, where I is an initiator precursor, I^* is an initiating species carrying a anionic center, and M is the monomer. For ideal living polymerization, the initiation step is almost instantaneous and is much faster compared to propagation.

$$\begin{aligned} &I \rightarrow I^* \\ &I^* + M \rightarrow I - M^* \end{aligned} \qquad \text{Eq. 2.1}$$

The most versatile and useful anionic initiators are the alkyllithium compounds, which are commercially available in hydrocarbon solvents such as hexane and cyclohexane and can be easily prepared by reacting the corresponding alkyl chloride with lithium metal. This type of initiator is very effective, as it operates by a direct anionic (nucleophilic) attack on the monomer, leading to a mono-functional chain growth reaction.

Propagation is the process in which reactive intermediates which differ in molar mass are continuously regenerated through a repetitive cycle of elementary steps, as shown in Eq. 2.2, where *n* denotes the degree of polymerization of a growing chain P_n^*.

$$\begin{gathered} I - M^* + M \rightarrow I - M - M^* \\ \vdots \\ I - (M)_{n-1} M^* + M \rightarrow I - (M)_n M^* \equiv P_{n+1}^* \end{gathered} \qquad \text{Eq. 2.2}$$

Termination is the step where the reactive intermediates are destroyed or rendered inactive, resulting in chain termination, as shown in Eq. 2.3, where *E* is the end group of the dead or inactive polymer chain contributed by a terminating agent, such as a –OH group from alcohol.

$$P_n^* \rightarrow P_n - E \qquad \text{Eq. 2.3}$$

2.2.2 Special features

In the absence of chain termination, anionic polymerization allows control of a wide range of compositional and structural parameters, including molecular weight, molecular weight distribution (polydispersity), branching, and chain-end functionality [15,77]. The special features of anionic polymerization are discussed in more detail below.

Molecular weight: From a simple stoichiometric balance on the number of moles of initiator and monomer, the average molecular weight (M_n) of the synthesized polymer can be predicted. For a monofunctional initiator that has only one reactive site, M_n can be calculated as shown in Eq. 2.4. Similarly, for an initiator with multifunctionality (*f*), M_n can be calculated according to 2.5.

M_n [g/mol] = mass of monomer / moles of initiator Eq. 2.4

M_n [g/mol] = (1/*f*) (mass of monomer /moles of initiator) Eq. 2.5

Molecular weight distribution: As recognized initially by Flory, polymers synthesized under termination-free chain addition polymerization have a Poisson distribution of molecular weights [78]. This is because in the absence of impurities all chains have the same probability for growth (*i.e.* the rate of initiation is competitive with the rate of propagation) and with a constant reactivity of the initiator, the polydispersity (M_w/M_n) can be assumed to have the Poisson form, *i.e.*

$$\frac{M_w}{M_n} = 1 + \frac{M_n - 1}{M_n^2} \approx 1 + M_n^{-1} \qquad \text{Eq. 2.6}$$

The approximation of Eq. 2.6 is valid for high molecular weight polymers. It can be readily seen that polydispersity decreases as chain length (*i.e.* M_n) increases. Theoretically, the distribution is remarkably narrow ($M_w/M_n \sim 1.01$) when $M_n = 100$. By definition, polymers with a narrow molecular weight distribution should exhibit a polydispersity of less than 1.1 [79]. By contrast, to obtain a broader molecular weight distribution, one can use a less effective initiator [80], a mixture of initiators [81], or the more controllable and practical approach of continuous addition of initiator in a continuous flow, stirred tank reactor [82].

Sequence distribution: In the absence of chain termination, all growing chains retain their active centers even when all of the monomers have been consumed. Therefore, when additional monomer is added into the system, chains will grow again up to the chain length calculated by Eq. 2.4 or Eq. 2.5. By sequential addition of several monomers into the living system, block copolymers such as A-B and A-B-A can be prepared [83], with each block having a controlled molecular weight and low polydispersity.

Branching: Star branched polymers can be prepared by reaction with multifunctional electrophilic linking agents. For example, using tri-functional methyl trichlorosilane as a linking agent to terminate the living chains will result in 3-arm star polymers [84]. This end-linking methodology provides better control of molecular weight and polydispersity than the use of a multifunctional initiator. Although the use of a multifunctional initiator in living anionic polymerization can yield similar branched structures, the initiation step now depends on the efficiencies and relative initiation rates of all the initiating sites of the rate of propagation [85] and is thus more vulnerable to heterogeneity in molecular weight.

Chain-end functionality: Since all growing chains can retain their active centers even when all monomers have been consumed, we are able to effectively control chain termination. By using appropriate electrophilic reagents to terminate the reaction, polymers with functional end groups can be formed [86]. Alternatively, the use of functionalized initiating species[87] will do the same job; since the functional group is incorporated into the initiator it will be at the initiating end of every molecule. In principle, this method ensures complete functionalization.

2.2.3 Control of process conditions

The excellent features of living anionic polymerization require careful experimental procedures [88] and proper selection of monomer, solvent, temperature and reaction time [15]. To obtain a well-defined polymer, the reaction conditions for living anionic polymerization must be precisely controlled. A summary of methods used to control reaction conditions and polymer characteristics is shown in Table 2.1.

In general, by varying the relative concentrations of initiator and monomer, one can control the molecular weight of the final product. To obtain a narrow molecular weight distribution, a rapid initiation process and a constant reactivity of the initiator are necessary to ensure that all chains grow simultaneously and in the same interval of time. Also, low reaction temperatures are required to eliminate chain transfer, and rigorous elimination of water and oxygen is generally required, since any impurities present will irreversibly destroy reactive chain ends, resulting in chain termination.

Table 2.1 Living anionic polymerization conditions required to control polymer characteristics

Polymer characteristic	Process condition
Molecular weight	Relative concentrations of initiator and monomer
Structure (*e.g*. multi-arm star polymers)	Functionality of initiator or choice of linking agent
Narrow molecular weight distribution	Rapid initiation and high purity of reagents
Microstructure (*e.g. cis*, *trans*, vinyl)	Choice of solvent and initiator
Reaction livingness	Choice of solvent and high purity of reagents
Constant reactivity of initiator	Choice of solvent and low reaction temperature

2.3 General experimental setup

This section describes the system assembled by the author to make linear polystyrene and polybutadiene.

A high vacuum line is generally used in anionic polymerization to ensure that reactive centers of initiators and the living polymer chains are free of contaminants such as oxygen, moisture and carbon dioxide. Details of high vacuum techniques and safety consideration are described in the literature [88,89].

Shown in Fig. 2.1 is a typical vacuum line that consists of (A) an oil pump, (B) a mercury diffusion pump, (C) a cold trap, (D) an upper and (E) a lower manifold with stopcocks. The combination of the oil pump and the mercury diffusion pump can bring down the pressure of the system to around 10^{-5}mmHg, while the use of a turbo pump alone is also adequate for this purpose. The cold trap is immersed in a bath of liquid nitrogen to condense any volatile substances in the system and to protect the pump from them. The upper and lower manifolds, separated by high vacuum Teflon stopcocks, allow individual operations involving reagent handling.

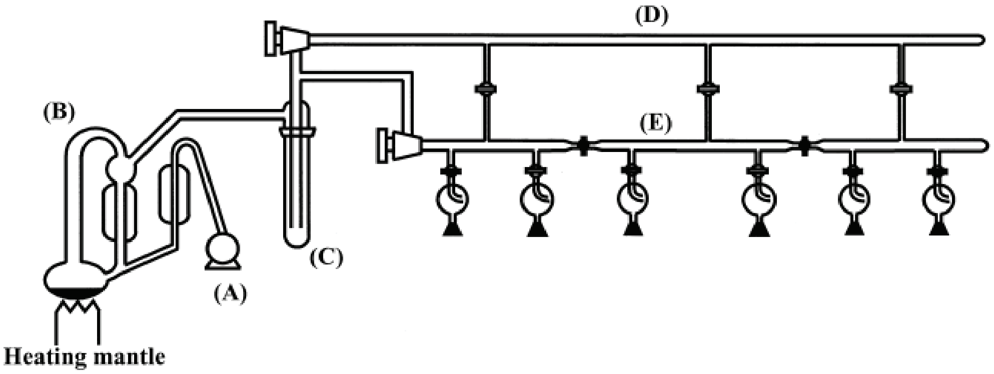

Figure 2.1 Typical vacuum line [88]

A Tesla coil is a convenient and reliable tool to check the quality of the vacuum and to detect the presence of pinholes in the evacuated glassware[90]. When the tip of the Tesla coil is held near the surface of the glassware, it is relatively quiet and does not discharge if the evacuated system is leak-free. The blue plasma line discharged by the Tesla coil in Fig. 2.2 indicates a leak in the system due to the failure of a Teflon stopcock.

Figure 2.2 Leak in vacuum line detected by the Tesla coil

To transfer reagents between two flasks in a contamination-free manner, distillation is generally used. The distillation setup used in preparing linear and star polymers is shown in Fig. 2.3. The setup consists of a source flask containing the solvent cyclohexane in this case, and the purifying chemical calcium hydride (CaH_2), a clean destination flask with a glass-coated Teflon stir bar inside, a solvent transfer manifold equipped with water jacket and an open port for connection to a vacuum line. The water jacket of the solvent manifold is connected to an external water circulation bath with the red arrow showing the water flow direction. To facilitate an effective reagent transfer, the setup is connected to a vacuum line. Only valve B is opened and the internal pressure of the destination flask, as well as the solvent transfer manifold, are brought down to around 100mtorr. The connection to the vacuum line is then closed, and the source flask is heated slowly by a heating mantle to the boiling point of the reagent. Valve A is then opened to allow reagent transfer. In this case CaH_2 is left in the source flask, while only the purified cyclohexane is transferred to the destination flask.

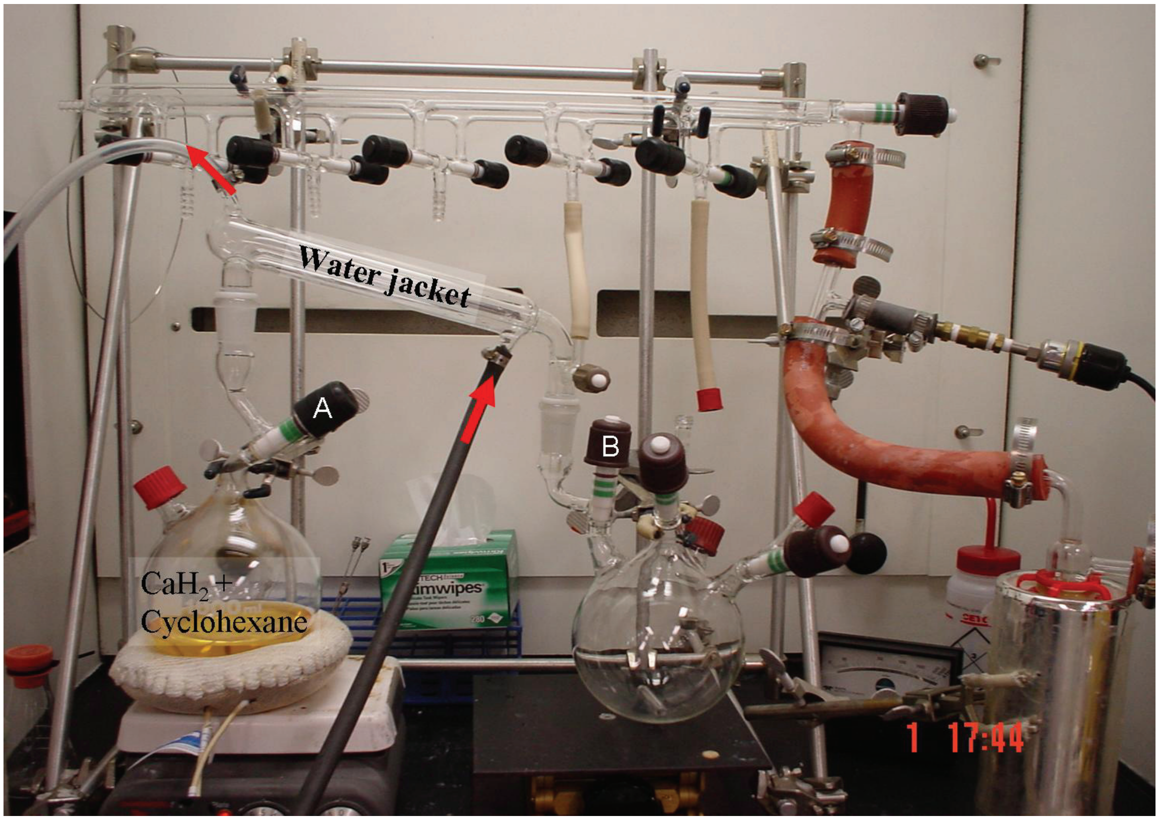

Figure 2.3 Reagents transfer line

2.4 Treatment of initiators, monomers, solvents and reagents etc

2.4.1 General

Aluminum oxide (Sigma-Aldrich, granular, 4-8 mesh), 1,2-Bis(Dichloromethylsilyl)ethane (DMSE) (Aldrich, 98%), Calcium hydride (Aldrich, coarse granules, -20mm, 95%), dibutylmagnesium (Aldrich, 1M in heptane), 1,1 diphenylethylene (DPE) (Aldrich, 97%), 2,6-di-tert-butyl-4-methyl-phenol (BHT) (Aldrich, 99+%), 1,1-Diphenylethylene (DPE) (Aldrich, 97%), anhydrous methanol (Sigma-Aldrich, 99.8%), methanol (Sigma-Aldrich, ACS reagent, $\geq 99.8\%$) and methyl chloride (Aldrich, $\geq 99.5\%$) were used as received without further treatment.

2.4.2 Initiators and their concentration

N-butyllithium (*n*-BuLi) (Aldrich, 2.5M in hexanes) or *sec*-butyllithium (*sec*-BuLi) (Aldrich, 1.4M in cyclohexane), shown in Figure 2.4, were used as received. Even though *n*-BuLi is not ionic, due to the large electronegativitiy difference between carbon and lithium, the C-Li bond is highly polarized and can often be considered to react as a butyl anion and a lithium cation. *Sec*-BuLi is more basic and sterically hindered than its primary organolithium reagent *n*-BuLi, but it has a higher initiation and propagation rate than *n*-BuLi. *Sec*-BuLi can be purified by distillation while *n*-BuLi is non-crystalline and has a boiling point (~60^{o}C – 80^{o}C) that is too high to be purified by distillation. Although the solutions are stable indefinitely if stored properly without contamination, in practice after a reagent bottle seal has been perforated, the solution degrades on aging, and its turbidity increases. This turbidity is due to the formation of lithium alkoxides by oxidation reactions or lithium hydroxides which exist in the form of a fine white precipitate by reaction with moisture. Knowing the exact amount of lithium byproducts in a given sample is thus crucial for an exact dosage of the reagent.

Several methods have been developed to examine the concentration of the active species in the initiators [91]. The oldest method is Gilman double titration [92], which determines the compositions of both the organolithium compounds and the lithium-alkoxides, thus providing an indication of the quality of the organolithium. The butyllithium solution is first reacted with benzylchloride to form neutral pentylbenzene while leaving all other basic impurities unaffected. The solution is then hydrolyzed and titrated with a hydrochloric acid standard using phenolphthalein as the indicator. The amounts of basic impurities can then be calculated. A second aliquot of the butyllithium solution is hydrolyzed and titrated with 1,2-dibromoethane. Since this step destroys the organolithium without producing lithium alkoxides, the difference of the two titrations gives the exact concentration of the organolithium.

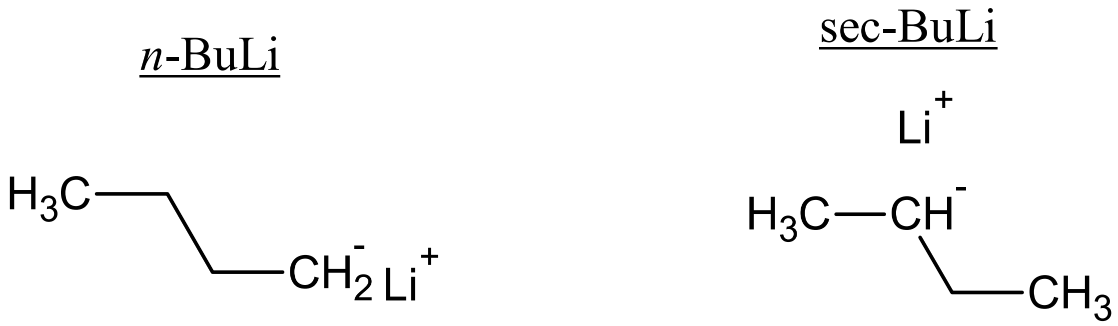

Figure 2.4 Molecular structures of initiators

In this project, we used a second method, the Watson-Eastham method [93]. This involves the use of a charge transfer (CT) complex indicator. The titration uses 2-butanol in dry hexane as titrant and 2,2 biquinoline as the CT complex indicator. The CT complex is only destroyed when all of the unreacted organolithium compound has been reacted with the alcohol; thus at the end point the solution's color changes from yellow to colorless. The molarity of a organolithium solution such as *n*-BuLi is calculated by Eq. 2.7. Details of the experimental procedures and sample calculations for this method are given in Appendix A.

$$\text{Molarity of } n\text{-BuLi} = \frac{\text{mass of BuOH}}{\text{mass of } n\text{ - BuLi}} \times \frac{\rho_{\text{n-BuLi}}}{M_{w,\text{BuOH}}} \times 1000 \ \text{(M)} \qquad \text{Eq. 2.7}$$

2.4.3 Styrene

Styrene (Sigma-Aldrich, ReagentPlus®, >99%) was purified in several steps. First, it was passed through a glass column filled with 90% aluminum oxide and 10% calcium hydride in a ratio of 1g mixture to 1.25 g styrene under a constant nitrogen purge. A 15 wt%

excess over the required amount was used to compensate for material loss while passing through the purification column. The receiving flask contained a glass- coated stir bar and a connecting adapter (Chemglass) equipped with a Chem-Vac^{TM} Chem-Cap® valve. Then, dibutylmagnesium solution was added into this flask under nitrogen purge by syringe and was stirred for 24 hours at room temperature. Afterwards, purified styrene was distilled into a clean flask and stored in a refrigerator (-15^{o}C) until use.

2.4.4 1,3-Butadiene

1,3-Butadiene (Matheson, 99wt% research grade) was purified immediately prior to starting a polymerization. Since the monomer is a gas at room temperature and atmospheric pressure and is highly reactive, all transfers of 1,3-butadiene were done at a temperature well below its boiling point of -4^{o}C. In the first step, 1,3-butadiene was transferred from the storage cylinder into a 300ml cylindrical flask containing calcium hydride under vacuum at a temperature of -78^{o}C, as shown in Fig. 2.5. The amount of 1,3-butadiene was measured by weighing the round bottom flask at the end of the transfer, and a 10 wt% excess over the required amount was transferred to compensate for material loss during the degassing process, which involved displacing the dissolved gas in the liquid system. Once the transfer was completed, the mixture was degassed and thawed. It was then stirred under calcium hydride for 5 hours in a dry-ice/isopropyl alcohol bath. In the second step, the 1,3 butadiene was distilled into a clean flask that had been evacuated and baked for 3 hours and contained solvent-free dibutylmagnesium. To facilitate distillation of the gas monomer, the dry ice/isopropyl alcohol bath of the feeder flask was removed, and the temperature was allowed to rise slowly back to room temperature, while the source flask was kept at -78^{o}C. After being degassed and thawed, the 1-3 butadiene was stirred with dibutylmagnesium for 5 hours in dry ice/acetone bath. In the third step, the 1,3 butadiene was distilled into solvent free n-butyllithium for 20 minutes in a dry ice/acetone bath. Finally, the purified 1,3-butadiene was collected by distillation in another 500ml round bottom flask, weighed and kept in freezer (-10 ^{o}C) until use.

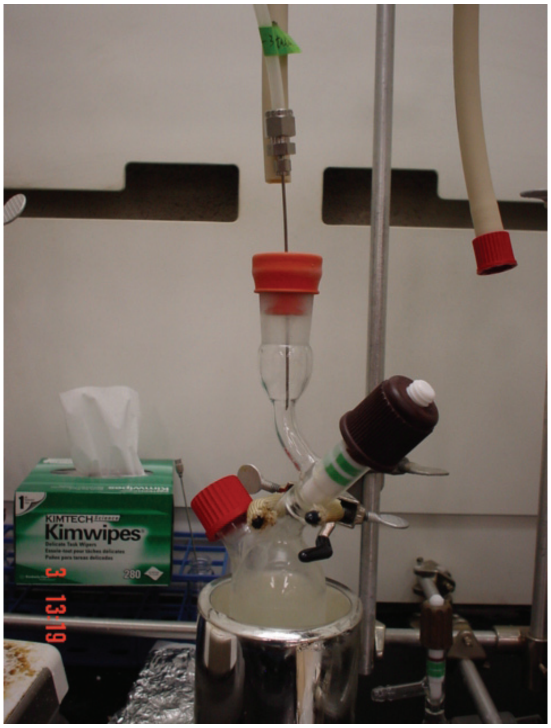

Figure 2.5 Transfer of 1,3-butadiene from gas cylinder into cylindrical flask at -78^{o}C

2.4.5 Cyclohexane

Cyclohexane (Sigma-Aldrich, ACS reagent, ≥ 99%) is purified by several purifying agents. It is first stirred with calcium hydride, then with dibutylmagnesium, and finally with *n*-BuLi with a few drops of purified styrene for 1 day each at room temperature. All transfers are done by distillation, with the feeder flask being heated while the receiving flask is kept in an ice/water bath. The golden color of the purified cyclohexane in *n*-BuLi with a few drops of styrene should persist until the solvent is ready to be transferred to the clean reactor. It is kept in a freezer until use.

2.4.6 Tetrahydrofuran (THF)

A solvent purification system was assembled based on the design of Pangborn *et al*. [94] for THF (Sigma, ≥ 99%) purification. The system contained two sequential purification columns. The first column contained activated alumina for removing polar impurities such as water, peroxides and inhibitors. The second column was copper oxide for removing traces of oxygen from the hydrocarbon. The whole setup was purged with nitrogen for 20 minutes before the solvent reservoir was filled. Before closing the two-way valve under the solvent reservoir, the nitrogen purge was stopped. This was to ensure that the internal pressure of the solvent reservoir was not higher than atmospheric pressure; otherwise solvent would spill over while filling the reservoir. To promote the flow of solvent through the columns the system was purged with nitrogen. The collection vessel was under static vacuum prior to being attached to the columns.

2.5 Synthesis of linear polystyrene

Linear polystyrene (PS) was prepared by anionic polymerization with THF as the solvent, DPE as an indicator and *n*-BuLi as the initiator. A schematic representation of the reactions is shown in Fig. 2.6.

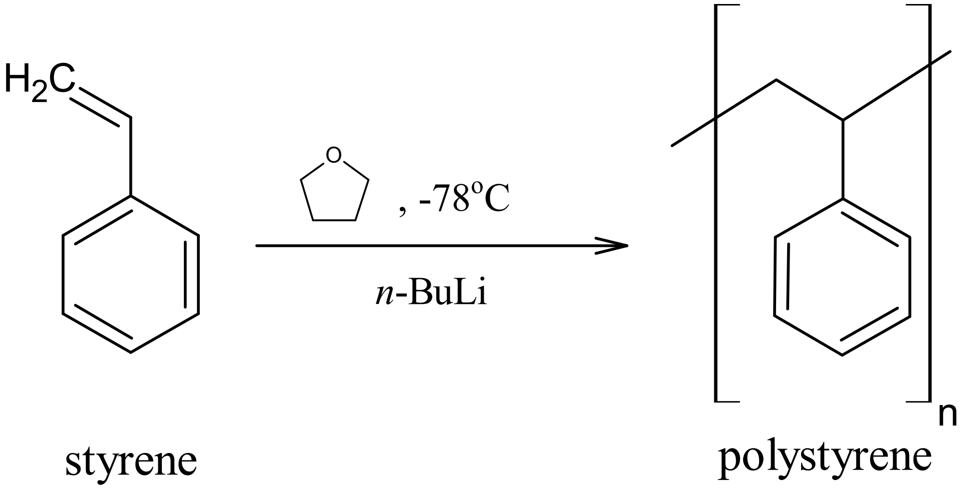

Figure 2.6 Anionic polymerization of linear Polystyrene with *n*-BuLi as initiator

2.5.1 Experimental section

Anionic polymerization of styrene under high vacuum conditions was performed in an all-glass (Pyrex ®) reaction system. A vacuum line connected with a two neck 250ml reactor, as illustrated in Fig. 2.7, was used, and the reactor was kept in a dry ice/acetone bath at -78° C during the reaction. The two-neck reactor was baked and evacuated with the vacuum line for 4 hours prior to use. Once the reactor was cooled down to room temperature, it was kept in a dry ice/acetone bath, and 100ml of THF was cannulated through the side arm of the reactor, which was capped by a rubber septum. Around 0.2g of DPE was injected with a syringe; this was followed by the injection of a small amount of *n*-BuLi until the solution's color changed from colorless to orange. This was to remove any traces of impurities by titrating them with the initiator *n*-BuLi. With the persistence of the orange color, the required amount of *n*-BuLi was injected into the reactor followed by 20g of styrene to start the reaction. The required amount of initiator can be calculated by Eq. 2.8 as follows:

$$mass\ of\ initiator\ (g) = \frac{mass\ of\ styrene\ added\ (g)}{target\ molecular\ weight\ (g/mol)} \times \frac{density\ of\ initiator\ (g/L)}{molarity\ of\ initiator\ (M)}$$

Since the septum was perforated after all the chemical additions, the reactor was filled with ultra-high purity nitrogen gas to minimize contamination by air. The reaction was terminated with anhydrous methanol after 6 hours in a dry ice/acetone bath. Reactions of *n*-BuLi in THF were typically conducted at low temperature to minimize deprotonation of THF by butyllithium, wherein butyllithium was consumed to produce butane. The solution was then poured into a large quantity of methanol with rigorous stirring to precipitate the polymer. The polymer was then filtered and dried in a vacuum oven at room temperature.

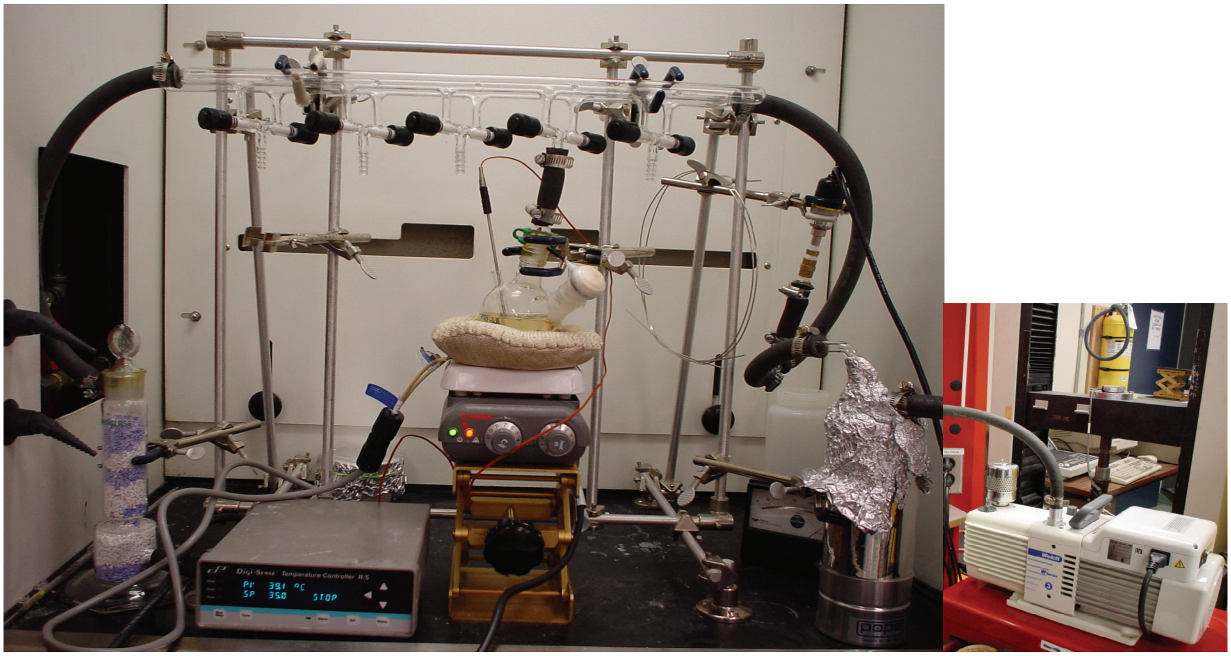

Figure 2.7 Vacuum line for anionic polymerization of linear polystyrene and polybutadiene

2.5.2 Result and discussion

Several batches of polystyrene were synthesized, and the molecular weight and molecular weight distribution were measured using gel permeation chromatography (GPC). A summary of samples prepared in this way is shown in Table 2.2 (at the end of section 2.7.3). The GPC system (Waters Breeze) consisted of an isocratic pump (Waters 1515), three HR Styragel columns (Waters) (HR1 with molecular weight measurement range of 100 to 5000 g/mol, HR2 with molecular weight measurement range of 500 to 20,000 g/mol and HR4 with molecular weight measurement range of 5,000 to 600,000g/mol), a guard column, a Waters 2487 UV detector and an RI 2410 differential refractive index detector. The measurement was done with THF as the mobile phase at a flow rate of 0.3mL/min with a column temperature of 40 ^{o}C. Concentration of the polymer was 4 mg/mL THF carrier phase. The GPC system was initially calibrated using narrow molecular weight distribution linear polystyrene standards, and the reported molecular weights of the samples are relative to the polystyrene standards.

When the target molecular weight was around 60kg/mol, anionic polymerization using the above method was generally satisfactory and constantly able to produce polymer with a narrow molecular weight distribution prior to any fractionation. A typical elution curve of a linear PS (PS-1) with a target molecular weight of 60kg/mol is shown in Fig. 2.8. The GPC measured molecular weight of this sample was 55kg/mol, the PDI (M_w/M_n) was 1.095, and around 90wt% of the monomer was polymerized. However, when the same method was used to prepare linear polystyrene with a target molecular weight around 100 kg/mol, a narrow molecular weight distribution could not be obtained. An elution profile of sample PS-2 with target M_n =110kg/mol is shown in Fig. 2.9. The GPC measured molecular weight was 96kg/mol, the PDI was 1.95 and around 90% of the monomer was polymerized.

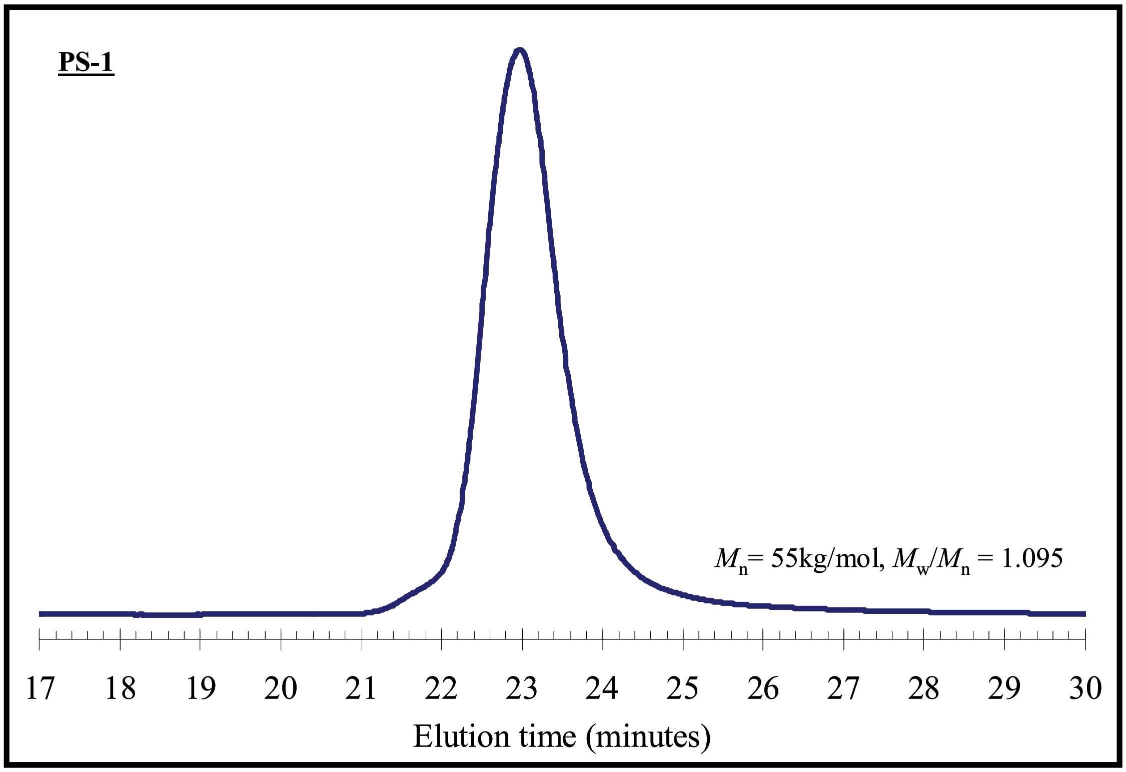

Figure 2.8 GPC elution profile of linear Polystyrene with target M_n = 60kg/mol and measured M_n = 55kg/mol.

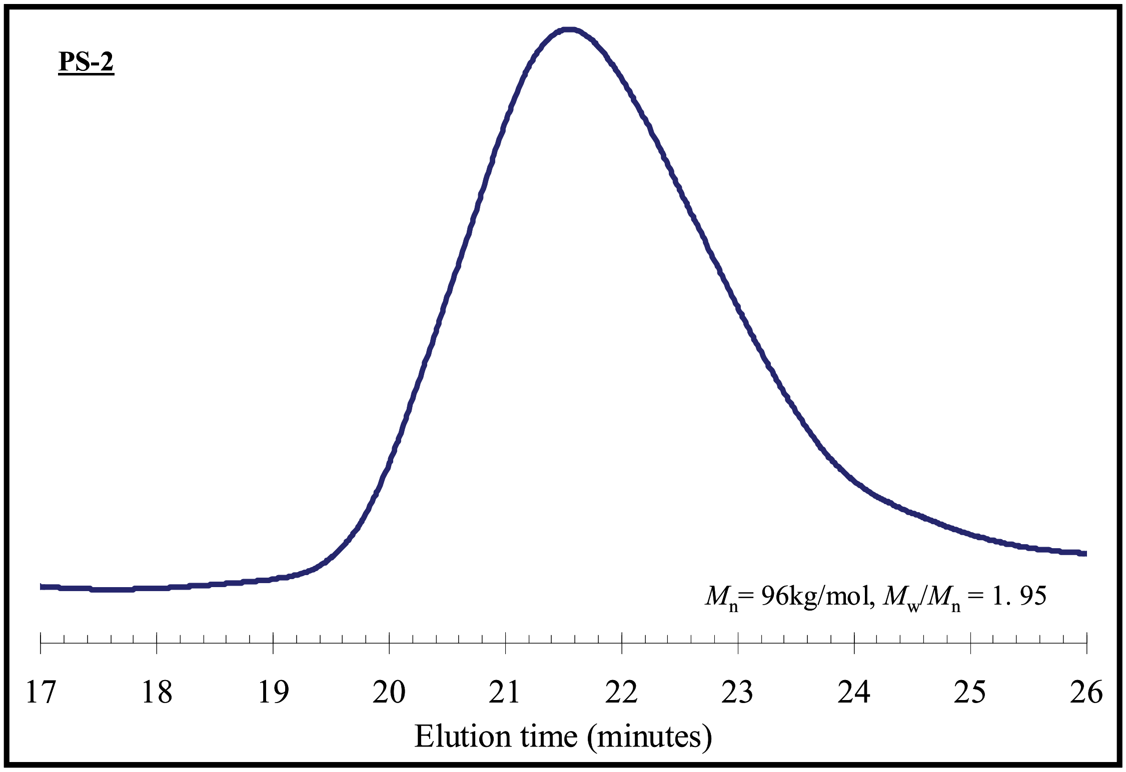

Figure 2.9 GPC elution profile of linear Polystyrene with target M_n = 118kg/mol and measured M_n = 96kg/mol.

With only 90% of the monomer consumed and a lower molecular weight than the target molecular weight, it was likely that the reaction had not proceeded to 100% completion. When the reaction was approaching 100% completion, the concentration of the available monomer was much lower that at the beginning, while the growing chains were already long enough to cause a significant hindrance between the reactive chain ends and the limiting monomer, which was indicated by the increased viscosity of the solution. Thus, a 6-hour reaction time may not be enough for complete polymerization, and the polymerization might also take a little longer due to the presence of lithium alkoxides formed in the titration of impurities.

However, according to the result shown in Fig. 2.8, a broadened molecular weight distribution resulted from the higher targeted molecular weight suggesting that initiation was slower than propagation or that the reactivity among initiators was not uniform. Based on Eq. 2.8, one can either increase the amount of monomer or decrease the amount of initiator when aiming at a higher target molecular weight. In the first case, increasing the concentration of monomer/solvent will considerably decrease the chances of an initiator molecule meeting a monomer molecule in the reactive mixture, which will slow down the initiation step. One way to solve this problem is to scale up the reaction system by using a larger reactor and more solvent, while keeping the monomer/solvent concentration below 20wt%. With the latter condition, the tolerance for impurities is reduced, since the amount of initiator required for polymerization will be comparable to the amount used for impurities titration, in which case the lithium alkoxides formed can considerably disturb the reactivity of the initiator. More vigorous control of the level of impurities is then essential to solve this problem. In the next section, modifications intended to improve impurities control in order to prepare polybutadiene are described.

2.6 Synthesis of linear polybutadiene

Linear polybutadiene (PBD) was prepared by anionic polymerization with cyclohexane as the solvent and *sec*-BuLi as the initiator. A schematic representation of the reactions is shown in Fig. 2.10.

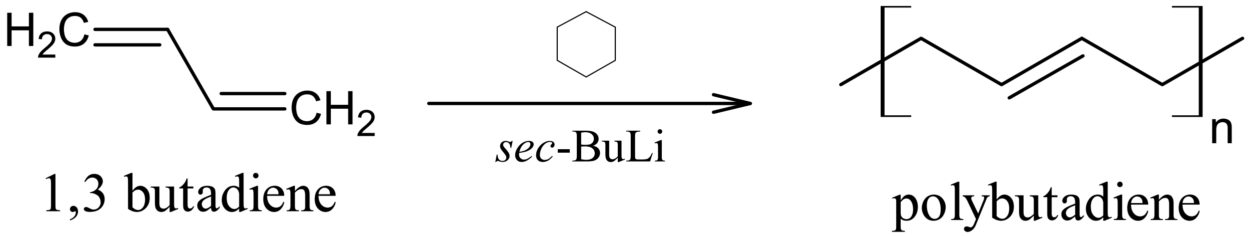

Figure 2.10 Anionic polymerization of linear Polybutadiene with *sec*-BuLi as initiator

When producing PBD by anionic polymerization using organolithium initiators, the concentrations of possible microstructures which are shown in Fig 2.11, can be varied by changing the reaction conditions. If the reaction is carried out in hydrocarbon solvents such as n-hexane and cyclohexane at ambient temperature, a product with about 94% 1, 4-addition typically results. Conversely, in polar solvents such as THF at relatively low reaction temperatures, 85-90% 1,2-vinyl addition is favored.

trans 1,4 polybutadiene	*cis* 1,4 polybutadiene	1,2 vinyl polybutadiene
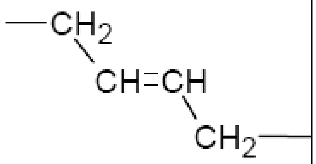	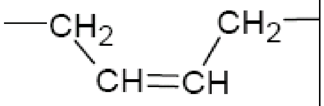	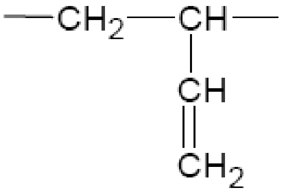

Figure 2.11 Various microstructures of polybutadiens

As shown in Fig. 2.12, the 1,2 addition results in a vinyl side group that form a branch, while the double bond on the vinyl side group is also vulnerable to cross-linking. The *trans* configuration allows the chain to stay rather straight and to have a more ordered alignment, so that chain section can form microcrystalline regions in the material. Meanwhile, the *cis* configuration causes a bend in the polymer chain, preventing the chains from lining up and form crystalline regions resulting in an amorphous region. To achieve the objectives of this project, samples that are vulnerable to cross-linking and contain many short chain branches are less suitable. Therefore, cyclohexane was chosen as the solvent to give a PBD high in the 1, 4-addition. However, since the reaction rate in hydrocarbon solvent is much slower than in polar solvent, *sec*-BuLi was used instead of *n*-BuLi, as the former is a more reactive initiator.

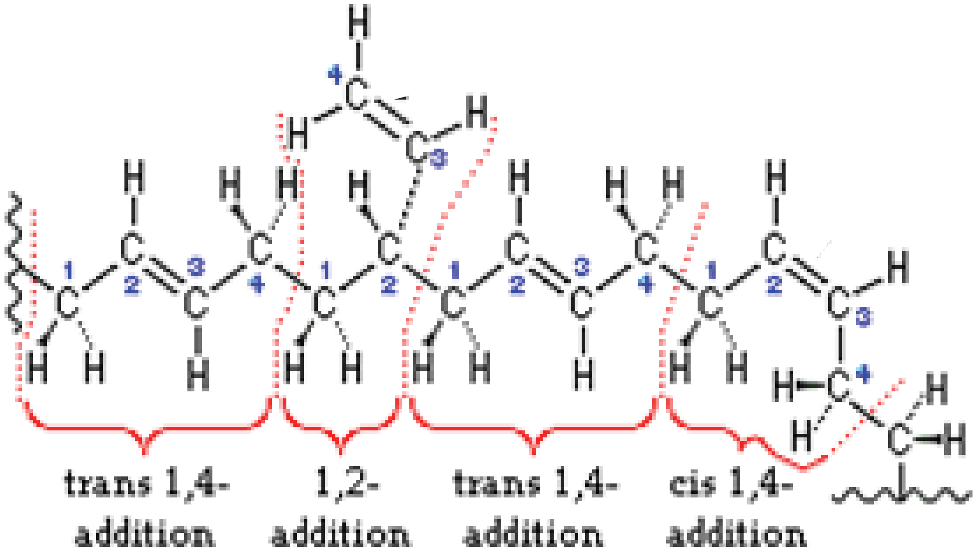

Figure 2.12 Schematic representation of a typical PBD chain configuration

2.6.1 Low molecular weight Polybutadiene (M_n ~30kg/mol)

Using an approach similar to that used to make polystyrene, PBD with a target molecular weight around 30kg/mol was made with *sec*-BuLi in cyclohexane at 40°C with DPE as an indicator, such that any impurities in the reaction mixture were titrated with the initiator prior to the initiation step. The experimental setup and procedures were same as those used in preparing linear polystyrene except that the DPE formed a yellow complex in cyclohexane, and the reaction time was 24 hours. A persistence of the golden-yellow color indicated the livingness of the reaction during the experimental time scale.

The GPC measured molecular weight was based on linear polystyrene standards, which can be approximately related to polybutadiene by the Mark-Houwink Equation as shown in Eq. 2.9 [95].

$$M_n(PBD) = \left[\frac{13.63}{25.6} \times M_n(PS)^{1.714}\right]^{1/1.74} \qquad \text{Eq. 2.9}$$

However, as shown in Fig. 2.13 for sample PBD-1, the molecular weight distribution of PBDs prepared by this method was much broader than that of linear PS with a PDI greater than 1.3 and with only 22% monomer consumption. The molecular weights corrected by Eq. 2.9 were 1/3 less than the target molecular weight. In addition to lithium alkoxides slowing down the reaction, the presence of DPE also disturbed the propagation step, especially when its concentration was comparable to that of the initiator. This was mainly due to steric hindrance arising from the bulky aromatic rings of DPE; therefore, DPE was not used in the subsequent experiments.

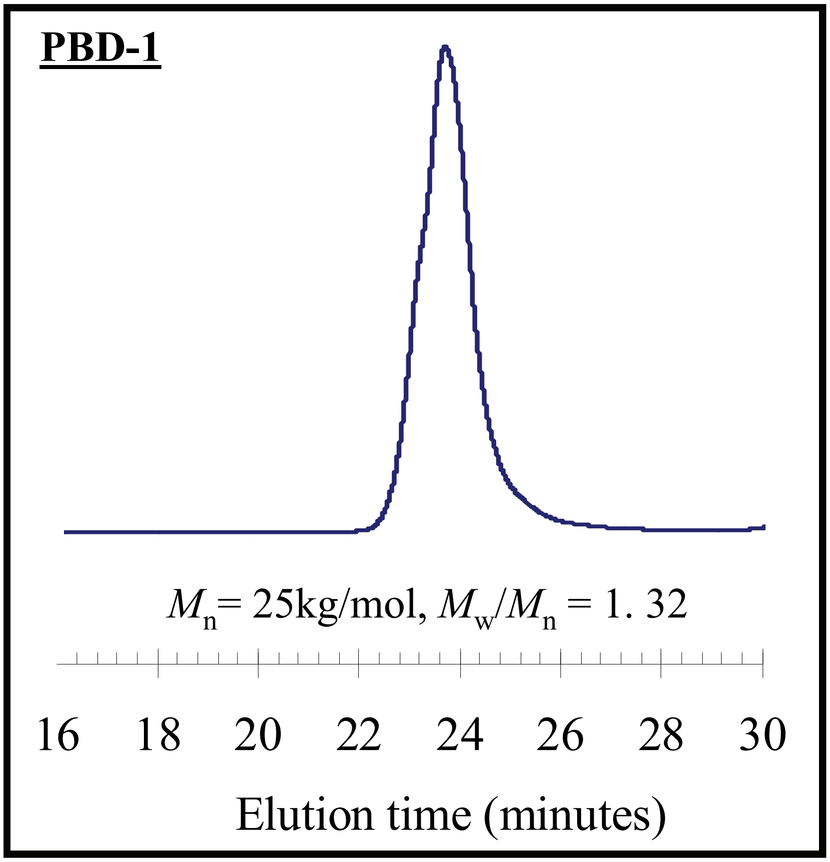

Figure 2.13 GPC elution profile of linear Polybutadiene with target M_n = 34kg/mol and calculated M_n = 25kg/mol from Eq. 2.9

2.6.2 High molecular weight Polybutadiene (M_n ~60kg/mol)

New difficulties were encountered with high molecular weight polybutadiene. First, the glass adapter required for connection between reactor and manifold required a thin layer of vacuum grease for a proper seal. However, not realizing that vacuum grease had gotten into the reactive solution and killed the reaction, I failed to synthesize PBD for several months. As the living initiator had a similar yellow color to the grease (Fig 2.14), it was difficult to tell if the mixture was grease-free. The only way to know was by terminating the reaction and pouring the mixture into an excess of methanol; the yellow color should completely fade away for a grease-free solution. Fig 2.15 shows the typical result for a grease-contaminated experiment; the mixture had a slight yellow color and did not show any polymer precipitate.

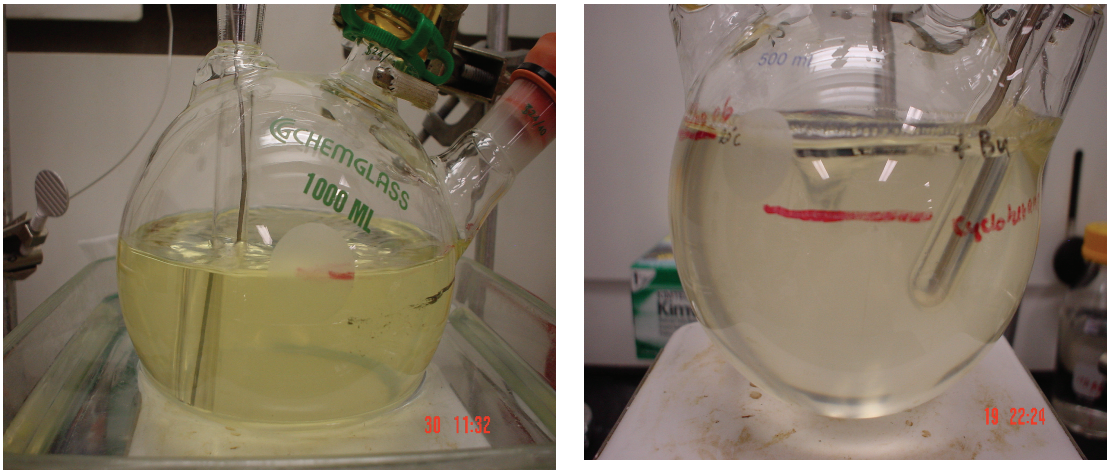

Figure 2.14 Left: Color of the reactive mixture without contamination of vacuum grease

Right: Reactive mixture with vacuum grease contamination

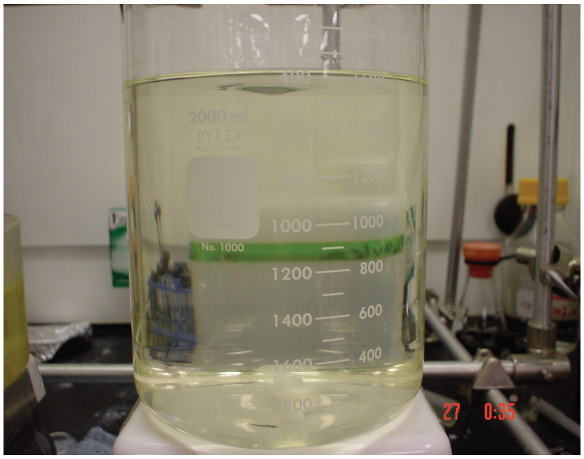

Figure 2.15 Typical result of grease contaminated reactive mixture in excess of methanol.

A new reactor (1L) with 2 necks and a thermowell was then custom-made at McGill University. The major neck connected to the manifold was made of an inverted ground glass joint and a drip tip to minimize vacuum grease contamination. This helped reduce the contamination problem but did not totally eliminate it. I also encountered a material loss problem during the early part of reaction. This was indicated by a drop in the liquid level of the reactive solution, especially in the first few hours of reaction. I suspected that this was due to the increased vapor pressure of butadiene when the solution was heated from room temperature to the polymerization temperature (~40^{o}C) and to a poor seal in the reactor glass joint.

Consequently, a 1L reactor with three side arms equipped with high-vacuum Teflon stopcocks, shown in Fig. 2.16, was used. One side arm was connected to the vacuum line, while the second was for initiator and monomer injection and was serum capped with Teflon coated silicone septa (Supelco, 22mm), and the third side arm was an adapter for solvent distillation. The Teflon stopcocks allowed isolation of the reactor from the vacuum line once the turbo pump was turned off and also protected the reactive mixture once the rubber septum had been perforated. A 25mm opening in the reactor allowed easy insertion of a glass-coated stir bar and could be screw capped. Instead of using a glass adapter to connect the reactor with the vacuum line, which required a thin layer of vacuum grease in the glass joint, the modified reactor did not require a glass adapter for connection with vacuum line, as shown in Fig. 2.17. Thus the use of vacuum grease was eliminated.

To minimize air contamination in the reactive mixture, a dual bank manifold was modified with the inclusion of a high-vacuum stopcock at one end to maintain the vacuum once the pump was off and a nitrogen/ argon outlet at the other end to facilitate inert gas purge on line. A check-valve oil bubbler was also incorporated to indicate excess inert gas.

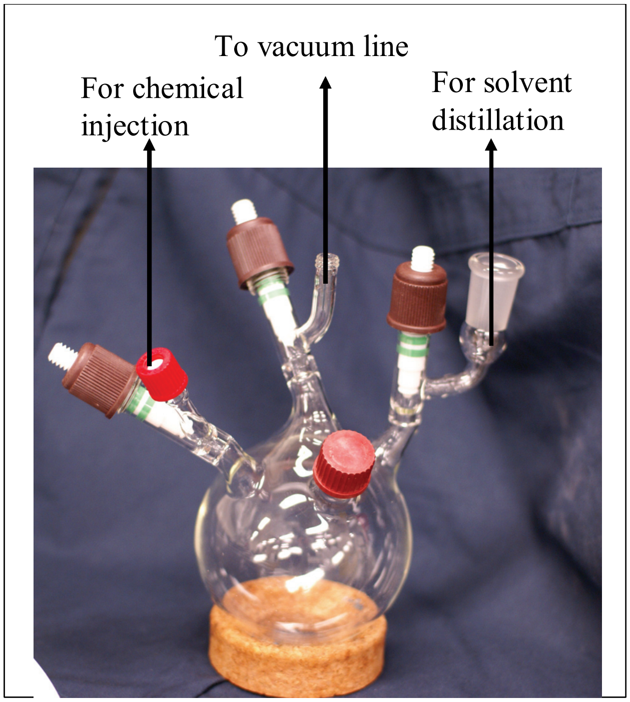

Figure 2.16 Modified reactor for use in high molecular weight PBD preparation

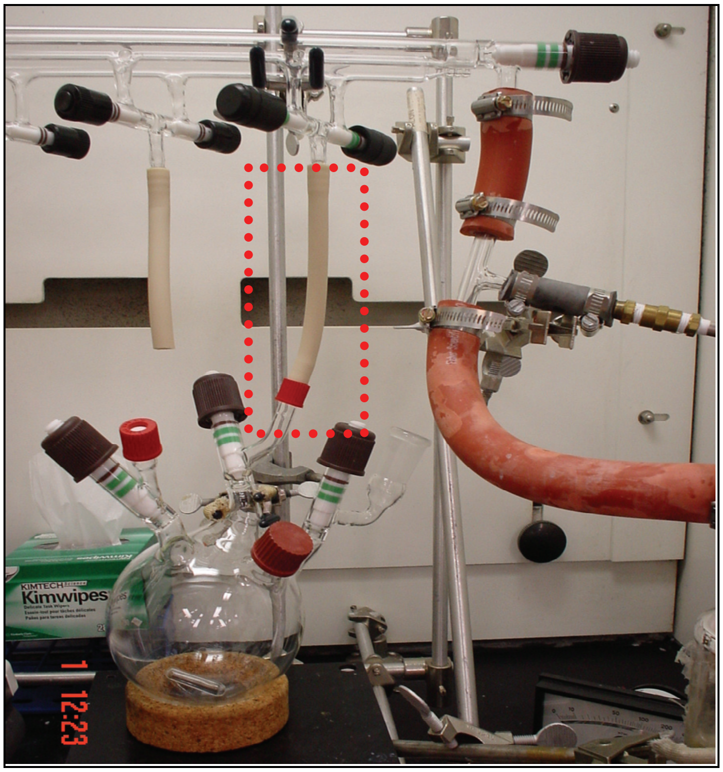

Figure 2.17 Modified connection of reactor with vacuum line

With the above modifications, several batches of linear PBD were synthesized at 20°C for 6 days to minimize material loss while compensating for the slow reaction rate at this lower temperature. The results are summarized in Table 2.2, which is shown at the end of section 2.6.3. Although the percent monomer consumption was improved (~73%, as shown in Fig. 2.18 for sample PBD-2, the calculated molecular weight from Eq. 2.9 was much smaller than the target molecular weight, suggesting that a considerable amount of the initiator was destroyed by impurities, thus forming lithium alkoxide which slowed down the reaction. This also explains why the reaction did not proceed to 100% completion after 6 days at 20°C. Moreover, chain-chain termination occurred as shown by the GPC elution curve, which revealed a bimodal distribution as shown in Fig. 2.18. The ratio of the peak heights showed that the longer chain (small peak) had twice the molecular weight of the shorter chain (major peak) and accounted for less than 20% of the total weight.

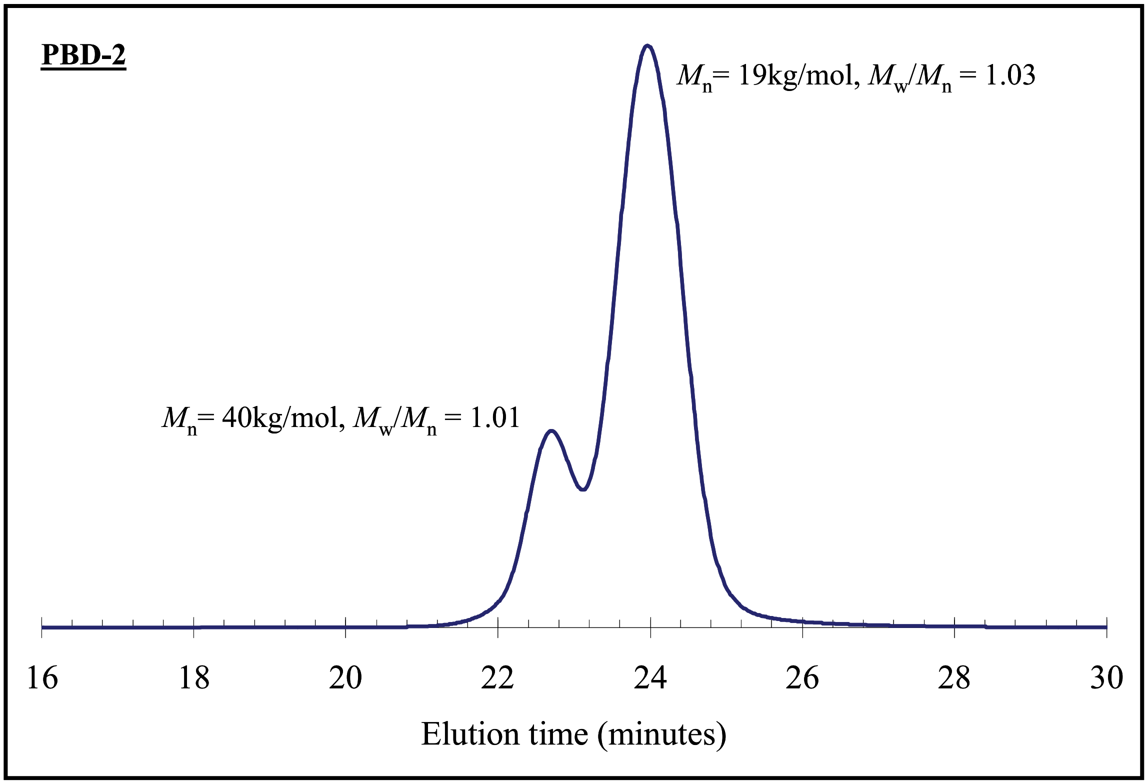

Figure 2.18 GPC elution profile of linear Polybutadiene with target M_n = 60kg/mol and calculated M_n (from Eq. 2.9) = 40kg/mol and 19kg/mol, respectively for the two components.

Therefore, to enhance the purity level of the solvent, the purification process for butadiene was modified by two treatments with solvent-free *n*-BuLi at -10^{o}C for 15 to 30 minutes; the butadiene was then used immediately for polymerization. Great caution was needed for this method, as the temperature was very close to the monomer boiling point (-4^{o}C); failure to maintain the cold bath can lead to a build-up of internal pressure and cause the glassware to explode. Therefore, purification of butadiene with solvent-free *n*-BuLi for some trails was carried out at -78^{o}C with a dry ice/acetone bath for 90 mins to compensate for the slower reaction rate. However, the polydispersity index of the product was still above 1.3, indicating that purification of butadiene needed to be done at a higher temperature with a salt/ice bath to speed up the purification process.

As pointed out by Dr. Jacques Roovers, who visited the lab during this work, some fractionation may have occurred when butadiene was taken from the gas cylinder, with the first few batches better than later ones. Moreover, he noted that a long storage time in a gas cylinder ca degrade the quality of butadiene through reaction with the metal cylinder. Therefore, a new batch of butadiene was used for the synthesis of high molecular weight PBDs.

Incorporating these two modifications of the monomer and the use of further degassed anhydrous methanol for termination, a few batches of PBD were polymerized at 40^{o}C for 24 hours. Although the second GPC peak was less significant, as shown in Fig. 2.19 for sample PBD-3, and the monomer consumption was close to 96%, the calculated molecular weight was still lower than the target molecular weight, and the polydispersity index of 1.2 was not narrow enough for this project's requirement.

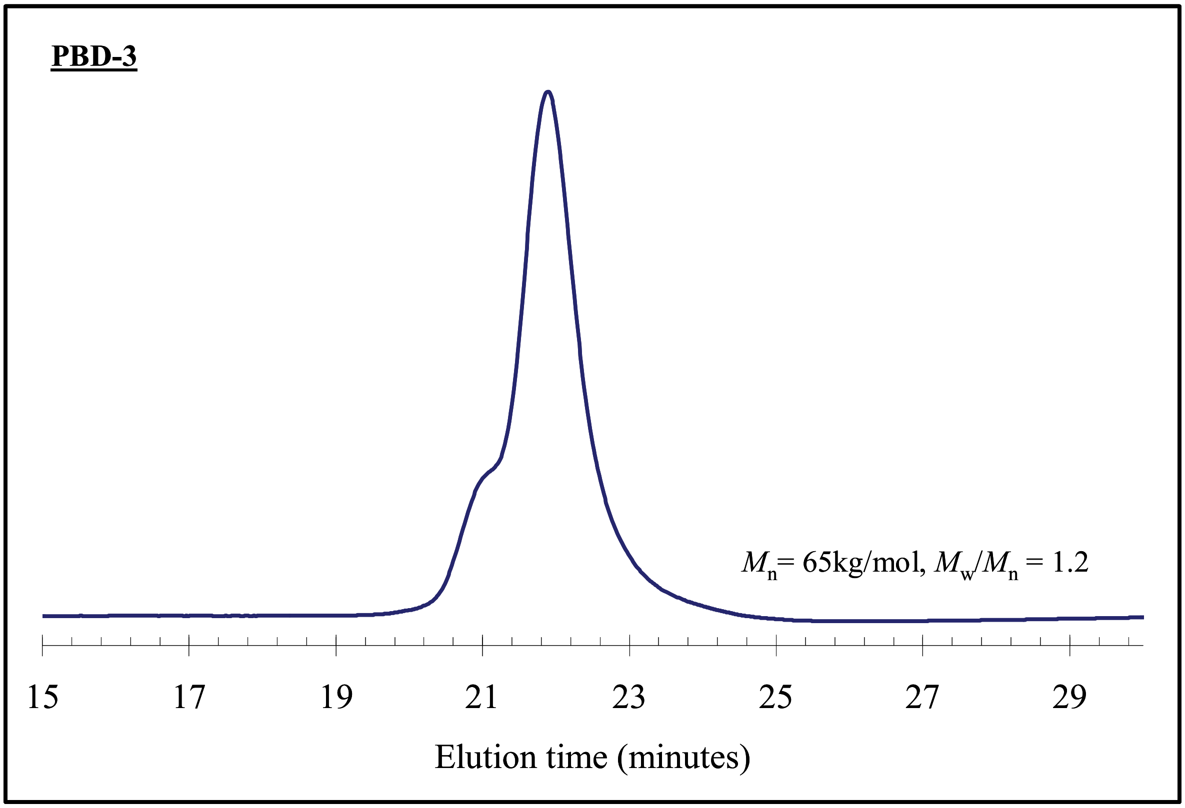

Figure 2.19 GPC elution profile of linear Polybutadiene with target M_n = 60kg/mol and calculated M_n = 65kg/mol from Eq. 2.9

2.7 Synthesis of 4-arm star polybutadiene

Star polymers are the simplest branched polymers and consist of several linear chains (arms) linked at a central branch point (core). The syntheses of star polymers from vinyl monomers using controlled/living polymerization has been described elsewhere [96,97].

2.7.1 Methods for preparing star polymers

There are essentially two strategies to prepare star polymers, the “core-first” approach [98] and the “arm-first” approach [99] which are shown in Fig. 2.20.

In the core-first approach, multifunctional initiators (core) capable of simultaneously initiate the polymerization of several branches are used to prepare a star polymer. To obtain star polymers with precise functionality and narrow molecular weight distribution, all the initiation sites have to be equally reactive and have the same rate of initiation. Furthermore, the initiation rate must be higher than the propagation rate. However, only a few multifunctional initiators can fulfill these requirements (*e.g.* divinylbenzene), and complications often arise from the insolubility of these multiply-charged initiators due to the strong aggregation effects.

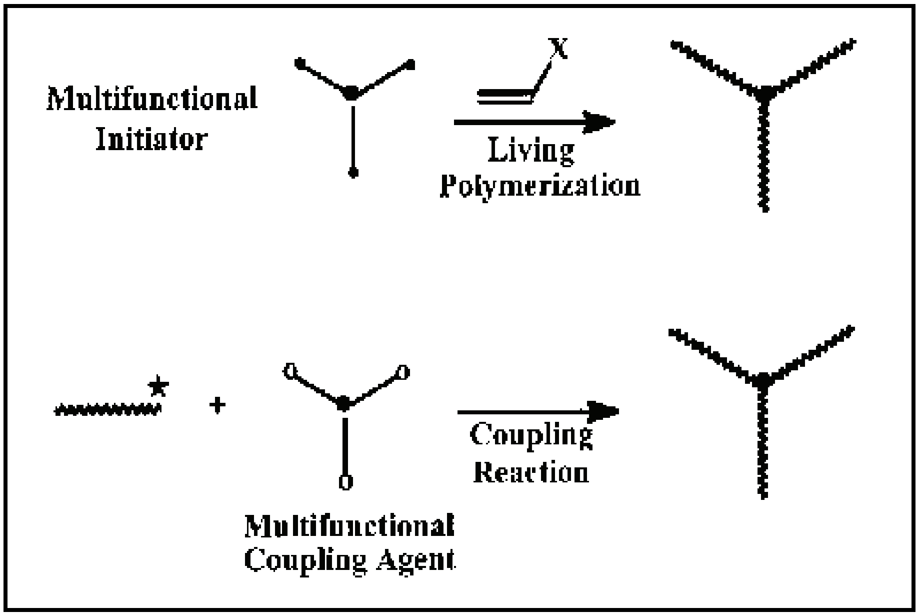

Figure 2.20 General synthetic method for star polymer

For the arm-first approach, living polymer chains (arms) are synthesized first in a one reactor and subsequently reacted with a multifunctional electrophile coupling agent, which is usually a chlorosilane, chloromethyl or a bromomethyl benzene derivative. This is the most efficient way to synthesize well-defined star polymers, as it provides absolute control of all the synthetic steps. As long as the linking reaction is quantitative and proceeds to completion, the number of arms is governed by the functionality of the linking agent. Since the living arms can be isolated and characterized independently along with the final star product, the functionality of the star and the molecular weight of the arms can be measured directly and accurately. However, this method is limited to stars based on polystyrene or polydienes derived from anionic polymerization [99], and in almost all cases a small excess of living arms is used to ensure complete coupling. Thus, there is a need to perform fractionation in order to obtain pure star polymers.

2.7.2 Experimental details

Preliminary preparations of 4 arms symmetric star-shaped PBD were carried out in cyclohexane with *sec*-BuLi at 20°C for 4 days, followed by 10 days for coupling. The experimental procedures and setup were exactly the same as in the case of linear PBD, with all modifications included except the termination step. Instead of adding degassed anhydrous methanol to the reactive mixture, 1,2-Bis(dichloromethylsilyl)ethane (DMSE), which is a coupling agent with 4 functionalities, was used [100]. Before injection of DMSE into the reactor, 3ml of the reactive mixture were extracted from the reactor into a clean glass tube, which contained degassed anhydrous methanol, for further GPC analysis. Samples of the reactive mixture were taken periodically for GPC analysis to probe the progress of the coupling reaction. An indicator of the coupling reaction could be seen from the fading yellow color of the reaction mixture, implying that the coupling step was actually terminating the living chains. To ensure complete coupling, the amount of coupling agent added is usually less than the stoichiometric amount calculated based on the molecular weight of the living arm near 100% conversion. In general, a perfect 4 arm star-shaped PBD with a fraction of lower molecular weight linear PBD are obtained by this approach, and the linear PBD can be removed by fractionation. However, this process reduces the overall yield of the polymer. In contrast, if the exact stoichiometric amount of coupling agent is added, coupling is more difficult, requires a longer coupling time, and produces a mixed product that cannot be fractionated.

2.7.3 Result and discussion

GPC analyses on living arms before coupling, after 1 day coupling and 10 days coupling, are shown in Fig. 2.21. The calculated molecular weight from Eq. 2.9 of the living arm was 29kg/mol which was very close to the target molecular weight of 30kg/mol and PDI of 1.15. However, the coupling reaction was not successful as can be seen from the elution curves after 1 day and 10 days coupling; these curves are almost the same as that of the living arm. This was likely due to the arms being no longer living before addition of the coupling agent, which also explained why the polymerization proceeded only to 80% completion even after 10 days of reaction.

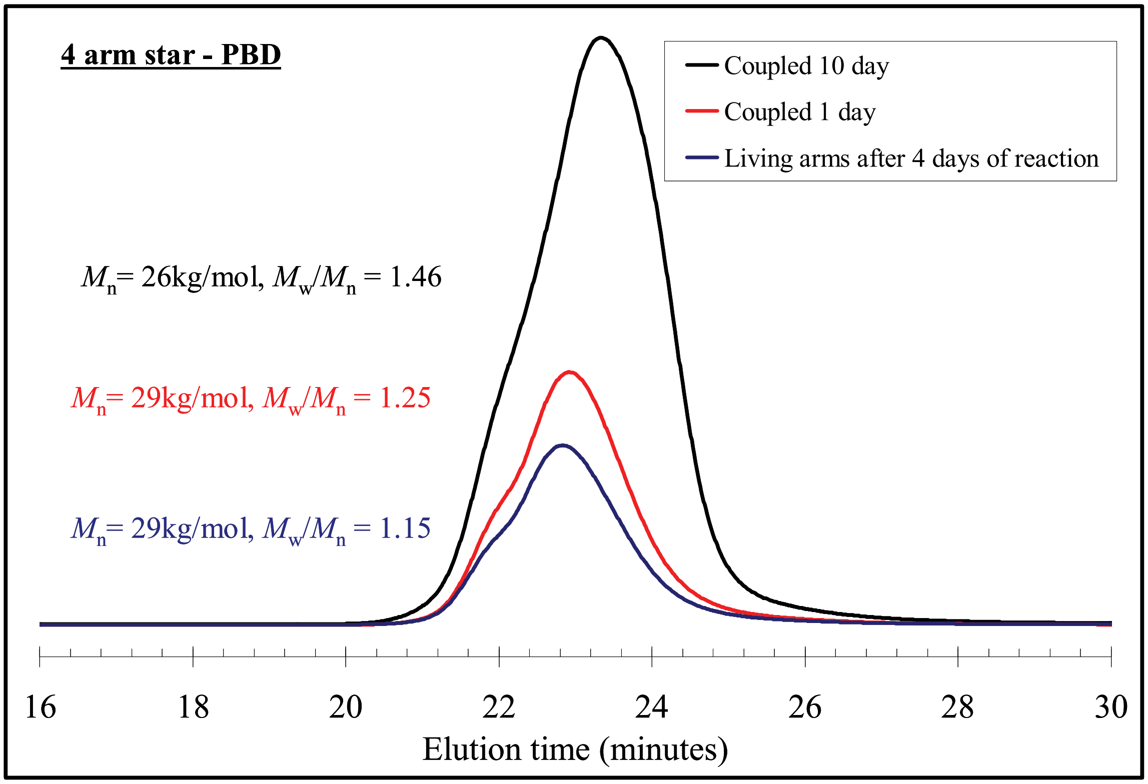

Figure 2.21 GPC elution profile of 4 arm star Polybutadiene with target M_n = 30kg/mol

Table 2.2 Summary of samples prepared in McGill University

Sample code	**Solvent**	**Initiator**	**Reaction temp (^{o}C)**	**Polymerization time (hr)**	**Mass of monomer (g)**	**Mass of initiator (g)**	**Mass of DPE (g)**	**Target M_n (kg/mol)**	**M_n (kg/mol) (Mark-Houwink)**	**PDI**	**Monomer conversion (%)**
PS-1	THF	*n*-BuLi	-78	6	21.5	0.099	0.02	60	--	1.095	90.2%
PS-2	THF	*n*-BuLi	-78	6	22	0.055	0.02	110	--	1.95	90.0%
PBD-1	cyclohexane	*sec*-BuLi	40	24	35.7	0.485	0.161	34	25	1.32	22.4%
PBD-2	cyclohexane	*sec*-BuLi	20	6 days	61	0.470	--	60	40 19	1.01 1.03	73.0%
PBD-3	cyclohexane	*sec*-BuLi	40	24	50	0.385	--	60	65	1.2	96.0%
4 arms star PBD	cyclohexane	*sec*-BuLi	20	14 days	56	0.862	--	30	29	1.15	78.6%

2.8 Conclusions

Living anionic polymerization is the best way for preparing well-defined model polymers due to the absence of chain transfer and chain termination. A relatively simple, small-scale vacuum line is constructed at McGill University; it fits into a standard fume hood and possesses most of the components of a typical vacuum line.

Procedures and apparatus are developed and used successfully to prepare modestly entangled polystyrene having a polydispersity index of 1.10. However, these are found to be unsuitable for the preparation of the branched samples required for this research. These samples are subsequently prepared in collaboration with Prof. Jimmy Mays at the University of Tennessee using the techniques described in the next chapter.

Chapter 3 Materials Used in This Project

To study structural and rheological relationships, PBD with a high concentration of 1,4 addition was chosen as the model polymer. This is due not only due to its relatively low entanglement molecular weight M_e among model polymers that can be synthesized by anionic polymerization (as shown in Table 1.1) but also due to the abundant literature data on PBD linears, stars and blends.

In this chapter, the sources of the samples used are provided, followed by a summary of anionic polymerization of H-shaped PBDs and a description of the preparation of binary blends and the procedure used to establish the molecular weights to be synthesized. Finally, analytical characterizations of molecular weight and microstructure are presented.

3.1 Source of materials

3.1.1 Reasons for outsourcing the materials

Based on the synthesis results presented in Chapter 2, we realized that the facilities and expertise required to synthesize linear and H-shaped PBDs with strict control of molecular structure were not available at McGill. For linear PBDs, the batch yield was around 30% (~10g), which, after several fractionations, would not be sufficient for rheological characterization. However, to ensure uniformity of a sample, it is crucial not to mix materials from different batches. Meanwhile, the quality of the linear PBDs described in Chapter 2 did not meet our requirements; the molecular weights and molecular weight distributions were out of control, and some samples contained a considerable amount of salt, which required several cycles of dissolution and precipitation to remove. Therefore, linear PBDs used in the rheological and modeling studies are provided by the Firestone Tire and Rubber Company. And for H-shaped PBDs special and delicate techniques are required to ensure species' livingness during each synthesis step. There are only a few experts in the world who have fully mastered these techniques; one of them is Prof. Jimmy Mays at the University of

Tennessee. Arrangements were thus made for our model H-shaped PBDs to be prepared by Dr. M.S. Rahman under the supervision of Prof. Mays using the techniques described in section 3.2.3. I visited their laboratory and participated in the synthesis process.

3.1.2 Naming of materials

Two linear PBDs, five H-shaped PBDs and a binary blend of H-shaped PBDs were studied in this project. For the linear PBDs, samples are named according to the number of components they have; “PBD2” indicates that the sample is a two-component blend while “PBD3” indicates that it is a three-component blend. For H-shaped PBDs, samples are named according to molecular weights of the arms and cross-bars; *e.g.* “HA12B40” denotes the H-shaped polymer with an arm MW of 12kg/mol and a cross-bar MW of 40kg/mol.

3.1.3 Preparation of linear PBDs

Linear PBDs were synthesized by classical anionic polymerization at the Firestone Tire and Rubber Company in a way similar to that described in Chapter 2. Purified 1,3 butadiene was transferred to clean hexane with *sec*-butyllithium as the initiator. Reactions were carried out in a 19L lab-scale batch reactor at 55-60^{o}C for 1.5 hours. The reaction was terminated and the product precipitated by discharging the polymer into a large amount of isopropanol containing a small amount of anti-oxidant, which was butylated hydroxytoluene (BHT). As reported by Firestone, the glass transition temperature (T_g) of these linear polymers was -90^{o}C, which they measured by differential scanning calorimetry with a heating and cooling rate of 5 ^{o}C/min.

3.2 Synthesis of H-shaped PBDs

The anionic polymerization of H-PBD is particularly challenging, especially for PBDs with high 1,4 addition, which requires that the reaction medium be a non-polar hydrocarbon. In general, anionic polymerization of H-shaped polymers involves the use of difunctional initiators, which are not commercially available and required a complicated preparation process. Furthermore, when compared with chains produced by monofunctional initiators such as *sec*-BuLi, the use of difunctional initiators in non-polar solvents generally broadens the molecular weight distribution of the crossbars [101]. It is also unavoidable that we would obtain a mixture of various branched polymers instead of pure H shaped polymers when using a multifunctional coupling agent. Each of these issues will be discussed in more detail in what follows.

3.2.1 Difunctional initiator for PBD in high 1,4 addition

Unlike polystyrene, which can be synthesized in polar solvent and thus has a wider choice of difunctional initiators such as alkali metal naphthalenide anion initiators [15,102,103], anionic polymerization of H-shaped PBD with high 1,4-addition has only limited coverage in the literature due to the difficulties in preparing a difunctional initiator that is soluble in hydrocarbon and still maintains equal activity at both reactive sites.

Two major methods for preparing an difunctional initiator for use in hydrocarbon solvents are described in the literature [39,104,105]. The first method involves an addition reaction of a mixture of *sec*-butyllithium/triethylamine in 1:1 mole ratio to 1,3-diisopropenylbenzene in 2:1 molar ratio in benzene at -10°C as shown in Fig. 3.1 [39,106]. Both reactants are commercially available from Aldrich, and the reaction is a one-step process with vivid color change as an indicator to the quality of the initiator. However, it is reported that even when the difunctional initiator is completely soluble in hydrocarbon solvent, it behaves as if it were a monofunctional initiator for butadiene [106].

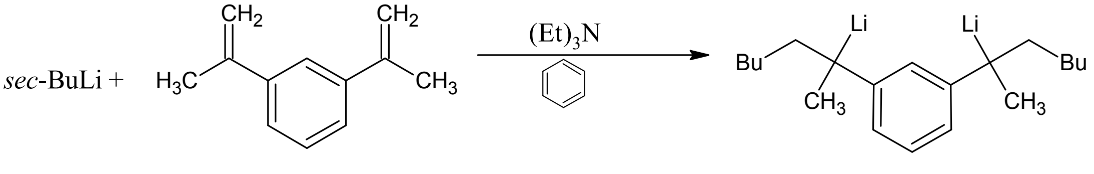

Figure 3.1 Schematic of method used to prepare difunctional initiator by Yu *et al.* [106]

A second method to obtain a difunctional initiator suitable for preparing polybutadiene with high 1,4 addition is a complicated process [104,105]. 1,2-diphenyl ethane first reacts with benzoyl chloride and after further reactions, filtration and crystallization, 1,2-Bis-(4-(1-phenylethenyl)phenyl) ethane is produced. This is reacted with *sec*-BuLi in a benzene/n-heptane solution under high vacuum to generate the difunctional initiator as shown in Fig. 3.2.

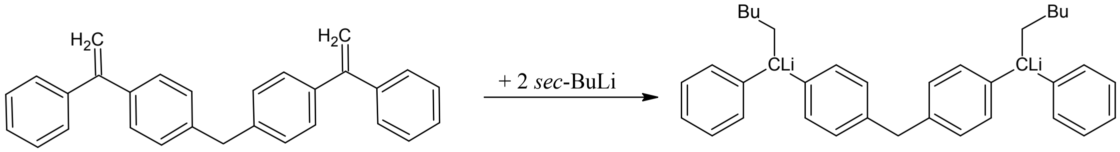

Figure 3.2 Schematic of method used to prepare difunctional initiator by Ikker *et al*. [105]

3.2.2 Earlier attempts to anionically polymerize PBD with high 1,4 addition

Using the difunctional initiator prepared by the second method and a trifunctional coupling agent, Perny *et al*. [29] prepared one H-shaped PBD with high 1,4 addition by the synthesis scheme shown in Fig. 3.3. First, a living chain was prepared with *sec*-BuLi and monomer. Meanwhile, a living difunctional crossbar was prepared by reacting the difunctional initiator with monomer in another reactor. Then the living crossbar was functionalized with excess methyltrichlorosilane at the two ends. Finally, the living linear chain was coupled with the functionalized crossbar to form the H polymer.

The polymer synthesized in this way was reported to be a mixture of various structures as shown in Fig. 3.4. The structure was determined by temperature gradient interaction chromatography (TGIC) [107], which is thought to have a higher resolution than size exclusion chromatography (SEC) for branched polymers [108,109]. TGIC analysis revealed that the sample contained 70% H shaped polymer, 25% low molecular weight byproduct and 5% high molecular weight byproduct. Formation of the low molecular weight byproducts was mainly due to incomplete coupling between the crossbar and the living arms. However, the formation of high molecular weight byproducts composed of two crossbars and up to five arms was due to reaction between two partially coupled intermediates, especially when the concentration of living arms is low while the concentration of partially coupled intermediate is high. Although the heterogeneous mixture of polymers could be separated by fractionation (a separation process that depends on the polymer-solvent interactions), and the molecular weight distribution could be made narrower, it was still challenging to separate high molecular weight by-products from the H polymers.

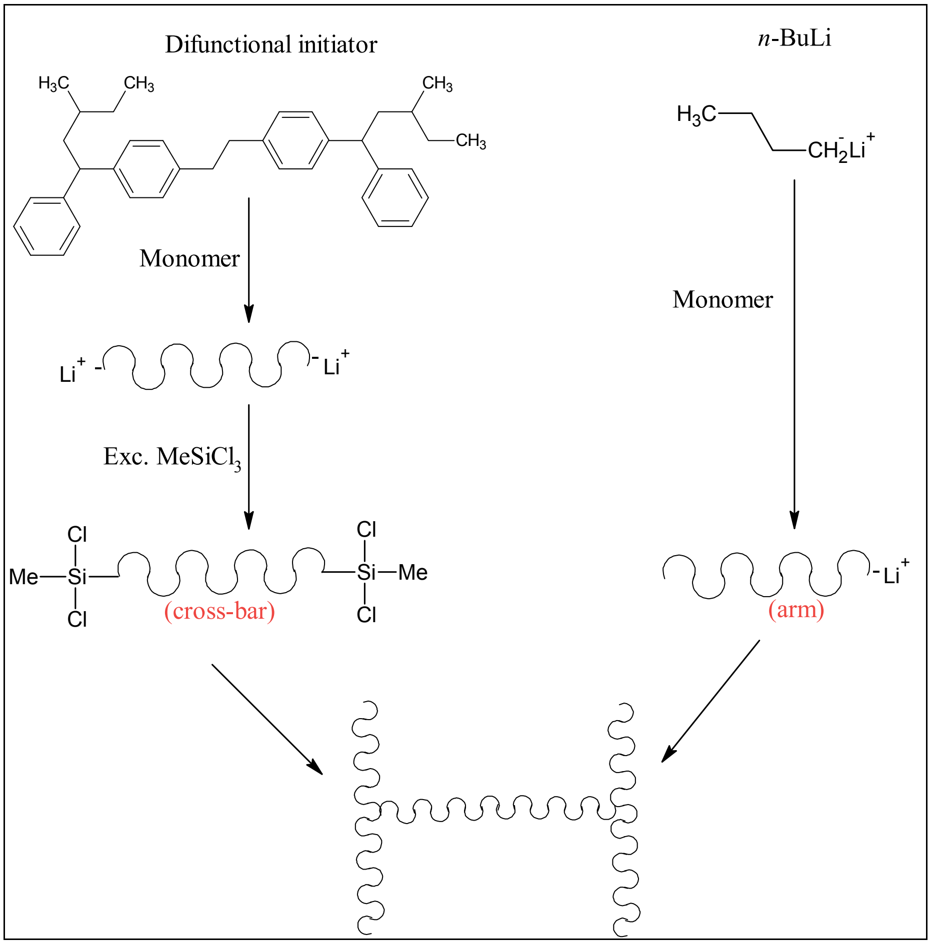

Figure 3.3 Schematic of method used to prepare H-shaped PBD by Perny *et al.* [104]

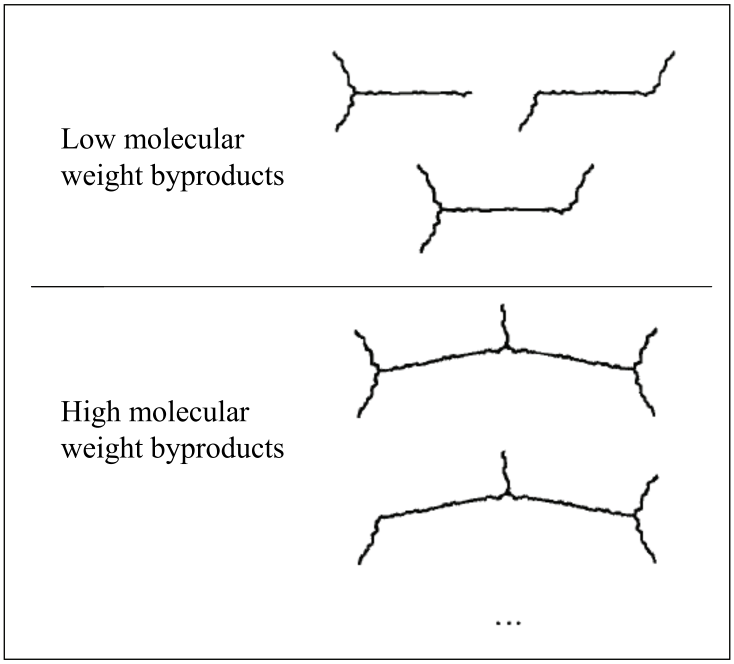

Figure 3.4 Possible byproduct structures in the H-shaped polymer prepared by Perny *et al.* [104]

3.2.3 Novel method of anionic polymerization of PBD with high 1,4 addition

High molecular weight byproducts obtained from the above method can significantly affect rheological properties. To minimize their formation, a novel strategy in preparing H-PBD by anionic polymerization was developed by Prof. Jimmy Mays [110]. It is based on the idea that coupling of two side arms with trichloromethylsilane prior to any reaction with the crossbar would significantly reduce the amount of these byproducts [102]. The method requires the use of high-vacuum and ampulization techniques [89]. Five H-shaped PBDs were prepared by researchers in Prof. Mays' research group. Dilute solution properties, such as radius of gyration and intrinsic viscosity of the resulting H-PBDs, can be found in their article [110]. To thoroughly understand this synthesis route, I was given the opportunity to work closely with the researchers at the University for one month. In general, the synthesis of model H-shaped PBDs involves a difunctional DPE-based coupling agent 4-(dichloromethaylsilyl)diphenylethylene (DCMSDPE), *sec*-BuLi and benzene. Details of the synthesis procedures are divided into five main steps.

Step 1: Preparing the DPE derivative as coupling agent

The difunctional DPE derivative (DCMSDPE) was prepared by a series of reactions using high-vacuum techniques and appropriate apparati. It was prepared from the Grignard reagent of 4-bromodiphenylethylene and trichloromethylsilane (99%, Aldrich), where 4-bromodiphenylethylene was obtained by the Wittig reaction of 4-bromobenzophenone (98%, Aldrich) with methyltriphenylphosphonium iodide (97%, Aldrich) in the present of *n*-BuLi [111,112]; the general reaction route is shown below:

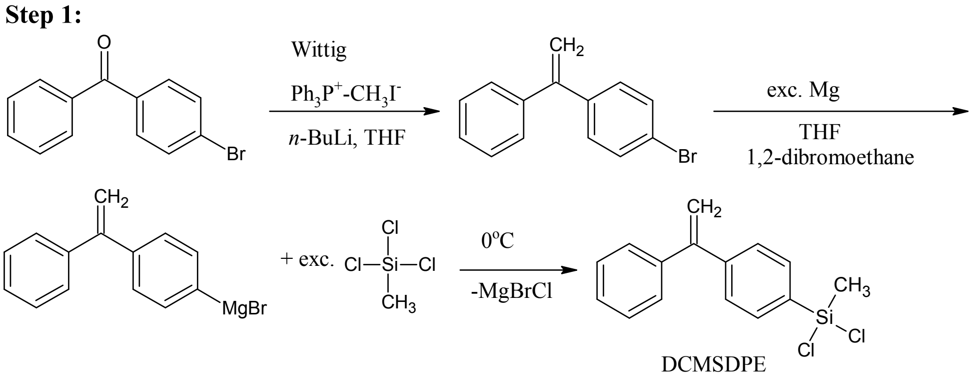

Figure 3.5 General reactions for the synthesis of 4-(Dichloromethylsilyl)diphenylethylene [111]

Step 2: Preparing the living arms

The living PBD-Li arms were made by polymerization of *sec*-BuLi and butadiene in the presence of benzene at room temperature for 24 hours as shown in Fig. 3.6. A small amount of the living arm solution was separated for characterization, while the rest was collected in a pre-calibrated ampoule equipped with break seals for the subsequent coupling reaction.

Step 3: Coupling of two living arms prior to reaction of crossbar

The living PBD-Li arms were added in a drop-wise manner to the DPE derivative (DCMS-DPE) in benzene under vigorous stirring by means of special glassware (Fig. 3.7). The slow addition was carried out over a period of 36 hours, and the coupling reaction was tracked by withdrawing an aliquot for SEC characterization from time to time. The coupling reaction has carried to completion when about two equivalent parts of living PBD-Li relative to DCMS-DPE were added. A doubling of the molecular weight of living arms and a narrow molecular weight distribution were observed in the SEC elution profile.

Step 4: Preparing half H-shaped molecules

After complete coupling of the two side arms, the double bond in DCMS-DPE was activated by *sec*-BuLi. The solution color immediately changed from yellow to deep red, indicating the reactivity of the double bond. The solution was then stirred for 48 hours at room temperature to ensure complete activation. Then freshly purified butadiene was added to produce half of the crossbar length to form an asymmetric three arm star (*i.e.* a half H).

Step 5: Coupling of two half H-shaped molecules

Dichlorodimethylsilane (99%, Aldrich), a difunctional coupling agent, was then added to terminate the reaction by connecting two of the half H molecules to produce one H-shaped molecule. Again, the coupling reaction was tracked by SEC from time to time. The solution was stirred for 3 weeks at room temperature to ensure complete termination.

To precipitate the final product, the solution was poured into a large excess of methanol with anti-oxidant BHT dissolved in it. Fractionation was performed with toluene/methanol as the solvent/non-solvent pair. The non-solvent was added to a polymer solution (0.5-2% w/v) to first precipitate species with relative higher molecular weight. The process was repeated until optimal results were obtained. The sample was then vacuum dried to a constant weight and stored in an amber glass container for further testing.

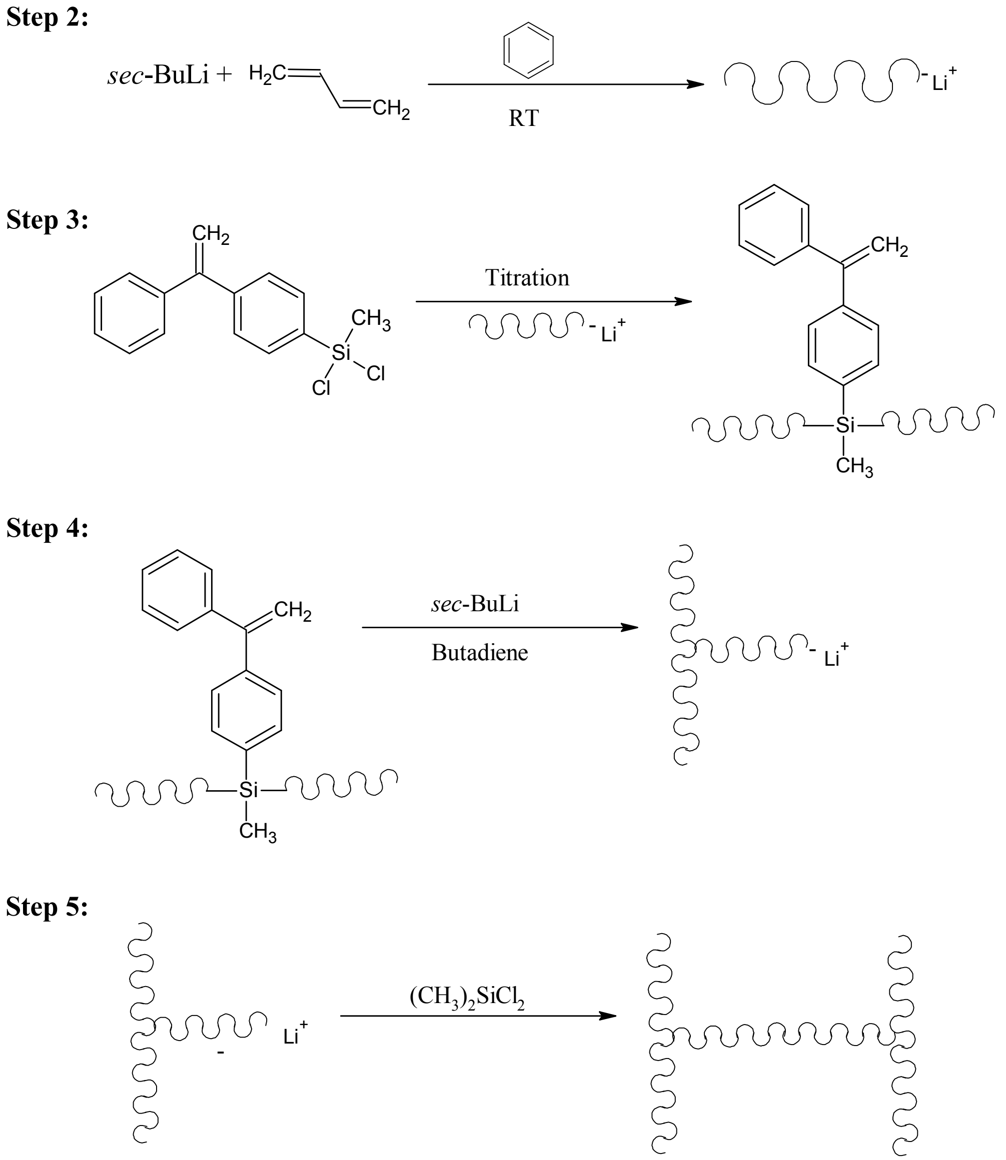

Figure 3.6 General reactions for the synthesis of H-shaped PBD [110]

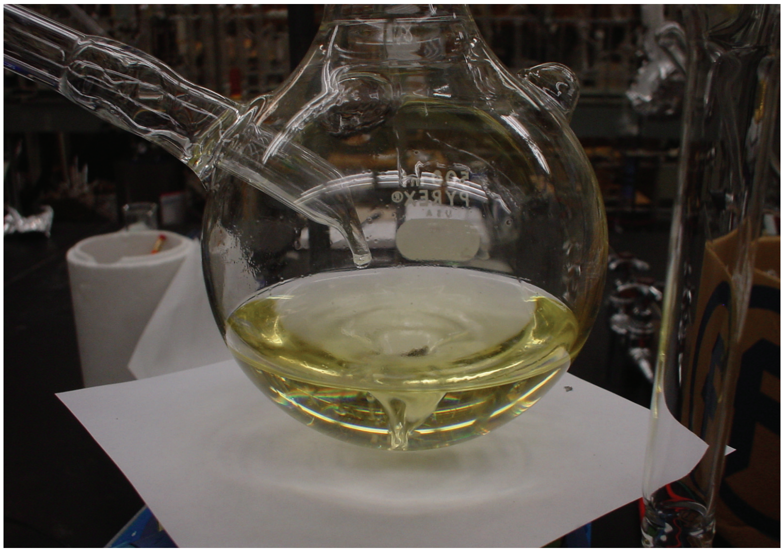

Figure 3.7 Special glassware used for the drop-wise addition of living arms to DCMSDPE

Additional experimental details are described in reference [110], and some major differences between the procedures described above and those used at McGill University (described in sections 2.4 to 2.6) are discussed below. First, the vacuum line used was a floor-to-ceiling glassware setup mounted on a metal rack as shown in Fig. 3.8. This consisted of a high-vacuum mechanical pump, a silicon oil diffusion pump, a cold trap, and a dual-bank manifold equipped with a Teflon-coated stopcock. This setup could be connected to an inert gas cylinder, a pair of oil bubblers, and a drying tower. Reagent handling such as purification, distillation, dilution and ampoulization were all done in custom-made glassware. The custom-made glassware for the entire polymerization process was made by the researcher. Newly blown components were baked overnight at 500^{o}C to remove any residual stresses. Ampoules (Fig. 3.9) containing the initiator and the monomer were then attached to the apparatus, and usually a purge section containing a side arm for injecting the purifying agent *e.g.* *n*-BuLi was attached to the setup as shown in Fig. 3.11(a). Purified solvent was docked to the vacuum line and distilled to the purge section by the opening and closing of various valves in the vacuum line. Then the whole setup was flame cut and detached from the vacuum line as shown in Fig. 3.11(b). Various ampoules were then broken to release the initiator and monomer into the reactor to start the polymerization reaction. It was extremely important that the entire polymerization process be carried in an impurities-free, closed system.

Figure 3.8 The vacuum line in Prof. Mays' laboratory

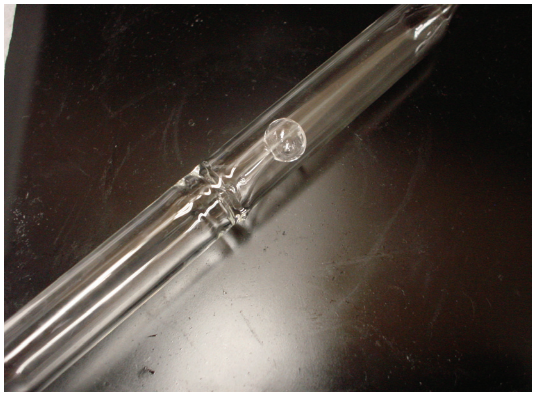

Figure 3.9 Break-seal ampoule

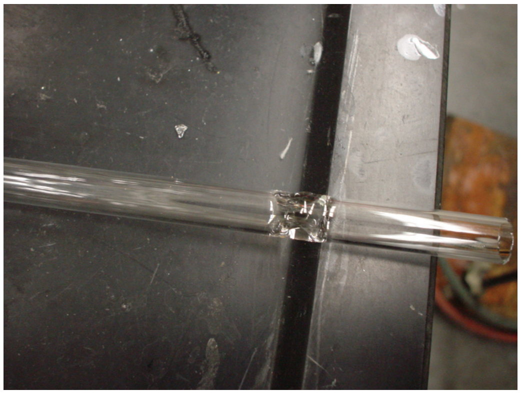

Figure 3.10 Constriction to facilitate removal of intermediate species

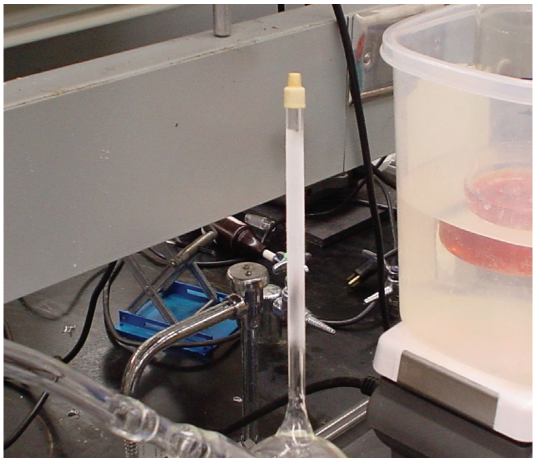

Figure 3.11(a) Side arm for purifying agent injection

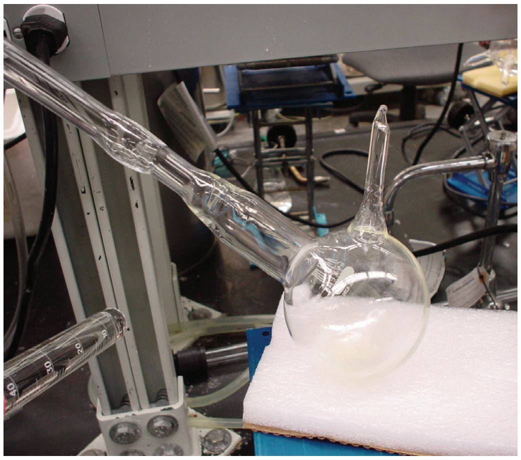

Figure 3.11(b) Side arm is flame cut after purifying agent injection.

Second, reagent purification and handling were done under high vacuum, all in *n*-BuLi-washed and benzene-rinsed reactors equipped with break-seals (Fig. 3.9) for reagent additions and constrictions (Fig. 3.10) for removal of intermediate species. Distillation of chemicals was performed without heating, except for very high boiling point chemicals such as DCMS-DPE. The destination flask was kept under high vacuum and cooled by a liquid nitrogen bath, while the source flask was submerged in a tape water bath. Opening and closing the appropriate valves in the vacuum line enabled the volatile solvent to be transferred to the destination flask for further dilution (Fig. 3.12) and ampulization if needed.

Lastly, *sec*-BuLi was prepared by reaction between lithium and butyl-chloride. It was then diluted with hexane and ampoulized using the dilution apparatus shown in Fig. 3.13. A colorless solution indicates that the initiator is free of impurities, while the solution we bought from Aldrich was slightly yellow in color and became turbid after the bottle seal had been perforated a few times.

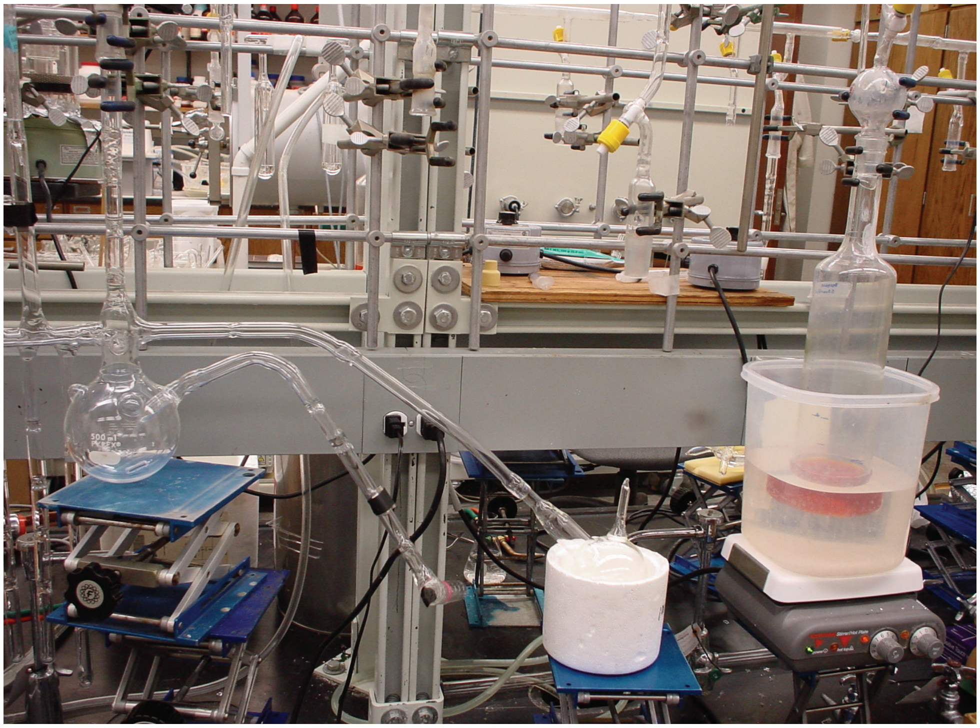

Figure 3.12 Distillation of benzene to a purge section of a reactor

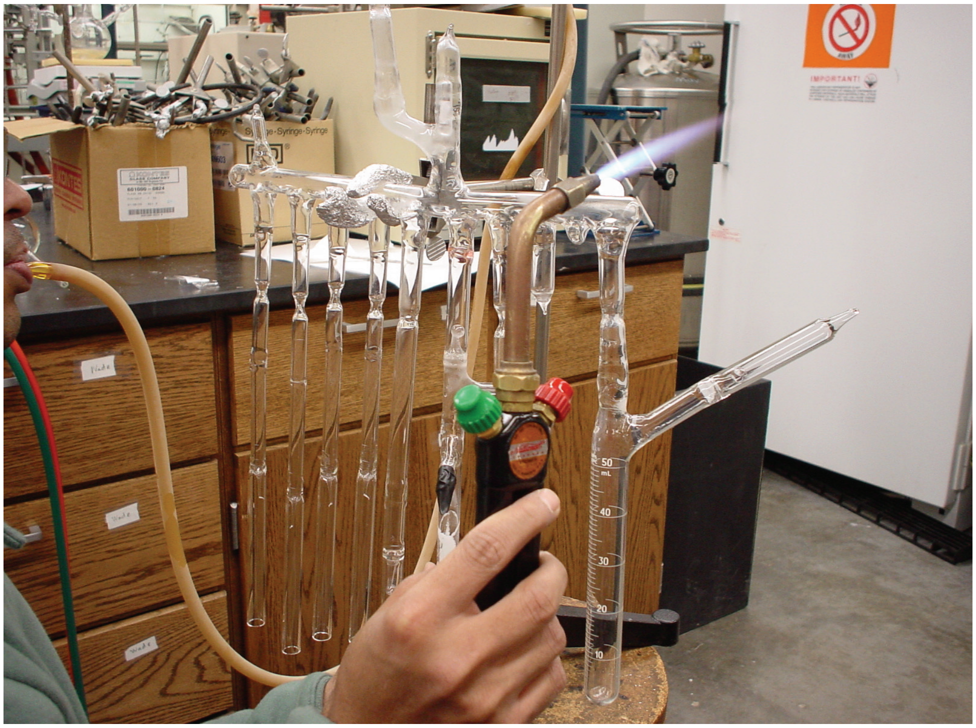

Figure 3.13 Typical dilution apparatus used for anionic polymerization

3.3 Preparation of binary blend

A binary blend of H-PBDs composed of HA12B40 and HA30B40 in 1:1 mole ratio was prepared by solution blending at McGill University. For a rubberlike material, mechanical mixing is not suitable, especially since the quantity available was not enough to go through a mechanical mixer. Although it has been suggested to use a 16mm twin-screw extruder for mixing small quantities [113], materials are sheared at a high shear rate (110 s^{-1}), and there is a risk of shear heating. Also, manual mixing usually leads to under-mixing of the material. Although solution blending involves dissolution of polymers [114], which is a slow process that takes days or even weeks for particularly high molecular weight polymers, the process can be accelerated by agitation. After the addition of solvent, a swollen gel is produced due to the gradual diffusion of solvent into the polymer. This gel gradually disintegrates as more solvent enters the gel. Eventually the polymer molecules are surrounded by solvent molecules (solvation) and are carried into the solution. Detailed procedures for preparing the binary blend by solution blending are described below.

After weighing the appropriate amount of each polymer, a total of 2.5g of material was added to 250ml of tetrahydrofurane (THF) inside a fume hood at room temperature in a clean wide mouth glass bottle capped with a plastic cover. The outside of the glass bottle was wrapped with aluminum foil to protect the sample from light-induced cross linking. The mixture was stirred continuously by a glass-encapsulated, Teflon-coated stir bar at room temperature for 48 hours to produce a viscous and transparent solution. After that, the stir bar and plastic cover were removed, and the top of the glass bottle was loosely covered with an aluminum foil with small holes made by a syringe needle. The bottle was placed inside a fume hood for a week until a thin and transparent layer of polymer formed at the bottom of the container. It was then further dried in a vacuum oven equipped with a cold finger to remove any residual solvent. Once there was no detectable smell of the THF solvent, and sample reached a constant weight, the materials were stored in closed containers and keep refrigerated until use.

3.4 Molecular weight selection

The molecular weights of the H-PBD arms and backbones were selected based on three criteria: 1. Feasibility to be synthesized by anionic polymerization in a laboratory scale reactor. 2. Accessibility of terminal viscoelastic behavior using available rheometers. 3. High degree of entanglement of the arms and crossbar.

Anionic polymerization is carried out in solution, which has the advantage of better control of the exotherm during reaction than in bulk polymerization. However, the reaction temperature is limited by the boiling point of the solvent, which in turn restricts the rate of reaction. Moreover, since a completely inert solvent is not known, chain transfer to the solvent, which adds a restriction on the molar mass of the product, is possible. It is also important to note the viscosity of the system during polymerization, since the solution viscosity is proportional to the molecular weight of the growing chain, and increases with reaction time. In an extreme case of a very viscous system where stirring becomes difficult, the polymer chains will have limited mobility and thus take a long time to react at the active sites. This not only limits the reaction rate but also results in non-uniform products. Therefore, there is a maximum molecular weight that one can achieve, which depends on the choices of monomer, solvent and temperature. Based on the experience of synthesizing linear PBDs and information in the literature, a maximum molecular weight (M) of 200 kg/mol for PBD synthesized in hydrocarbon solvent at room temperature was set as a safe target for a laboratory scale reactor. In terms of degree of entanglement, as illustrated in Fig. 3.14, this molecular weight is equivalent to a degree of entanglement of 100. The degree of entanglement is defined as M/M_e where M and M_e are the molecular weight of the chain and the molecular weight between entanglements, respectively. By analogy with the theory of rubber elasticity, an entanglement is thought of as a topological restriction on the motion of one molecule imposed by neighboring molecules, although a precise definition has not been agreed upon.

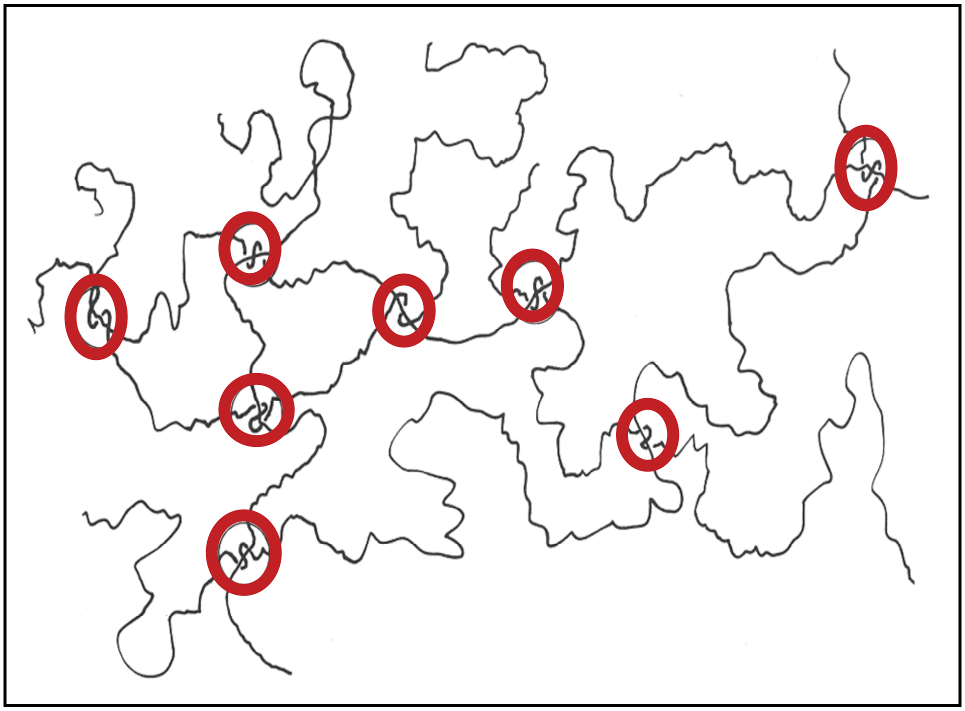

Figure 3.14 Schematic representation of entanglements, with the red circles indicating entanglements

As mentioned in Chapter 1, the zero shear viscosity is sensitive to molecular structure and can be obtained only when the polymer chains are fully relaxed, which happens in the terminal zone at a low frequency. Performing small amplitude oscillatory shear (SAOS) at very low frequencies is problematic, since either the torque may reach the lower limit of the transducer or the large shear strain may break the sample. In addition, to obtain a datum at a frequency as low as 10^{-4} rad/s requires about 17 hours for only one cycle, which yields minimum precision. Although performing the experiment at a higher temperature accelerates the relaxation process, PBD is susceptible to thermal degradation. While there are other methods to indirectly obtain information at a low frequency, there are always concerns about instrument precision and experimental time, the details of which will be covered in Chapter 4. Considering that the H-PBDs are precious samples, we want to avoid experimental temperatures above 25°C so that material can be reused. Therefore, a frequency range between 10^{-5} rad/s and 10^{-6} rad/s was taken to be the experimentally accessible range.

While high molecular weight polymers are more difficult to prepare and characterize than low molecular weight polymers, it is desirable that the molecular weights selected be comparable to those used in previous studies of H-shaped polymers [20-23,41,104,115-117]. A detailed summary of these studies is provided in Table 3.1, which includes information on polymer type, molecular weight and molecular weight distribution, rheological measurements, and modeling work.

Based on the above criteria, it was estimated that the H-shaped PBDs shown in Table 3.2 would be optimal for this project. In terms of degree of entanglement, the molecular weights selected cover the high ends of degree of entanglement of arms and crossbar used in other studies of H-shaped polymers as illustrated in Fig. 3.15. To verify that terminal behavior could be reached at frequencies above 10^{-6} rad/s, the original hierarchical molecular model [60] , Hierachical-2.0, was used to predict the rheological behavior of these polymers at 25°C, using the parameter values suggested by Park *et al.*[60] and assuming the samples to be monodisperse (details about the model are provided in Chapter 6). The predicted rheological behavior at 25 °C is shown in Fig. 3.16 for a set of samples with equal arm lengths and in Fig. 3.17 for a second set of samples with equal crossbar lengths. All the predictions suggested that terminal behavior would be observed well above a frequency of 10^{-5} rad/s.

Once the molecular weights were selected, the design of the binary blend was relatively straight forward. As one of the objectives was to study the effect of polydispersity on rheological behavior, and the dominant effect on rheology is contributed by the arms rather than the crossbars, two H-PBDs in 1:1 mole ratio with equal crossbar lengths but very different arm lengths were thought to be appropriate. As illustrated in Fig. 3.18, a preliminary model prediction for the binary blend showed behavior significantly different from those of the monodisperse components.

Table 3.1 Summary of literature studies of H-shaped polymers

Reference	**Material**	**Arms**		**Crossbar**		**H Polymer**		**Rheological measurement in LVE region**		**Modeling**
		Degree of entanglement (M/M_e)	M_w/M_n	Degree of entanglement (M/Me)	M_w/M_n	Mn (kg/mol)	M_w/M_n	Experimental temperature range (^oC)	Frequency covered (rad/s)	
Roovers 1981 [102]	Polystyrene	1.2	--	1.2	--	--	--	140 to 250	10^{-2} to 10^{2}	No
		2.6	--	2.6	--	--	--			
		5.4	--	5.4	--	--	--			
		7.5	--	7.5	--	--	--			
		11.6	--	11.6	--	--	--			
		18.8	--	18.8	--	--	--			
McLeish 1988 [22]	Polystyrene	11.6	--	11.6	--	--	--	140 to 250	10^{-2} to 10^{2}	Yes
Hakiki 1996 [23]	Polyisoprene	3.6	--	54.8	--	334	1.11	No		No
		8.0	--	32.8	--	324	1.06			
		11.7	--	43.0	--	460	--			
		12.6	--	39.6	--	460	1.33			
		27.0	--	50.6	--	--	--			
McLeish 1999[118]	Polyisoprene	4.0	--	30.0	--	--	--	No		Yes
		6.0	--	30.0	--	--	--			
		8.0	--	30.0	--	--	--			
		6.0	--	20.0	--	--	--			
		6.0	--	25.0	--	--	--			
		4.0	1.01	22.2	1.13	198	1.11	-30 to 150	10^{-6} to 10^{5}	Yes
		8.0	1.05	32.8	1.3	324	1.06			
		12.6	--	39.6	--	460	1.33			
		10.5	--	22.2	--	310	1.08			
Daniels 2001[115]	Polyisoprene	4.0	--	22.2	--	198	1.11	-70 to 100	10^{-3} to 10^{5}	Yes
		12.6	--	39.6	--	460	1.33		10^{-6} to 10^{6}	
Heinrich 2002 [116]	Polyisoprene	10.5	--	22.2	--	--	--	-30 to 90	10^{-5} to 10^{5}	Yes
Perny 2001 [104]	Polybutadiene	12.5	1.02	28.6	1.04	161	1.04	No		No
Heinrich 2004[41] and 2002 [117]	Polybutadiene	12.5	1.02	28.6	1.1	--	--	-35 to 100	10^{-5} to 10^{6}	Yes

Table 3.2 Molecular weights of H-PBDs selected for use in this project

Sample code	M_{arm} **(kg/mol)**	**Degree of entanglement of arms** M_{arm}/M_e	$M_{crossbar}$ **(kg/mol)**	**Degree of entanglement of cross bars** $M_{crossbar}/M_e$	**Total molecular weight,** M **(kg/mol)**
HA12B40	12	6	40	20	88
HA30B40	30	15	40	20	160
HA40B40	40	20	40	20	200
HA12B60	12	6	60	30	108
HA12B100	12	6	100	50	148
HA1230B40	HA12B40 and HA30B40 in 1:1 mole ratio				

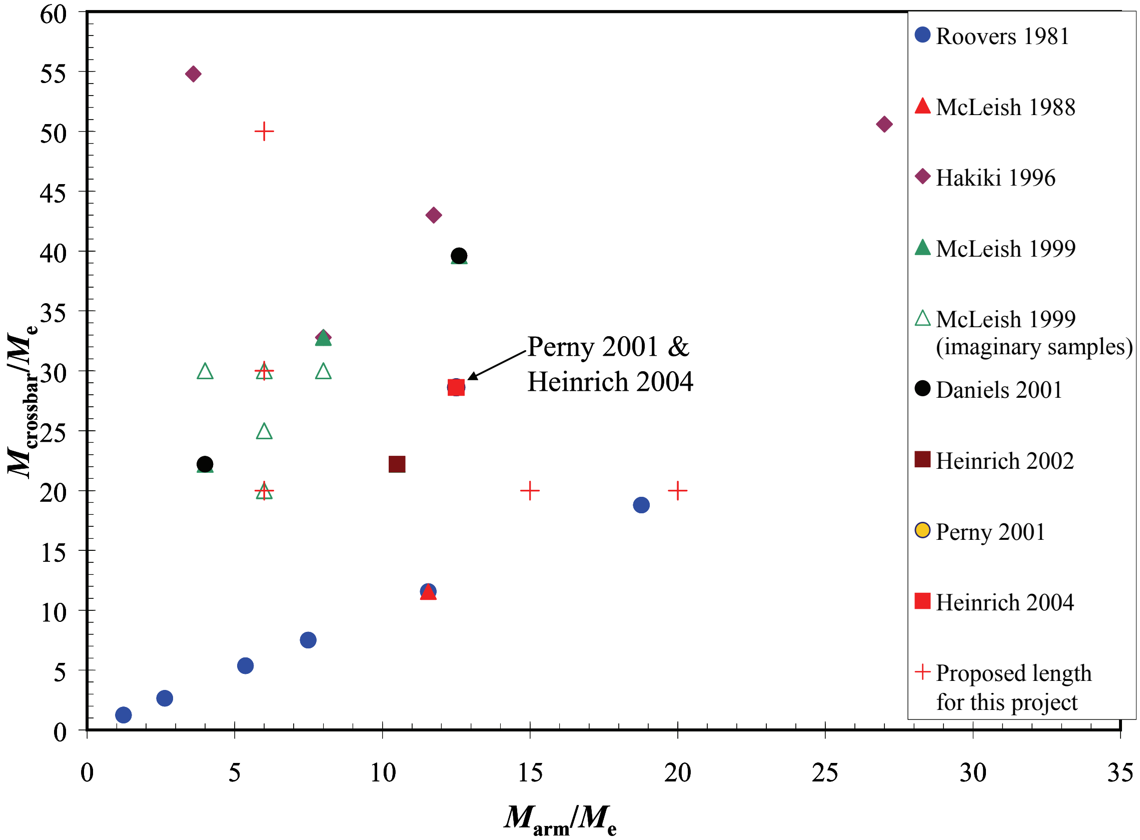

Figure 3.15 Comparison of selected molecular weights with those used in previous studies in terms of degree of entanglement (M/M_e)

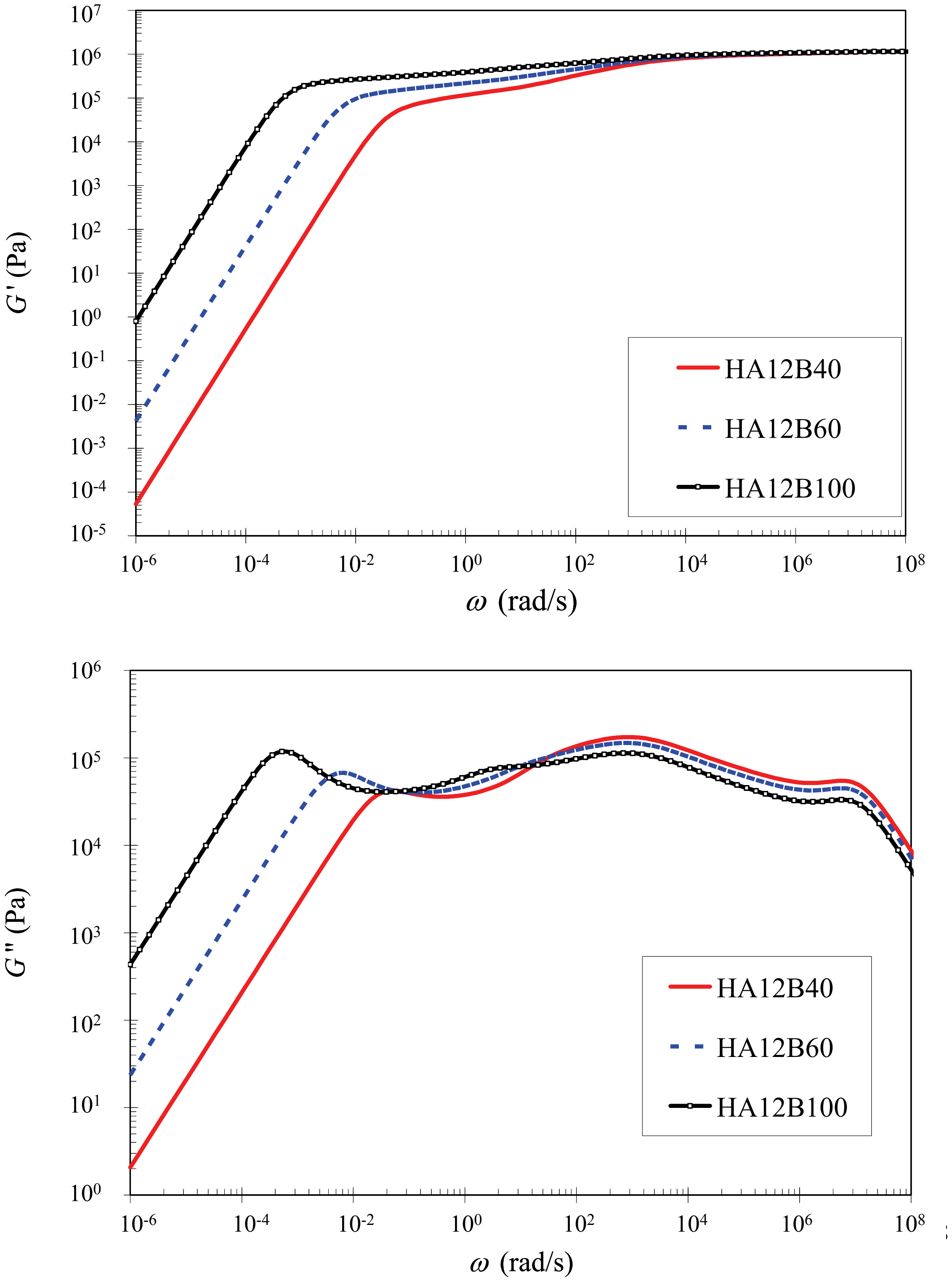

Figure 3.16 Storage and loss moduli G' and G'' as predicted using the original hierarchical model for H-PBDs with equal arms lengths at 25°C

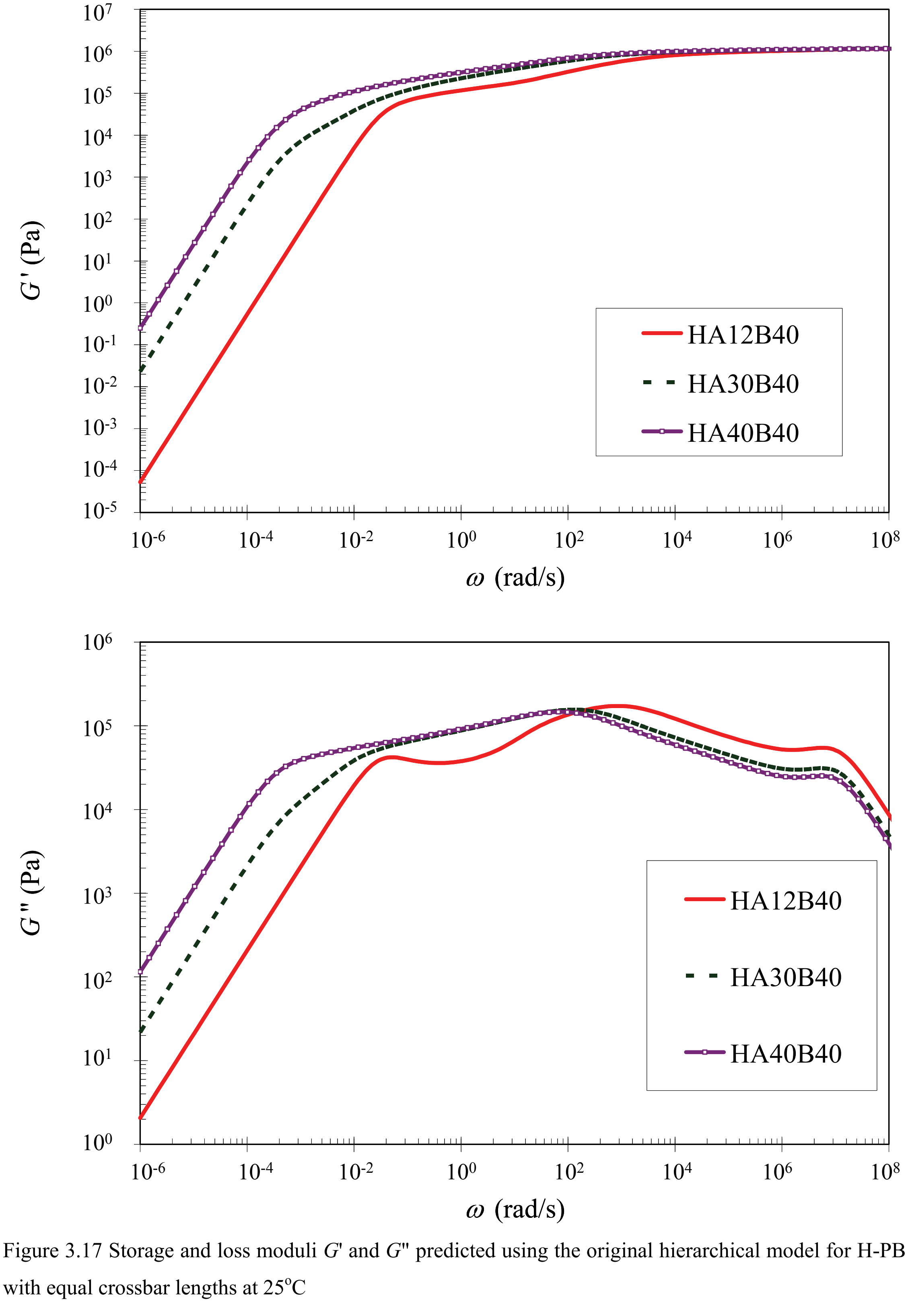

Figure 3.17 Storage and loss moduli *G*' and *G*'' predicted using the original hierarchical model for H-PBDs with equal crossbar lengths at 25°C

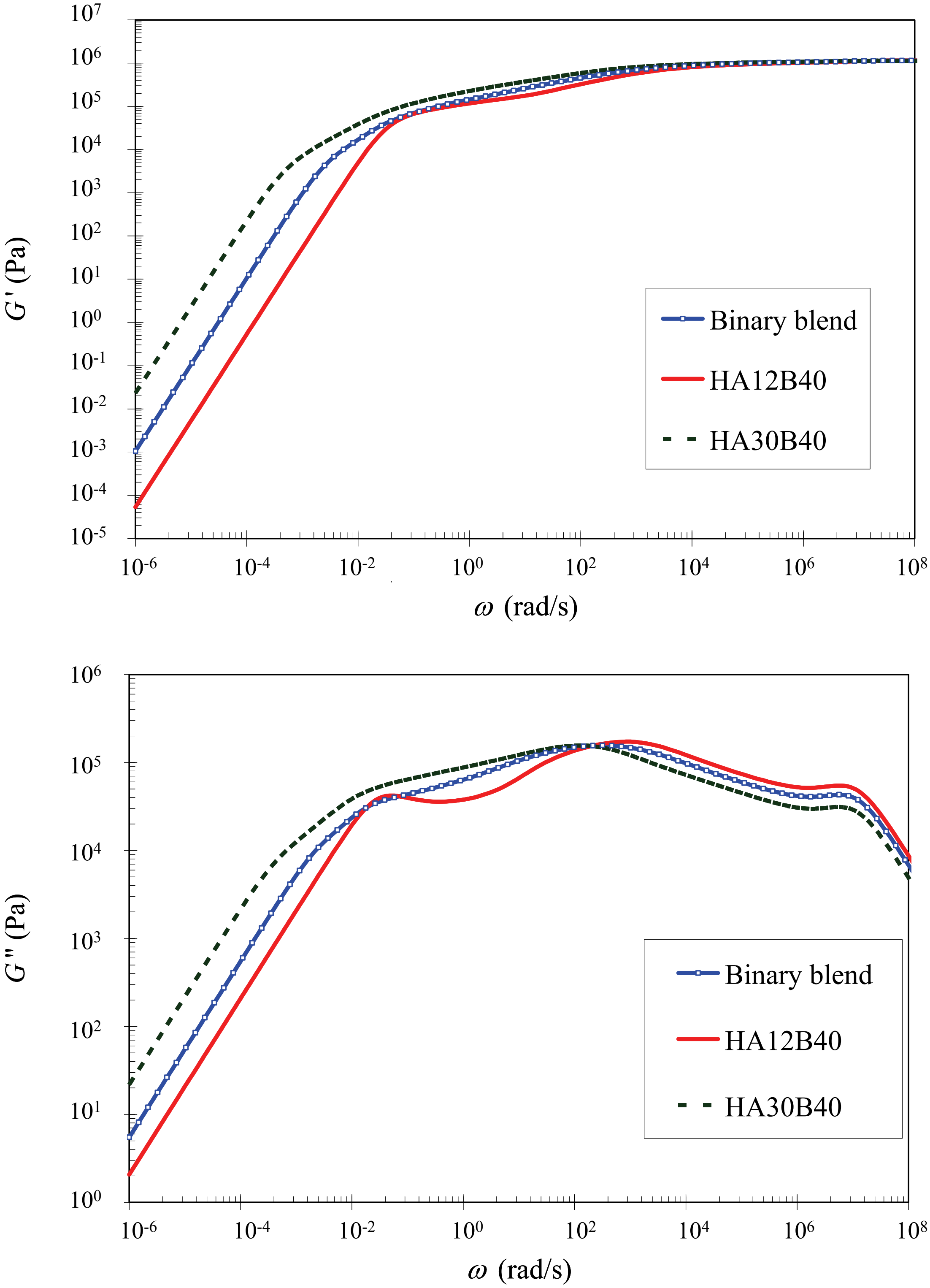

Figure 3.18 Storage and loss moduli *G*' and *G*" predicted by the original hierarchical model for a binary blend and its components at 25°C

3.5 Characterization

3.5.1 Molecular weight

Molecular weights of the linear PBDs were determined by two different methods. The first method was used by the Firestone Tire and Rubber Company who used an SEC (Waters^{TM} Model 150-C) equipped with a refractive index detector (SEC/RI), operated at 40°C with THF as the mobile phase. Molecular weights based on polystyrene standards were related to polybutadiene by Mark-Houwink equation. The second method was performed at the University of Tennessee by SEC with Two-Angle Laser Light Scattering (SEC/TALLS). The system was also connected to a refractive index detector and a Viscotek differential viscometer, which were used to determine the precursors and final products. The columns used are Waters Ultrastyragel HR series, HR-2, HR-4, HR-5E, and HR-6E, with pore sizes 10^3, 10^4 and 10^5 Å. The measurement was done at 40 °C with THF as the mobile phase at a flow rate of 1.0mL/min. Results obtained from these two methods are shown in Table 3.3.

Table 3.3 Molecular weight characterization of linear PBDs

Sample	**Molecular weights (kg/mol)**				
	SEC/RI		SEC/TALLS		
	M_n	M_w/M_n	M_n	Composition (wt%)	M_w/M_n
PBD2	75	1.04	130	10	1.13
			92	90	1.02
PBD3	184	1.06	284	10	1.03
			260	40	1.03
			245	50	1.03

Molecular weights of the H-PBDs were determined by various methods, and the results are summarized in Tables 3.4 and 3.5. The first characterization was performed at the University of Tennessee using SEC/TALLS using the apparatus described above. Since the molecular weight characterization was performed in parallel with the synthesis, it is the only one that provided information on precursors at various stages of polymerization. In other words, it contains molecular weight information on arms and half-Hs. Complete elution curves at various stages of polymerizations of each sample can be found in

Appendix B. Generally, the SEC/TALLS elution profiles of precursors and final products as shown in Fig. 3.19 had single peaks and narrow distributions.

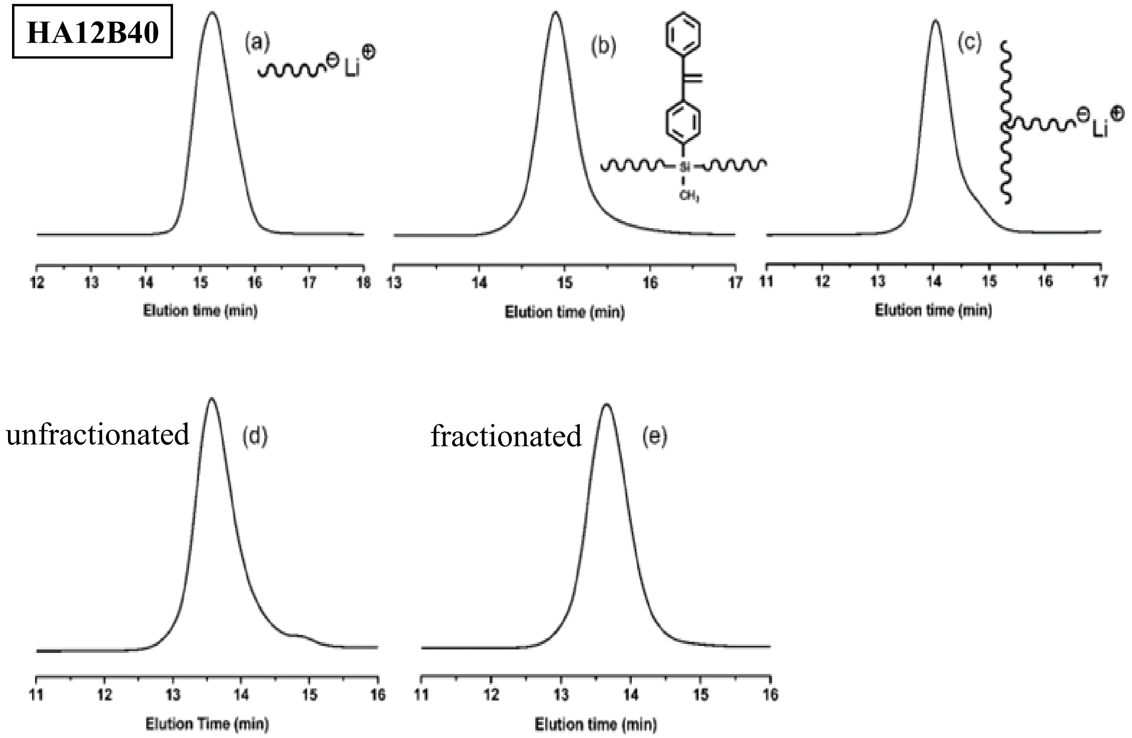

Figure 3.19 SEC/TALLS (LS response at 15°) elution profiles of precursors and final product of HA12B40: (a) living PBD arm, (b) coupled PBD arms, (c) living half-H, (d) unfractionated product, and (e) fractionated product, as measured at the University of Tennessee

The second molecular weight characterization was performed by Dow Chemical on the fractionated product, using conventional SEC/RI with Polymer Labs Polypore column (5μm). Measurement was done at 40°C with THF as the mobile phase at a flow rate of 1.0ml/min and using polybutadienes as standards. The SEC profiles obtained by Dow Chemical had double peaks for most of the samples, except HA12B40 and HA12B60, as shown in Fig. 3.20. The molecular weights of the two peaks were in a ratio of about 1:2, suggesting the presence of half -Hs which are equivalent to asymmetric three-arm stars. The weight fraction calculated from the area under the peaks after curve fitting the RI signal with Gaussian distribution is also presented in Table 3.4.

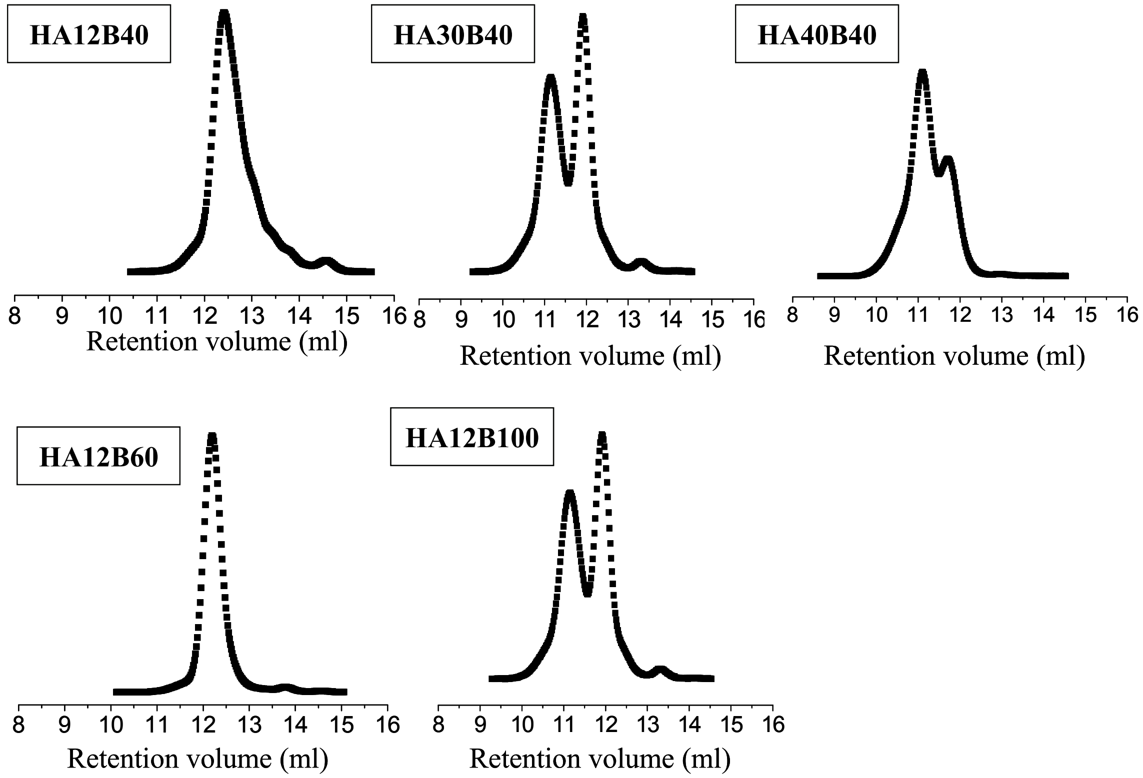

Figure 3.20 SEC/RI elution profiles on fractionated polymers, as measured by Dow Chemical

The third molecular weight characterization was performed on the fractionated products at Pohang University of Science and Technology. The characterization was performed at 40°C with THF as the mobile phase at a flow rate of 0.8ml/min. The SEC was equipped with a Wyatt MiniDawn light scattering detector (LS), a Younglin UV detector (UV) and a Shodex RI-101 refractive index detector (RI). A PLgel mixed-C 2EA column (5μm particle size) was used, with THF as the mobile phase in a 0.8mL/min flow rate. The elution curves from the SEC/Triple detectors are shown in Fig. 3.21.

The distributions measured at these three institutions were very different from each other. The SEC/TALLS data from the University of Tennessee suggested that all the fractionated samples were nearly monodisperse, H-shaped polymers, while SEC/RI results obtained from Dow Chemical suggested that most of the fractionated samples were mixtures of H-shaped and asymmetric three arm star (half-H) molecules. Although the molecular weights of fractionated HA30B40 and HA40B40 found by SEC/Triple detectors were comparable to those found by SEC/TALLS, most samples had narrower molecular weight distributions in SEC/TALLS curves, as shown in Fig. 3.21.

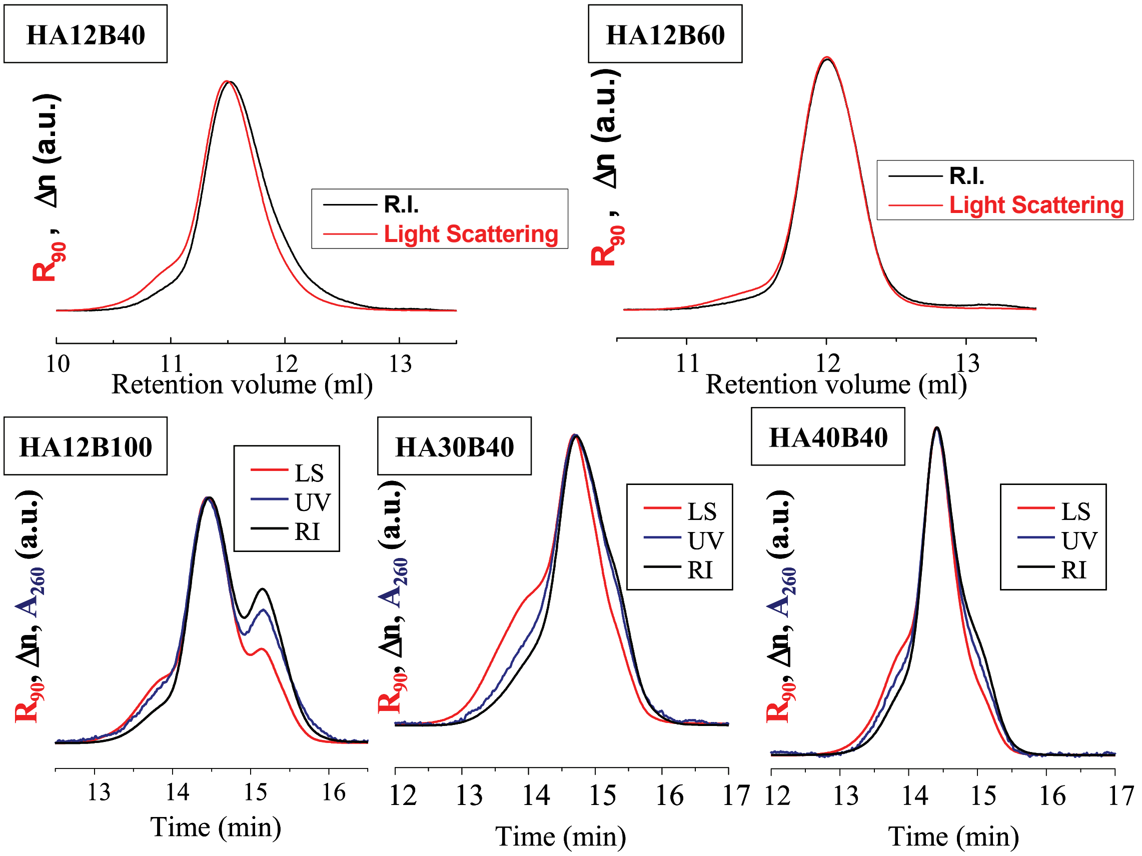

Figure 3.21 SEC/Triple detector elution profiles on fractionated polymers, as measured at Pohang University of Science and Technology

Table 3.4 Summary of molecular weights characterization by SEC from different institutions

Sample	Molecular weights (kg/mol)										
	SEC/TALLS (University of Tennessee)						SEC/RI (Dow Chemical Co.)			SEC/Triple detectors (Pohang University of Science and Technology)	
	M_n (arm)	M_w/M_n (arm)	M_n (half H)	M_w/M_n (half H)	M_n (fractionated product)	M_w/M_n (fractionated product)	M_n (fractionated product)	Composition (wt%)	M_w/M_n (fractionated product)	M_n (fractionated product)	M_w/M_n (fractionated product)
HA12B40	10.6	1.01	41	1.11	82.3	1.03	70.8	100	1.25	64.2	1.12
HA30B40	29.6	1.01	80.2	1.05	161	1.06	93.3 174	8 92	1.32	164	N/A
HA40B40	41.6	1.01	106	1.06	212	1.05	109.6 218.8	23 77	1.22	216	N/A
HA12B60	11.6	1.01	49.5	1.19	98.5	1.03	87.1	100	1.11	85.4	1.04
HA12B100	15.3	1.03	82.4	1.07	158	1.04	81.3 170	47 53	1.28	114 196	N/A

The final method used to characterize the structures of the H-PBDs was TGIC [107,119], which was performed at Pohang University of Science and Technology. Unlike SEC, TGIC is an interaction chromatographic technique in which the separation is driven by enthalpic interactions between the sample and the stationary phase. The strength of separation is controlled by varying the column temperature, and the molecular weight resolution is little affected by the chain architecture. Therefore TGIC is believed to be more sensitive to chemical structure [119-121] and to have a higher resolution than SEC [104,108,122,123]. The TGIC experiments were carried out using a standard HPLC system equipped with a C_{18} bonded silica column (Alltech, Nucleosil, 300 $\overset{\circ}{A}$ pore, 150 ×4.6mm, 5 μm particle size for samples HA12B100, HA30B40 and HA40B40, 500 $\overset{\circ}{A}$ pore, 150 ×4.6mm, 7 μm particle size for samples HA12B40 and HA12B60), with a mobile phase of 1,4-dioxane at a flow rate of 0.5mL/min. The system was equipped with a light scattering detector (Wyatt miniDAWN) and a refractive index detector (Shodex RI-101). The temperature profiles of column as well as the chromatograms are shown in Fig. 3.22. The molecular weights corresponding to each peak, *i.e.* M_p are shown in Table 3.5.

Chromatograms obtained by TGIC suggested that even after fractionation samples were mixtures of several components, mainly in low molecular weight by products. However, TGIC results do not reveal branching structures.

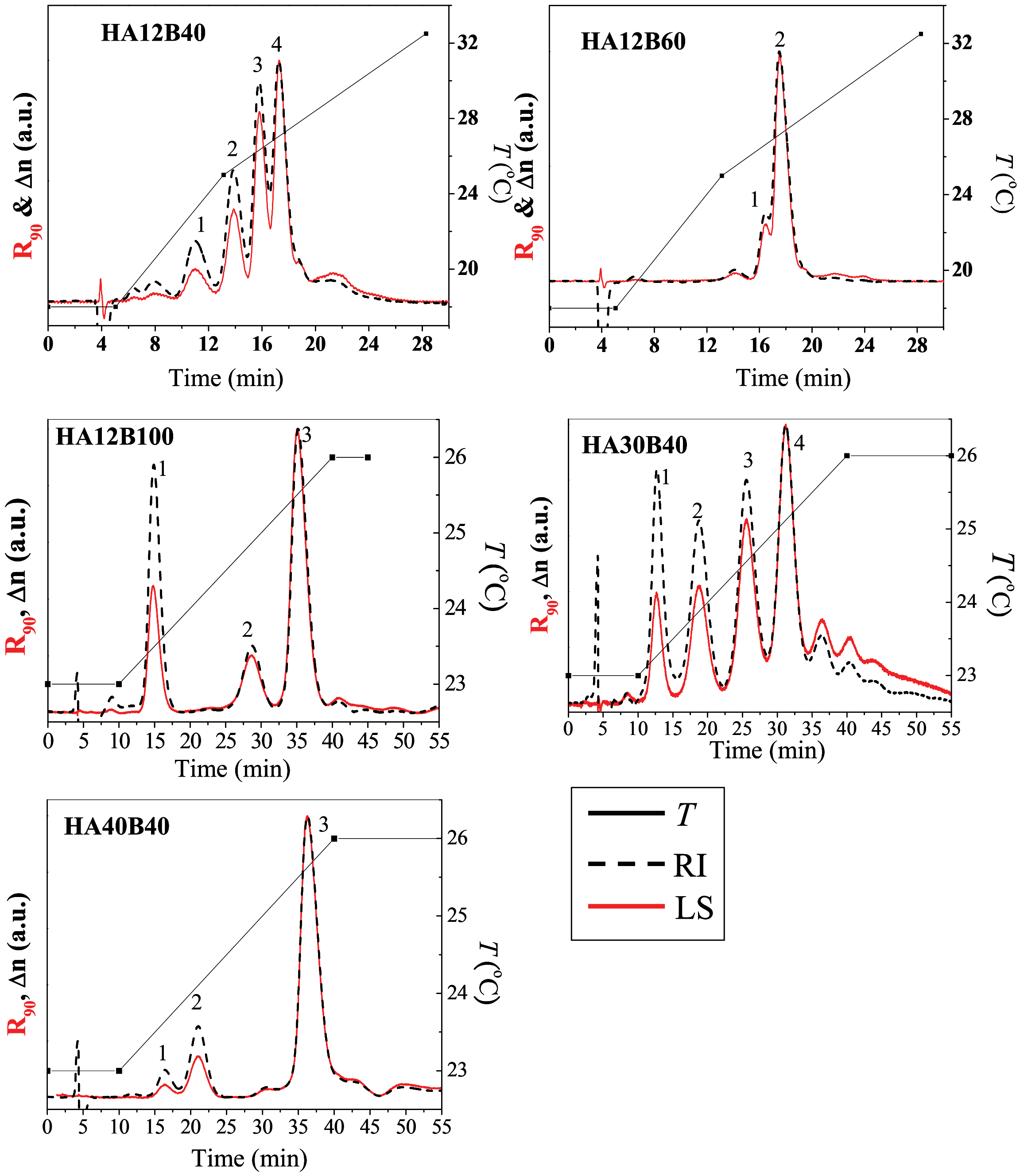

Figure 3.22 Chromatograms from TGIC analysis of H-shaped PBDs

Table 3.5 Molecular weight characterizations by TGIC from Pohang University of Science and Technology

Sample	Molecular weights, M_p (kg/mol)					
	Peak 1	Peak 2	Peak 3	Peak 4	Peak 5	Peak 6
HA12B40	45	57	70	81	N/A	N/A
HA30B40	65	117	131	164	336	N/A
HA40B40	110	121	205	343	N/A	N/A
HA12B60	80	99	N/A	N/A	N/A	N/A
HA12B100	103	170	198	N/A	N/A	N/A

3.5.2 Microstructure

To elucidate the microstructures of the PBDs, ^{1}H nuclear magnetic resonance (NMR) is a useful technique. As the sensitivity and resolution of NMR spectra increase with magnetic field strength, the characteristic peaks for *cis* and *tran*s configurations can be resolved by use of a 500 MHz magnetic field strength. NMR studies were carried out on all samples on a 500 MHz Varian unity spectrometer at room temperature. The spectrometer was operated with software VNMR 6.1C on a SUN Ultra 5 workstation. 10mg of sample were dissolved in 0.7ml of deuterated chloroform (Cambridge Isotope Laboratories Inc.) in 5mm 508 Up NMR tubes. The samples were injected into the probe, shimmed and scanned 32 times. Characteristic peaks for the *cis*/*trans* 1,4 and 1,2 vinyl configurations were indentified [124,125] and the corresponding areas under the peaks were calculated by the operating software. Microstructure characteristics of linear PBDs and H-PBDs are shown in Table 3.6. NMR spectra of each sample and the area under each characteristic peak can be found in Appendix C.

Table 3.6 Microstructure characteristics of linear and H-shaped PBDs

Microstructure (%)	**Samples**						
	PBD2	**PBD3**	**HA12B40**	**HA30B40**	**HA40B40**	**HA12B60**	**HA12B100**
cis 1,4	41	43	42	41	42	44	43
trans 1,4	49	47	46	43	45	45	45
vinyl 1,2	10	10	13	16	13	11	12

3.6 Conclusions

The materials used in this project have similar microstructures, being high in the 1,4 configuration. However, there is poor agreement between molecular weight distributions determined by conventional SEC from three reputable institutions. The TGIC analysis revealed that the H-shaped PBDs contain several components having various molecular weights that are not revealed by conventional SEC. The novel synthesis strategy developed by Prof. Jimmy Mays did minimize the formation of high molecular weight by-products, but there are low molecular weight components. The use of SEC/TALLS alone is not adequate to track the reaction progress, and this may have provided a misleading indication of the end point of the coupling reaction, resulting in incomplete coupled molecules.

Chapter 4 Rheological Characterization of Linear and H-shaped Polybutadienes in LVE region

Part I: Procedures

Rheology is the science dealing with the way materials deform when stresses are applied to them. For viscoelastic materials such as polymers, linear viscoelasticity (LVE) is the simplest type of rheological behavior: it describes how the material responds to a deformation that is very small or very slow, or when the material is in the very early stages of a large and fast deformation, or where the departure of the chain from its equilibrium state is negligible. Within the linear regime, the viscoelastic response is independent of the kinematics of the deformation and is governed by Boltzmann's superposition principle. Linear viscoelastic properties such as complex viscosity $|\eta^*|$ and storage and loss moduli $G'(\omega)$, $G''(\omega)$ are generally used to reveal important information regarding the molecular structure of a polymer because the measurement techniques offer high precision and ease of use.

The objective of this chapter is to describe the LVE properties of polymers mentioned in Chapter 3. The chapter starts with an introduction on obtaining rheological data over a broad range of frequencies, followed by an exposition of critical but often neglected experimental details that are required to obtain accurate and precise data. Then experimental procedures, including oscillatory shear, creep and recoil are described. Linear viscoelastic properties such as the plateau modulus, zero shear viscosity, and steady state compliance are defined in terms of raw data. A discussion of the relationship between rheological behavior and molecular structure, particularly the effects of branching structure and molecular weight distribution is presented in Chapter 5.

4.1 Methods to obtain rheological data over a board range of frequencies

If the storage and loss moduli are known with sufficient precision over the range of frequencies from zero to a frequency high enough to reveal high frequency limiting behavior, rheological response to any type deformation in the LVE region can be predicted. However, data at very low frequencies are rarely attainable by dynamic experiment because of instrument limitations and the extremely long experimental time required. To obtain data over the broadest possible range of frequencies, time-temperature superposition of oscillatory shear data along with creep experiments are usually required.

4.1.1 Time-temperature superposition

For thermorheologically simple materials [126] time-temperature superposition can be used to shift properties measured at several temperatures over a given frequency range onto a "master curve" showing behavior over a much larger frequency range, all at a single reference temperature. Both vertical (b_T) and horizontal (a_T) shift factors at each test temperature are required, although the vertical shift is often neglected. The long-time (low-frequency) portion of the master curve comes from high temperature data and the short time (high frequency) portion comes from low temperature data.

The vertical shift factor operates on a measured stress quantity to yield a reduced modulus $G_r \equiv G(T)/b_T$ where $G(T)$ is the modulus at the test temperature, and b_T is defined by Eq. 4.1 where T_0 and ρ_0 are the temperature and density at the reference temperature.

$$b_T = \frac{T\rho}{T_0\rho_0} \qquad \text{Eq. 4.1}$$

Similarly, the horizontal shift factor operates on frequency to yield a reduced frequency $\omega_r \equiv \omega\, a_T$. Two commonly used empirical expressions for a_T are described below, where E_a is the activation energy for flow, R is the universal gas constant, and A and B are empirical constants.

Arrhenius dependence $\left(T > T_g + 100\ ^{o}C\right)$

$$a_T(T) = \exp\left[\frac{E_a}{R}\left(\frac{1}{T} - \frac{1}{T_0}\right)\right] \qquad \text{Eq. 4.2}$$

WLF dependence[127] $\left(T \text{ close to } T_g\right)$

$$a_T(T) = \frac{-A(T - T_0)}{\left[B + (T - T_0)\right]} \qquad \text{Eq.4.3}$$

However, for thermorheologically complex materials such as some long-chain branched polyethylenes [128] for which time temperature fails to produce a master curve while the accessible frequency range is limited. In this case, creep or creep/recovery experiment may help to extend the low frequency end of the characterization.

4.1.2 Storage and Loss moduli inferred from transient data

When time-temperature superposition fails, or a sample cannot be subjected to high temperatures due to thermal degradation, combining transient data from creep (or creep/recovery) tests with dynamic data from oscillatory shear tests may be useful to extend an LVE characterization curve to lower frequencies. Several methods for combining transient and dynamic data have been suggested [43,129,130]. Generally, a retardation spectrum inferred from transient data or a relaxation spectrum inferred from dynamic data is used as an intermediary, since if the spectrum is known, all other linear rheological functions can be calculated. However, determination of the spectrum is an ill-posed problem [131] that involves solving the nonlinear Fredholm integral equation of the first kind like that given by Eq. 4.4. For such a problem, linear regularization methods can be used to infer a modulus from dynamic data [132,133]. Instead of having a unique solution for each set of experimental data, a number of solutions each equally fitted to the original data were inferred. Various mathematical approximations are used to yield either a discrete or continuous spectrum which have been reviewed by Tschoegl [134].

$$J(t) = J_g + \int_{-\infty}^{\infty} L(\tau)\left(1 - e^{-t/\tau}\right) d\ln\tau + t/\eta_0 \qquad \text{Eq. 4.4}$$

When transient data are used to infer either a discrete or continuous retardation spectrum $L(\tau)$, the storage $J'(\omega)$ and loss compliances $J''(\omega)$, and hence the storage $G'(\omega)$ and loss moduli $G''(\omega)$, can be calculated by the following equations where J_g is the instantaneous compliance, which is of the order of 10^{-9} Pa^{-1} [135] and is neglected for melts.

$$J'(\omega) = J_g + \int_{-\infty}^{\infty} L(\tau) \frac{1}{1+\omega^2\tau^2} \, d\ln\tau \qquad \text{Eq. 4.5}$$

$$J''(\omega) = \frac{1}{\omega\eta_0} + \int_{-\infty}^{\infty} L(\tau) \frac{\omega\tau}{1+\omega^2\tau^2} \, d\ln\tau \qquad \text{Eq. 4.6}$$

$$G'(\omega) = \frac{J'(\omega)}{J'(\omega)^2 + J''(\omega)^2} \qquad \text{Eq. 4.7}$$

$$G''(\omega) = \frac{J''(\omega)}{J'(\omega)^2 + J''(\omega)^2} \qquad \text{Eq. 4.8}$$

4.2 Critical experimental issues for accurate and precise rheological data

To obtain accurate and precise rheological data in LVE region, great care must be taken to minimize the effects of normal stress develops during sample loading, frost formation at low temperature, shape of the sample edge and presence of dissolved gas or residual solvent. The results of failing to deal with these problems are described below.

4.2.1 Normal stress effect

Normal stress normally develops during sample loading and may take a long time to relax to zero, especially in high molecular weight branched polymers that have very long relaxation times. To reveal the effect of normal stress on shear stress measurements, a sample of PBD2 was subjected to oscillatory shear at 25°C using parallel plate fixtures and the stress was measured at various times after loading. A base case was established by waiting 3 hours to allow the normal stress to relax to a zero reading. The percent difference between complex viscosities measured at various times and the base case value was calculated by Eq. 4.9.

$$\frac{|\eta^*_{\text{normal stress}}| - |\eta^*_{\text{base case}}|}{|\eta^*_{\text{base case}}|} \times 100\% \qquad \text{Eq. 4.9}$$

Figure 4.1 shows that normal stress results in a reduction in complex viscosity, the bars representing a ± 2.5% range, which is the normal run-to-run variation. For highly entangled branched polymers, it can take days or even weeks for the normal stress to go to zero. As a compromise, therefore, all the data acquisition was done when the normal stress fall below 5g_f; which resulted in, at most, a ± 2% variation from the base case.

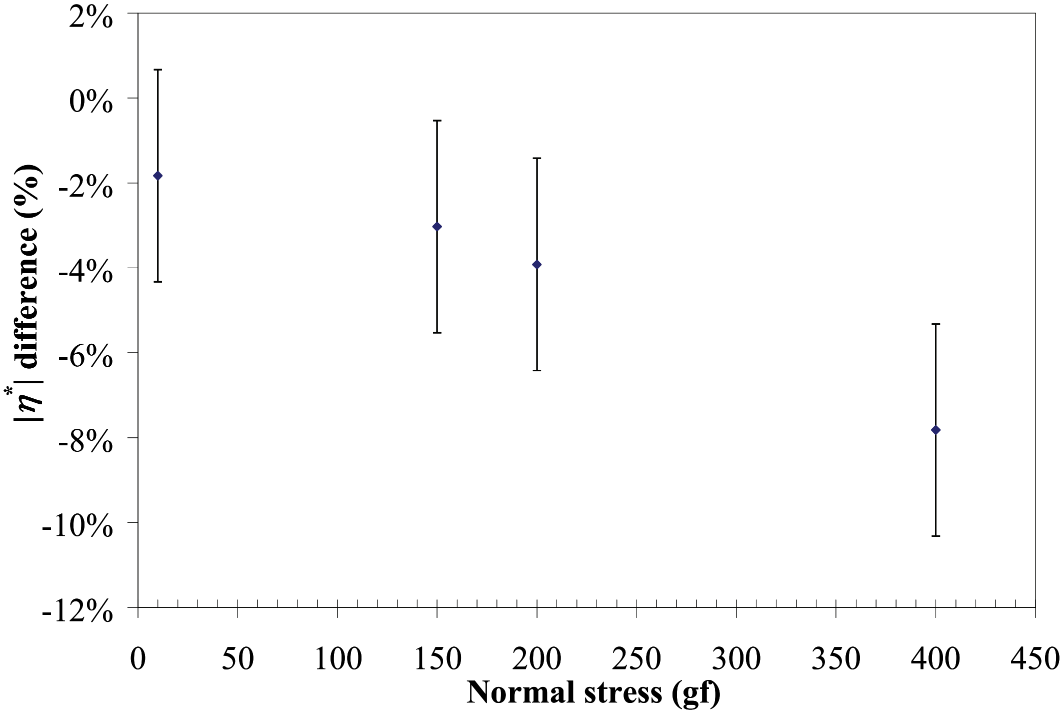

Figure 4.1 Effect of normal stress on complex viscosity (PBD2 at 25°C)

4.2.2 Gap variation due to temperature change

To minimize frost formation at low temperatures, sample loading was done at 25°C for all experiments. This also reduced the time required for relaxation of the normal stress due to the fact that relaxation is faster at 25°C than at lower temperatures. Changing the temperature to the value of a measurement causes a change in the plate spacing due to thermal expansion or contraction of the test fixtures. Therefore, it was necessary to correct the effect of thermal expansion by a correction factor α' as defined in Eq. 4.10, which was measured as a function of temperature.

$$\alpha' = \frac{\Delta L}{\Delta T} = \frac{L_T - L_{Tref}}{T - T_{ref}} \qquad \text{Eq. 4.10}$$

Two methods were used to obtain the value of α when using the 25mm diameter stainless steel plates. The first method was a discrete measurement method. The two plates were bought into contact with each other with a normal force of 200g_f at 25°C, and this position was set as the zero gap. Then the two plates were separated by 1mm, and the test temperature was changed to 10°C. Once the instrument reached the desired temperature and after waiting 30mins to reach equilibrium, the gap was manually adjusted until the two fixtures were in contact with each other with a normal force of 200g_f, and the gap reading shown in the instrument control panel was recorded. Due to metal contraction at a lower temperature, this gap reading was always negative, indicating the upper fixture had to go further down from the zero position to contact the lower plate with the same normal stress. By repeating this procedure, reducing the temperature 10°C each time, a correlation between the thermal contraction of the tools and temperature was constructed. Similarly, a correlation for temperatures above 25°C was developed by increasing the temperature at 10°C intervals. The second method was a continuous measurement method involving a continuous temperature change from T_{ref}=25°C, performed using the manufacturer's suggested protocol ($\omega = 6.283$ rad/s , $\gamma = 0.00001\%$, time per measurement = 10s, ramp rate = 3.0 °C/min when $T>T_{ref}$ or ramp rate = -3.0 °C/min when $T<T_{ref}$). These two methods were complementary since each measurement in method 1 was done at conditions such that fixtures had enough time to respond to the temperature changes, while method 2 provided data at smaller temperature intervals, which allowed a more precise determination of the linear fit function.

The correction factor was then determined from the slope of the curves as shown in Figs. 4.2 and 4.3 for temperature above and below T_{ref} (25°C). The values of α obtained from the two methods were found to agree with each other, with an average value of $\alpha' = 0.00250\, mm/^{o}C$ for $T > T_{ref}$ and $\alpha' = 0.00215\, mm/^{o}C$ for $T < T_{ref}$. The actual gap at the test temperature was then calculated by Eq. 4.11.

$$Actual\ gap = instrument\ display\ gap + \alpha'\left(T - T_{ref}\right) \qquad \text{Eq. 4.11}$$

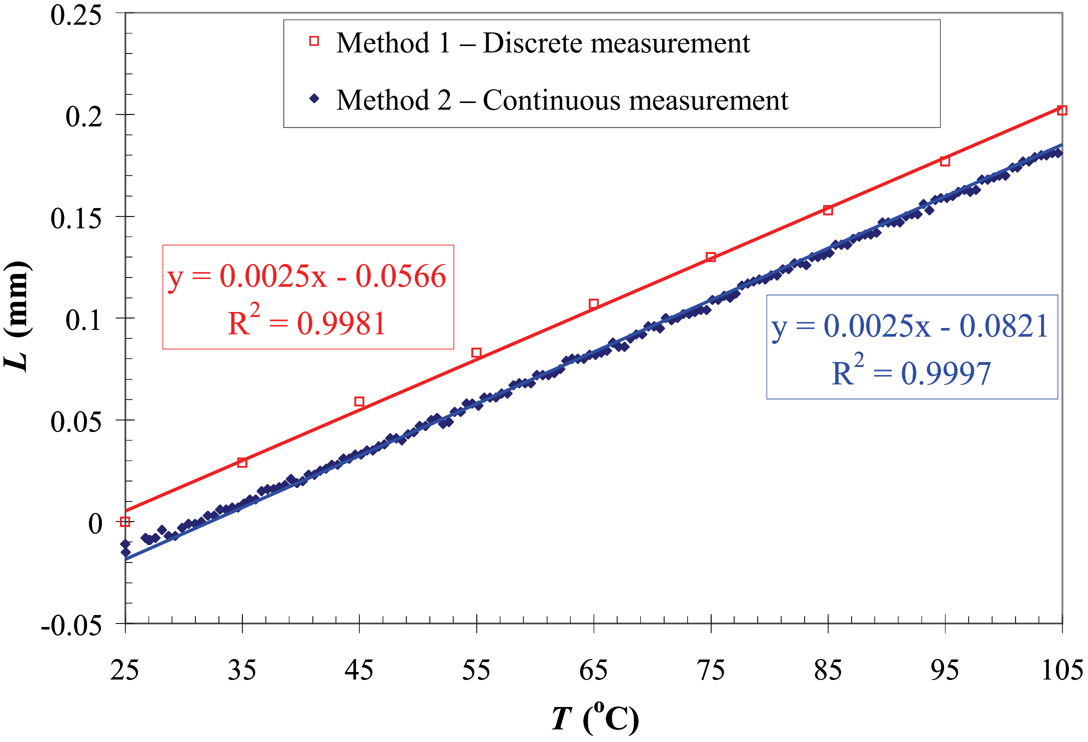

Figure 4.2 Thermal expansion of fixtures above reference temperature = 25°C

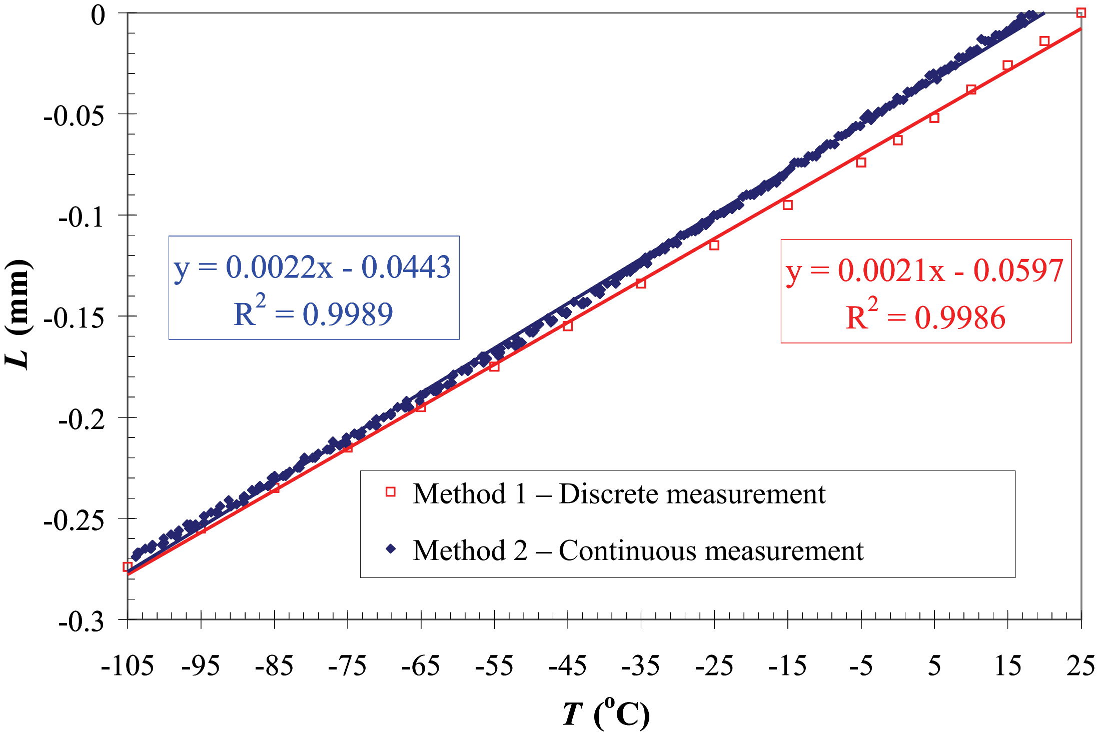

Figure 4.3 Thermal expansion of fixtures below reference temperature =25°C

4.2.3 Sample edge meniscus

After a sample was loaded between the fixtures, it was trimmed with a bronze knife and squeezed by reducing the gap a little bit to form a curved meniscus at the edge of the sample. The extent of squeezing directly influences the shape of the meniscus, which has a significant effect on rheological measurements. To determine the uncertainty arising from this effect, meniscuses having two very different shapes were studied at 25°C using PBD2. Both were formed initially by setting the gap at 1mm, trimming the sample and beginning measurements only when the normal stress fell below $5g_f$. As shown in Fig. 4.4, a "good" meniscus shape was formed by slightly reducing the gap by 2%, while a "bad" shape was formed by reducing the gap by 10%. The "good" shape is generally accepted as optimal for parallel plate fixtures. The difference between complex viscosities measured for the two shapes are plotted as a function of frequency in Fig. 4.4, which shows that the "bad" meniscus resulted in a complex viscosity 5% higher than the good meniscus.

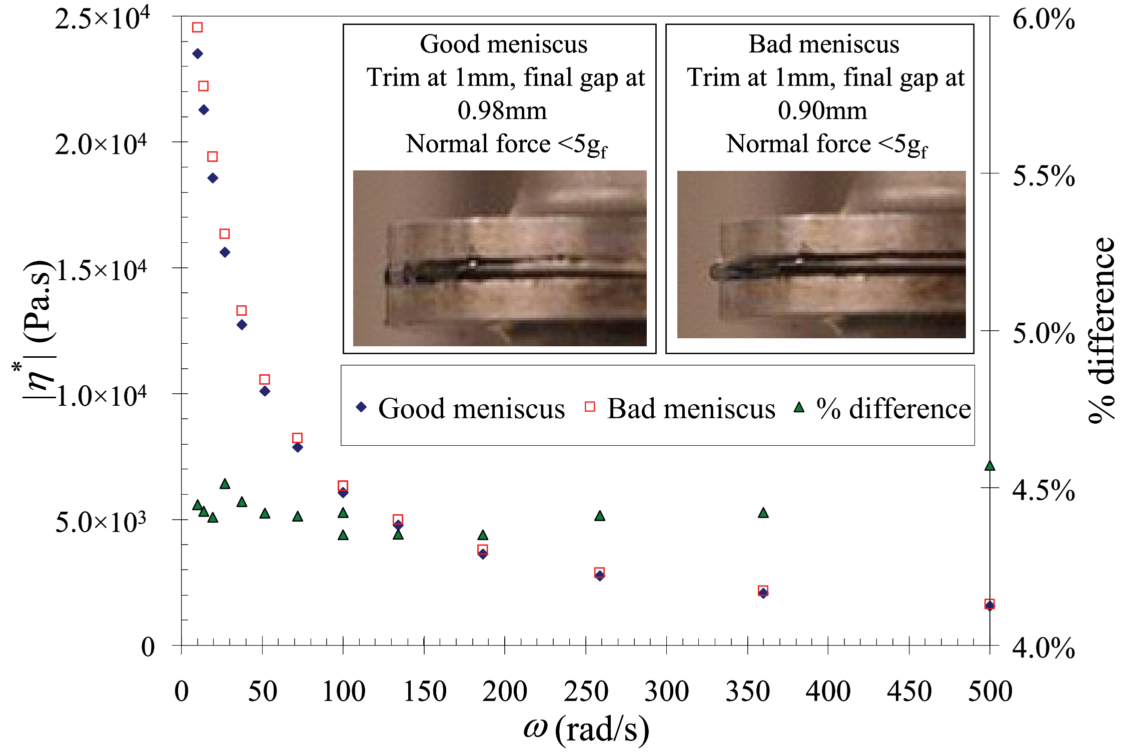

Figure 4.4 Effects of meniscus shape on complex viscosity (PBD2 at 25°C)

4.2.4 Dissolved gases

Dissolved components such as air, water and solvent are small molecules that reduce viscosity. Their presence was revealed by the appearance of many bubbles during vacuum drying, as shown in Fig. 4.5. A sample that is properly dried has a constant weight and a smooth surface. A sample that has not been dried is called a raw sample, and its complex viscosity is compared with that of fully dried sample in Fig. 4.6.

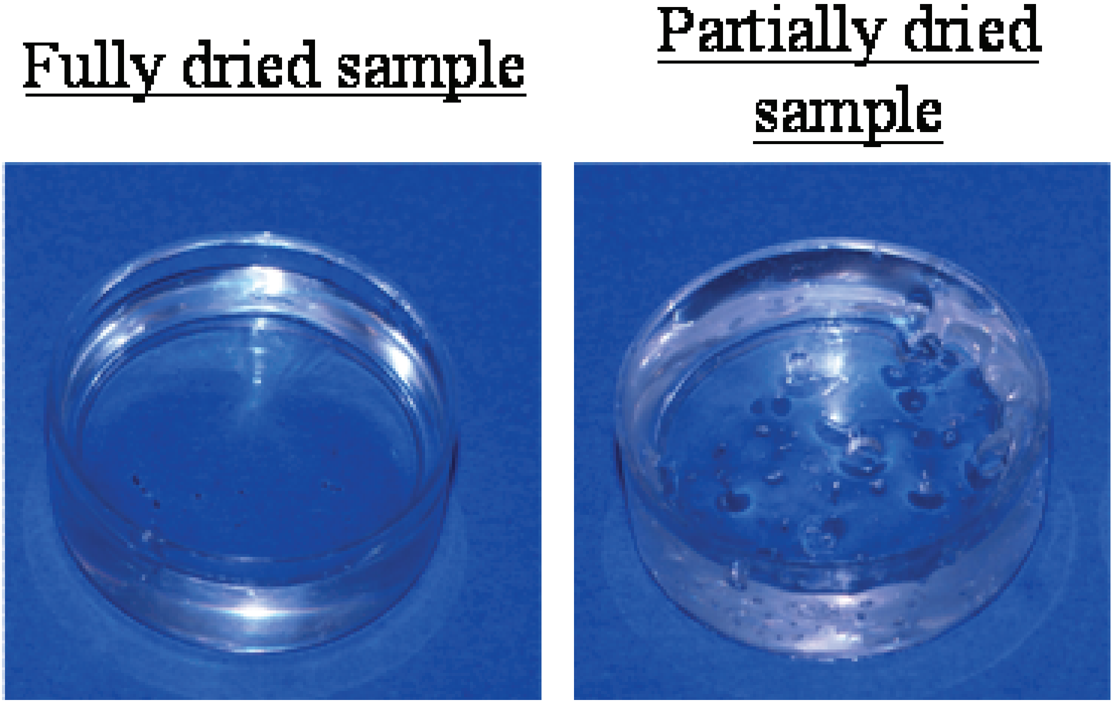

Figure 4.5 Appearance of fully dried and partially dried samples

At a frequency below 10 rad/s, complex viscosity of the thoroughly dried sample that contained no dissolved gases and volatile components was approximately 5% higher than that of the raw sample. The discrepancy became more significant at high frequency, resulting in a 20% difference between the two samples at 500rad/s. Therefore, it is very important to ensure that the samples are in good conditions as the maximum frequency is much higher than 500rad/s when constructing the master curves on each of the test materials.

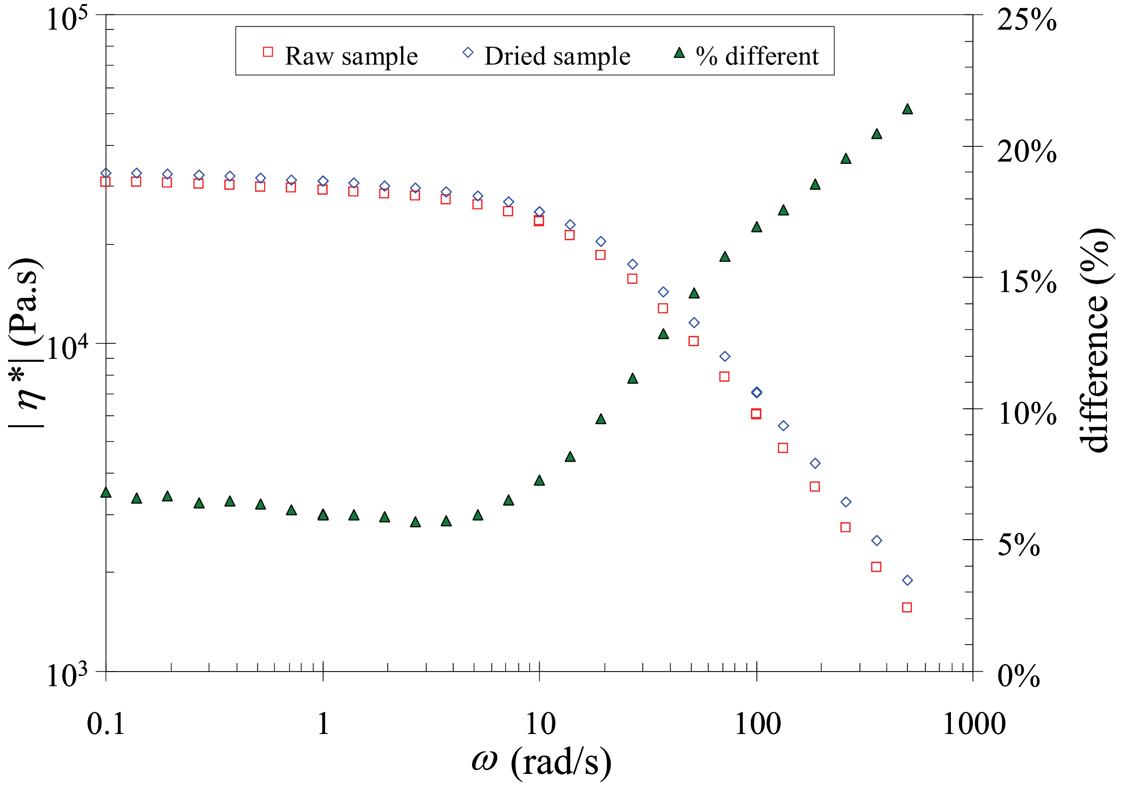

Figure 4.6 Effect of sample drying on complex viscosity of PBD2 at 25°C

4.3 Polymer storage and sample preparation

To prevent degradation due to light and heat, polymers were stored in a freezer in a wide mouth glass container wrapped with aluminum foil. Two months prior to making a measurement, the material to be used was dried in a vacuum oven at room temperature and its weight was monitored. A sample was considered thoroughly dried when no more bubbles appeared visually, and it had a constant weight.

To prepare circular 25mm diameter disks for experiments, compression molding was used to minimize strain and thermal histories. The mold was a 1.19mm thick stainless steel plate with nine 25mm-diameter circular holes in it. About 0.5g of polymer was placed in each hole. The filled mold was sandwiched between Teflon sheets and placed between two heavy metal plates. This assembly was then pressed at 25°C under 5000 tons force for the period of time shown in Table 4.1. The sample disks were then stored in a vacuum oven set at 30inHg at room temperature prior to rheological measurement.

Table 4.1 Molding time of samples at 25°C under 5000 tons force

Samples	**Molding time**
PBD2	2hr
PBD3	2 hr
HA12B40	2 hr
HA30B40	1 day
HA40B40	14 days
HA12B60	2 days
HA12B100	2 days
HA1230B40	1 day

4.4 Experimental procedures and calculation of properties

Detailed experimental procedures for the rheological measurements and by several methods for determining material constants such as plateau modulus G_{N}^{0}, zero shear viscosity η_0 and steady state compliance J_s^0 are described below. Results for a few samples are shown to illustrate procedures, while data for the remaining samples are provided in Appendix D.

4.4.1 Rheometers and fixtures

A strain-controlled rheometer ARES (Advanced Rheometric Expansion System) and a stress controlled rheometer SR5000 (Stress Rheometer 5000) were used for the rheological measurements. To eliminate noise and spikes in the power supply, an uninterrupted power supply (Tripp-Lite, SU6K) was inserted between the AC line and the rheometers. Based on the distinct capabilities of the instruments, the ARES was used for high frequency measurements, while the SR5000 was used for low frequency and creep measurements. Since the SR5000 was used for long-time (low-frequency) experiments, it was mounted on an air table to minimize the influence of vibrations.

While parallel plate fixtures do not generate uniform shear strain as do cone and plate fixtures, this does not affect their use for measurement of linear properties. And the ease of sample preparation and sample loading afforded by the former make them much more convenient for the measurement of LVE properties. Parallel plates with 25mm diameters were used in this study.

4.4.2 Small amplitude oscillatory shear (SAOS)

To perform small amplitude oscillatory shear in the ARES, the parallel plates fixtures were mounted on a common axis of symmetry and the sample loaded between them. The bottom fixture rotates sinusoidally while the torque M is measured on the upper fixture. Before making measurements on a particular polymer, a sample underwent a thermal stability test to find the maximum experimental time before degradation, and a strain sweep test to find the limit of LVE behavior at each frequency.

4.4.2.1 Thermal stability test

The thermal stability of a sample was determined by a time sweep experiment. The sample was subjected to oscillation at a constant strain amplitude and frequency, while the torque was recorded. Thermal degradation results in either a monotonic increase or decrease of the complex viscosity with time, depending on whether the material is undergoing cross-linking or chain-scission. The strain amplitude selected for use is not necessary to stay within the LVE region but be large enough to be within the precision range of the torque transducer. Similarly, the chosen frequency cannot be so low that one datum takes a long time to obtain or so high that sample breakage may occur. Therefore, frequency of 10 rad/s and strain amplitude of 1% were chosen for PBD2.

Time sweep results for PBD3 at 25^{o}C and PBD2 at 75^{o}C are shown in Figs. 4.7 and.4.8. The sample is deemed to be thermally stable at the test temperature as long as the change in the absolute value of complex viscosity is less than 3%. As shown in Fig. 4.7, PBD3 was stable for almost 3 days at 25^{o}C, during which the viscosity increased by only 2%. Figure 4.8 shows that PBD2 was stable for almost 2 days at 75^{o}C with a total viscosity increase of about 2%. Due to the limited quantities of H-shaped PBDs, thermal stability tests were not carried out on these polymers. Since the same anti-oxidant as in the linear PBDs had been added to H-shaped PBDs, and the highest experimental temperature was 25^{o}C, we assumed the H-shaped PBDs were thermally stable at all test temperatures.

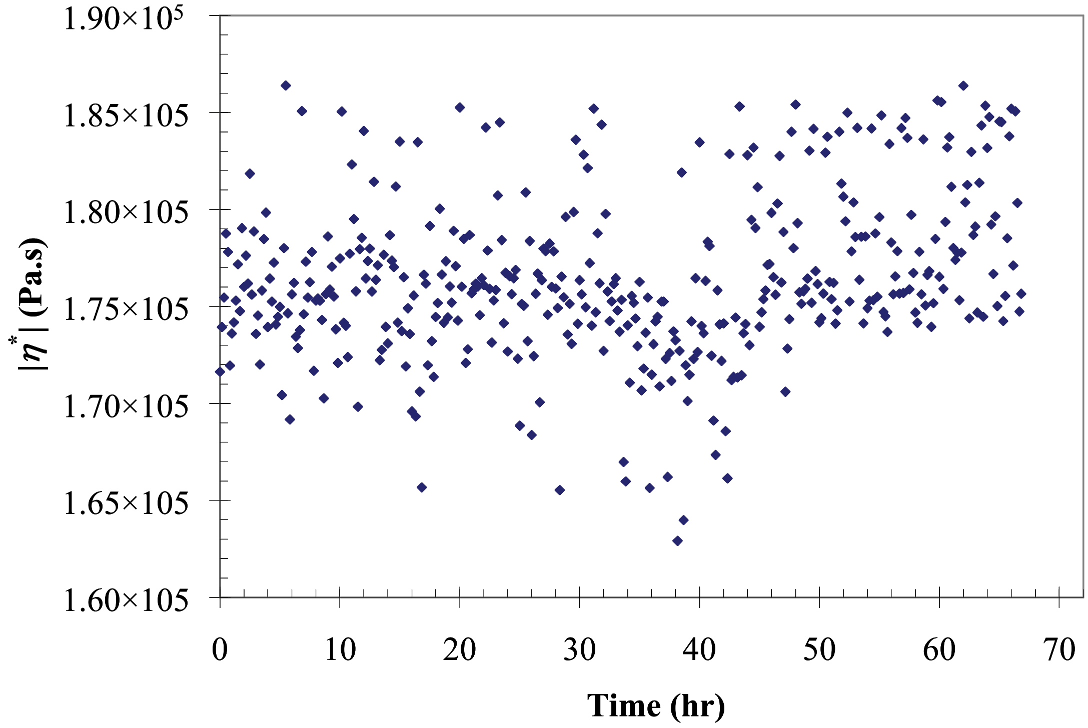

Figure 4.7 Thermal stability test of PBD3 at 25^{o}C, ω = 10rad/s and γ =1%

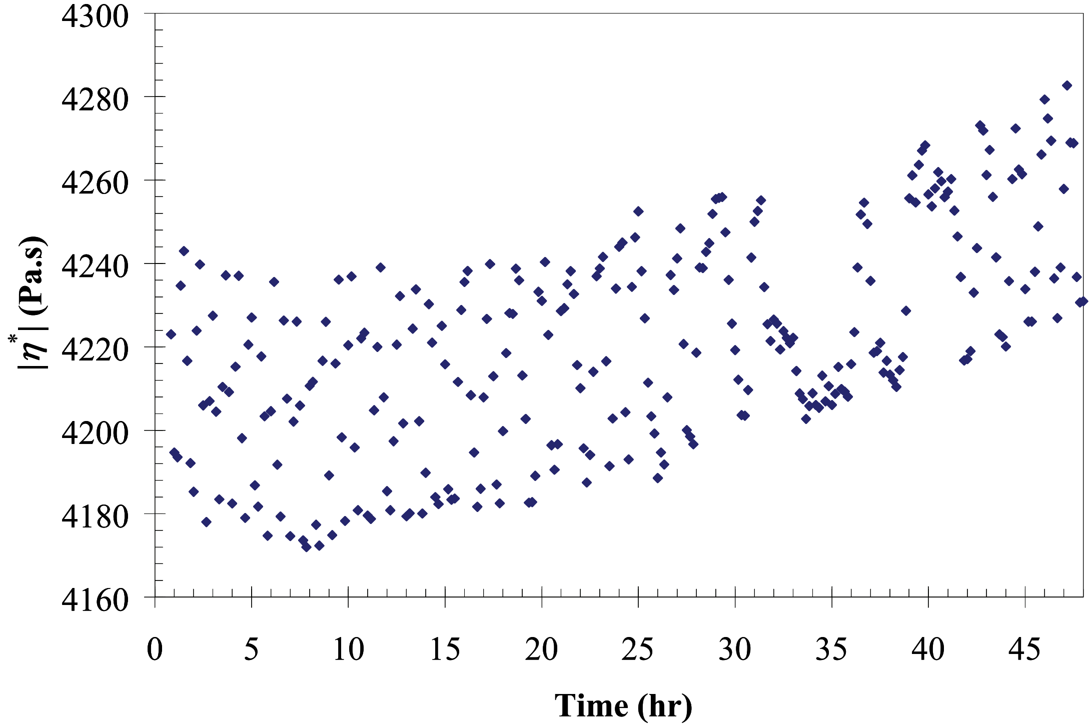

Figure 4.8 Thermal stability test of PBD2 at 75^{o}C, ω = 10rad/s and γ =1%

4.4.2.2 Determination of linear regime

Strain sweep tests were performed to determine the limit of linear viscoelastic behavior while maintaining the precision of torque data. If the strain amplitude is too small, the torque value will be below the useful range of the transducer. If it was too large, the behavior will be non-linear, leading to incorrect modulus data. Since the limiting strain depends on frequency, the experimental frequency range was divided into decades, and the maximum strain in each decade was determined by strain sweep tests. In such a test, the sample is subjected to varying strain values at a fixed frequency and the torque signal is recorded. As long as the strain is within the linear region, the calculated moduli will not vary with strain.

Strain sweep tests were carried out on all samples and at each test temperature to ensure linearity and precision. The command strain values finally selected are listed in Appendix D. It is generally true that as the temperature falls, a polymer behaves more like a solid, and a small strain is sufficient to generate sufficient torque. As the frequency is reduced, polymer behaves more like a liquid, and a larger strain is required to obtain a precise torque signal. Although the command strains at -75^{o}C were higher than at 25^{o}C, the actual strains experienced by the sample, especially at low temperature, were less than the command strain values; the actual strain thus decreased with temperature.

4.4.2.3 Dynamic frequency sweep test

To minimize thermal degradation on the limited quantity of H-shaped PBDs, dynamic frequency sweep tests were performed at 25^{o}C, 0^{o}C, -25^{o}C, -50^{o}C and -75^{o}C using the predetermined command strain values. Following those critical experimental techniques mentioned in section 4.2, a thoroughly dried sample as treated by the procedures shown in section 4.3 was loaded at 25^{o}C under a nitrogen purge. Once the normal stress developed during sample loading had fallen below 5g_f, the sample was trimmed and the gap was adjusted to give the desired shape of the meniscus.

Each data point shown in Fig. 4.9 and in Appendix D is an average of at least three runs performed under the same conditions but with different sample disks. Due to the limited amount of material, samples were recycled and remolded for further tests. Therefore, some runs were performed with fresh samples, while others were performed with recycled samples. The run-to-run variation, which is the maximum deviation between any two runs, was $\pm 2.5\%$. This was deemed to be an acceptable level of precision. A matter of special concern in this work was that after each test the sample was recycled back to the vacuum oven, then molded and loaded for another experiment. However, after being recycled a sample still produced data within $\pm 2.5\%$ of previous data. It was thus concluded that the experimental protocol used produced data that were suitable for the objectives of this research.

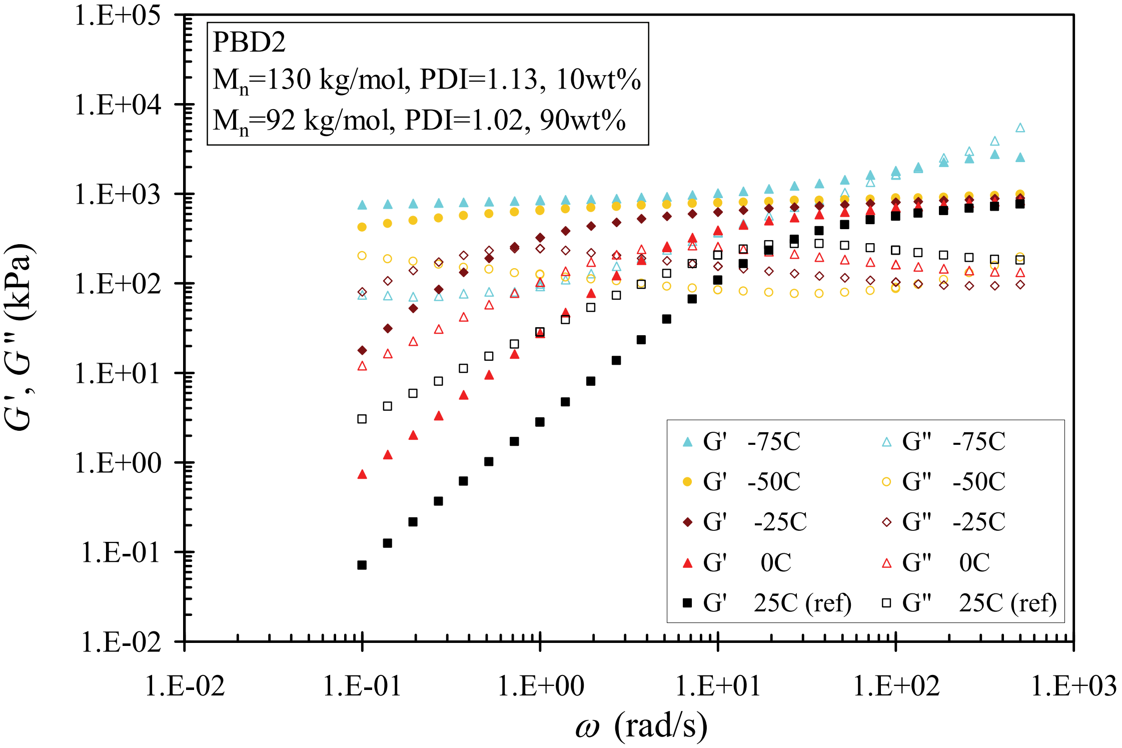

Figure 4.9 Storage and loss moduli of PBD2 measured at temperatures between 25°C and 75°C

4.4.3 Creep/recovery experiment

Small-amplitude oscillatory shear provides data mainly at relatively high frequencies (short times), and these were complemented by data from creep/recovery tests to obtain information about long-time (low-frequency) behavior. To minimize thermal degradation, especially in the case of polybutadiene, creep/recovery experiments were performed at

$25^{o}C$. Experiment was performed on SR5000 at a set temperature of $26.17^{o}C$ due to a different heating mechanism of SR5000 compared to ARES, a different set temperature had to be used in order to compare data from these two instruments under the same actual temperature which was 25 ^{o}C. The sample preparation and loading methods were the same as that used in ARES.

4.4.3.1 Linearity of applied stress

Preliminary creep tests with various applied stresses and creep time were performed to locate the optimal test conditions. If the deformation is within LVE region, the creep compliance $J(t)$ will be independent of the applied stress. As shown in Fig. 4.10 was the creep compliance of PBD2 obtained from various applied stresses, it is found that $J(t)$ superposed perfectly with a 200s creep time, suggesting even the maximum strains reached by these stresses are still within the linear region. The optimal stress and creep time of each sample were then found as listed in Table 4.2 and the corresponding results on all samples are shown in Appendix D.

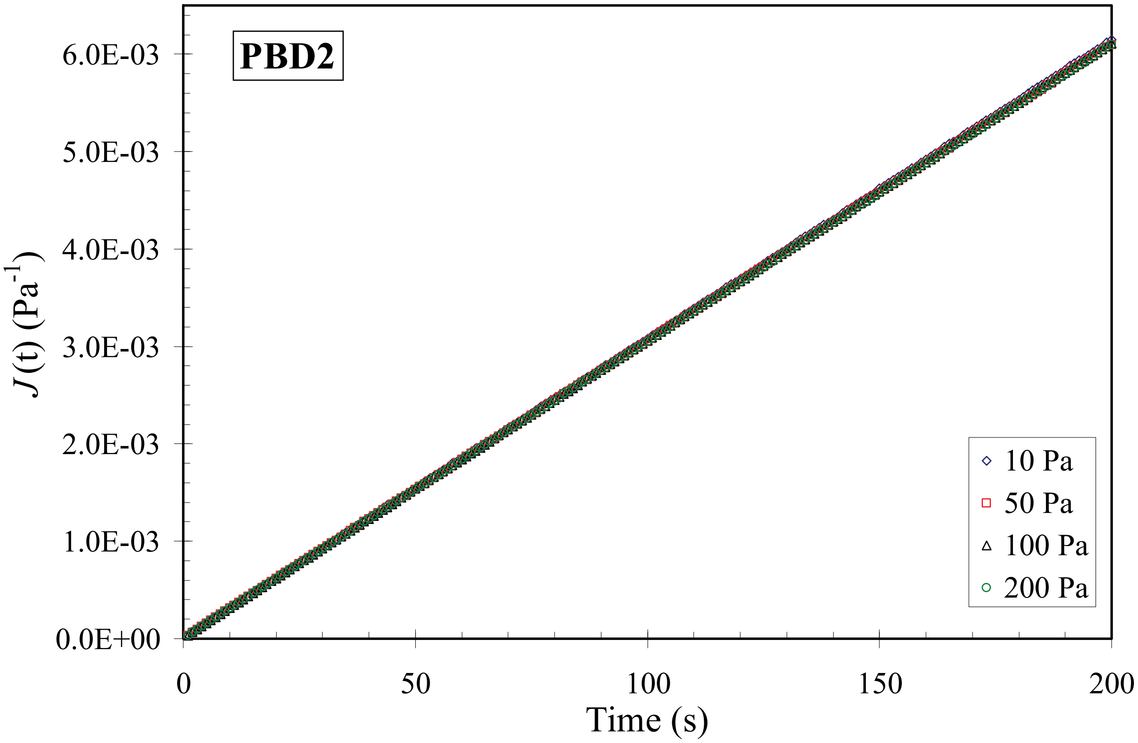

Figure 4.10 Creep compliance of PBD2 at various applied stresses in 200s creep time (T=25^{o}C)

Table 4.2 Optimum stress and creep time used for creep and recovery experiment

Sample	Stress (Pa)	Creep time (s)
PBD2	10	200
PBD3	150	200
HA12B40	300	200
HA30B40	200	200
HA40B40	150	200
HA12B60	150	200
HA12B100	300	1000
HA1230B40	250	200

4.4.3.2 Strain behavior and composite creep curve

Creep/recovery experiments on all samples were performed on the optimal stress and creep time as listed in Table 4.2. The shear strain measured during the recovery process that lasted up to 2 days was used to construct the composite creep compliance over the entire experimental time by Eq. 1.8 and Eq. 1.9. The composite creep compliance and strain behavior of PBD2 are shown in Fig. 4.11 while those of other samples are shown in Appendix D. The long time composite creep compliance data was best-fitted with a straight line which together with the equation of the best fit line, are shown in the insert of Fig. 4.11 and those in Appendix D. Recalling Eq. 1.10, when the creep compliance reaches steady state, the slope of the best fit line gives the inverse of zero shear viscosity while the intercept gives the steady state compliance. More detailed discussion on these rheological functions is presented in Chapter 5.

Similar to SAOS measurement, each data point shown in Fig. 4.11 and those in Appendix D for transient experiment was the average of at least three runs performed under the same conditions but with different sample disks. Due to the limited amount of materials, samples are recycled for further experiments. The run-to-run variation of composite $J(t)$ in the creep/recovery experiment was $\pm 2\%$.

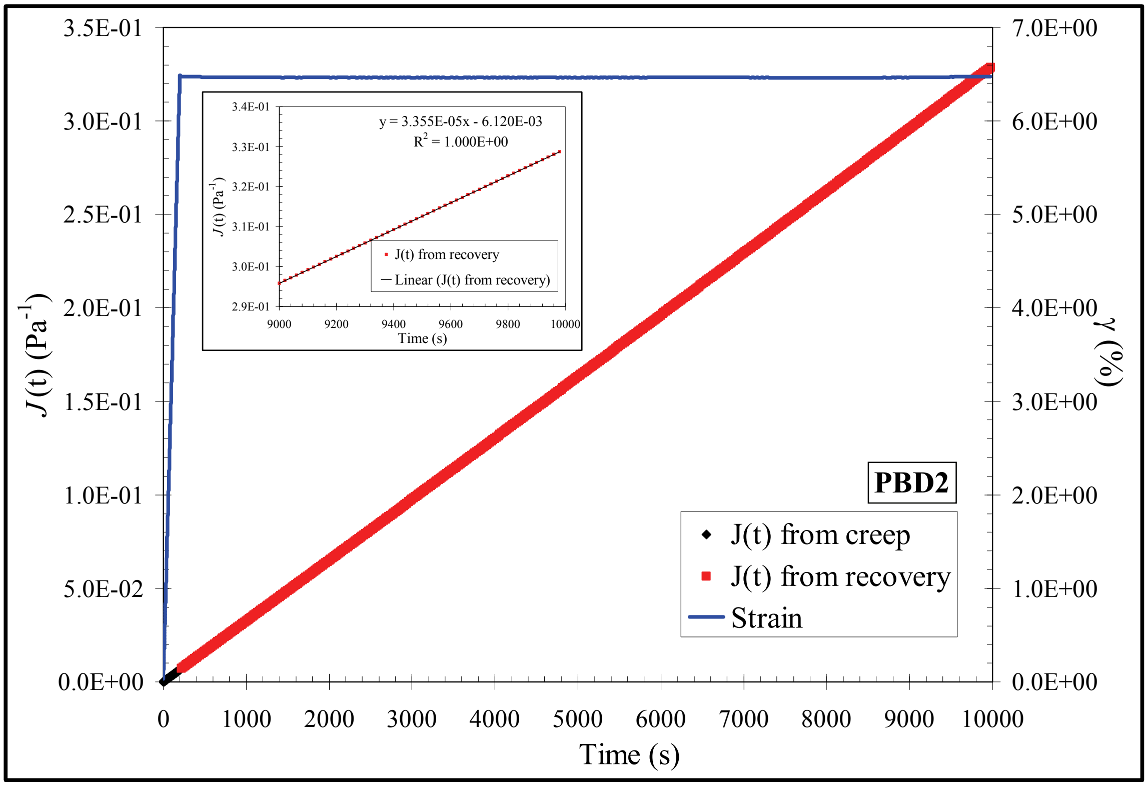

Figure 4.11 Strain and creep compliance as a function of time for PBD2 at 10 Pa, 25°C

4.4.3.3 Recoverable compliance J_r(t)

In creep/recovery experiment, the final part of the strain curve is a horizontal straight line, *i.e.* $\lim_{t\to\infty}\gamma_r(t) = \text{constant}$ as shown in Fig. 1.2. According to Eq. 1.7, the recoverable compliance $J_r(t)$ should reach a constant value at long time. However, commercial rotational rheometers equipped with air bearing[136], such as SR5000, is unlikely to achieve an exactly zero torque in the recovery stage due to the presence of residual torque arising from the air bearing that is dependent on the air pressure and the temperature of the bearing[137]. Therefore, the sample would be subjected to a non-zero stress during the recovery period. This resulted in a drift of $J_r(t)$ especially at long time. The drift direction of $J_r(t)$ depends on the direction of residual torque which is a random event. Therefore, from the behavior of $J_r(t)$ especially at long time, one can probe the effect of the residual torque on the sample response. Typical results of $J_r(t)$ that is affected by the residual torque and that is free from the effect of residual torque are shown in Figs. 4.12 and 4.13, respectively. $J_r(t)$ of the rest of the samples are shown in Appendix D.

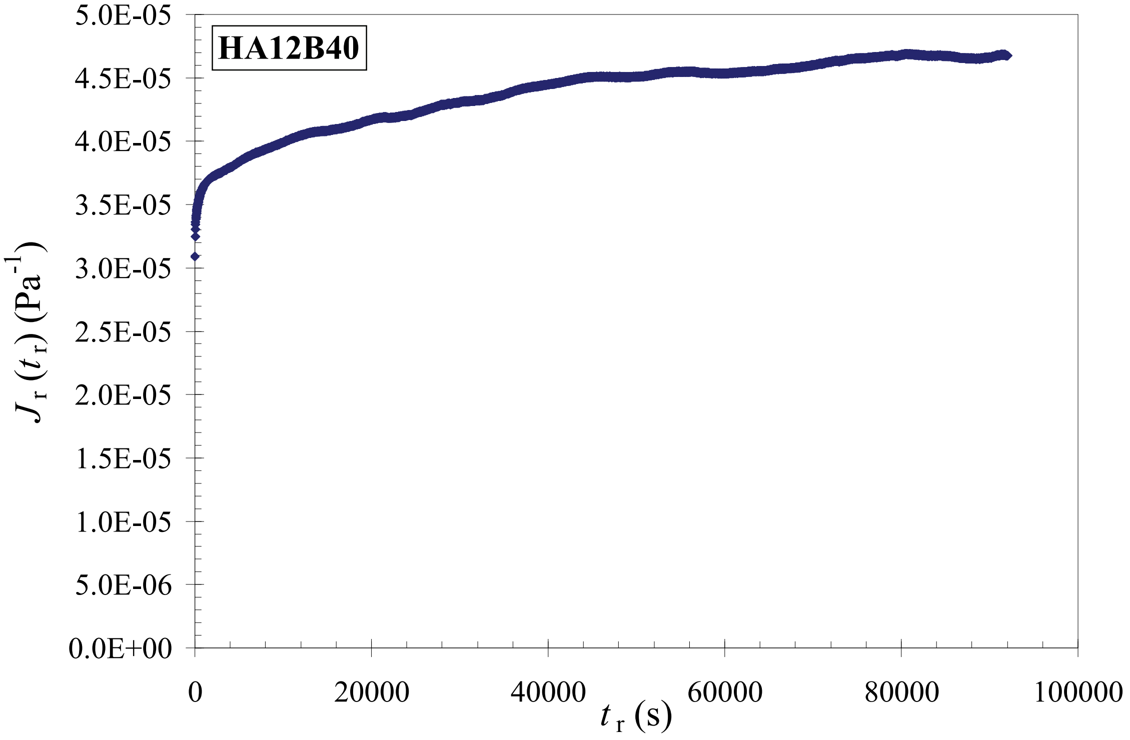

Figure 4.12 Recoverable compliance of HA12B40 which is affected by residual torque

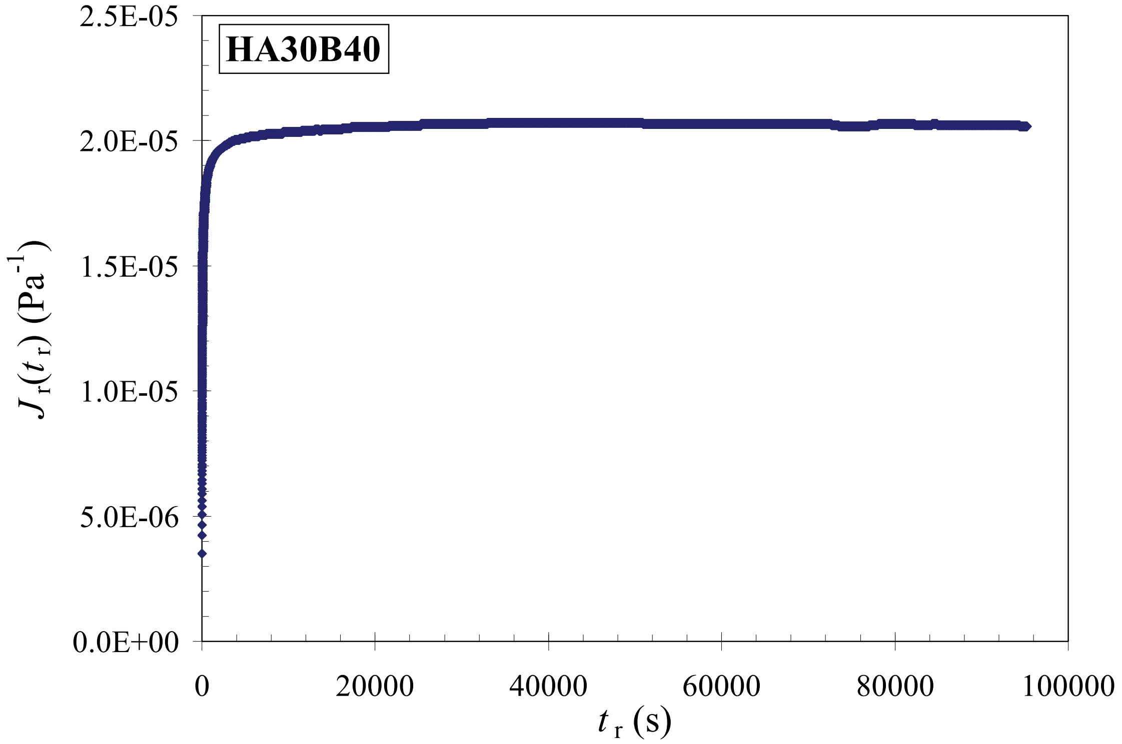

Figure 4.13 Recoverable compliance of HA30B40 which is free from residual torque

4.4.4 Creep experiment

For HA12B40 and HA40B40, whose recoverable process is strongly affected by the residual torque of the instrument as revealed by the drift in recoverable compliance at long time, creep only experiment was also performed. Again, preliminary creep tests with various applied stresses were performed for up to 24 hours to confirm the linearity of applied stress. The optimal stress and creep time of HA12B40 and HA40B40 were listed in Table 4.3 and the corresponding data is shown in Appendix D

Table 4.3 Optimum stress and creep time used for creep experiment

Sample	Stress (Pa)	Creep time (hrs)
HA12B40	30	25
HA40B40	200	22

Creep compliance as calculated by Eq. 1.5 from creep experiment are then compared with those obtained from creep/recovery experiment at the same reference temperature (T_{ref} = 25 °C), as shown in Figs. 4.14 and 4.15.

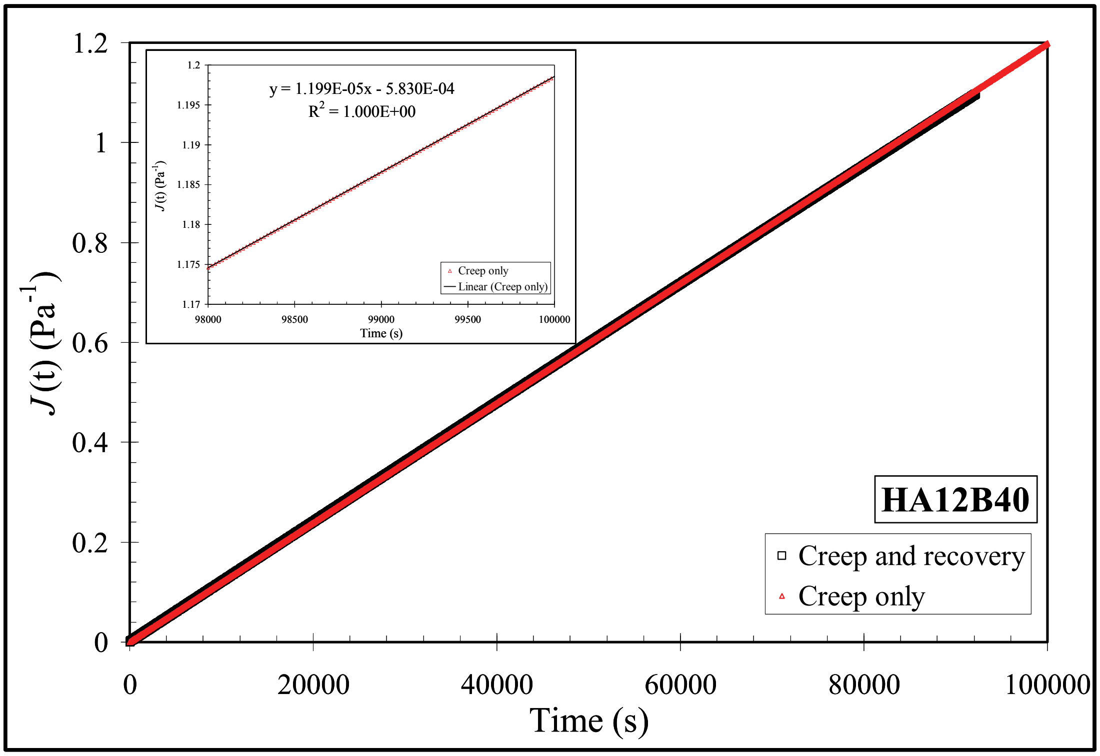

Figure 4.14 Comparison of J(t) obtained from creep and creep/recovery experiment of HA12B40

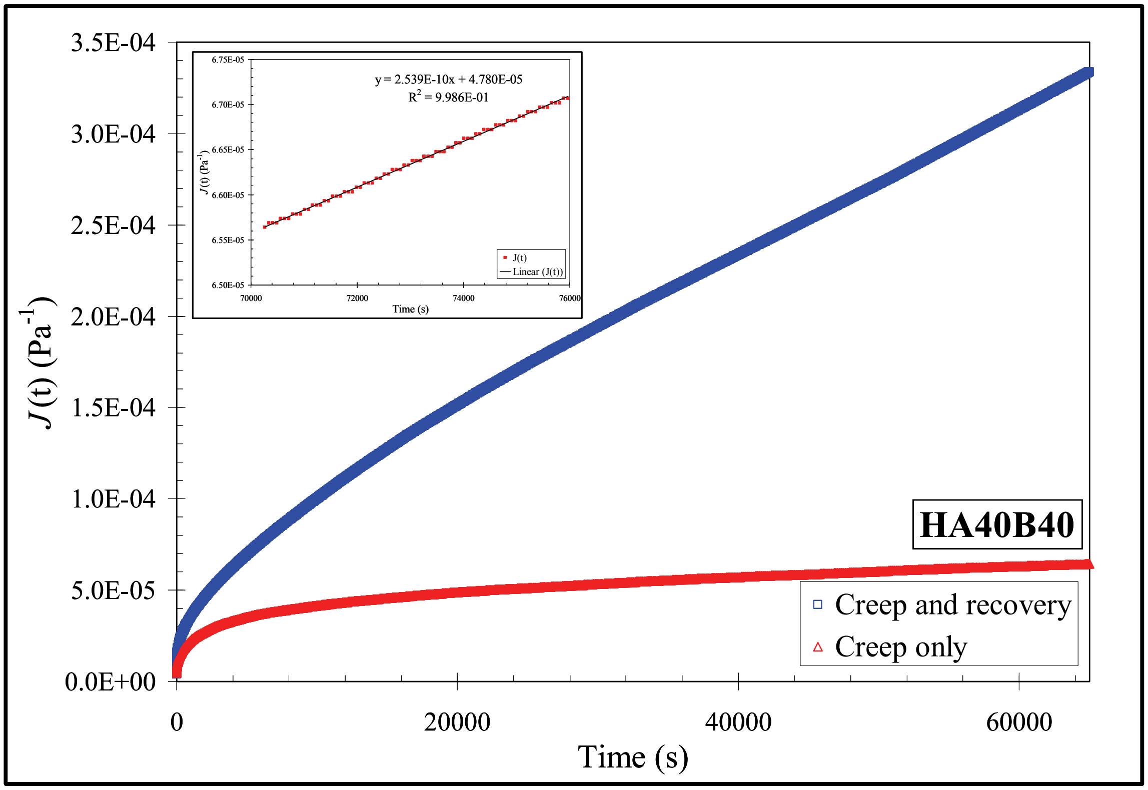

Figure 4.15 Comparison of *J*(t) obtained from creep and creep/recovery experiment of HA40B40

4.4.5 Calculation of viscoelastic properties

Experimental data must be handled in the way as mentioned in section 4.1 so that the transient and dynamic data can be shifted to a common temperature, T_{ref} =25°C. Then, properties that are sensitive to molecular structure and molecular weight distribution can then be determined. In this section, methods used to evaluate key properties, particularly zero shear viscosity η_0 , plateau modulus G_{N}^0 and steady state compliance J_s^0 are described. The resulting master curves property values are presented in Chapter 5.

4.4.5.1 Plateau modulus G_{N}^0

A plateau region appears in the storage modulus of a monodisperse polymer when its molecular weight exceeds the entanglement molecular weight, M_{e}, However, except for very high molecular weight, monodisperse samples, a truly flat plateau region is not observed. For polydisperse samples it is not straightforward to infer the plateau modulus from experimental data. Therefore, plateau moduli of samples studied in this project were estimated by the minimum phase angle. Detailed discussions of methods for determining a value for the plateau modulus can be found in the literature [46,138] as well as in Appendix F.

For linear polymers with high molecular weight and narrow molecular weight distribution, a value of plateau modulus G_{N}^{0} can be determined from G' where the corresponding G'' reaches a minimum [135] as shown in Eq. 4.12.

$$G_{\mathrm{N}}^{0} = G'(\omega)_{G''\to\text{minimum}} \qquad \text{Eq. 4.12}$$

However, for polydisperse systems for which a minimum in G'' is not always present, Eq. 4.13 was used to account for the minimum of phase angle $\delta = \tan^{-1}\left(G''/G'\right)$ [139] in the rubbery plateau region of the material.

$$G_{\mathrm{N}}^{0} = G'(\omega)|_{\delta=\min} \qquad \text{Eq. 4.13}$$

4.4.5.2 Zero shear viscosity η_0

As introduced in Chapter 1, η_0 is an important quantity in describing how readily a material can flow. It has a strong dependency on molecular weight (M) for entangled linear polymer melts. Several empirical relationships of M-η_0 have been developed, such as the power law relationship which is particularly useful for linear polymers. However, there is little experimental data available for branched polymers at a sufficiently low shear rate such that the viscosity is constant. Thus, η_0 of a series of linear PBDs blends and H-PBDs were determined by the methods presented below.

For sample that has reached terminal behavior by SAOS experiment, such as PBD2, η_0 is determined from the complex viscosity. In the terminal region, storage modulus $G'(\omega)$ and loss modulus $G''(\omega)$ are proportional to ω^2 and ω respectively. This proportionality happens at very low frequency (long time) where the polymer chains are completely relaxed and free of stress. The absolute magnitude of complex viscosity in this regime is equivalent to η_0 as shown in Eq. 1.2.

While for PBD3 and H-shaped PBDs where terminal zone cannot be reached by SAOS experiment, η_0 is determined from the creep compliance $J(t)$ as shown in Eq.1.10. The long time $J(t)$ is best fitted with a linear relationship where the inverse of its slope gives η_0 .For HA12B40 and HA40B40, $J(t)$ obtained from creep only experiment (section 4.4.4) was used to obtain η_0, results are shown in Figs. 4.14 and 4.15, respectively. While for HA12B60, HA12B100 and HA30B40, the composite $J(t)$ obtained from creep/recovery experiment (section 4.4.3) was used to obtain η_0, corresponding $J(t)$ curves and best fit line are shown in Appendix D.

4.4.5.3 Steady state compliance J_s^0

J_s^0 is a measure of average molecular distortion of a polymer coil during flow, when sufficient time is given, the molecular distribution function would be independent of time [135]. As J_s^0 is related to the second moment of the relaxation time distribution, it is much more sensitive to the molecular weight distribution compared to average molecular weight. It characterizes the elastic features of the polymer responses in a steady-flow situation and is a difficult quantity to measure compared to η_0 due to its relative small order of magnitude.

As shown in Eq. 1.10, the intersection on $J(t)$ extrapolated from long time is equal to J_s^0 Except sample HA12B40 and HA40B40, J_s^0 was determined from $J(t)$ obtained from creep/recovery experiment (section 4.4.3) where results are shown in the insert of Figs. 4.11 and in Appendix D. For HA12B40 and HA40B40, due to the significant effect of residual torque in the recovery process, J_s^0 of these samples was determined from $J(t)$ obtained from creep only experiment (section 4.4.4) as shown in the insert of Fig. 4.14 and Fig. 4.15.

Chapter 5 Rheological Characterization of Linear and H-shaped Polybutadienes

Part II: Results and Discussion

In this chapter we presented master curves of storage and loss moduli and complex viscosity prepared by combining data from oscillatory shear with those from creep or creep/recovery tests. These master curves will be used to evaluate two molecular models in Chapter 6. Results of estimating the material constants: plateau modulus G_N^0, steady-state compliance J_s^0 and zero-shear viscosity η_0 are presented, and the effects of molecular structure on the LVE properties are discussed in detail.

5.1 Time-temperature superposition of data

The vertical shift factor b_T defined by Eq. 4.1 involves the melt density, which can be measured directly. Carella *et al*. [140] measured the density of a series of linear polybutadienes with various vinyl contents at 25°C using a density gradient column or by a neutral buoyancy method and found the density to be independent of microstructure and to have values of $\rho = 0.896 g/cm^3$ at low vinyl concentration and $\rho = 0.890 g/cm^3$ at 99% vinyl concentration. Literature data for a linear PBD from 30.2°C to 235.8°C were extrapolated down to -75°C to obtain the density at our experimental temperatures[141]. An empirical relationship of density valid from -90°C to 90°C is shown in Eq. 5.1 where *T* is the temperature of interest in Kelvin. Due to the lack of literature data on H-shaped PBD, we assumed that it has the same density as linear PBDs as calculated from Eq. 5.1.

$$\rho(T) = \frac{1}{0.918871 \exp(0.000681 \times T)} \qquad \text{Eq. 5.1}$$

After applying b_T, the horizontal shift factors a_T were obtained by shifting the modulus data until those at lower temperature overlapped with those at the reference temperature using a plot with linear scales as illustrated in Figs. 5.1 and 5.2.

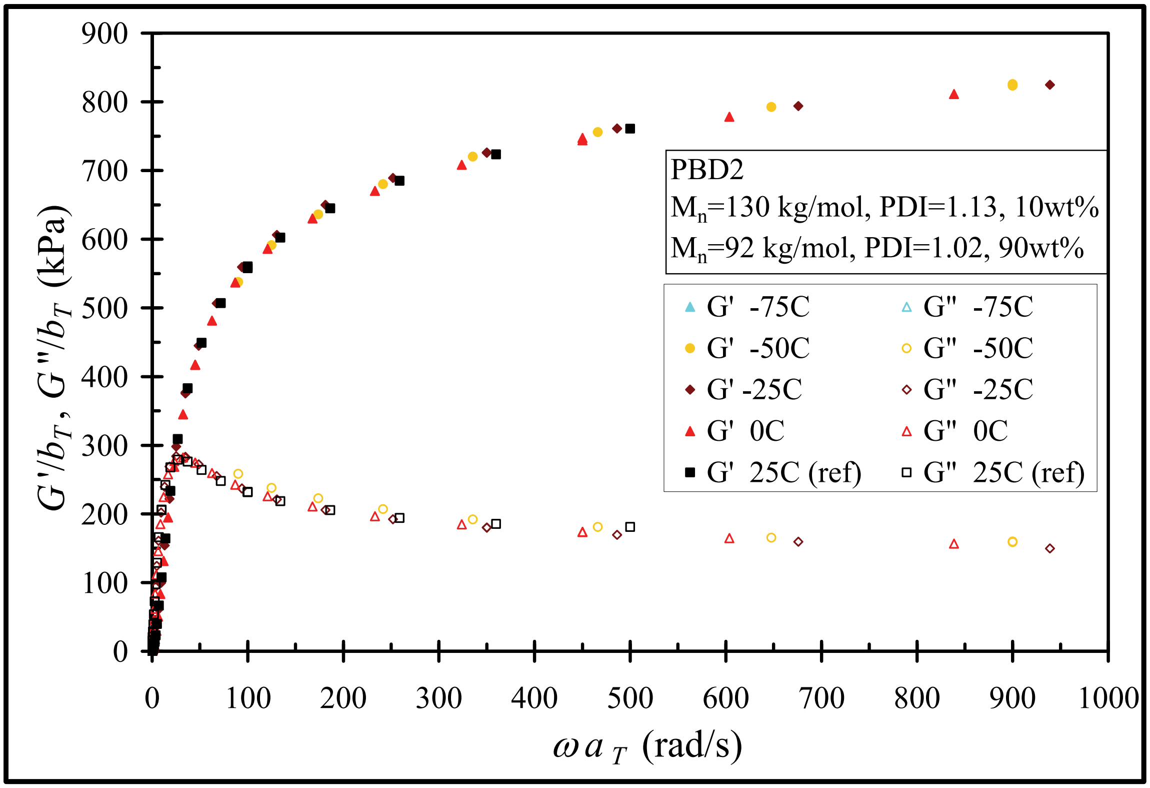

Figure 5.1 Master curves of storage and loss moduli of PBD2 for T_{ref}=25ºC using linear scales

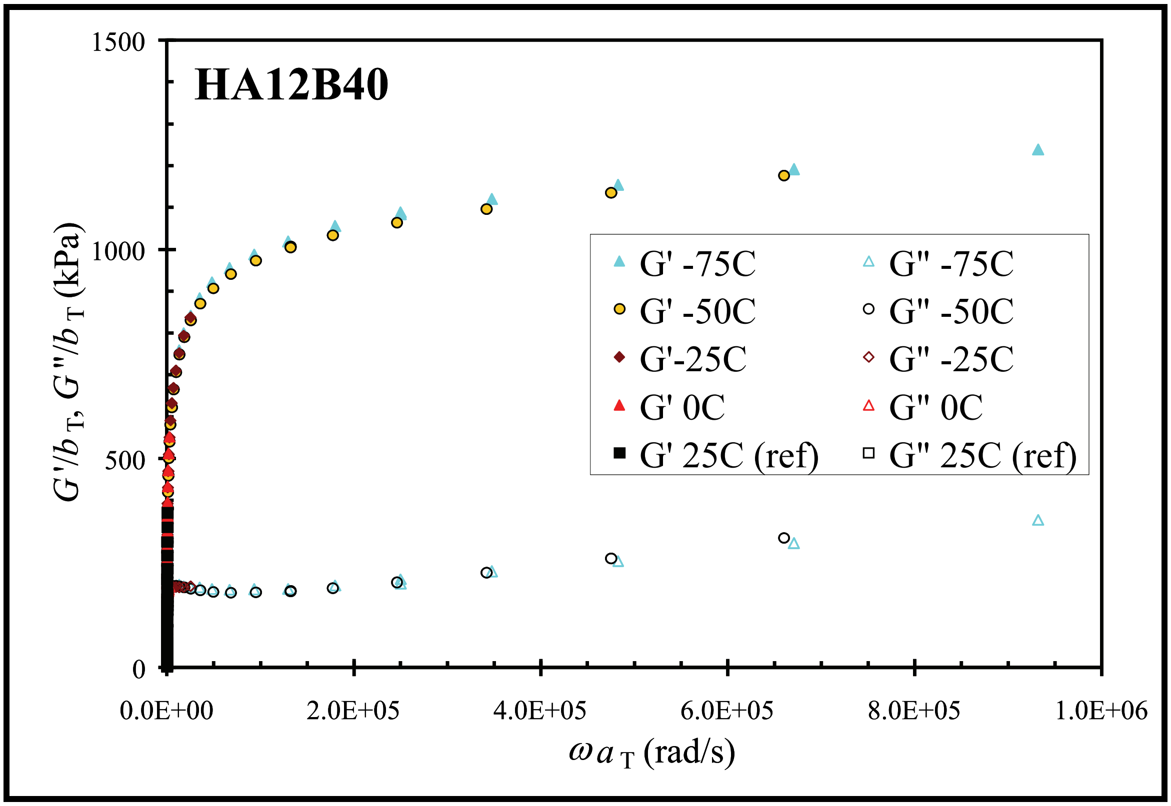

Figure 5.2 Master curves of storage and loss moduli of HA12B40 for T_{ref}=25ºC using linear scales

Contrary to $b_{T,}$ a_T decreases with increasing vinyl content [140]. Despite the small difference in vinyl content among various H-shaped PBDs (11% to 16% vinyl content), a single set of a_T values is good enough to shift the modulus data for all H-shaped PBDs. When the shifted modulus and frequencies were plotted in a linear-linear scales, as suggested by Wood-Adams *et al.* [142] and Dealy *et al.* [143] to confirm the thermorheological behavior , both the linear and H-shaped PBDs were found to be thermorheologically simple. Another technique to judge the success of superposition is to use plot of loss angle (*i.e.* δ) versus log $|G^*|$ or commonly known as van Gurp-Palmen plot [144], which is attached in Appendix F. For each temperature, only a single pair of shift factors was required for satisfactory superposition of both storage and loss moduli. It is found to be thermorheologically simple on other branched polymers, such as H-shaped Polyisoprenes [21,115], H-shaped Polybutadiene [41], comb Polybutadienes[29,33] and comb Polyisoprene [27].

The shift factors used for linear and H-shaped PBDs are shown in Fig. 5.3. Although same vertical shift factors were used for both H-shaped and linear PBDs, it was found that the horizontal shift factors of linear PBDs were lower than those of H-shaped PBDs and this difference increased as temperature decreased. From the microstructures revealed by ^{1}H NMR shown in Chapter 3, we know that the linear and H-shaped PBDs have similarly high 1,4 contents. Thus, the larger a_T of H-shaped PBDs must be the result of long-chain branching. Such a_T enhancement due to the presence of LCB, even in a small amount (0.06LCB/1000C), was also observed on Polyethylene as reported by Park *et al.*[145].

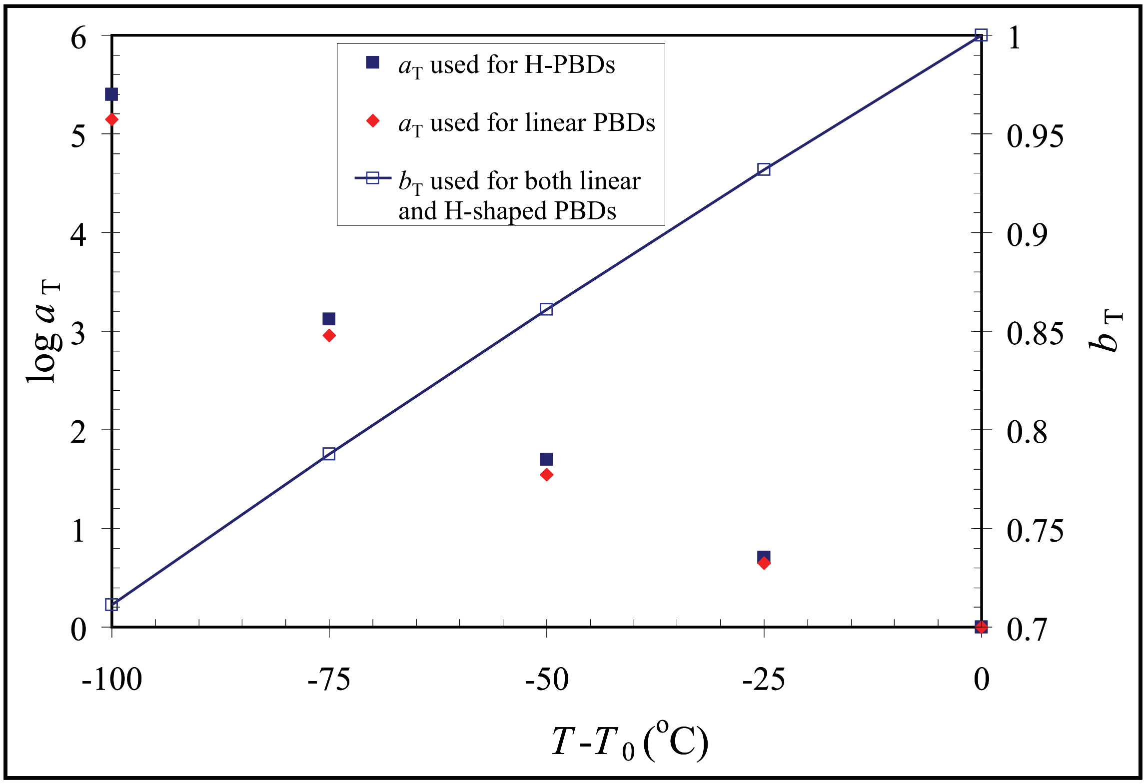

Figure 5.3 Vertical and horizontal shift factors for linear and H-shaped polybutadienes

Horizontal shift factors a_T were found to obey the WLF equation, Eq. 4.3. By inverting Eq.4.3, the coefficients of A and B can be found from a plot of $1/\log(a_T)$ versus $1/(T-T_0)$ as shown in Fig. 5.4, where the slope of the best fit line gives -B/A while the intercept gives -1/A. The WLF relations for linear and H-shaped PBDs that were found to be valid over the experimental temperature ranging from 25°C to -75°C are as follows:

$$\text{Linear PBDs:} \quad \log a_T = \frac{-3.98(T-T_0)}{177.5+(T-T_0)} \qquad \text{Eq. 5.2}$$

$$\text{H-Shaped PBDs:} \quad \log a_T = \frac{-4.42(T-T_0)}{181.0+(T-T_0)} \qquad \text{Eq. 5.3}$$

When compared under similar microstructure (~10% vinyl) at the same reference temperature (*i.e.* T_{ref}=25°C), the WLF coefficients of the two linear PBDs are found to be consistence with literature values, with A = 3.64 and B = 186.5°C as reported by Valentine *et al*. [146] and A=3.48 and B=163 °C as reported by Colby *et al.*[147]

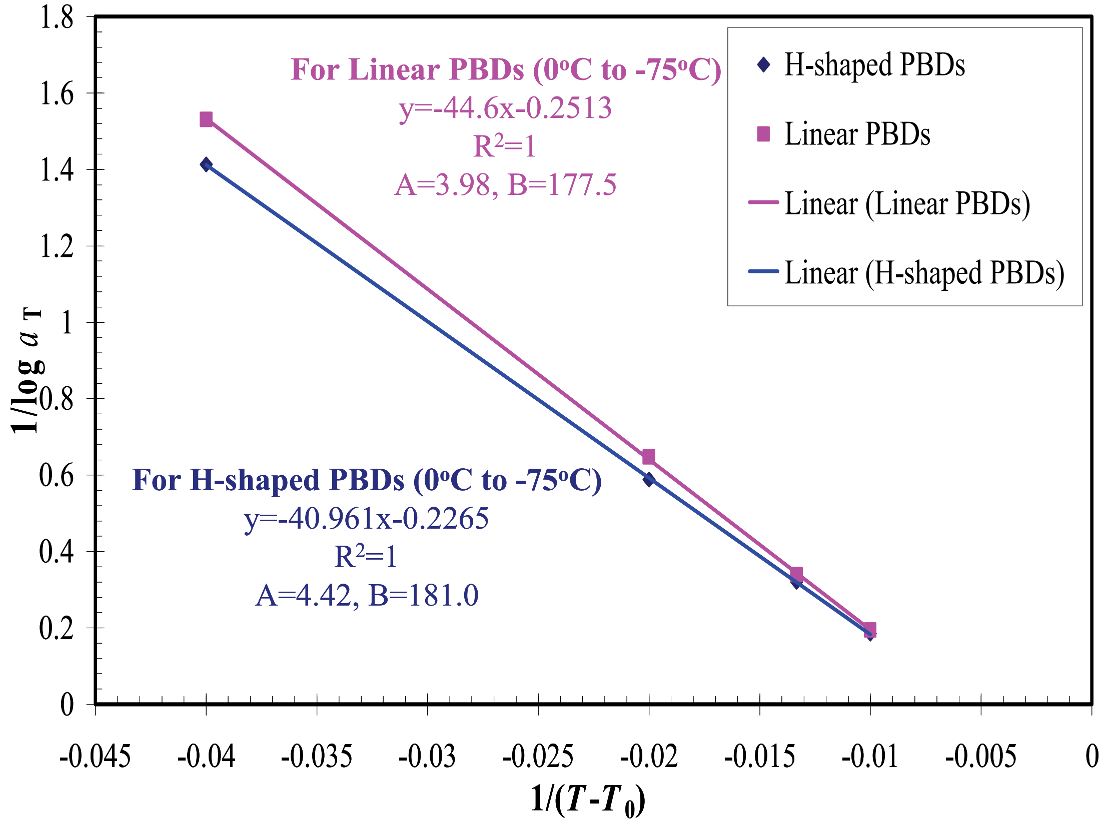

Figure 5.4 Horizontal shift factors a_T for linear and H-shaped PBDs using WLF plot

Using these shift factors, the data obtained at various temperature were shifted to the reference temperature T_{ref}=25°C, as shown in Fig. 5.5 and Appendix E, and the corresponding complex viscosity curves are shown in Fig. 5.6 and in Appendix E. We see that even the data obtained at the highest temperature are often still far from the terminal zone. In order to obtain information in the terminal zone, creep or creep/recovery measurement was performed at T_{ref}.

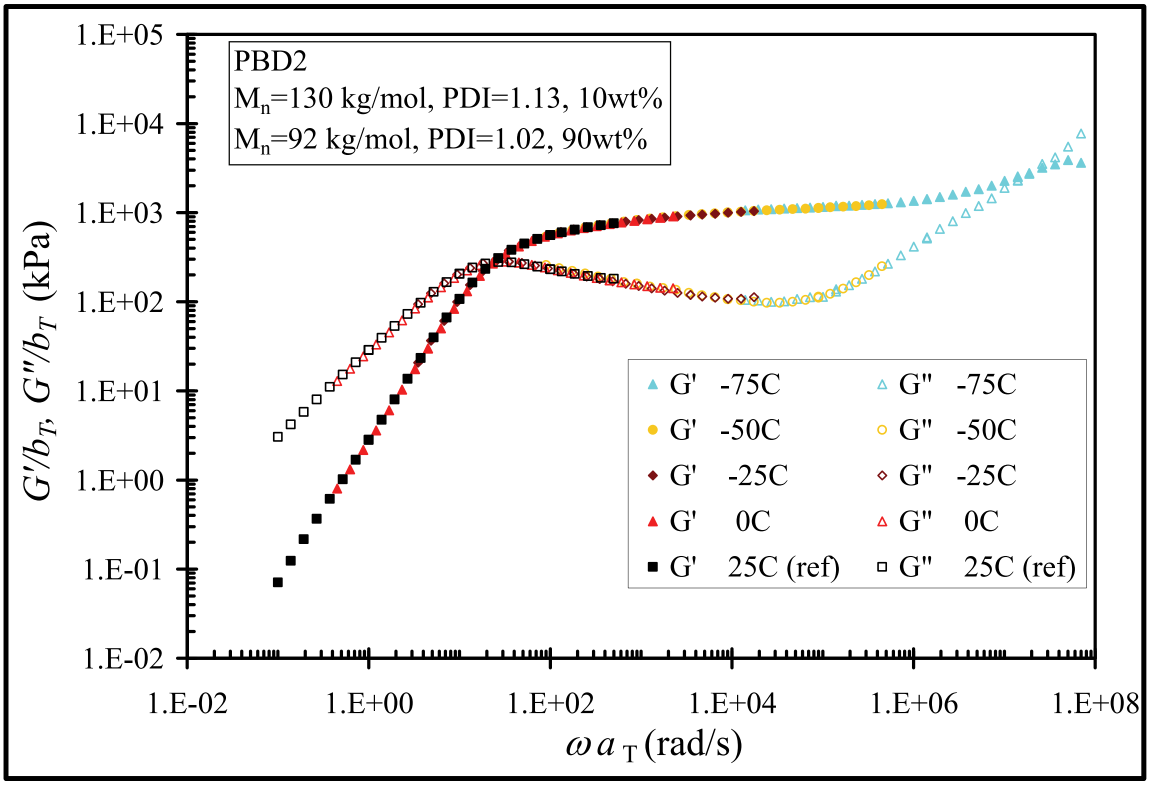

Figure 5.5 Master curves of storage and loss moduli of PBD2 shifted to T_{ref}=25°C

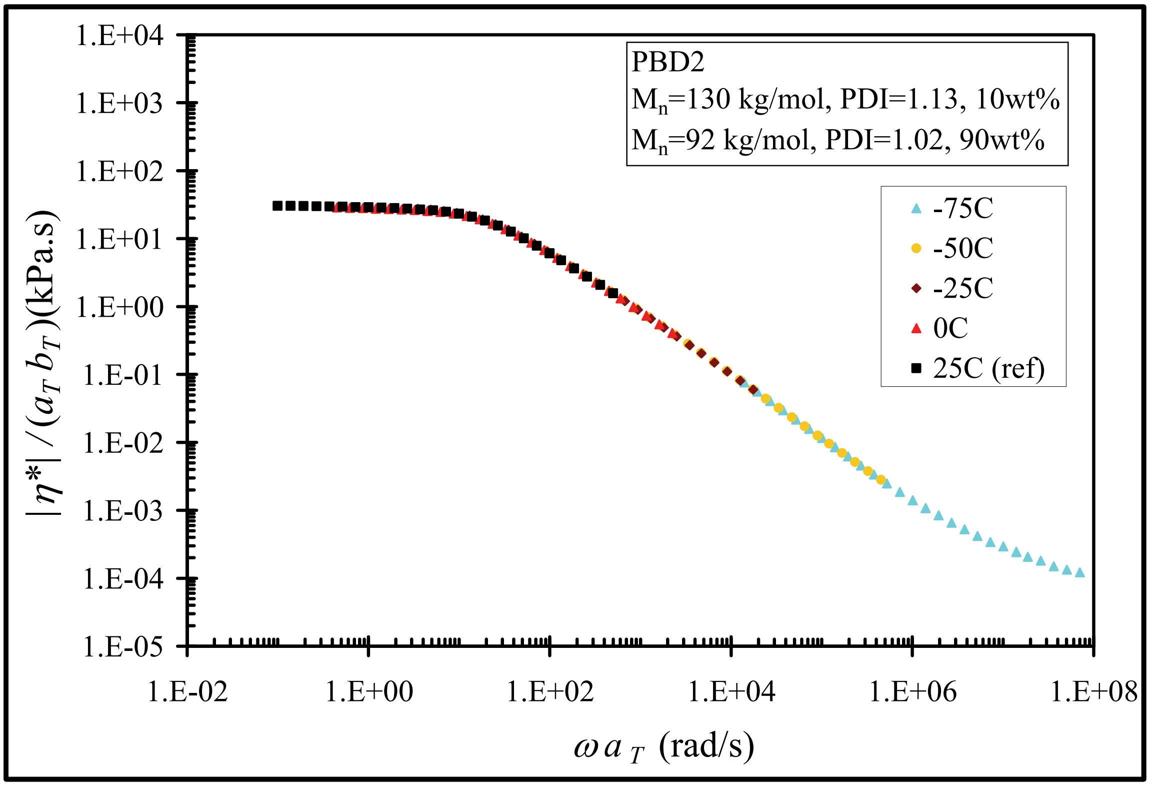

Figure 5.6 Complex viscosity of PBD2 shifted to T_{ref}=25°C

5.2 Moduli inferred from a retardation spectrum

Creep compliance data *J*(t) obtained by means of creep or creep/recovery experiments were used to infer a retardation spectrum by the nonlinear regression with regularization program (NLREG) (Freiburg Materials Research Center, version 2929, January 2, 2008) [132,148,149] as mentioned in section 4.1.2. This technique has been shown to yield moduli that are in excellent agreement with values obtained by SAOS for several polymers [6]. This algorithm is an iterative multi-data method that always gives positive retardation strengths having logarithmically equidistant retardation times. From the inferred retardation spectrum, the storage and loss compliance, and thus the storage and loss modulus, were calculated by use of Eqs. 4.5 to 4.8.

It is noted that for sample HA12B40 and HA40B40, transient data obtained from creep only experiments were used to construct the master curves of dynamic modulus and complex viscosity due to the non steady state of recoverable compliance at long time which was discussed in section 4.4.3.3.

5.3 Master curves of storage and loss moduli and complex viscosity

On master curves obtained by combining transient and dynamic data, data from the two techniques overlapped over at least two decades of frequency. To increase the overlap range, small amplitude oscillatory shear experiments were performed on some samples at 25^{o}C using the SR5K which is able to generate smaller torques and detect frequencies down to almost 10^{-3} rad/s. Modulus data obtained in this way overlapped with those from the ARES instrument over at least two frequency decades.

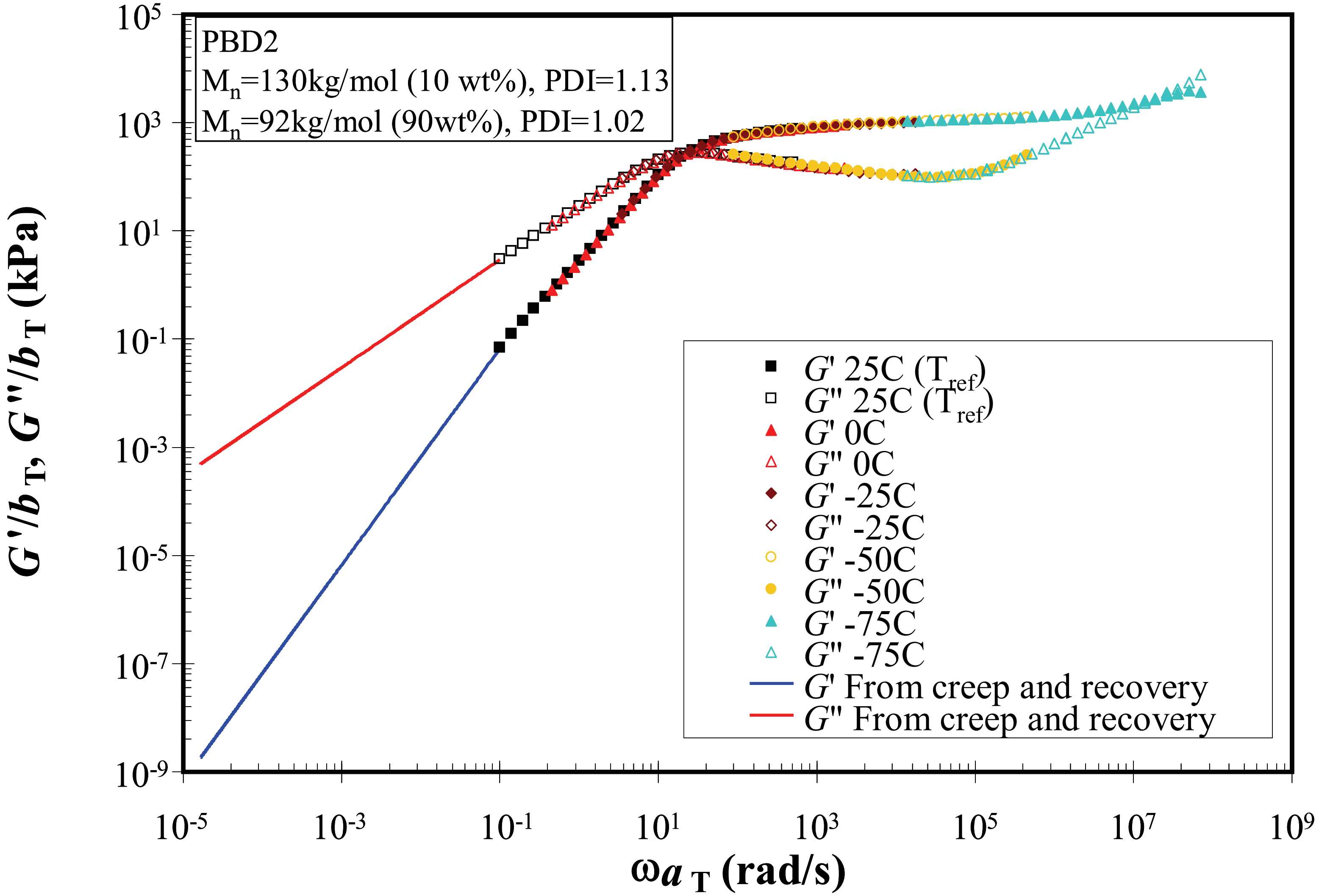

Figure 5.7 Master curves of storage and loss moduli for PBD2 at 25°C

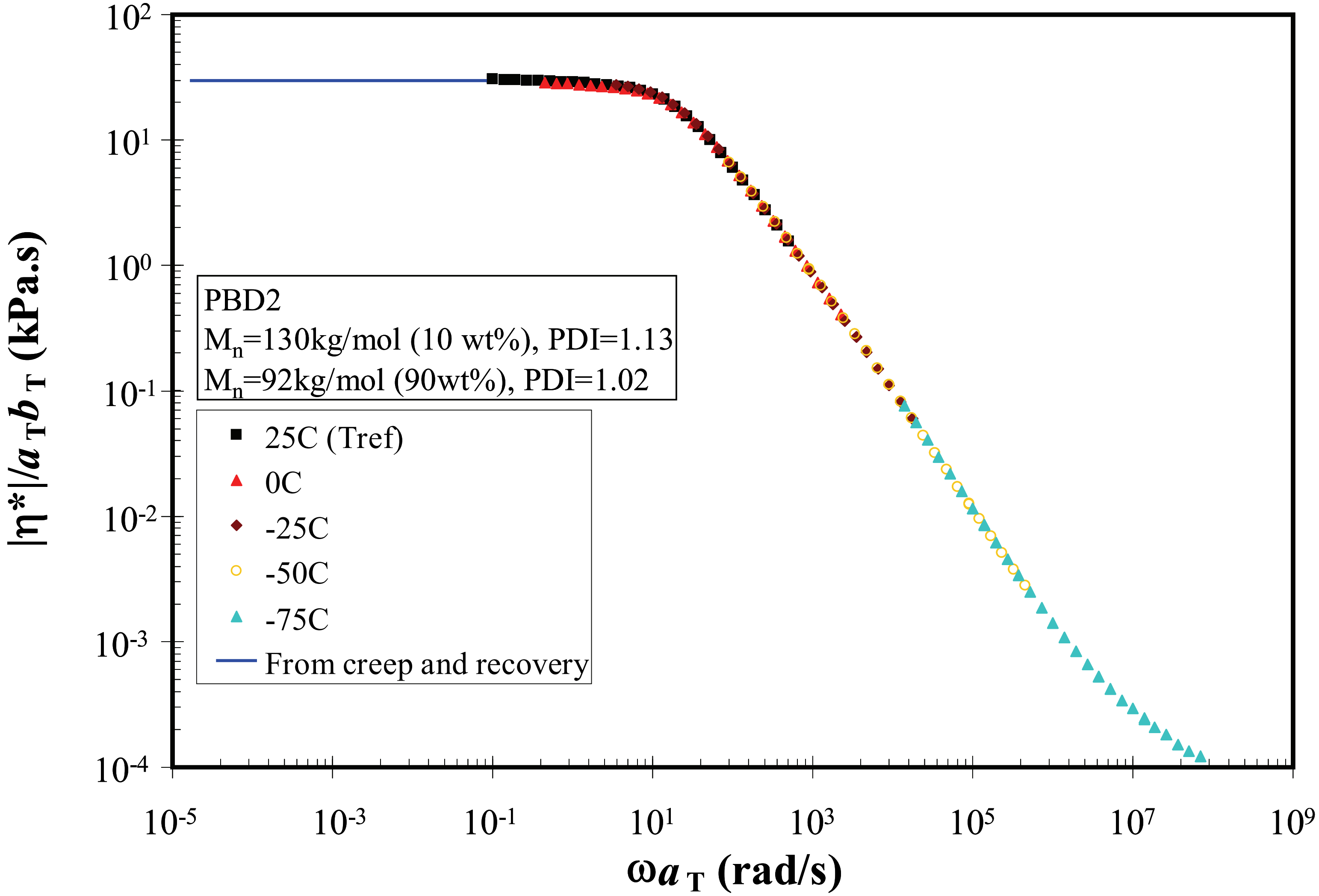

Figure 5.8 Complex viscosity master curve of PBD2 at 25°C

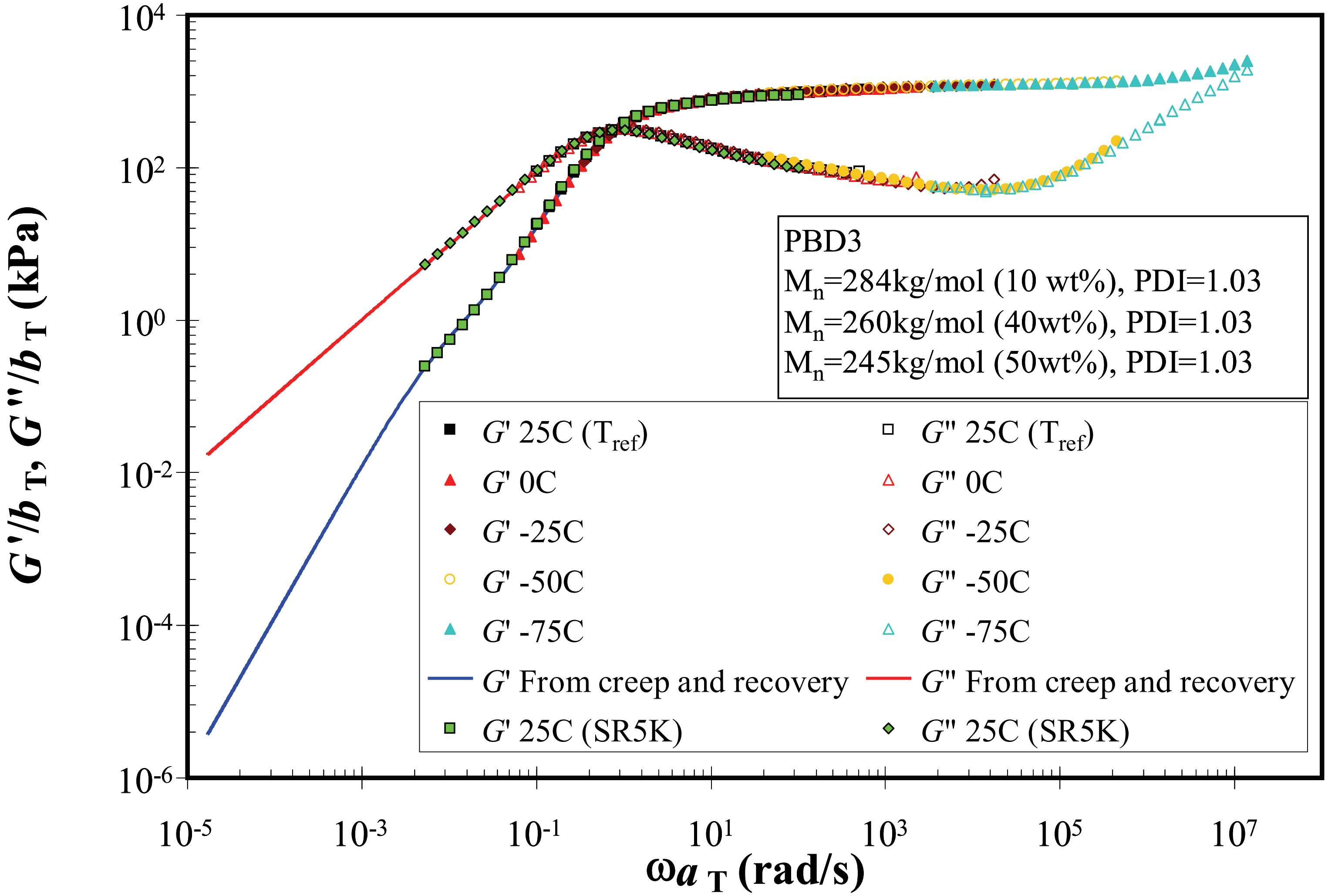

Figure 5.9 Master curves of storage and loss moduli for PBD3 at 25°C

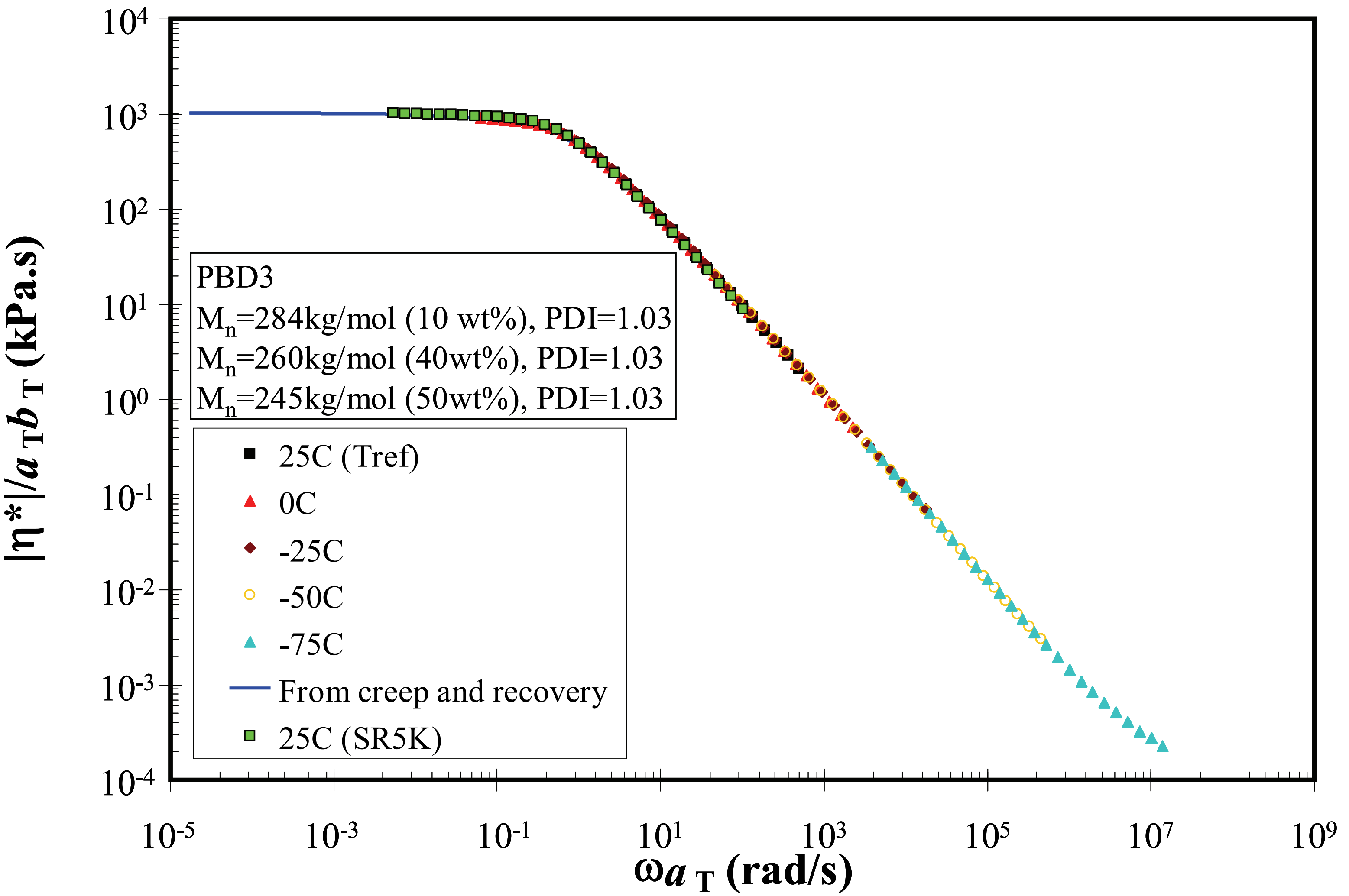

Figure 5.10 Complex viscosity master curve of PBD3 at 25°C

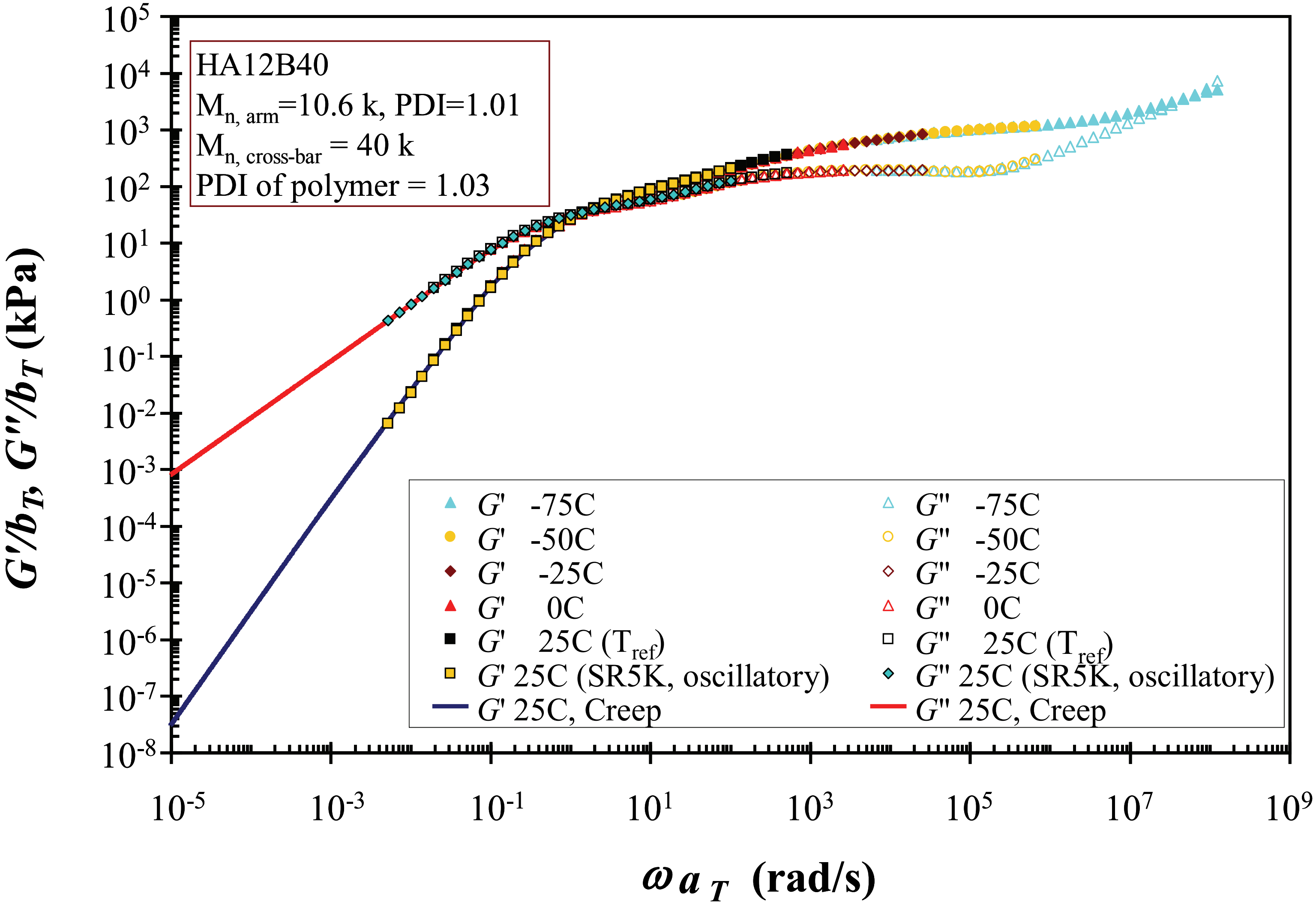

Figure 5.11 Master curves of storage and loss moduli for HA12B40 at 25°C

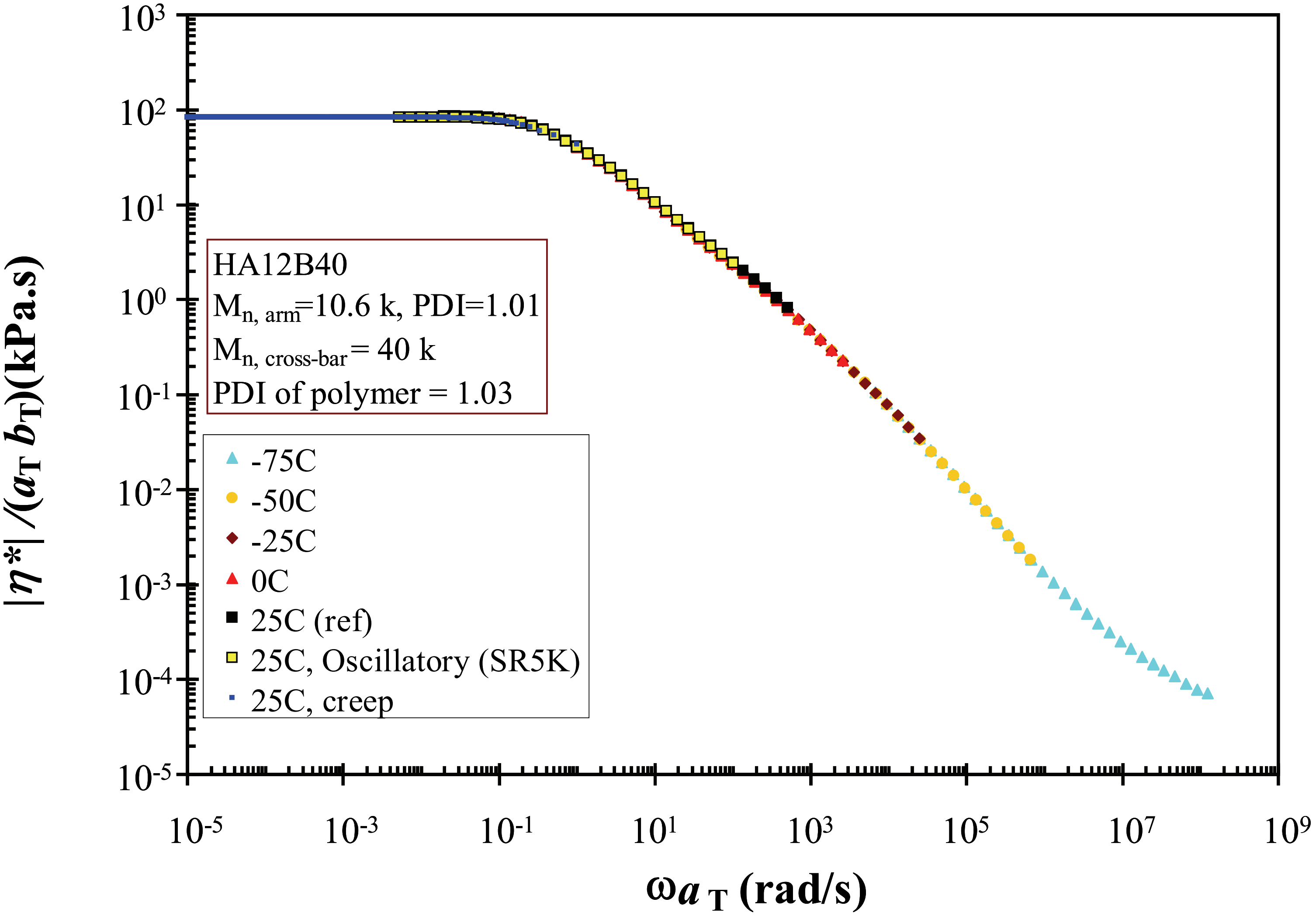

Figure 5.12 Complex viscosity master curve of HA12B40 at 25°C

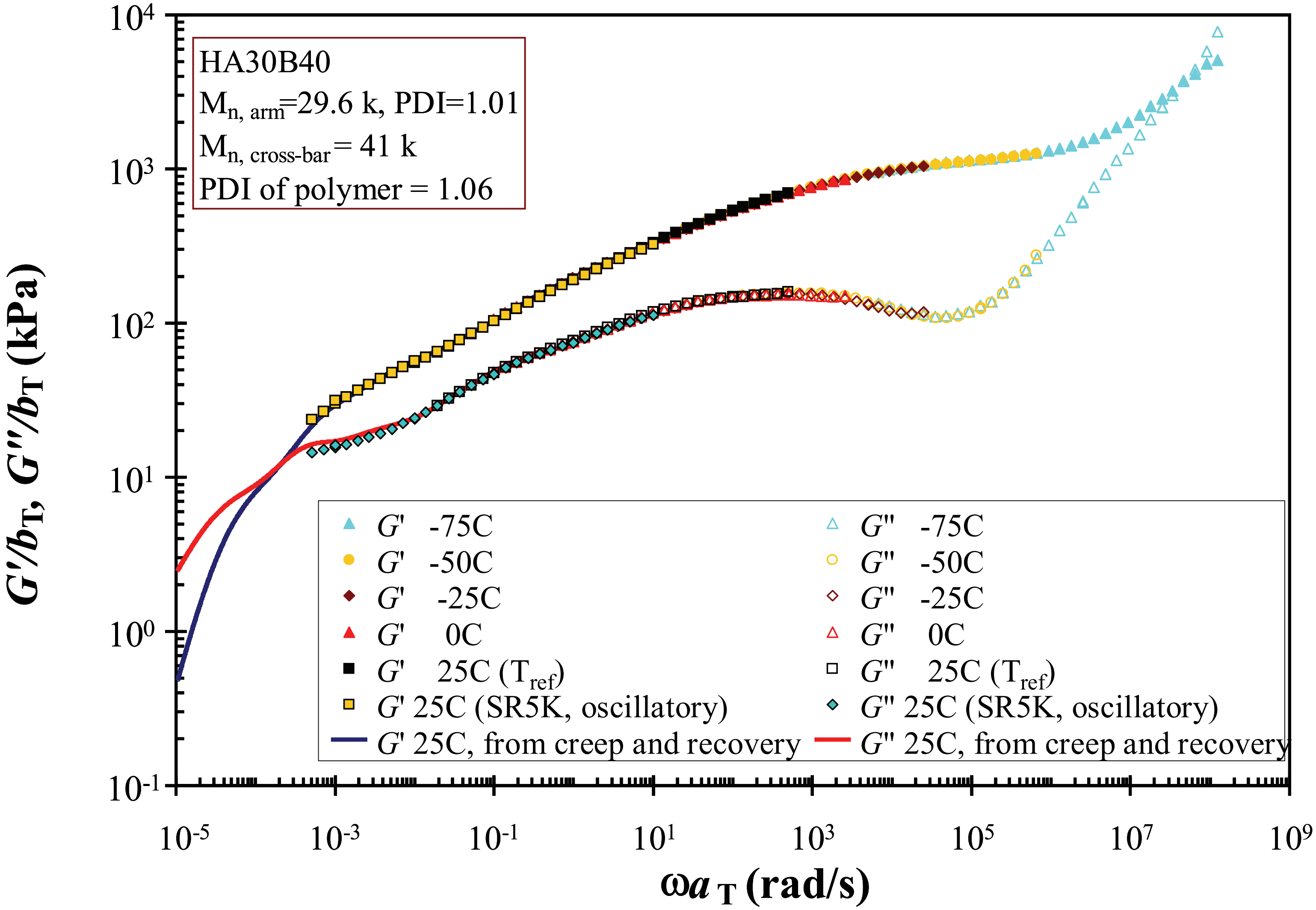

Figure 5.13 Master curves of storage and loss moduli for HA30B40 at 25°C

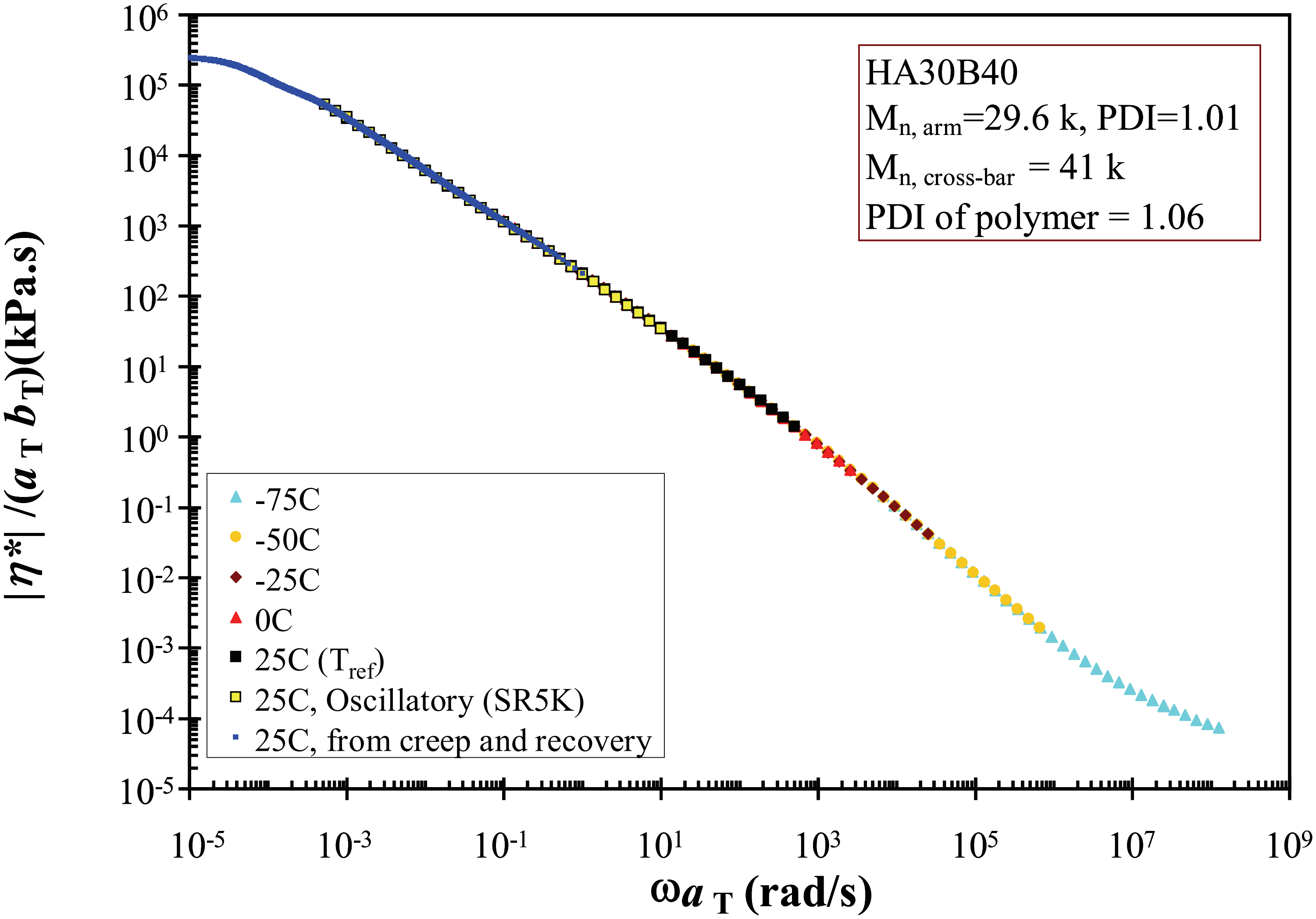

Figure 5.14 Complex viscosity master curve of HA30B40 at 25°C

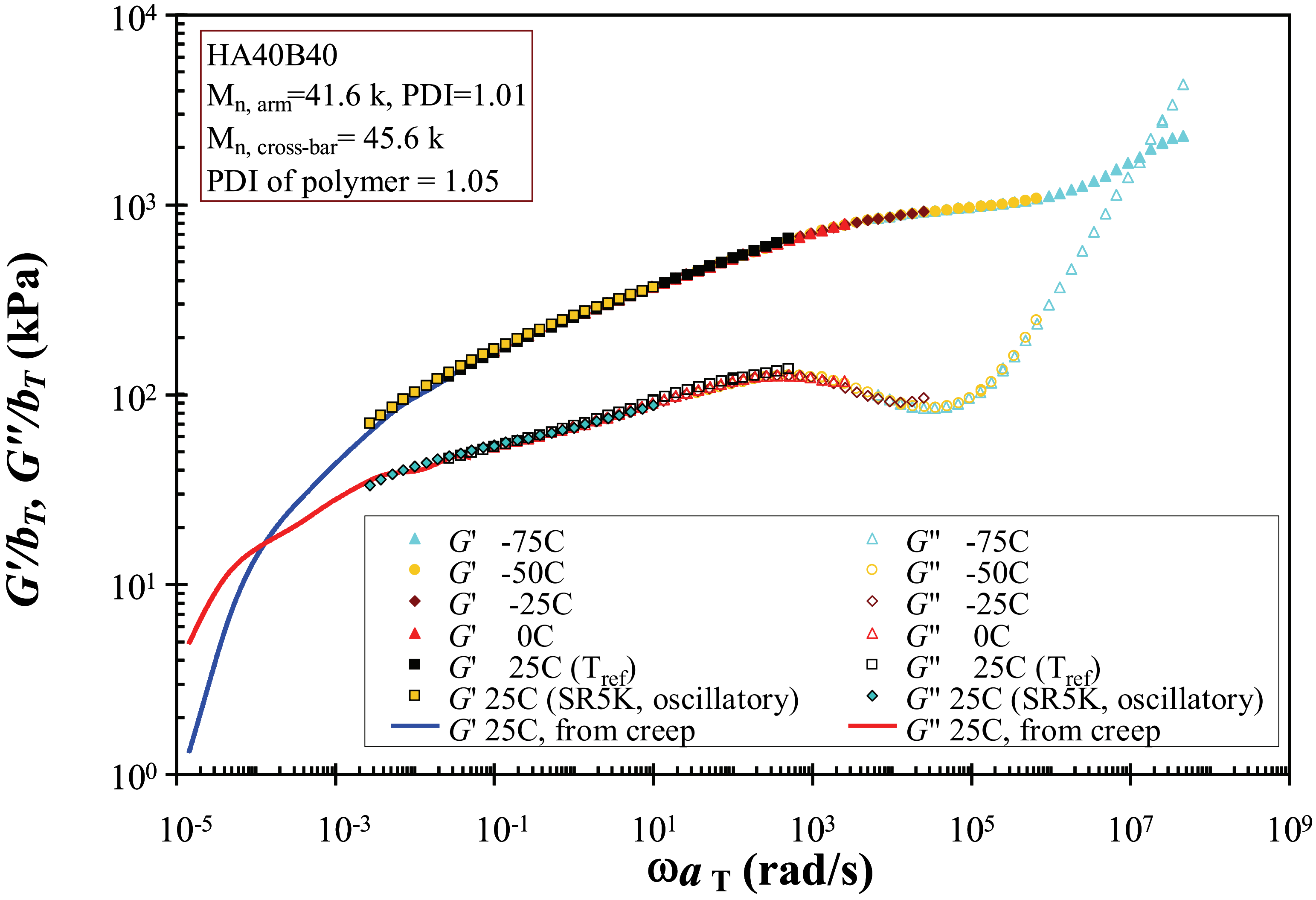

Figure 5.15 Master curves of storage and loss moduli for HA40B40 at 25°C

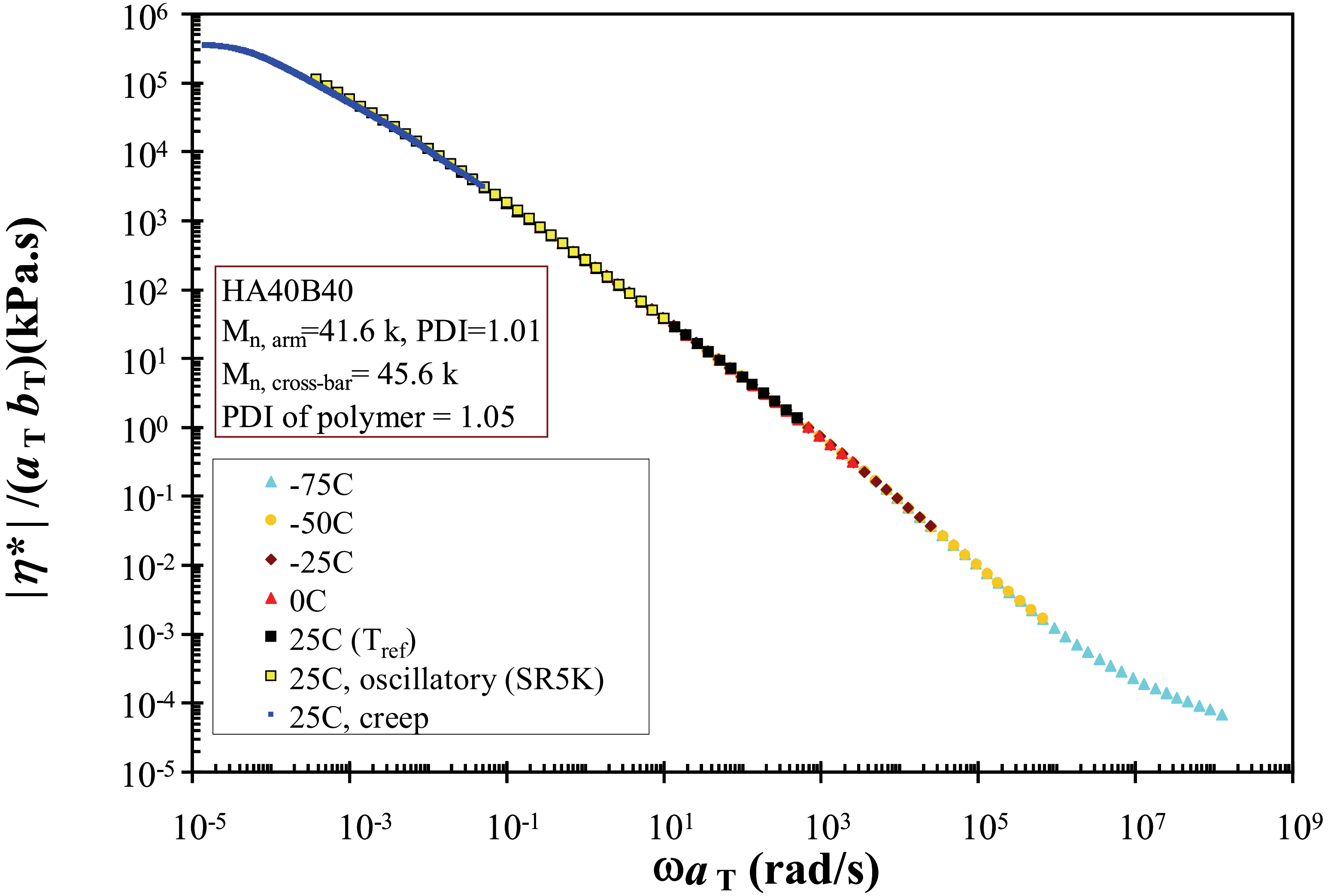

Figure 5.16 Complex viscosity master curve of HA40B40 at 25°C

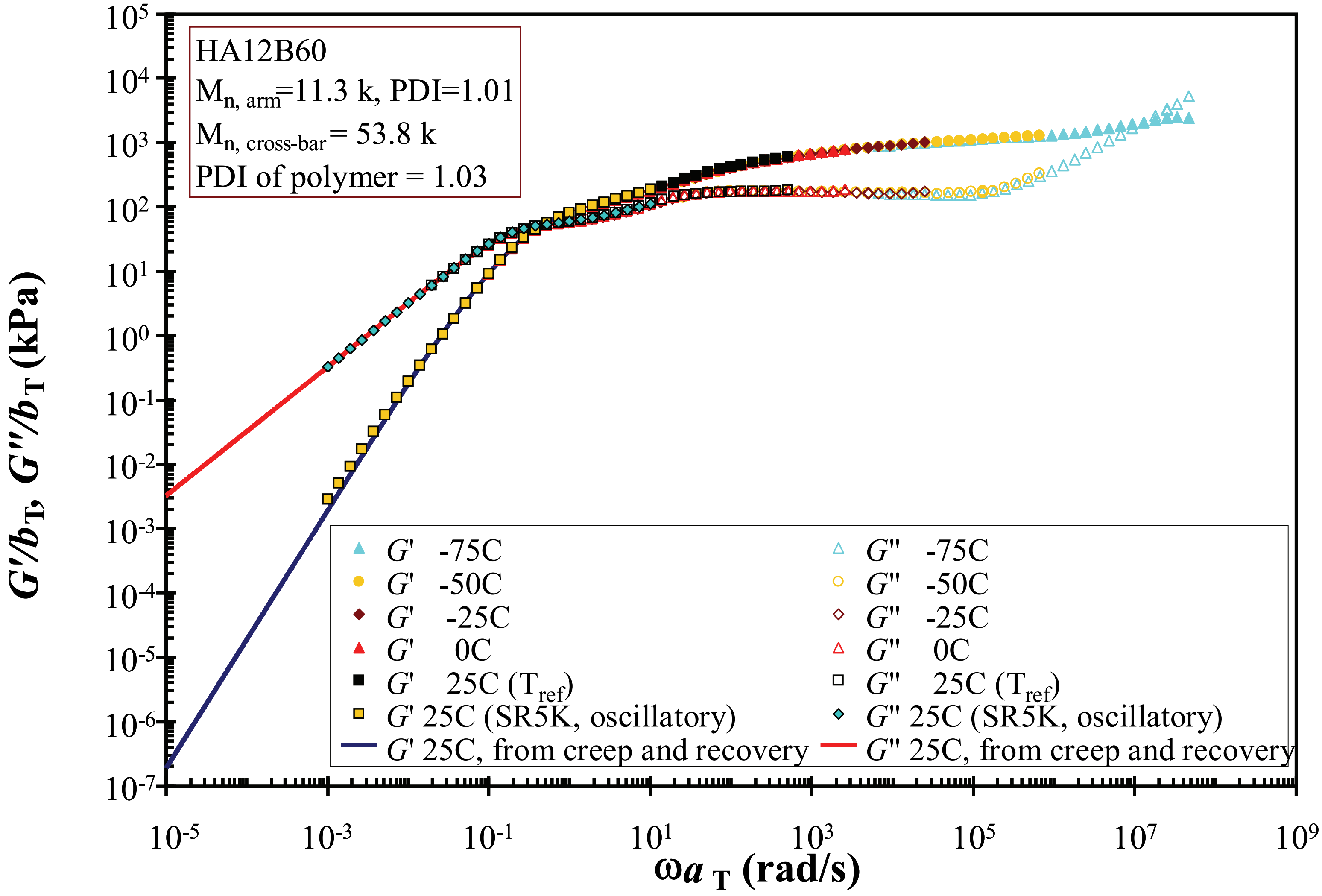

Figure 5.17 Master curves of storage and loss moduli for HA12B60 at 25°C

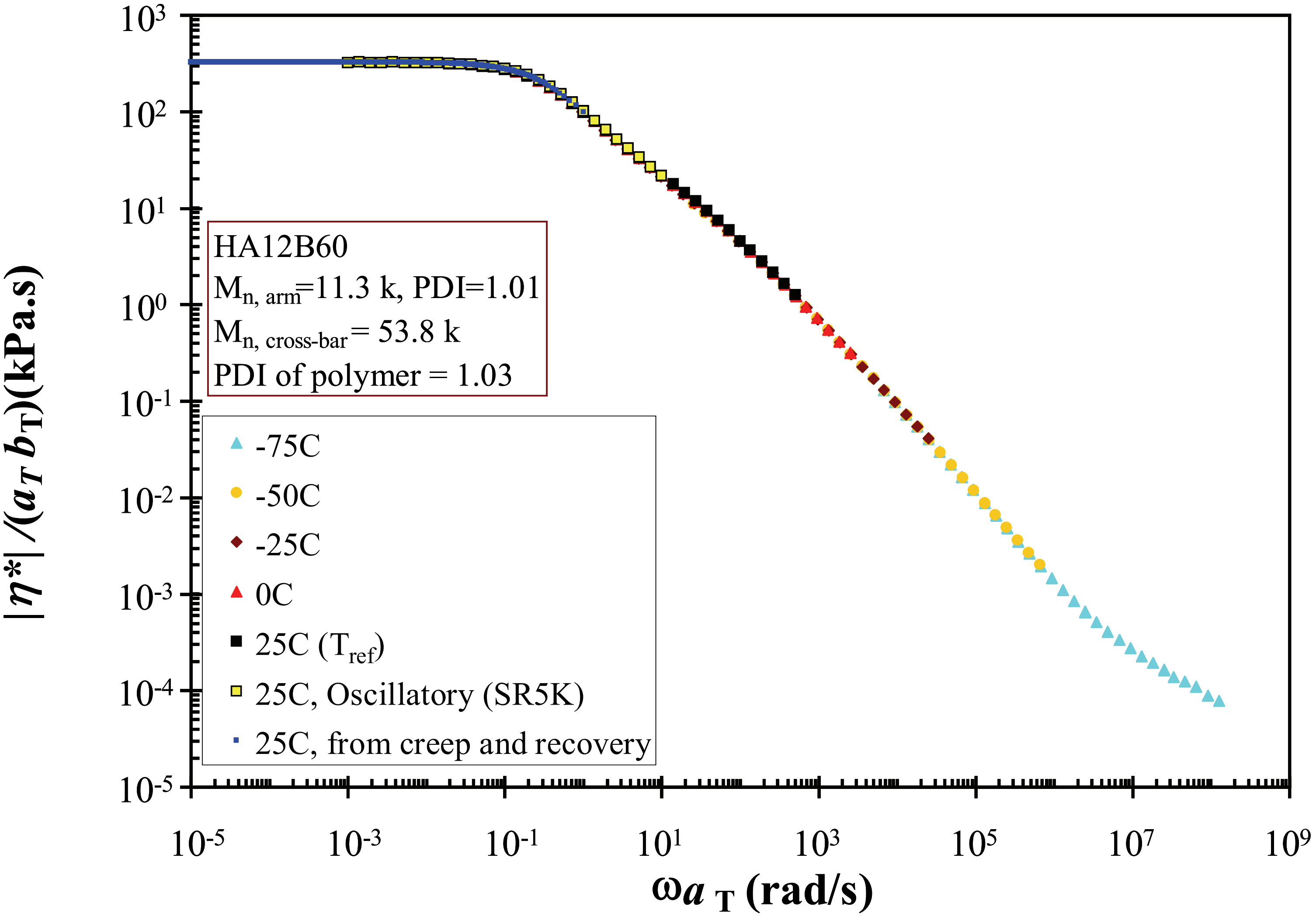

Figure 5.18 Complex viscosity master curve of HA12B60 at 25°C

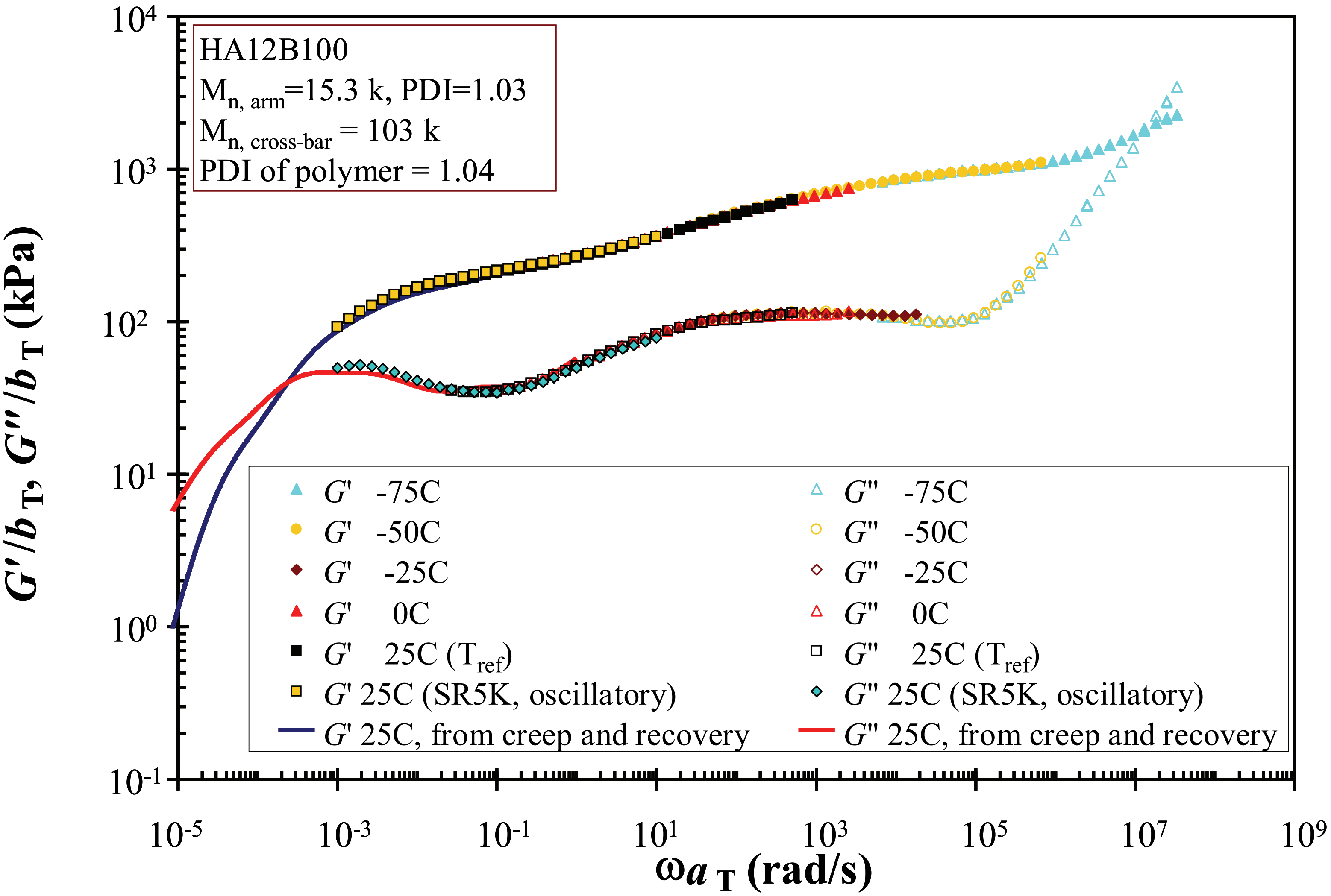

Figure 5.19 Master curves of storage and loss moduli for HA12B100 at 25°C

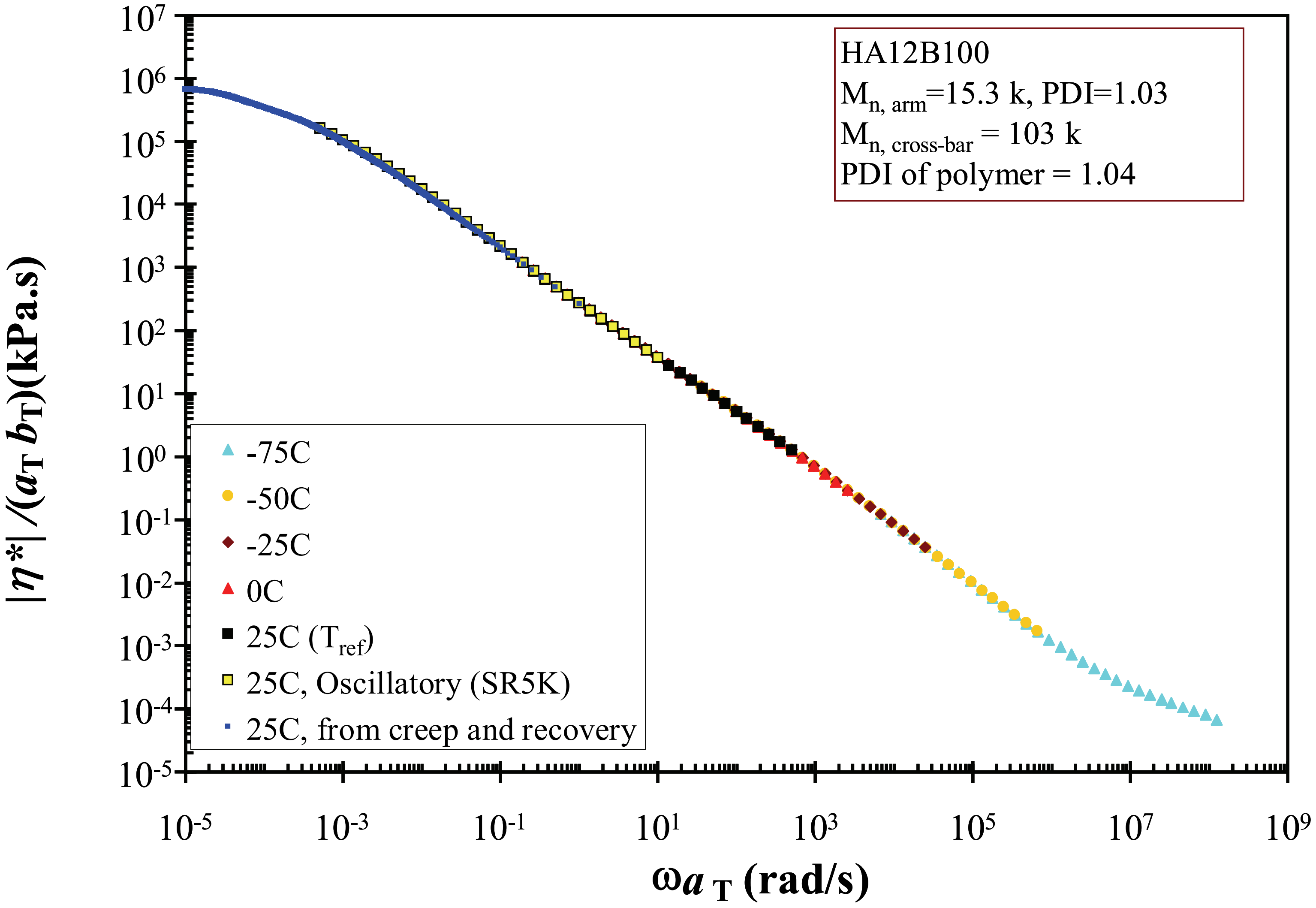

Figure 5.20 Complex viscosity master curve of HA12B100 at 25°C

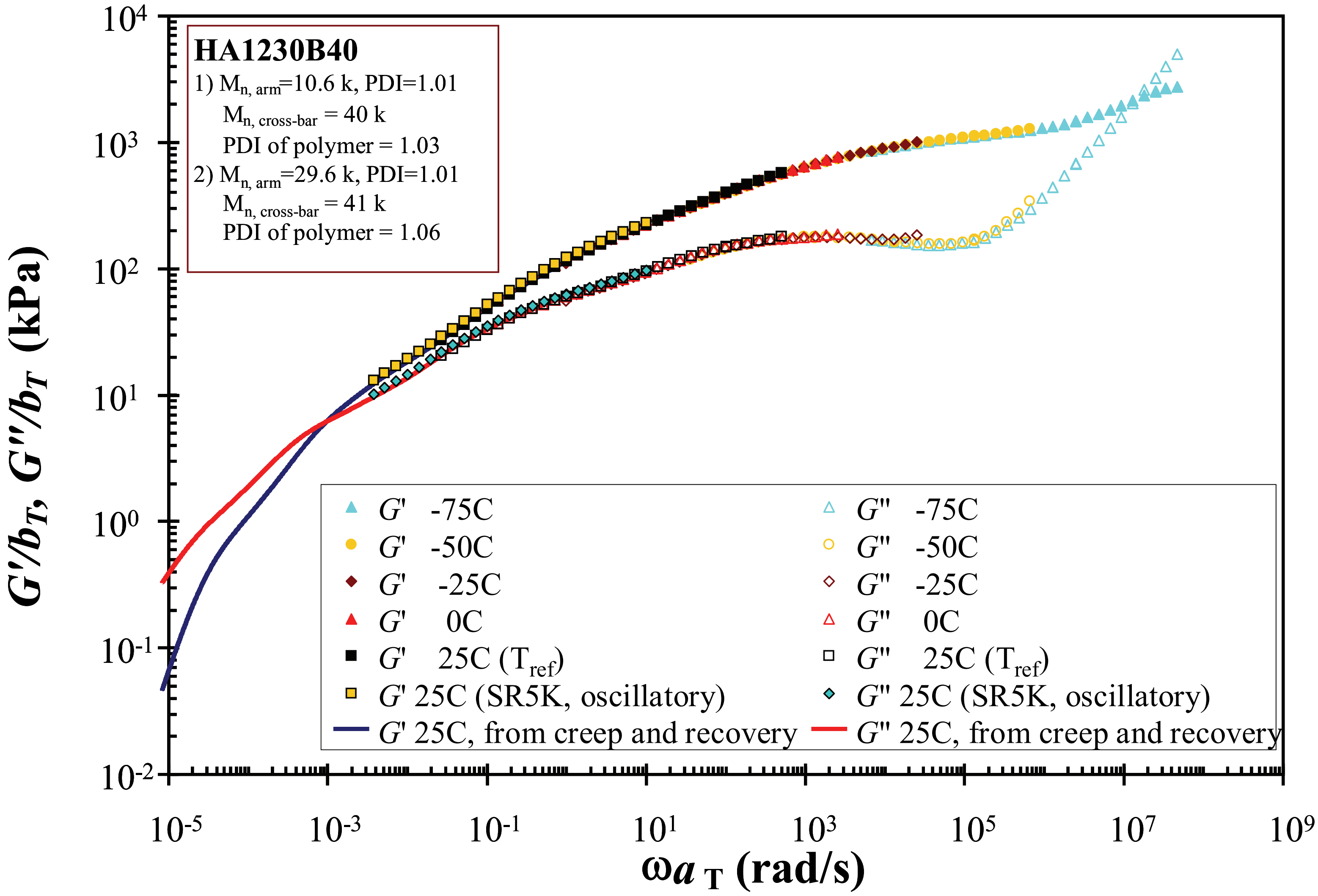

Figure 5.21 Master curves of storage and loss moduli for HA1230B40 at 25°C

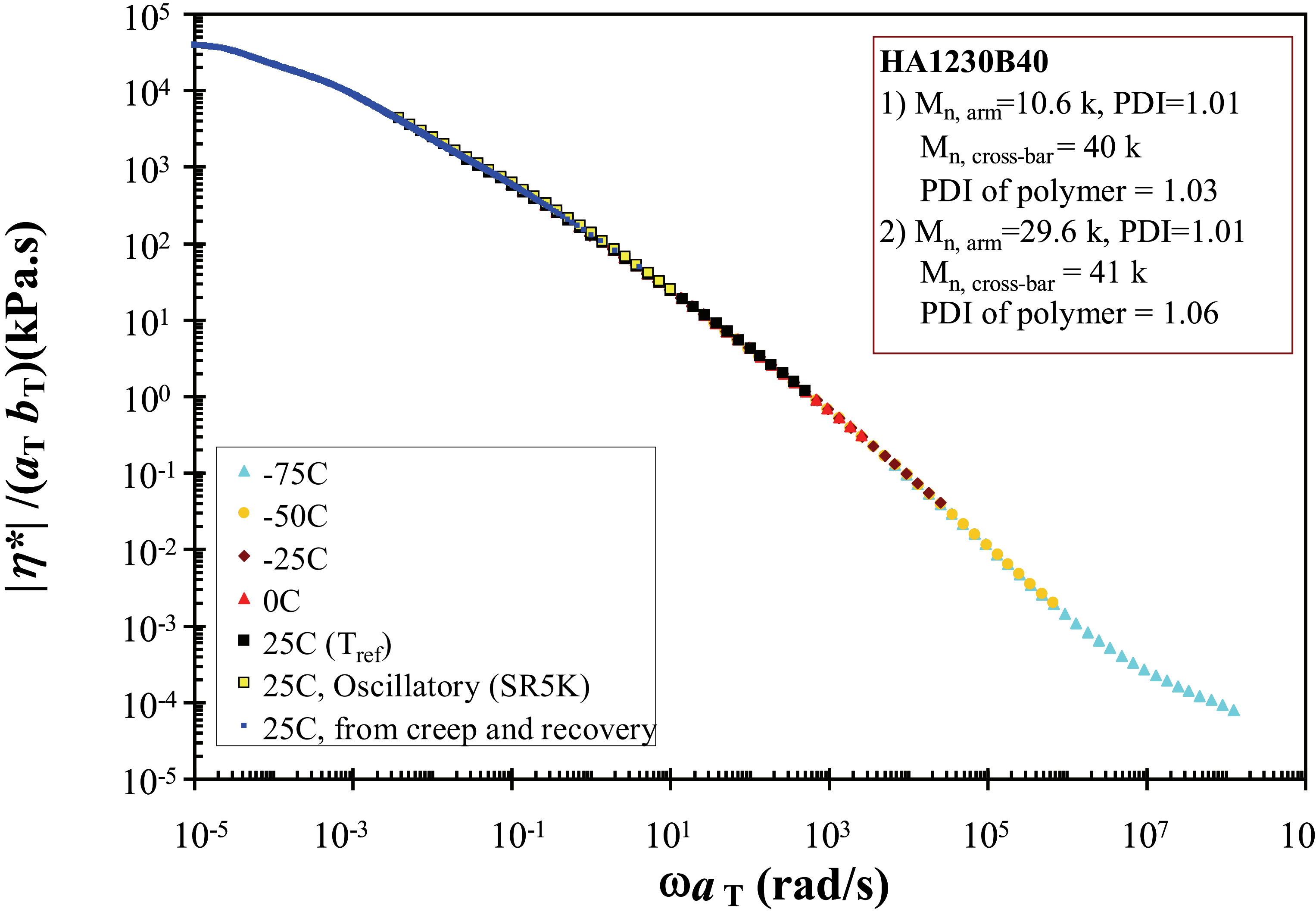

Figure 5.22 Complex viscosity master curve of HA1230B40 at 25°C

5.4 Estimation of material constants - G_N^0, η_0 and J_s^0

The values of G_N^0, η_0 and J_s^0 estimated from raw data by methods described in section 4.4.5 are summarized in Table 5.1.

Table 5.1 Material constants of linear PBDs blends and H-shaped PBDs estimated from raw data at T_{ref}=25°C

Sample	G_N^0 (MPa)	η_0 (Pa.s)	J_s^0 (Pa^{-1})
PBD2	1.06	2.97×10^4	N/A
PBD3	1.17	1.03×10^6	N/A
HA12B40	1.05	8.34×10^4	N/A
HA30B40	1.1	2.32×10^8	5.32×10^{-5}
HA40B40	0.94	3.94×10^9	4.78×10^{-5}
HA12B60	1.13	3.25×10^5	N/A
HA12B100	0.97	8.50×10^8	3.04×10^{-5}
HA1230B40	1.08	3.51×10^7	7.10×10^{-4}

Compared with literature data on various linear monodisperse PBDs, G_N^0 determined from the minimum phase angle (Eq. 4.13) has a range from 1.13 to 1.18 ± 0.07 MPa [46]. The linear PBDs studied in this project show similar results with G_N^0 range from 1.12 ± 0.06 MPa as determined by the same method. According to Eq. 1.11, the average entanglement molecular weight for the linear PBDs blends is M_e = 1600g/mol, which is within ±10% of reported values by Fetters et al. [150]. For H-shaped PBDs, the average G_N^0 is 1.05 ± 0.12 MPa which gives an average M_e = 1700g/mol. The estimated values of G_N^0 as shown in Table 5.1 are then used in evaluating two tube-based models in Chapter 6. More details in estimating G_N^0 by other methods can be found in Appendix F, which includes a composition rule with vinyl content [151], an empirical relationship with packing length [152] and crossover-modulus [153], as well as determination from Van Gurp-Palmen- Plot [144].

As introduced in Chapter 1, η_0 has a strong dependency on molecular weight (M) for entangled linear polymer melts. Several empirical relationships of M-η_0 have been developed, such as the power law relationship which is particularly useful for linear polymers. Comparison of η_0 for linear PBDs with literature data is given in section 5.5. However, there is little experimental data available for H-shaped PBD at a sufficiently low shear rate such that the viscosity is constant [41].

J_s^0 as determined by best fitting the raw data *J*(t) is very sensitive to the attainment of steady state at long time and is prone to severe extrapolation error. We noted a negative J_s^0 in a few samples, suggesting this method is not appropriate to provide a good estimation for our samples. In addition, the tube-based models evaluated in this project (Chapter 6) has no use of J_s^0, therefore, no further discussion of J_s^0 is included in this Chapter. Nevertheless, details in estimating J_s^0 by other methods that use data inferred from the raw data *J*(t) can be found in Appendix F.

5.5 Effects of molecular weight on rheological properties of linear PBDs

When comparing the master curves of PBD2 and PBD3 as shown in Fig. 5.23, the width of the plateau region depends strongly on molecular weight whereas high molecular weights broaden the plateau region but the values of G_{N}^0 is essentially independent of molecular weight. The presence of the fairly flat plateau region on a log-log plot indicates the rubber-like elastic properties in the intermediate frequency region. It is noted that although PBD2 and PBD3 are actually blends of linear PBDs (*i.e.* polydisperse PBDs), the values of G_{N}^0 are in good agreement with the literature data of linear monodisperse PBDs as discussed in section 5.4. This confirmed that G_{N}^0 is independent of molecular weight distribution for linear polymers.

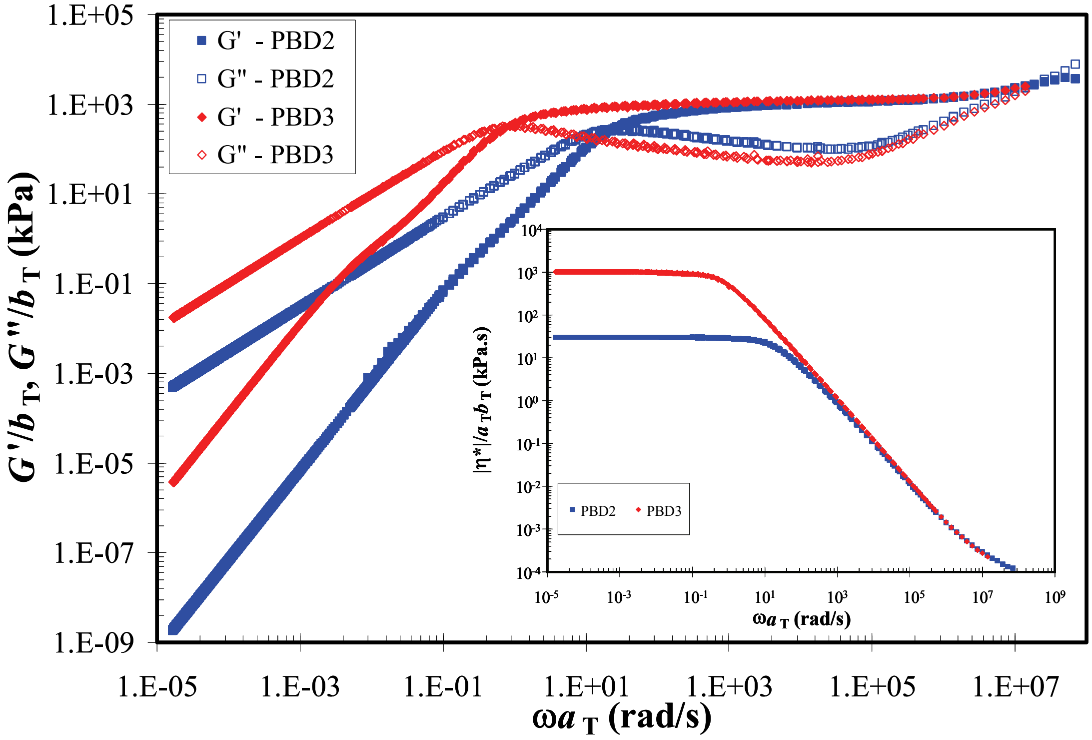

Figure 5.23 Comparison of properties of PBD2 and PBD3 at 25°C

In general, for polymer chains beyond a critical molecular weight, M_c, which is approximately equal to $2.5M_e$ (*i.e.* ~5000g/mol for PBD) [154], η_0 has a power law dependence on the weight-average molecular weight (M_w) with a power law index *a* commonly found to be 3.5 ± 0.2. Colby *et al.* [147] used a series of narrow distribution polybutadienes with low vinyl content to test the range of validity of the 3.4 power law, and significant departures from 3.4 were observed beyond M/M_e~200. Also, there is controversy centered on the value of *a* for a specific polymer because there are huge variations between values reported by different groups for the same chemistry and structure as shown in Fig. 5.24. Until more studies on linear PBD blends, we cannot conclude the dependence of η_0 on M_w for the linear PBD blends studied in this project.

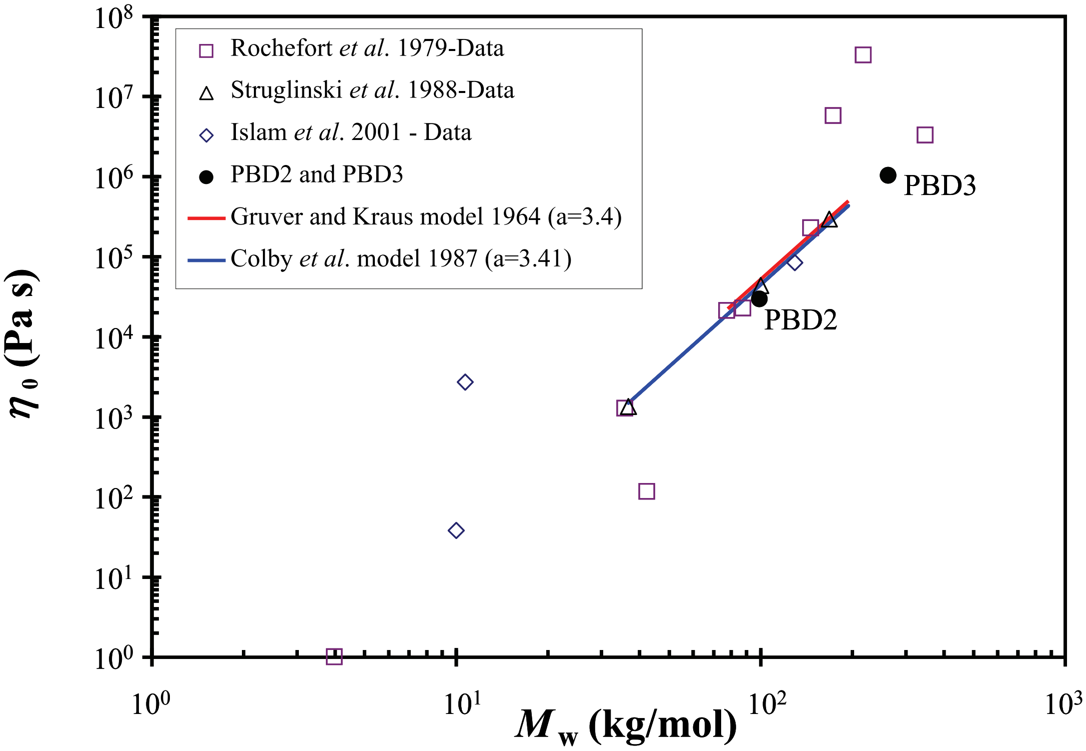

Figure 5.24 Comparison of η_0 values of PBD2 and PBD3 with those reported in the literature for linear monodisperse polybutadienes at T=25°C

5.6 Effects of LCB on rheological properties

The dynamic moduli-frequency curves of the H-shaped PBDs are quite different from those of the linear PBD blends although they merge together in the high frequency Rouse regime despite different structures as shown in Fig. 5.25. For linear PBD blends, a fairly flat plateau region is seen in the intermediate frequency range. For H-shaped PBDs, the region is much broader than those of the linear polymers and is less well defined, which exhibits a "shoulder" feature in $G''(\omega)$ and a maximum in $G''(\omega)$ near the cross-over frequency ω_c . Both the "shoulder" feature and a maximum on $G''(\omega)$ near ω_c are obvious rheological signatures as expected for entangled H-shaped polymers [20-22,115,118]. As mentioned by McLeish *et al*.[21], the dynamic moduli-frequency curve contains features of both star and linear polymers, represented by a broad shoulder in $G''(\omega)$ and a well-defined peak in $G''(\omega)$ at the inverse of relaxation time of arms and cross-bar, respectively. The prominent features on $G''(\omega)$ suggested that there are more than one relaxation mechanisms for the H-shaped PBDs.

Values of G_N^0 of H-shaped PBDs is essentially identical to that of linear PBDs estimated by the same method, which suggested that G_N^0 is fairly independent of the presence of long chain branching. Although the presence of LCB did not affect the value of G_N^0, it did broaden the plateau region and changed the curvatures of $G'(\omega)$ and $G''(\omega)$ in the plateau region.

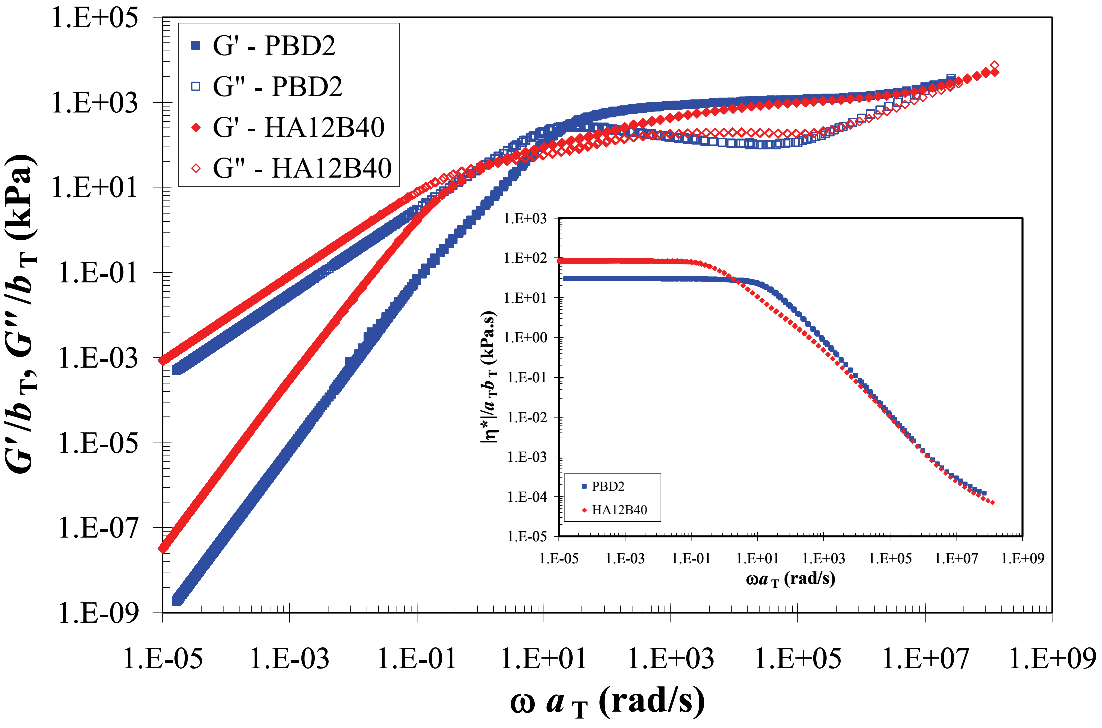

Figure 5.25 Comparison of properties of PBD2 and HA12B40 at 25°C

When comparing η_0 of linear PBDs blends with H-shaped PBDs under the same total weight-average molecular weight, M_w, the presence of LCB shows a drastic increase of η_0 as shown in Fig. 5.25. The η_0 enhancement on H-PBDs compared to linear PBDs blends can be explained in terms of relaxation mechanism differences among the two structures. A plot of loss tangent versus reduced frequency at reference temperature (i.e.

tan δ versus ωa_T) is shown to be more sensitive in distinguishing features of the relaxation process [33]. As shown in Fig. 5.26 and Appendix E, the collapse of high-frequency data into one curve confirms the data quality, as molecular movement at high frequencies is limited to local transitional Rouse-like and segmental glassy motions which have no molecular weight or structural dependency. For PBD2, only one minimum is seen in tan δ which marks the onset of chain relaxation by reptation, which is a slow relaxation process that molecule escapes from its imaginary tube by sliding back and forth in it only [52]. While for HA12B40, two local minima are seen in tan δ, as indicated by the arrows in Fig. 5.26, suggested more than one relaxation mechanisms are taking place. Since the cross-bar is topologically constrained up by the attached arms at both ends, it can relax only until the attached arms have fully relaxed. Thus, the intermediate frequency minimum in tan δ indicates the onset of arms relaxation by primitive path (or contour length) fluctuations which is a process that rapidly relax the ends of the chain due to Brownian motion [55,56,155], while the lower frequency minimum in tan δ indicates the onset of cross-bar relaxation by reptation.

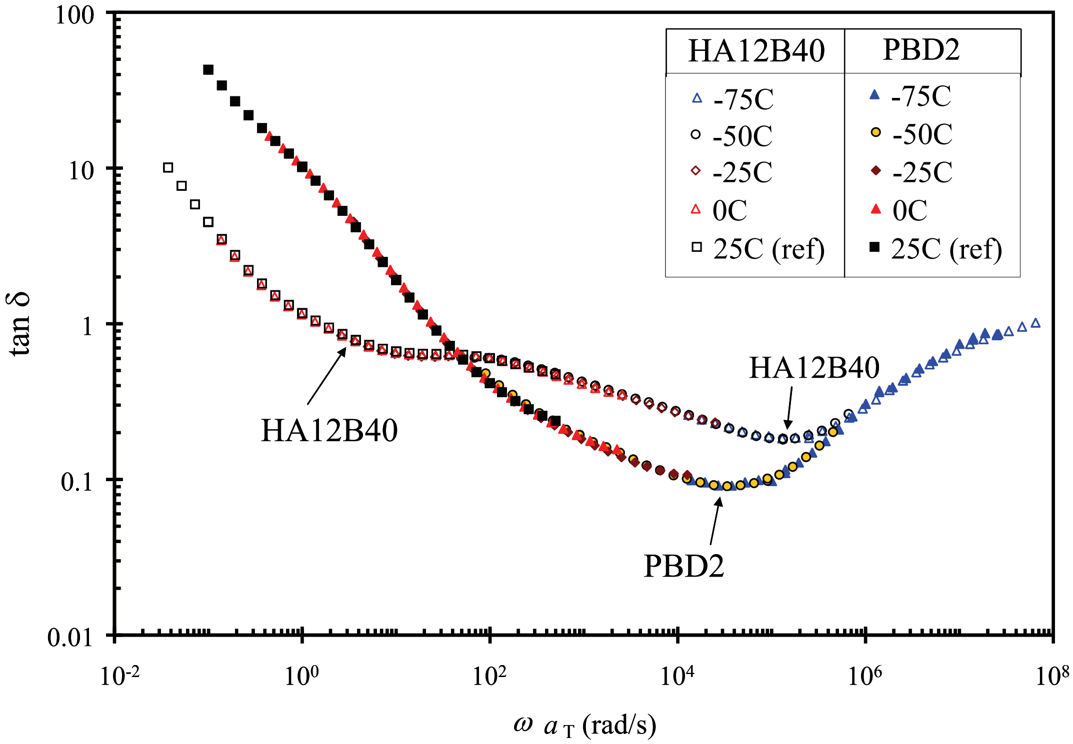

Figure 5.26 Comparison of loss tangent of PBD2 and HA12B40 at 25°C

5.7 Effects of cross-bar length on rheological properties of H-shaped PBDs

At high frequencies where molecular movement has no dependency on molecular weight or molecular structure, the dynamic modulus of HA12B40, HA12B60 and HA12B100 collapse into one curve despite different cross-bar lengths as shown in Fig. 5.27. Moving down to the intermediate frequencies, an increase in cross-bar length did broaden the plateau region but not the values of G_N^0 as seen in Table 5.1. The low frequency peak on $G''(\omega)$ that was responsible for the cross-bar relaxation was shifted to lower frequencies with a longer cross-bar. The magnitude of this peak also increased as the volume fraction of cross-bar increased, and thus contributed to the dynamic modulus. It is observed that for H-shaped polymers with highly entangled cross-bar, this peak is better defined (*e.g.* HA12B100).

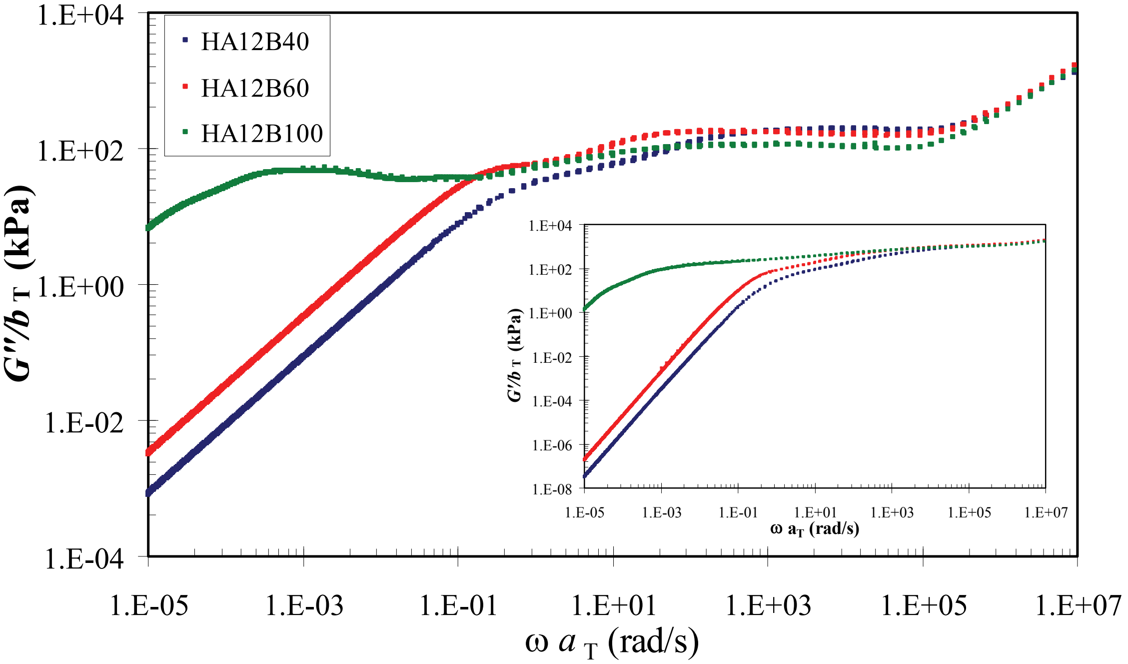

Figure 5.27 Comparison of moduli of H-shaped PBDs having equal arm length but various cross-bar lengths

It is noted that η_0 increased drastically as shown in Fig. 5.28 and in Table 5.1 when arms lengths were essentially the same but cross-bar length increased. As observed by Roovers [20] and Archer *et al.*[39] on H-shaped Polystyrene and Polyisoprenes, respectively, η_0

increased exponentially with arm lengths. It suggested that the relaxation mechanisms of cross-bars and arms are not the same with the relaxation mechanism of cross-bar being a much slower process than that of arms.

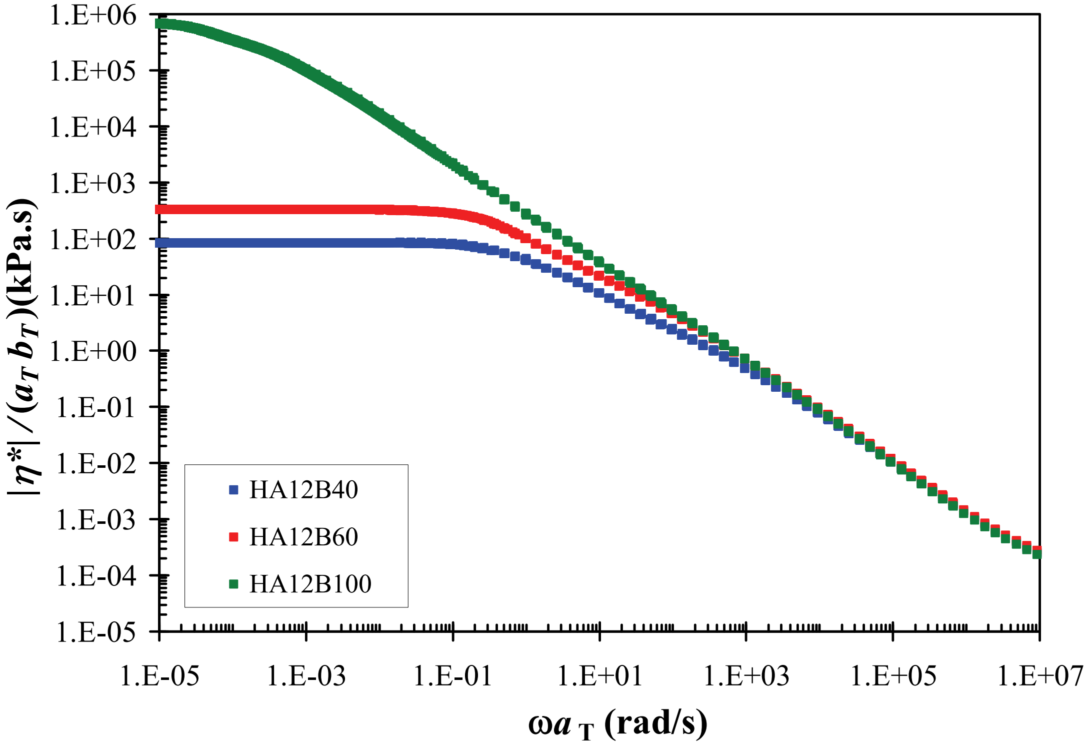

Figure 5.28 Comparison of η_0 of H-shaped PBDs having equal arm length but various cross-bar lengths

5.8 Effects of arm length on rheological properties of H-shaped PBDs

The prominent "shoulder" feature as shown in $G''(\omega)$ was a clear signature of arm relaxation, increasing the arm length but keeping the cross-bar length the same increased this shoulder width as shown in Fig. 5.29 for sample HA12B40, HA30B40 and HA40B40. It also smeared out the maximum peak in $G''(\omega)$ which corresponded to cross-bar relaxation due to an increase in volume fraction of the arm segment. Despite widening the transition from plateau to terminal region, there was no obvious change on the value of G_N^0 with different arm length. Similar to the effect of an increase in cross-bar lengths, there is a drastic enhancement on η_0 with longer arm lengths.

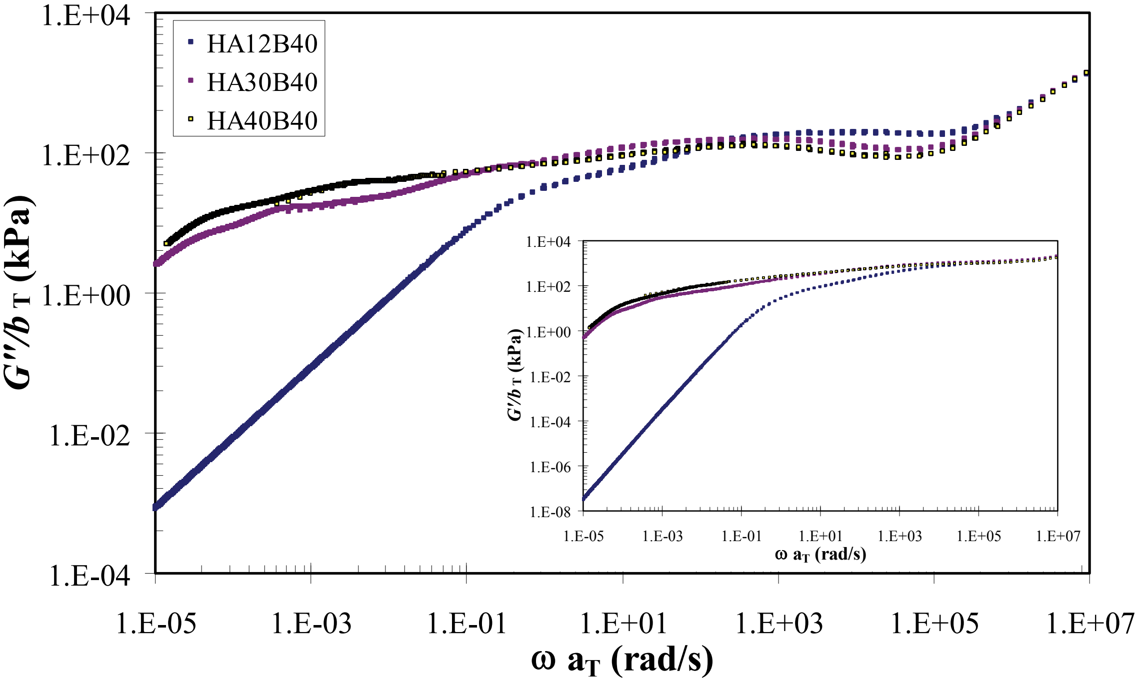

Figure 5.29 Comparison of moduli of H-shaped PBDs having equal cross-bar length but various arm lengths

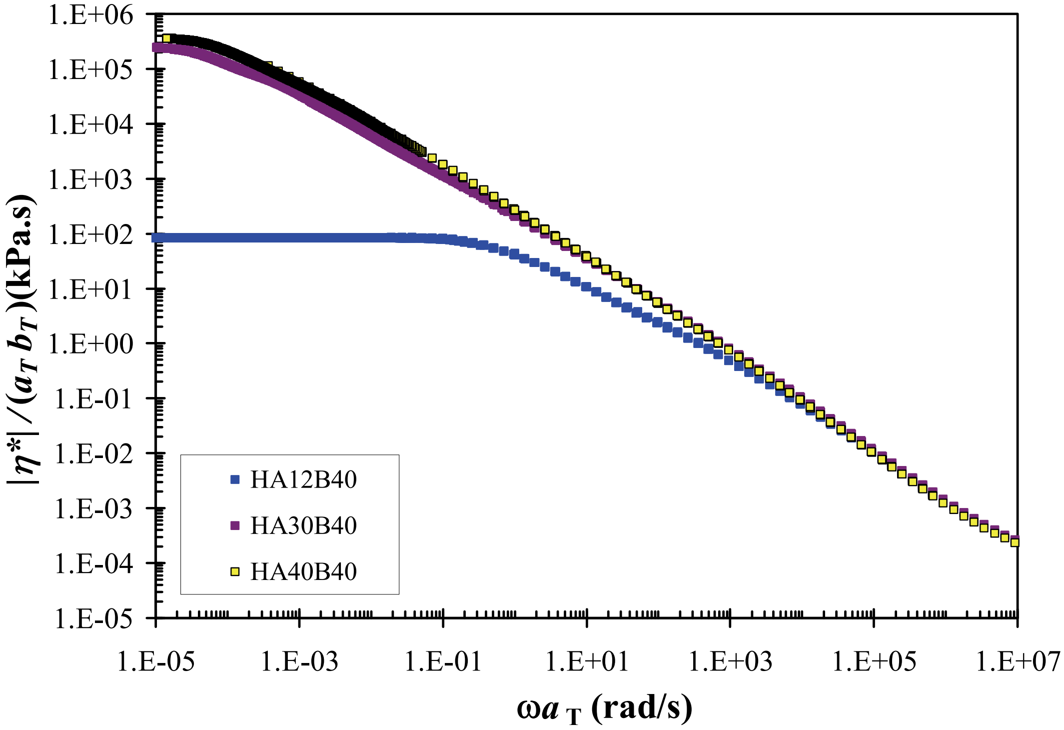

Figure 5.30 Comparison of η_0 values of H-shaped PBDs having equal cross-bar length but various arm lengths

The qualitative effect of arm length on the overall polymer relaxation behavior can also be seen by comparing the crossover frequencies ω_c as listed in Table 5.2 [39], where $G_c = G'(\omega) = G''(\omega)$. When comparing HA12B40 with HA30B40, where these two samples have the same cross-bar length but arm lengths differed by a factor of 3, ω_c was found to decrease by four orders of magnitude. Similar result was found when comparing HA12B40 with HA40B40. Again, this is due to the fact that relaxation of cross-bar is a much slower process than the relaxation of arms.

Table 5.2 Crossover frequencies and crossover modulus on H-PBDs with equal cross-bar length

Sample	ω_c **(rad/s)**	***G***
HA12B40	1.39E+00	34.9
HA30B40	1.64E-04	10.9
HA40B40	1.11E-04	16

5.9 Effects of polydispersity of arms on rheological properties

A binary blend of H-PBD (HA1230B40) composed of an equimolar mixture of HA12B40 and HA30B40, where these two samples differed only in the arm lengths, was purposely prepared by solution blending to study the effects of polydispersity of arms in H-shaped polymers. HA1230B40 is expected to have the broadest molecular weight distribution among the other H-shaped samples. It is interesting to note that by incorporating 34 wt% of HA12B40 to HA30B40 in making the equimolar blend, which is essentially diluting the highly entangled HA30B40 by adding the less entangled HA12B40, η_0 of the blend is around 7 times smaller than that of HA30B40 as shown in Fig. 5.32. The dynamic modulus – frequency curve of HA1230B40 is very similar to that of HA30B40, except the terminal behavior shows up earlier than HA30B40 as shown in Fig. 5.31.

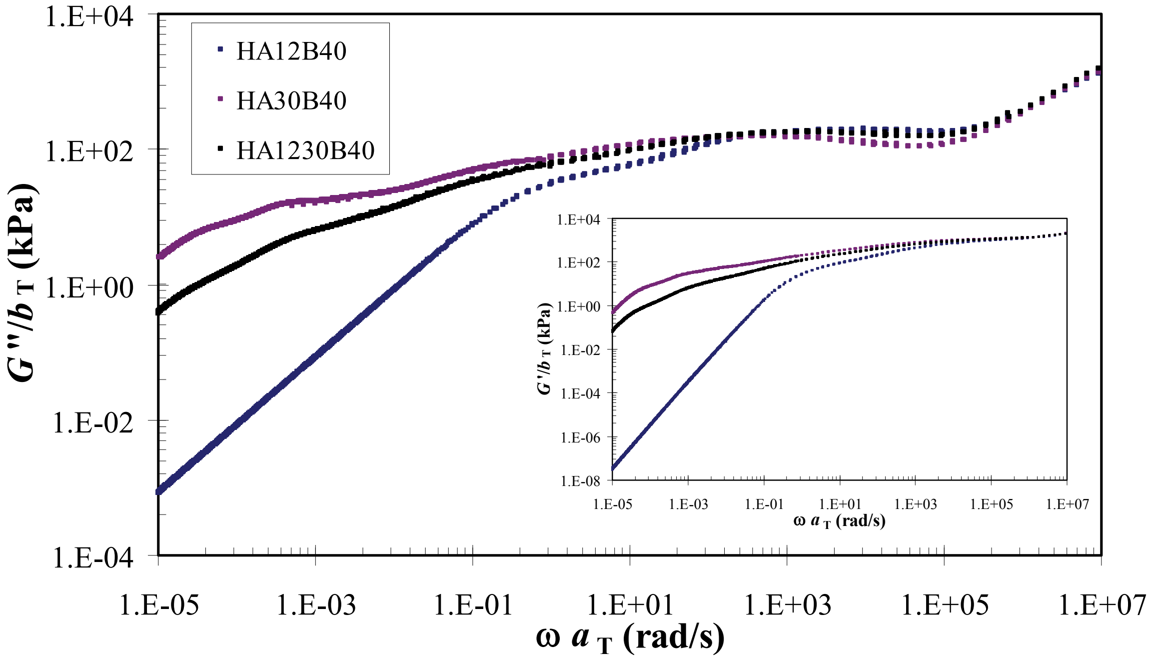

Figure 5.31 Comparison of moduli of H-shaped PBDs and their blend

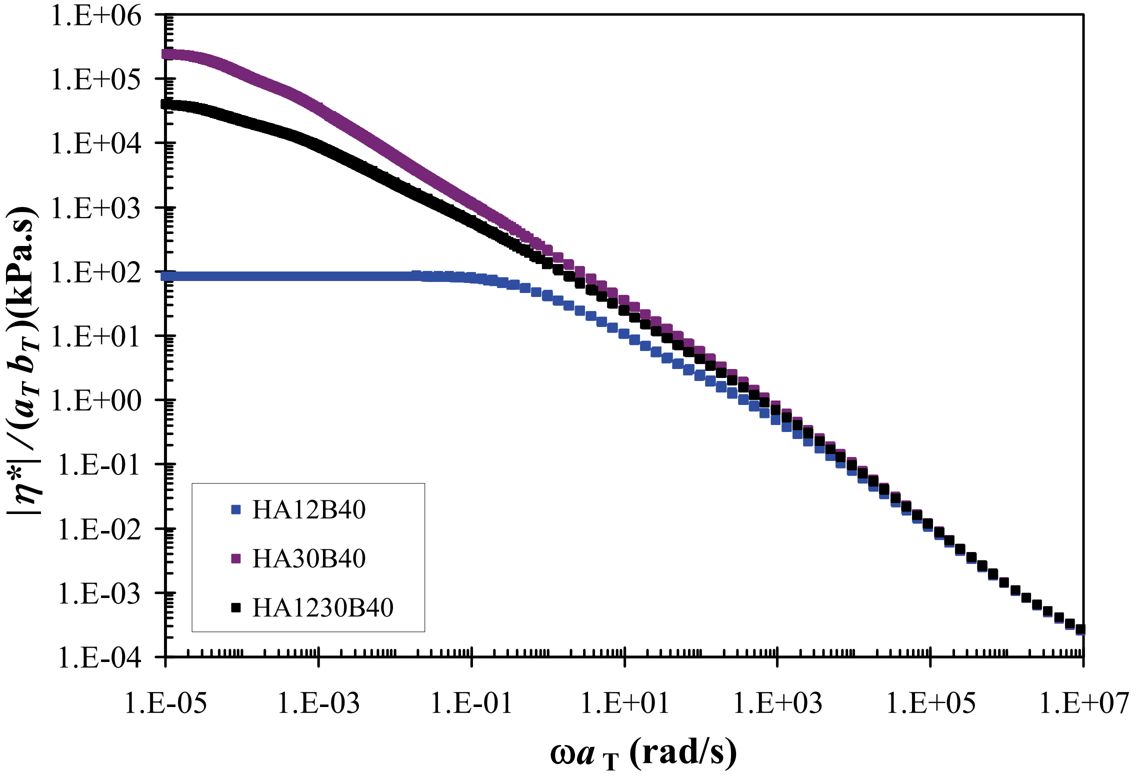

Figure 5.32 Comparison of η_0 values of H-shaped PBDs and their blend

5.10 Conclusions

A few critical but commonly ignored experimental issues are studied and taken care of, which include normal force build up during sample loading, frost condensation on the sample at low experimental temperature, meniscus of the sample and thermal expansion (contraction) of fixtures at various test temperatures. Rheological studies within the LVE regime on two linear PBDs blends, five H-shaped PBDs and one H-shaped blend were conducted that are free from the uncertainties caused by the above issues.

The linear PBDs blends and H-shaped PBDs are found to be thermorheologically simple. The horizontal shift factors that account for the frequency dependence on temperature are found to obey the WLF relationship and have higher values at the presences of LCB. Three material constants, plateau modulus G_{N}^{0}, zero shear viscosity η_0 and steady state compliance J_s^0 are estimated from raw data. G_{N}^{0} is essentially constant among the linear PBDs blends and H-shaped PBDs, regardless of the molecular weight distribution, molecular weight and long chain branching. Presence of LCB resulted in a strong enhancement of η_0 when comparing samples with the same total molecular weight. Negative J_s^0 is found in a few samples when estimated from the raw data J(t) at long time due to extrapolation error. As shown from the studies of a binary H-PBD blend, a change of the molecular weight distribution of arms with fixed cross-bar lengths only sped up the relaxation process slightly, suggesting that the relaxation of the cross-bar is the slowest relaxation step.

Chapter 6 Evaluation of Molecular Models

6.1 Introduction

According to The Council for Regulatory Environmental Modeling [156], model evaluation is a process of generating information to determine the quality of a model and its analytical results. This recommended model evaluation process involves scientific peer review, sensitivity and uncertainty analyses, and model corroboration. This was the process used to evaluate the molecular models of interest here.

Specifically, the first objective is to determine whether a model is able to qualitatively and quantitatively predict the LVE behavior of a polymer without fitting input parameters. In this chapter, two molecular models are evaluated: the BoB model developed by Das *et al.* [59] and the Hierarchical-3.0 model developed by Larson *et al.* [60,61,63]. These models were chosen because abundant documentation on the theory as well as computational algorithms are available, as well as information about input parameters for a wide range of molecular structures. However, thorough evaluations of these models following the procedures outlined above have not been done. It is interesting to note that both models are based upon similar theories but are implemented in very different ways in the algorithm, as described in the following sections. Thus, the second objective is to compare the performance of the two models.

A description of each model is presented, followed by a summary of previously published comments ("scientific peer review"), sensitivity and uncertainty analyses, and finally a comparison of predictions with the experimental data presented in Chapter 5 ("corroboration"). Traditionally, model predictions and experimental data are compared by plotting both in the same figure, typically $G'(\omega)$ and/or $G''(\omega)$ versus ω. However, this procedure does not lend itself to quantitative comparison, especially when more than one model is of interest. First of all, the high-frequency data are not affected by entanglements and are not related to molecular structure, thus these high-frequency data are not of interest to us. Furthermore, the sensitivity and uncertainty analyses need to be compared with specific values, and I chose to use the zero shear viscosity η_0 to represent the terminal region and the cross-over frequency and modulus ω_c and G_c to represent the transition region. In comparing model predictions with experimental data, the traditional graphical representation as well as the quantitative comparison of η_0, ω_c and G_c were used.

All simulations presented in this chapter were done using the Krylov cluster at CLUMEQ, the Quebec high-performance computing center located in Montreal. Krylov is a heterogeneous system comprising a Sun Fire X4100 system and an Advanced Clustering Technologies system for a total of 300 cores in 2.2GHZ with 8 GB Ram and 2.3GHz with 16 GB Ram, respectively.

6.2 Description of the Hierachical-3.0 model

Theories combining reptation, primitive path fluctuations, and constraint release that were developed by Milner and McLeish and coworkers for stars [157], linear polymers [158], and mixtures thereof [159,160] are referred to here as the "Milner-McLeish theory". It is based on the tube concept proposed by Edwards [51] and applied to melts by Doi and Edwards [54-56] along with the mechanisms of constraint release by dynamic dilution (*i.e.* the relaxed segments act as solvents to the rest of the polymer since they will no longer hold entanglements, thus the entanglement network becomes increasingly diluted and so the tube diameter) [161,162] and constraint release Rouse motion [163]. The theory has found to be useful for monodisperse linear and star polymers, which contain only one branch point per molecule. The next simplest structure to test the model would be H-shaped polymer, which contains two branch points per molecule. Molecules with at least one internal segment are of special interest to the plastics industry because of their greatly enhanced ease of processing.

Larson [61] generalized and extended the Milner-McLeish theory to predict relaxation of arbitrarily branched melts including linear, star, H, comb-shaped molecules and mixtures thereof. This model and its associated algorithm was the original Hierarchical model called “Hierachical-1.0” by Wang *et al.* [63]. A brief summary of the model development and the relaxation pathway assumed is presented below.

In Hierachical-1.0 [61], it was assumed that the melt is a mixture of linear, star and comb molecules with no branch-on-branch structure. The model also neglected both “early-time” fluctuations and high-frequency Rouse motions that lead to deviations between experimental data and predictions at high frequencies. Predictions of Hierachical-1.0 were found to be semi-quantitatively accurate only for linear and star polybutadienes and mixtures of these.

In Hierachical-2.0 [60] , the early time fluctuations introduced by Milner and McLeish [157] were included, and the waiting time concept in late-time fluctuations was eliminated so that a fitting parameter was no longer required. The definition of M_e was also corrected in Hierachical-2.0 to be consistent with the definition of the tube diameter a . A single set of model parameters (except G_N^0 , which was directly taken from experiments [164,165]) that was independent of polymer architecture were obtained by fitting the predictions of Hierachical-2.0 to data for monodisperse linear and star molecules, particularly polyisoprene and polybutadiene. Without adjusting the parameter values and extending the model to binary blends, predictions from Hierachical-2.0 were reported to be in good agreement with experimental data for linear/linear and linear/star polybutadiene blends. However, only the general trend was captured for asymmetric-star, H and comb polymers. For H polymers with polydisperse arms, the predictions depended on the order in which the arms were numbered in the algorithm. Moreover, a very large number of ensembles were required to represent highly polydisperse systems. Due to the linear time-stepping method used in the calculation of arm-end retraction and among other things, the computation time required for 10,000 ensembles of as an H-shaped structure was above 300 hours on a 21 dual-socket, dual-core 2.2GHz supercomputer.

To overcome the above deficiencies, an updated version of Hierachical-2.0 was recently developed [63,66]. Hierachical-3.0 achieved improved computational efficiency by implementing a logarithmic time-stepping method instead of the linear method used in its predecessor. To process 10,000 ensembles using the same supercomputer, Hierachical-3.0 took only about 30 minutes. In order to correct the problem arising from the order in which the arms are numbered in the algorithm, especially for H-shaped molecules, a segment-partitioning technique was implemented. The calculation of the total friction of the effective linear chain for a branched polymer was also modified, resulting in a faster reptation time than for Hierachical-2.0. To enhance flexibility in the use of Hierachical-3.0, three options are available to deal with arm retraction in the constraint-release Rouse regime. In addition, the input parameters were modified slightly by relating G_{N}^{0} directly to M_e using Eq. 6.1 and letting G_{N}^{0} = 1.095MPa instead of 1.15MPa for polybutadienes at 25°C.

$$M_e = \frac{4}{5}\frac{\rho RT}{G_{\mathrm{N}}^{0}} \qquad \text{Eq.6.1}$$

In the hierarchical model, the melt is represented by a discrete but large set of molecular ensembles. Each ensemble carries information about the number of arms, arm length, backbone length, as well as the volume (or mass) fraction of the ensemble in the sample. Since branch-on-branch structure is not allowed, every molecule in the hierarchical model can be treated as a comb-branched polymer.

The conceptualization of the relaxation pathway of the comb-branched polymer is shown in Figure 6.1. Shortly after imposing a small deformation (Step 1), only the arms can relax, by primitive path fluctuations, while the backbone segment remains frozen until one of its ends is released by complete relaxation of the attached arms. The shortest arm relaxes first by early-time fluctuations that are limited to small fractional excursions toward the branch point. Then it relaxes by late-time, deep-arm retractions. Once the arm is relaxed (Step 2) it is “pruned away” in the model and replaced by an effective frictional “bead” at the branch point at which it is attached. Now the partially relaxed molecule is equivalent to an “H” molecule. Further relaxation of the arms results in a star (Step 3) and eventually an effective linear molecule (Step 4) that consists of two relaxing compound “arms”.

An arm containing more than one localized drag point or bead left behind by a collapsed side arm is called a compound arm. In Hierachical-3.0, relaxation of compound arms is treated in the same way as that of a simple arm by taking all the friction arising from collapsed arms into consideration. Before reptation of the residual “linear molecule” takes over to complete the relaxation process, it retracts from its free ends in a “thin” tube by the constraint release Rouse mechanism. Due to the segment-partitioning strategy, the original backbone segment is shared between the two compound arms instead of being merged with only one of them.

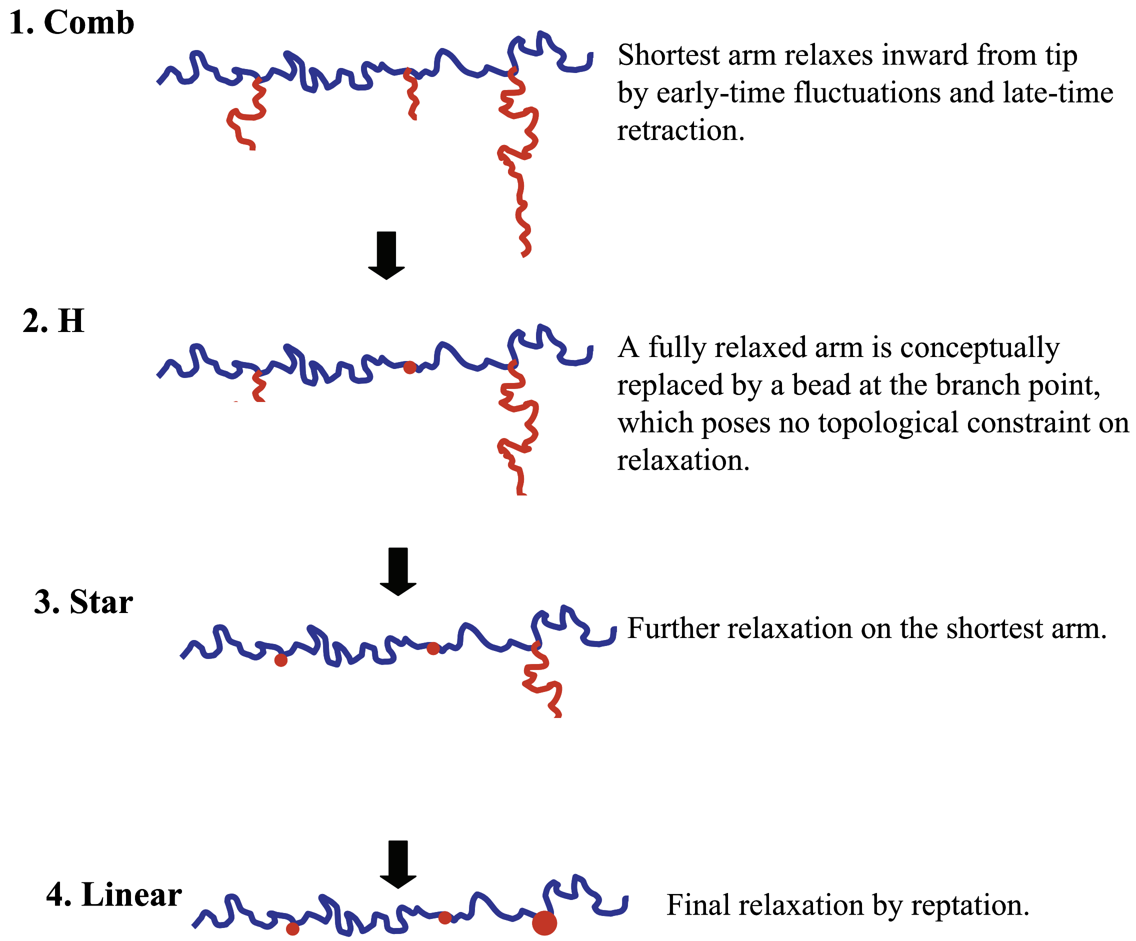

1. Comb

Shortest arm relaxes inward from tip by early-time fluctuations and late-time retraction.

2. H

A fully relaxed arm is conceptually replaced by a bead at the branch point, which poses no topological constraint on relaxation.

3. Star

Further relaxation on the shortest arm.

4. Linear

Final relaxation by reptation.

Figure 6.1 Conceptualization of relaxation pathway in the Hierarchical-3.0 model

6.3 Description of the Branch on Branch (BoB) model

The Branch-on-Branch (BoB) model is a general algorithm developed to predict the linear rheology of an arbitrary architecture based on the tube-theory framework similar to the one used by Hierachical-3.0 [59]. In the BoB model, the stress relaxation due to a small step strain of a polydisperse, branched polymer (including branch-on-branch structure) is considered. The polydisperse melt is viewed as a spectrum of elements with various architectures, each relaxing with its own relaxation time and mechanism. This section describes the relaxation pathway used by BoB and the differences between BoB and Hierarchical-3.0. A detailed description of the BoB algorithm and its use can be found in reference [59], while the computational differences between the two models are described in reference [63] .

The Bob model considers the relaxation modulus *G*(*t*) as the sum of fast and slow contributions: $G(t) = G_{fast}(t) + G_{slow}(t)$. $G_{fast}(t)$ describes the high frequency (short time) relaxation that is due to sub-tube-diameter Rouse modes, which are not accounted for in Hierachical-3.0. $G_{fast}(t)$ accounts for relaxations that are faster than, or comparable to, the entanglement time τ_e (which is defined as the Rouse time of the chain segment between entanglements) by two relaxation pathways, fast Rouse motion inside the imaginary tube and longitudinal Rouse motion along the tube. While $G_{slow}(t)$ describes relaxation due to the escape of chain segments from the deformed tube and relaxation of the tube itself through the mechanism of constraint release Rouse motion.

As in Hierchical-3.0, a linear molecule is looked on as a two-armed star. The relaxation pathway of simple arms is the same as in Hierachical-3.0, except that different mathematics is used to estimate the effective potential for arm retraction and late time arm retraction τ_{late}. During arm retraction, chain segments between branch points remain topologically constrained. When an arm relaxes completely, it is replaced by a drag point at the branch point to which the relaxed arm is attached. This branch point is free to move (diffuse) with time unless it is trapped by other unrelaxed branches at that time. Therefore, the extra friction imposed by the collapsing arm is represented by a time-dependent function in BoB, instead of a time-independent function in the undilated tube in Hierachical-3.0. The use of a time-dependent function in branch point friction is justified by the three-dimensional diffusive motions of branch point and a continually dilating tube diameter over time. Due to a different selection of friction constant of the branch point in BoB, a value of the branch point hopping fraction $p^2 = 1/40$, instead of $p^2 = 1/12$ used in Hierachical-3.0, was found to provide the best fit to experimental data on polyisoprene asymmetric star and H polymers.

A compound arm retracts in a way similar to a simple arm except that a new effective potential is calculated at each time. Only the portion of the compound arm that moves coherently with the chain end is used to calculate the new effective potential, which becomes the effective free-arm length. Therefore, the extra drag contributed from the branch points along the compound arm is effectively included into the new potential. When the same concept is applied to branch-on-branch structures that are not considered in Hierachical-3.0, a new effective free-arm length is considered at each time, then associated with the effective friction and potential since the side arms are themselves compound arms.

When only two arms are left during the relaxation process, the chain becomes effectively linear. Arm retraction continues in the free end until reptation takes over. In BoB, polymer chains are assumed to reptate in the undilated tube. Due to the differences in considerations regarding the tube diameter in which the chain reptates, the reptation time in BoB is longer than that in Hierachical-3.0 for a simple linear chain with no branch points. On the other hand, the reptation time in BoB is shorter than that in Hierachical-3.0 for an effective linear chain composed of compound arms. This is due to the dominant effect of branch point friction, which is lower value in BoB than in Hierachical-3.0.

6.4 Summary of published comments on the models

6.4.1 Published comments on the BoB model

The BoB model has been tested mainly by comparison with data for polyisoprenes and polybutadiens having various structures. For polyisoprenes, linear [166], asymmetric and symmetric three-arm stars [166] and H-shaped [21] structures were used to fix the values of dilution exponent α and the branch point hopping fraction p^2, which were expected to depend on temperature but not on the polymer chemistry. Data sets were selected based on the criterion that the frequency-dependent moduli that should be independent of architecture overlapped when $\omega > 1/\tau_e$ at a given temperature. By fitting model predictions to data at T=25ºC, values of M_e and τ_e for polyisoprene at T=25ºC were determined.

Once the input parameters had been fixed, BoB predictions were compared with data for a series of star-linear polyisoprene blends having various compositions [167]. The temperature for these data (T=28^{o}C) was somewhat higher, but all the parameters were assumed to be the same as at T=25^{o}C except τ_e, which was adjusted by time-temperature superposition. Predictions for the star-linear blends were found to be slightly lower than the experimental data; in particular a lower plateau region and hence G_{N}^{0} were predicted for these asymmetric stars. The authors [59] attributed these reductions to the use of $\alpha = 1$ rather than the temperature effect on G_{N}^{0}, which is related to M_e by Eq. 6.1. Since G_{N}^{0} should vary with temperature according to the shift factor b_T [168], *i.e.*

$$G_{\mathrm{N}}^{0}(T) = b_{\mathrm{T}}(T)\, G_{\mathrm{N}}^{0}(T_0) \qquad \text{Eq.6.2}$$

an increase in temperature should lead to an increase in b_T as shown in Fig. 5.2 and thus a lower G_{N}^{0}. It is interesting to note that in the following sensitivity analysis of the BoB model, predictions are more sensitive to G_{N}^{0} than to α under the same fractional change of parameter.

To further explore the model's applicability to more complex systems, a series of four comb-shaped PBDs [29] with various backbone lengths and numbers of side arms were studied. The material-independent parameters α and p^2 were the same as the values used for polyisoprenes, while the material-dependent parameters M_e and τ_e were obtained by fitting predictions for the comb-shaped PBDs to experimental data.

For their simulation, the value of M_e was not related to G_{N}^{0} by Eq. 6.1 but was slightly lower than the value calculated from the experimental value of G_{N}^{0}. Predictions for the comb-shaped PBD with the largest number of side arms in the series failed to capture quantitatively the terminal behavior and led to an underestimation of the relaxation time. It was a common failure among these four comb-shaped PBDs that the curvatures of G' and G'' at intermediate frequencies were not correctly captured. Parameter values suggested by the model developers for PBD for use in BoB simulations are given in Table 6.1.

BoB predictions were also compared with data for a series of metallocene-catalyzed polyethylenes (m-PE) [20]. The material-dependent parameters M_e and τ_e were chosen as before. Predictions for systems having branch-on-branch architectures with various degrees of branching (from 1/2 to 15 branch points per molecule) agreed well with the experimental results. However, we note that although $\alpha = 1$ worked best for branched metallocene-catalyzed polyethylenes, $\alpha = 4/3$ was found to work better for simpler architectures such as linear polymers and symmetric stars. The dependence of α on material architecture suggested that a better understanding of branched structures is needed.

Recently, the algorithm for BoB predictions was thoroughly reviewed by Wang *et al.* [63]. Although their principal objective was to compare the effects of various physical mechanisms on predictions of both models, several pieces of information relevant to the performance of BoB can be extracted. Wang *et al.* reported an error in BoB when evaluating the reptation time of a one-arm chain that arose from the collapse of another arm into an effective linear chain with only two relaxing arms. Their analysis of data sets different from those used by Das *et al.*[59] also indicated that BoB actually works better with $\alpha = 4/3$ for simple structures such as monodisperse linears and symmetric 3-arm stars [169], and the use of $\alpha = 1$ under-estimates the relaxation modulus of these systems, especially at low frequencies. However, in more complicated structures such as asymmetric stars [166] and linear-linear binary blends [170], the use of $\alpha = 1$ gave better predictions. The exception was star-linear binary blends; while Das *et al.* always observed under-estimation of the relaxation modulus at low frequencies, model predictions obtained by Wang *et al.* for another set of data [169] was higher than the data in a case where the volume fraction of star molecules was low (20%). Further testing of more complicated structures such as H-shaped [21], comb [29] and branched metallocene catalyzed polyethylenes led to the same conclusions reported by Das *et al.*, suggesting that $\alpha = 1$ works better than $\alpha = 4/3$ for these systems and that further refinement of the relaxation mechanisms of H and comb shaped structures will be necessary to deal with the under-estimation of the relaxation modulus.

6.4.2 Published comments on the Hierarchical-3.0 model

The only review paper on Hierachical-3.0 is that of Wang *et al.*[63], in response to the recent release of the updated version [66]. Selection of the material-independent parameters such as $\alpha = 4/3$ was based on intensive comparison of model predictions with experimental data for linear, star, and star-linear blends of PBDs, without changing other input parameters [171]. For p^2, they followed the example of McLeish *et al.* who found that $p^2 = 1/2$ gave the best fit for H-shaped polyisoprenes [21]. As for the material-dependent parameters, G_N^0 for PBD was obtained by slight adjustment of the experimental value measured by Fetters *et al.*[164], while G_N^0 for the polyisoprenes was taken from Pearson *et al.* [165]. The corresponding M_e was related to G_N^0 by Eq. 6.1 with a slight adjustment to make its value an integral multiple of the monomer molecular weight. The values of τ_e for both polymers were obtained by fitting the zero-shear viscosities of linear and star PBDs using the Milner-McLeish theory [60]. A list of the parameter values suggested by the model developers for PBD to be used in Hierarchical-3.0 is given in Table 6.1.

Once the input parameters were fixed, Hierachical-3.0 predictions were compared with experimental data for simple structures such as monodisperse, linear PBDs and monodisperse, symmetric 3-arm star PBDs [169]. Without adjusting any input parameters, a simultaneous fit to the experimental data of all the above systems can be achieved. For star-linear, binary blends of PBDs [169], model predictions were higher than experimental data in one case where the volume fraction of star molecules was low (20%) while the model gave good quantitative predictions for other blend compositions.

The authors reported that enabling the disentanglement relaxation mechanism sped up the relaxation of diluted star components in the linear matrix and thus eliminated the discrepancy between predictions and experimental data [63].

However, for more complicated structures such as asymmetric stars [166] and linear-linear binary blends [170], the model commonly predicted a lower relaxation modulus, especially in the terminal zone. To obtain a better fit to experimental data for such systems, the disentanglement relaxation mechanism had to be enabled and a different value of α used.

Model predictions for several H-shaped polyisoprenes [21] and a series of comb shaped PBDs [29] further probed the limits of Hierarchical-3.0; the predicted terminal behavior appeared much sooner than the measured behavior, and G_{N}^{0} was under-estimated. To simulate metallocene-catalyzed polyethylenes [8], experimental G_{N}^{0} and the corresponding M_e values were used for modeling. Again, much faster relaxation was predicted, and the results for the m-PEs were not well separated from each other despite differences in their degrees of branching. A better prediction for the m-PEs with the lowest branching level was obtained when the simulation time step was reduced and the no-arm retraction method was applied in the constraint release Rouse region. However, the authors also noted that the computation time for this modification is extremely long and would increase further with an increase in branching degree.

Table 6.1 Suggested parameter values for use with PBD in the BoB and Hierarchical-3.0 models

Parameter	Suggested Values		Description
	BoB	Hierarchical-3.0	
p^2	1/40	1/12	Prefactor in branch point diffusion coefficient
α	1	4/3	Dilution exponent
N	10,000	10,000	Number of molecules used in calculation
M_o	54.09	54	Molar mass of monomer [g/mol]
N_e	33.9	N/A	Number of monomers in an entanglement length
M_e	(1836)	1650	Molecular weight between entanglements [g/mol]
G_N^0	0.97	1.15	Plateau modulus [MPa]
ρ	0.895	0.895	Density of polymer [g/cc]
τ_e	2.75E-07	3.70E-07	Entanglement time [s]
T	298.15	298.15	Temperature [K]

6.5 Sensitivity analysis

Sensitivity analysis is defined as a local measure of the effect of changes in input values or assumptions on a model's predictions [172]. It is recommended as the principal evaluation tool to identify the most and least important sources of input variables in a model. In a one-at-a-time (OAT) sensitivity analysis, base values of input variables are chosen and each variable is subjected to perturbation by a given percentage away from its base value, while all other input variables are kept at their base values. In this way one can relate output changes solely to the variation of that particular input variable. It is noted that an OAT sensitivity analysis usually yields local measures of sensitivity that depend on the base values.

6.5.1 Base values and standard case

Since a considerable amount of work has been done in modeling PBD, the input values suggested by Chinmay *et al.* and Larson *et al.* for PBD at 25^{o}C were chosen as base values for the OAT sensitivity analysis. Since both models require information on molecular structures such as M_w and polydispersity index (PDI) of arms and cross-bars ($M_{w,arm}$, $M_{w,cross\text{-}bar}$, PDI$_{arm}$, PDI$_{crossbar}$), sample HA12B40 was chosen as an example for the OAT sensitivity analysis due to the detailed characterization of its molecular structure. Among several sets of molecular structure data, the one from the University of Tennessee was chosen to establish base values for these input variables, as it was the only source that provided information on the molecular weight and polydispersity index of the arms. Referring to Table 3.1, Sample HA12B40 had a polydispersity of only 1.03, and we assumed that it consisted entirely of H-shaped molecules. The value of $M_{\text{n,cross-bar}}$ was then calculated by subtracting four times $M_{\text{n,arms}}$ from $M_{\text{n,H}}$. Knowing $M_{\text{n,cross-bar}}$, $M_{\text{w,cross-bar}}$ was then determined by trial-and-error. For this purpose, the program named "mwdh.f", kindly provided by the team at the University of Michigan, was used. The program reads values of $M_{\text{w,arm}}$, $M_{\text{n,arm}}$, $M_{\text{w,cross-bar}}$ and $M_{\text{n,cross-bar}}$, and generates 10,000 ensembles with log-normal distributions to represent the melt. Using these 10,000 ensembles, $M_{\text{w,H}}$ and $M_{\text{n,H}}$ are calculated by Eq. 6.3 and compared with values measured at the University of Tennessee; the trial-and-error procedure stops when the calculated and measured values differ by less than 2%, and the assumed value of $M_{\text{w,cross-bar}}$ is taken as $M_{\text{w,cross-bar}}$ for modeling. $\text{PDI}_{\text{cross-bar}}$ is then calculated from the ratio of $M_{\text{w,cross-bar}}$ and $M_{\text{n,cross-bar}}$.

$$M_n = \frac{\sum M_i}{N} \text{ and } M_w = \frac{\sum M_i^{\,2}}{M_i} \qquad \text{Eq. 6.3}$$

where Mi [g/mol] = molar mass of individual ensemble and N = number of ensemble.

Based on the kinetics of the reactions used to make H-shaped PBD (described in Chapter 3) and the molecular weight information revealed from TGIC, the most probable by-products are shown in Fig. 6.2. It is noted that the high molecular weight by-products observed by Perny *et al.* [104] are less likely to form in our case [110].

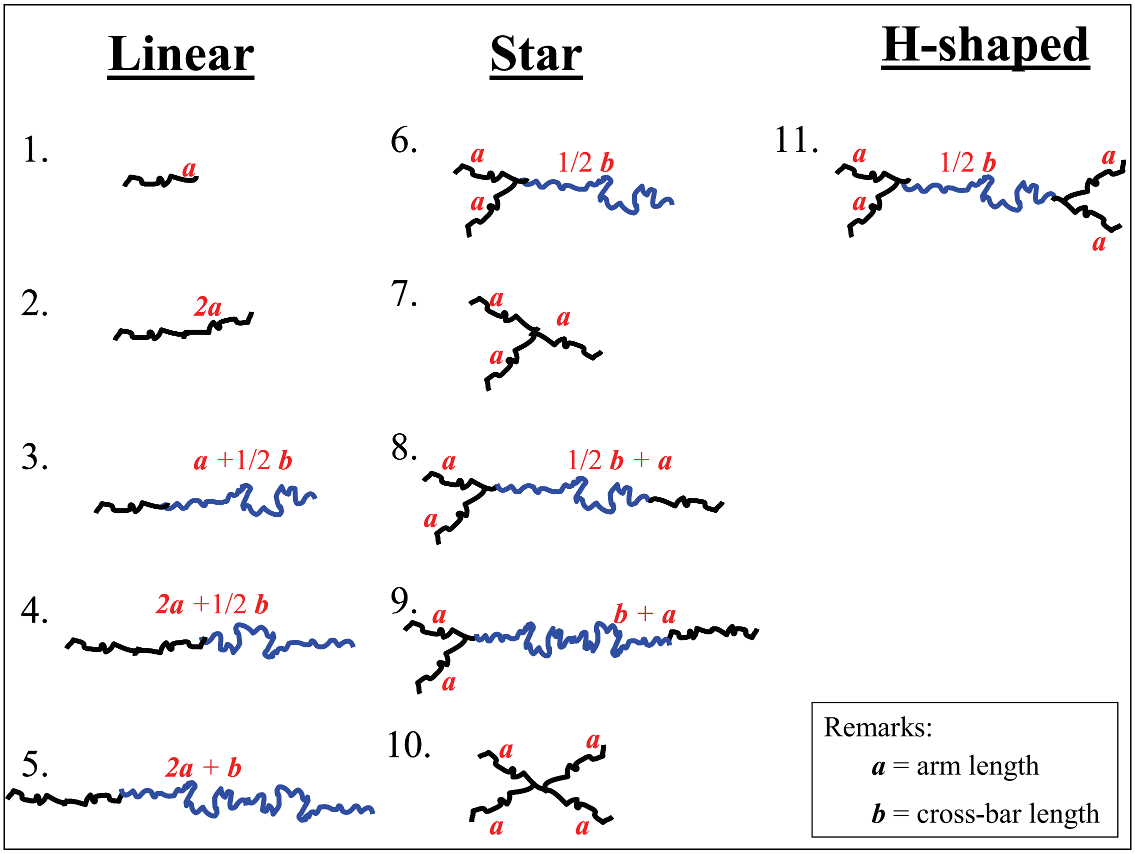

Figure 6.2 Schematic representations of the most probable structures of low molecular weight by-products

A list of input variables subjected to OAT sensitivity analysis along with their base values and ranges of perturbation are listed in Table 6.2. To quantify the degree of sensitivity of each input variable, values of η_0, ω_c and G_c were determined from the predictions and compared with those predicted when the base values were used for the input variables. To be consistent with BoB, it is noted that the disentanglement relaxation mechanism in Hierachical-3.0 was switched off for the following analyses.

Table 6.2 List of input variables for OAT sensitivity analyses on sample HA12B40

Variable	Base Values		Range of Perturbation
	BoB	Hierachical-3.0	
α	1	4/3	+100% to -80%
G_N^0	0.97	1.095	
p^2	1/40	1/12	
τ_e	2.75E-07	3.70E-07	
$M_{\mathrm{w,\ arm}}$	10.7 kg/mol		
$M_{\mathrm{w,\ cross\text{-}bar}}$	45.1 kg/mol		
$\mathrm{PDI}_{\mathrm{arm}}$	1.01		Monodisperse to +100%
$\mathrm{PDI}_{\mathrm{cross\text{-}bar}}$	1.13		
Distribution	log-normal		Gaussian distribution and Poisson distribution
Number of ensemble	10,000		10 to 500,000
Structures	100% H-shaped		composition of reaction by-products (as shown in Fig. 6.2) vary from 1wt% to 50wt%

6.5.2 One-At-a-Time (OAT) sensitivity analysis of the BoB model

I. Sensitivity to G_{N}^0, τ_e, α and p^2

As shown in Figs. 6.3 and Fig. 6.4, increases in G_{N}^0 and τ_e lead to increases in η_0 and G_c, while an increase of the material-independent parameters α and p^2 result in decreases in η_0 and G_c. Among these four input variables, G_{N}^0 has the largest effect on η_0 which varies by about 10 orders of magnitude, while η_0 varies by only about 1 order of magnitude in response to the same level of perturbation in τ_e. Moreover, the effect of τ_e on G_c is negligible, having a maximum variation of only 3%. It is noted that sensitivities to α and p^2 approach saturation when the perturbation is more than plus 50%.

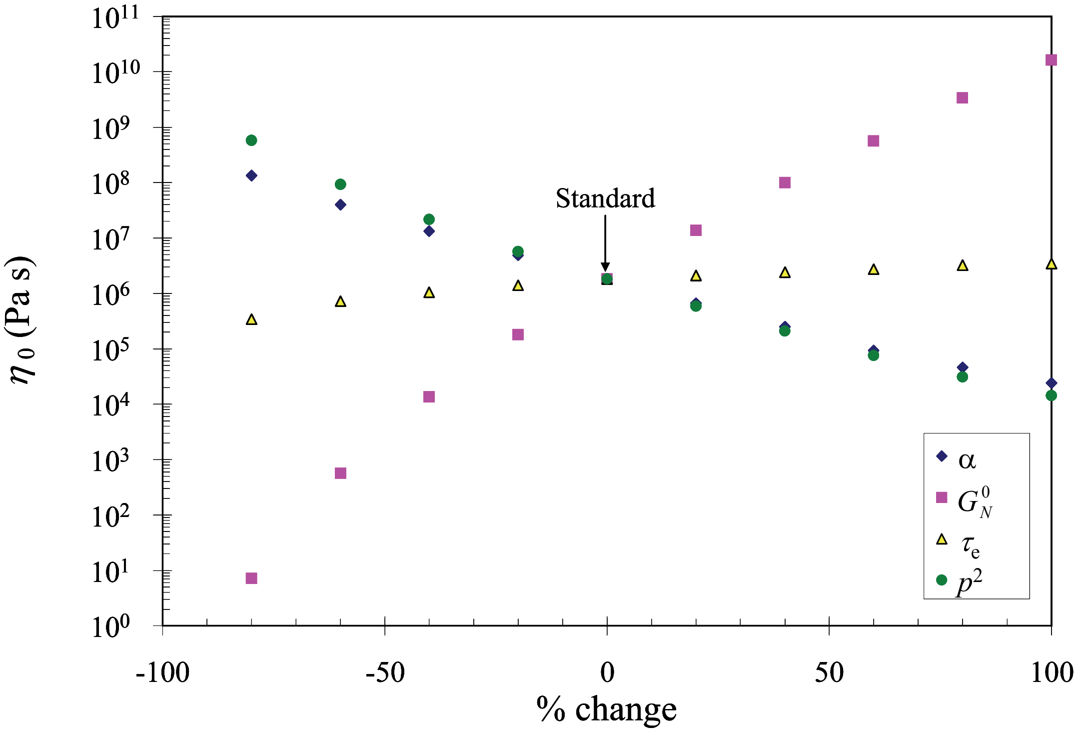

Figure 6.3 Sensitivity to G_{N}^0, τ_e, α and p^2 of η_0 as predicted by the BoB model

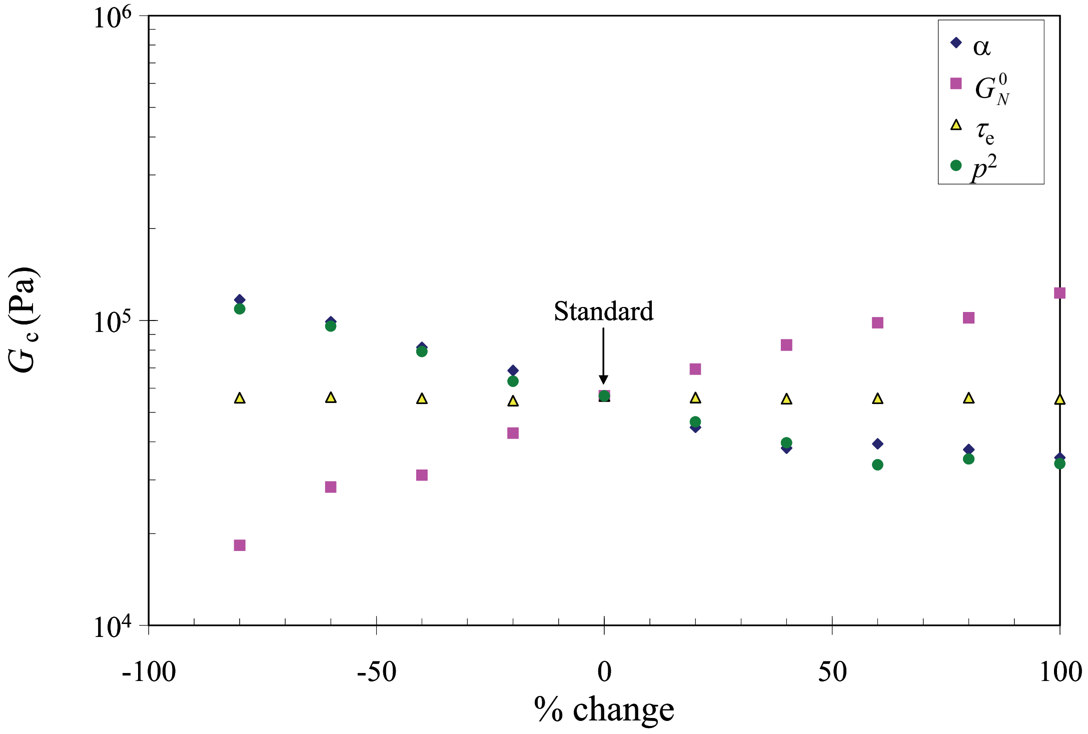

Figure 6.4 Sensitivity to G_{N}^0, τ_e, α and p^2 of the BoB prediction of G_c

On the other hand, an increase in G_N^0 would result in a decrease in ω_c while the opposite trend was observed on α and p^2 as shown in Fig. 6.5. τ_e was slightly more sensitive on ω_c than G_c and η_0. Therefore, the degree of sensitivity among these four input variables was G_N^0 (most sensitive) >> $p^2 > \alpha > \tau_e$ (least sensitive).

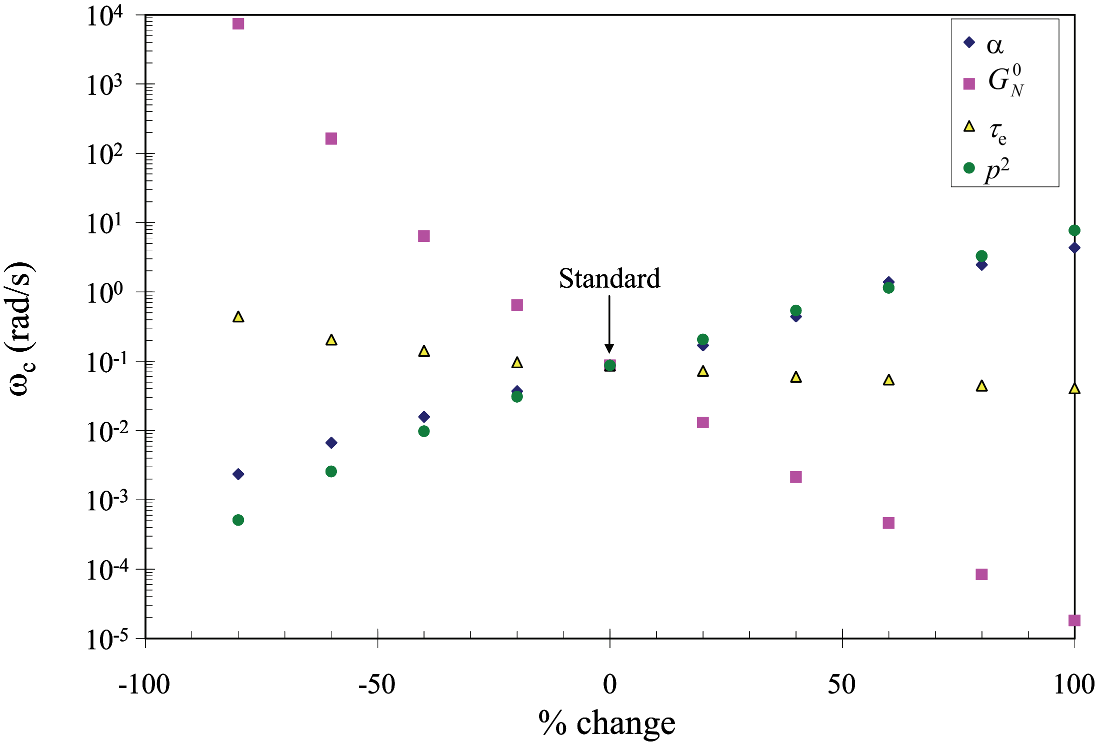

Figure 6.5 Sensitivity to G_N^0, τ_e, α and p^2 of ω_c as predicted by the BoB model

II. Sensitivity to $M_{w,cross\text{-}bar}$, $M_{w,arm}$, PDI_{arm} and $PDI_{cross\text{-}bar}$

As shown in Fig. 6.6, the effect of $M_{w,cross\text{-}bar}$ on η_0 was found to be stronger than that of $M_{w,arm}$, while PDI_{arm} was slightly more sensitive than $PDI_{cross\text{-}bar}$. It was obvious that η_0 increased with either increasing $M_{w,arm}$ or $M_{w,cross\text{-}bar}$ at the same molecular weight distribution because there would be more entanglements. The stronger dependence of $M_{w,cross\text{-}bar}$ on η_0 than $M_{w,arm}$ did was due to different relaxation mechanism of the arms and cross-bar. The cross-bar was trapped by two branch points at the ends which was frozen in motion until the braches (arms) were fully relaxed by primitive path fluctuation.

Therefore, relaxation of cross-bar was a much slower process compared to the relaxation of arms.

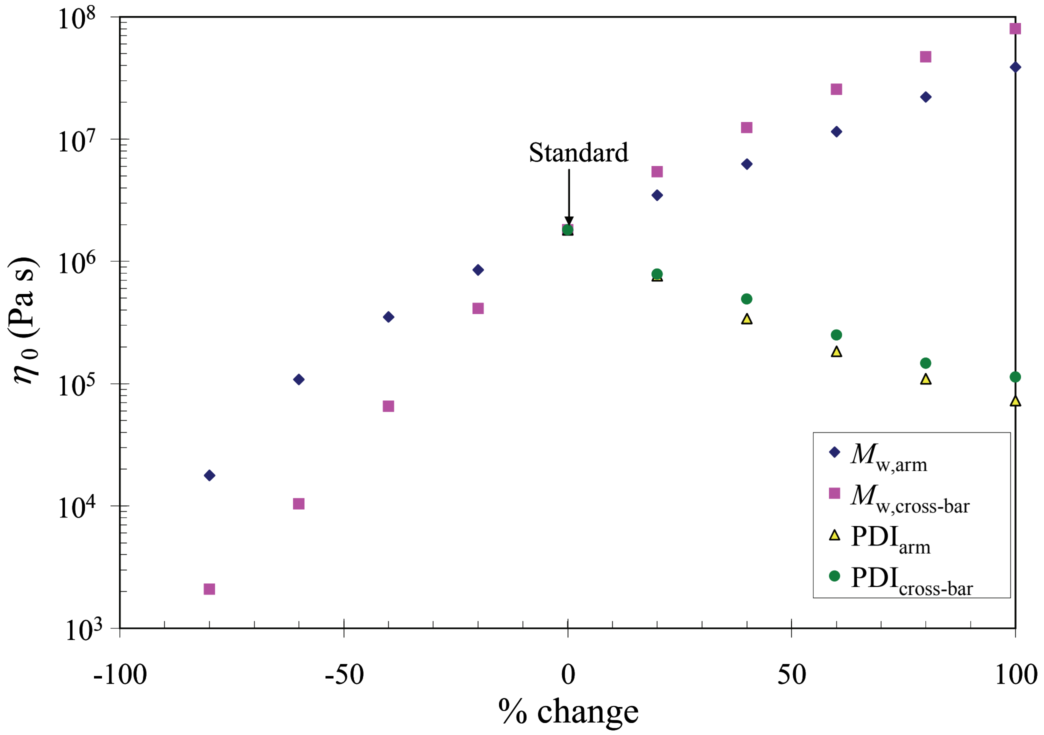

Figure 6. 6 Sensitivity to molecular weights and distributions of η_0 values predicted by BoB

Fixing M_w and the other input variables, while increasing polydispersity, a decrease in the predicted η_0 was observed. This seems to contradict the general observation that η_0 is remarkably insensitive to polydispersity unless a significant number of unentangled chains are present [173,174]. However, since constraint release is taken into account in the BoB algorithm, the presence of unentangled chains in a sample would be expected to yield such a prediction. Figure 6.7 is a sketch of the molecular weight distributions of two hypothetical samples having the same peak value (which means the same M_w for these symmetric distributions) but having different molecular weight distributions. Since the PDI of sample 2 is much larger than that of sample 1, sample 2 will have more unentangled chains, for which $M < M_c$, and this could lead to a reduced value of η_0.

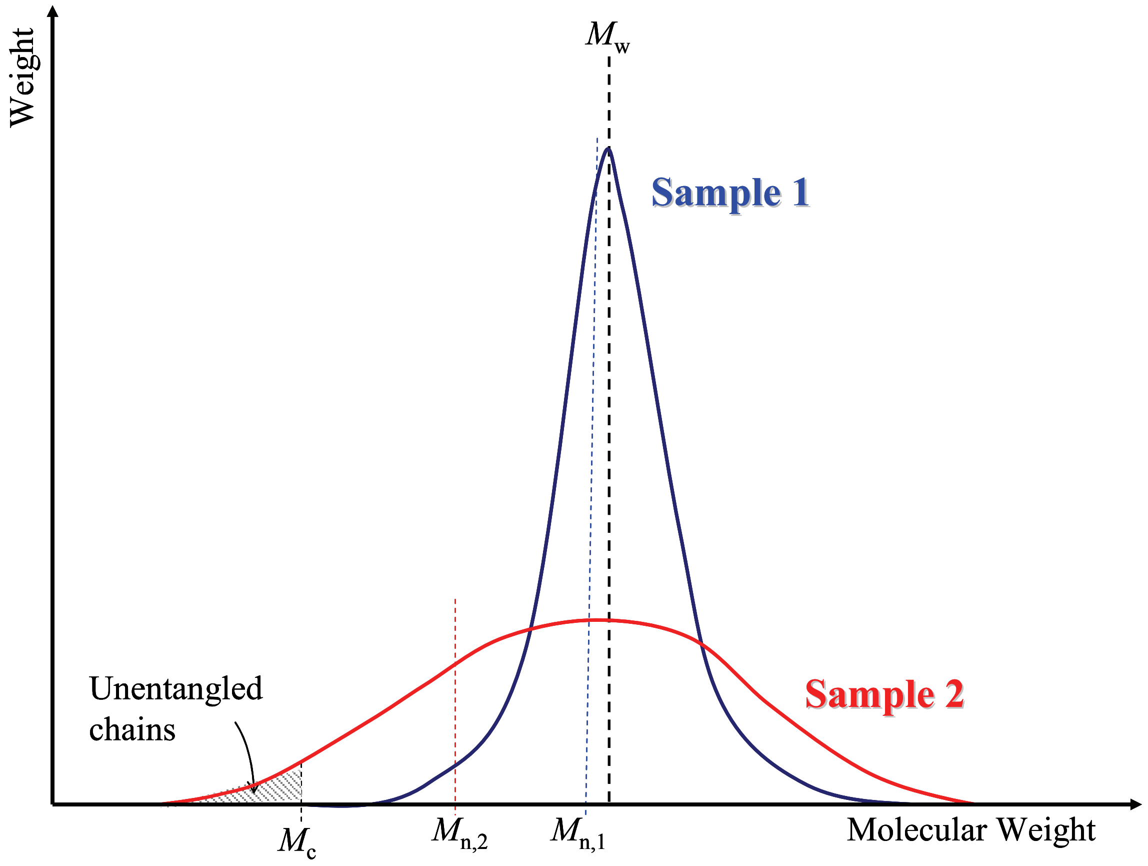

Figure 6.7 Sketch of molecular weight distribution of two samples having the same Mw but different molecular weight distributions

As shown in Fig. 6.8, increases in $M_{w,\text{cross-bar}}$ or PDI_{arm} both increase G_c to similar extents, but the opposite trend is observed for $M_{w,\text{arm}}$ and $\text{PDI}_{\text{cross-bar.}}$ The effect of $M_{w,\text{cross-bar}}$ on G_c is stronger than that of $M_{w,\text{arm}}$, and PDI_{arm} has a slightly stronger effect than $\text{PDI}_{\text{cross-bar}}$.

It is interesting to note that a very different dependence of ω_c on these four parameters was observed. As shown in Fig. 6.9, an increase in $M_{w,\text{arm}}$ or $M_{w,\text{cross-bar}}$ results in a decrease in ω_c, while an increase in PDI_{arm} or $\text{PDI}_{\text{cross-bar}}$ results in an increase in ω_c. Unlike the stronger sensitivity to $M_{w,\text{cross-bar}}$ than $M_{w,\text{arm}}$ observed in η_0 and G_C, the effects of these two parameters on ω_c were similar.

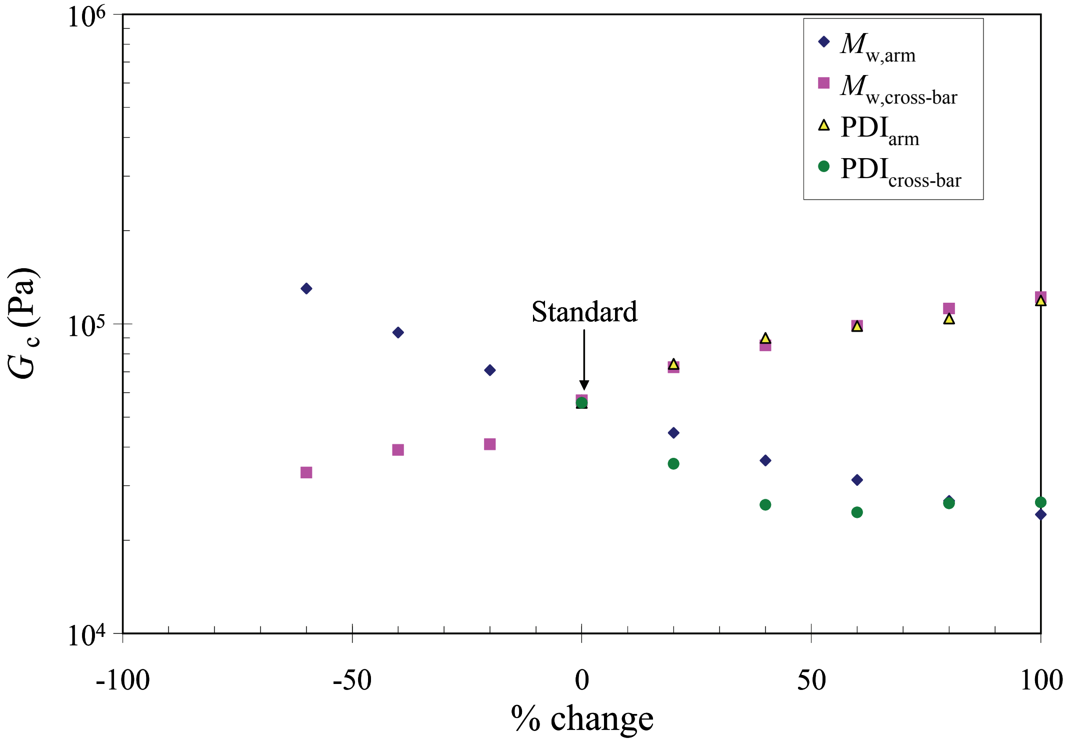

Figure 6.8 Sensitivity to molecular weights and distributions of G_c values predicted by BoB

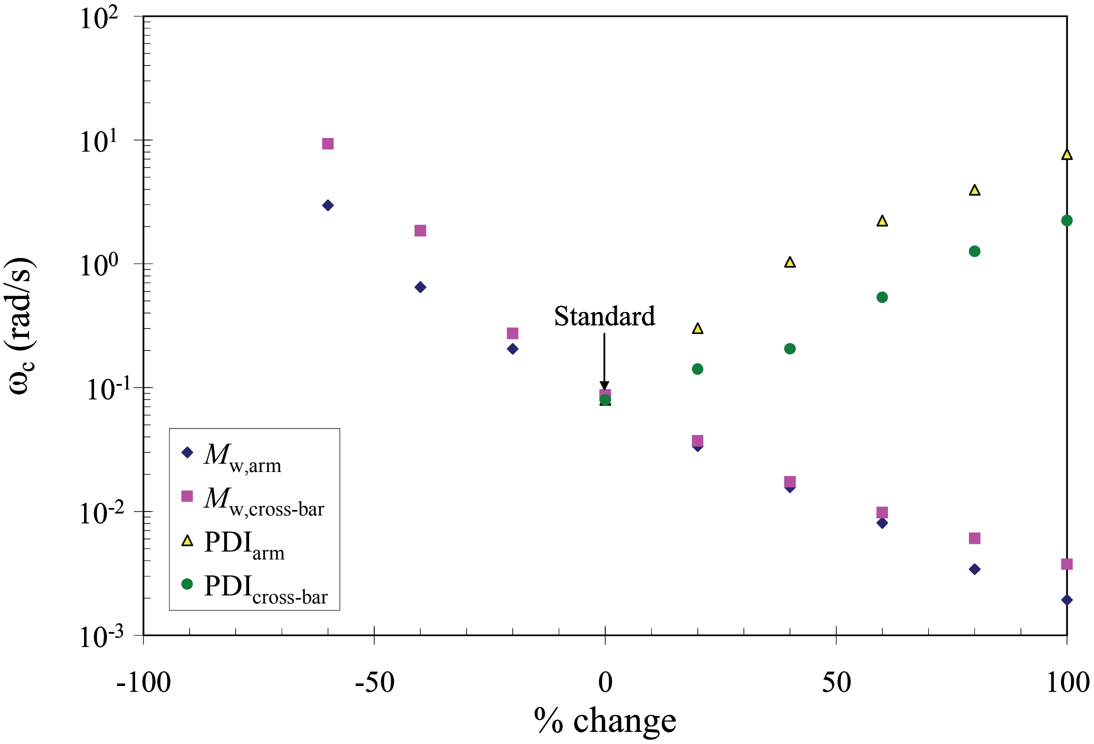

Figure 6.9 Sensitivity to molecular weights and distributions of ω_c values predicted by BoB

III. Sensitivity to mode of distribution

Three modes of molecular weight distribution were compared: log-normal (base case), Poisson and Gaussian, although additional modes are available in the BoB algorithm. The Flory distribution was not included as it assumes a constant monomer concentration during polymerization, which was not the case in our synthesis method.

When the PDIs of arms or cross-bars are small, as in Table 6.2, there is only a 2% variation over a wide range of frequencies ($\omega = 10^{-6}$ to 10^{8} rad/s) in predictions using the three distribution modes, as is illustrated in Fig. 6.10. This, of course, is not unexpected.

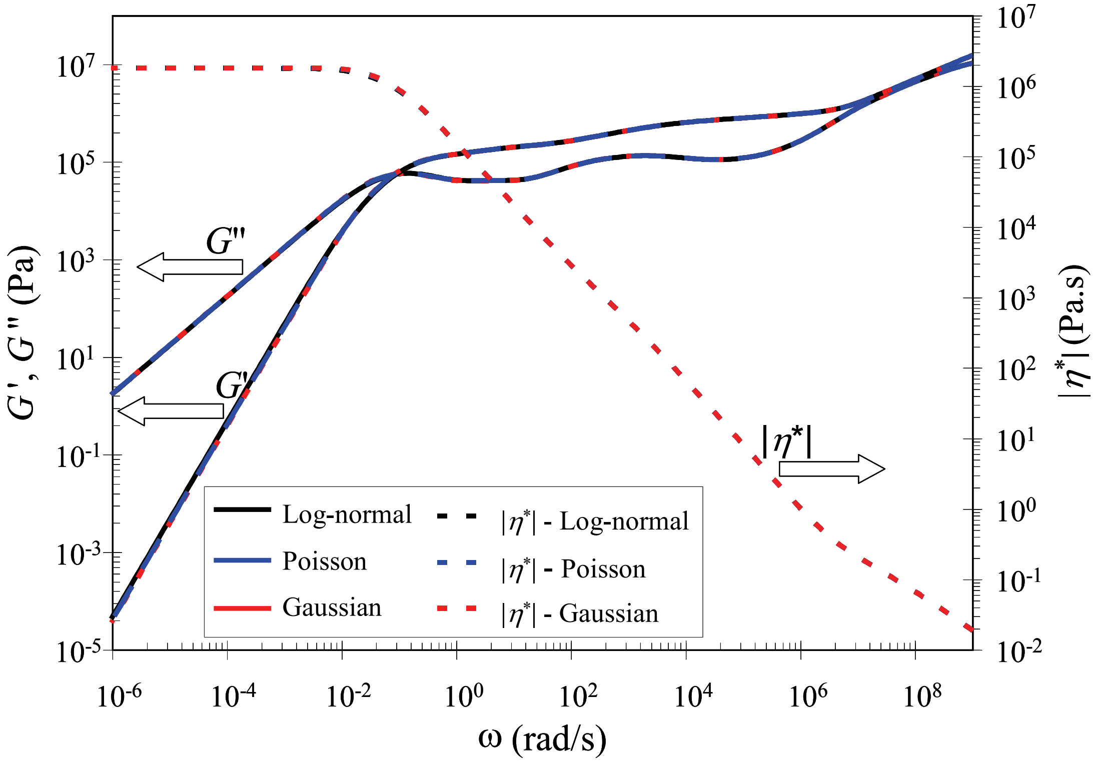

Figure 6.10 Sensitivity to mode of molecular weight distribution of BoB predictions for a nearly monodisperse system

However, when the PDIs of the arms and cross-bar are increased to 2, the Poisson distribution fails to generate ensembles that can describe the system, as only a living polymerization can generate a Poisson distribution with a PDI usually less than 2. Figure 6.11 compares the log-normal and Gaussian distributions and shows that the Gaussian distribution results in smaller values of G_c (20%) and ω_c (10%) than the log-normal distribution but a 10% higher η_0. The BoB user manual [175] recommends the Gaussian distribution for use with highly monodisperse polymers and the log-normal distribution when little is known about the synthesis process.

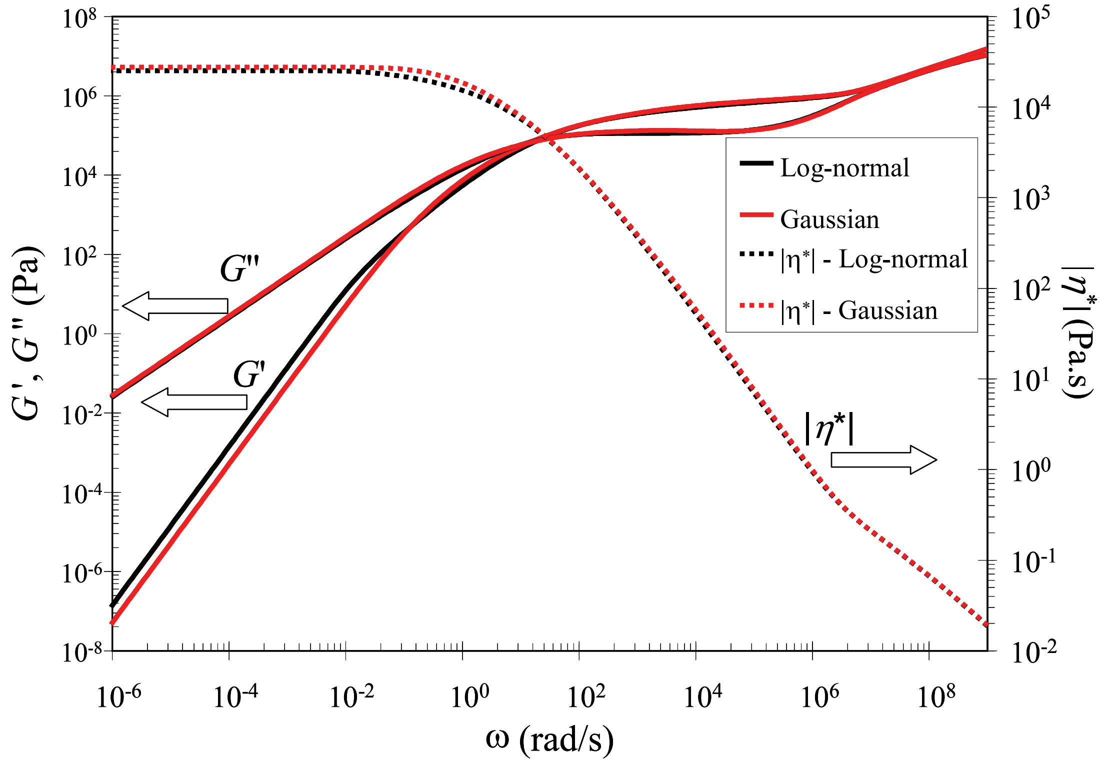

Figure 6.11 Sensitivity to mode of molecular weight distribution of BoB predictions for a polydisperse system

IV. Sensitivity to number of ensembles

The number of ensembles generated by the model to represent the system should not affect the prediction. However, as shown in Fig. 6.12, when the number of ensembles is below 10,000, there is a significant fluctuation in η_0 (also in G_c and ω_c, which are not shown). Predictions become independent of the number of ensembles when it is greater than 10,000.

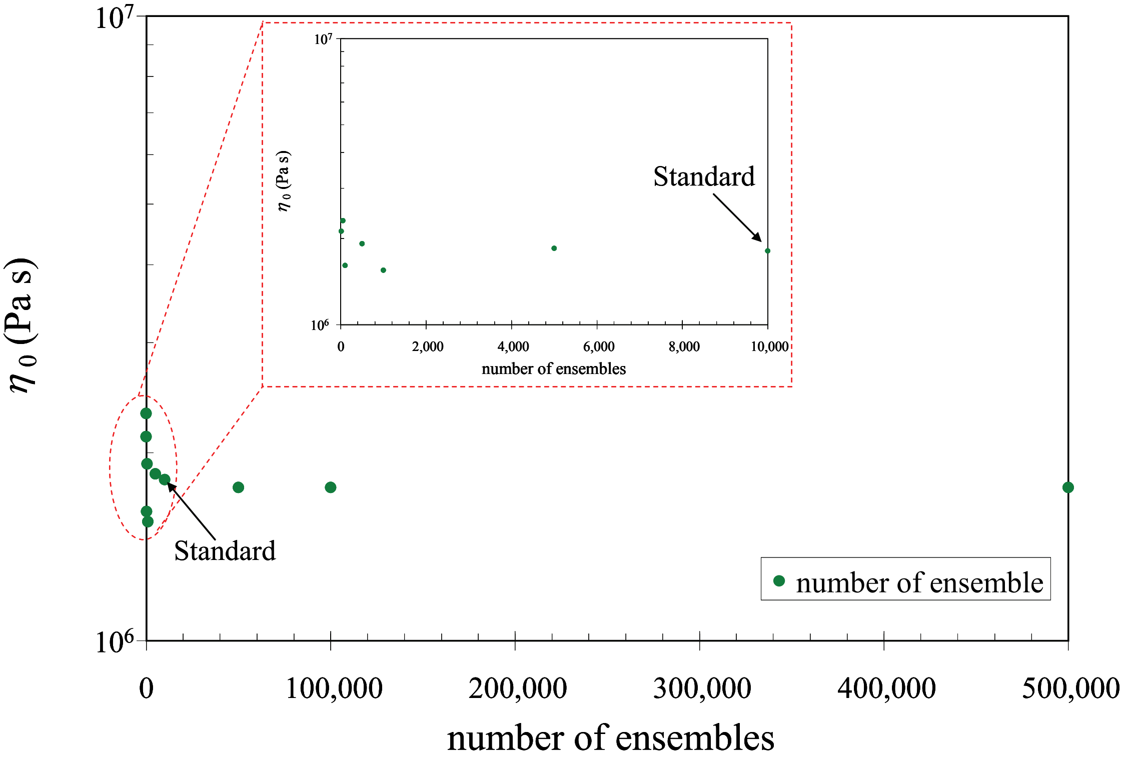

Figure 6.12 Sensitivity to number of ensembles of η_0 predicted by BoB

V. Sensitivity to the presence of reaction by-products

As mentioned in the previous section, a number of unexpected by-products were generated during synthesis, and their structures are shown in Fig. 6.2. Sensitivity to the presence of these structures was studied by adding them one at a time to pure H, the base case, to form various binary blends. The objective was to see what structures and compositions have the largest effects on predictions. For linear and star structures (*structures 1* to *10*), I assumed linear chains or arms with PDIs of 1.01, while for the H by-product (*structure 11*) PDI values of 1.01 and 1.13 were assumed for arms and cross-bars, respectively.

As shown in Figs. 6.13 to 6.15 the inclusion of any amount of by-product reduces η_0 and G_c and increases ω_c, showing that smaller by-products speed up the relaxation of pure H. This effect becomes important when the fraction of by-product reaches 5%.

When comparing *structures 1* to *5*, which are linear molecules, the sensitivity of η_0 and ω_c decreases with increasing chain length. However, the inclusion of linear by-products has a similar effect on G_c regardless of chain length up to 30wt% content as shown in Fig. 6.14. For asymmetric stars (*structures 6*, *8* and *9*) the sensitivity of η_0, G_c and ω_c decrease with increasing arm length. It is interesting to note that *structure 7* (3-arm symmetric star) and *structure 10* (4-arm symmetric star) has almost the same effect on η_0, G_c and ω_c over the entire range of compositions. This is expected, since the relaxation of a star molecule is mainly by primitive path fluctuations, constraint release, and high frequency Rouse modes, which depend only on arm length. It has been observed that η_0 depends exponentially on arm length but not on number of arms [14,18,19,48]. The addition of *structure 11*, which is an H with half the cross-bar length of the base case, results in a maximum of one order of magnitude variation in η_0, G_c and ω_c.

Among all the by-products, an asymmetric 3-arm stars (*structure 9*), which is an H with a missing arm, shows the least sensitivity of η_0, G_c and ω_c up to 50 wt% concentration. Whereas the most dangerous structure for η_0 and ω_c is a linear molecule with the length of an arm of an H (*structure 1*); an inclusion of 50 wt% of *structure 1* results in a decease of more than two orders of magnitude in η_0 and an increase of two orders of magnitude in ω_c. Similarly, the most dangerous structure for G_c is a linear molecule with the length of two arms plus half a cross-bar (*structure 4*). The maximum reduction in η_0 is more than 2 orders of magnitude, while for ω_c it is 2 orders of magnitude, but for G_c it is less than 1 order of magnitude.

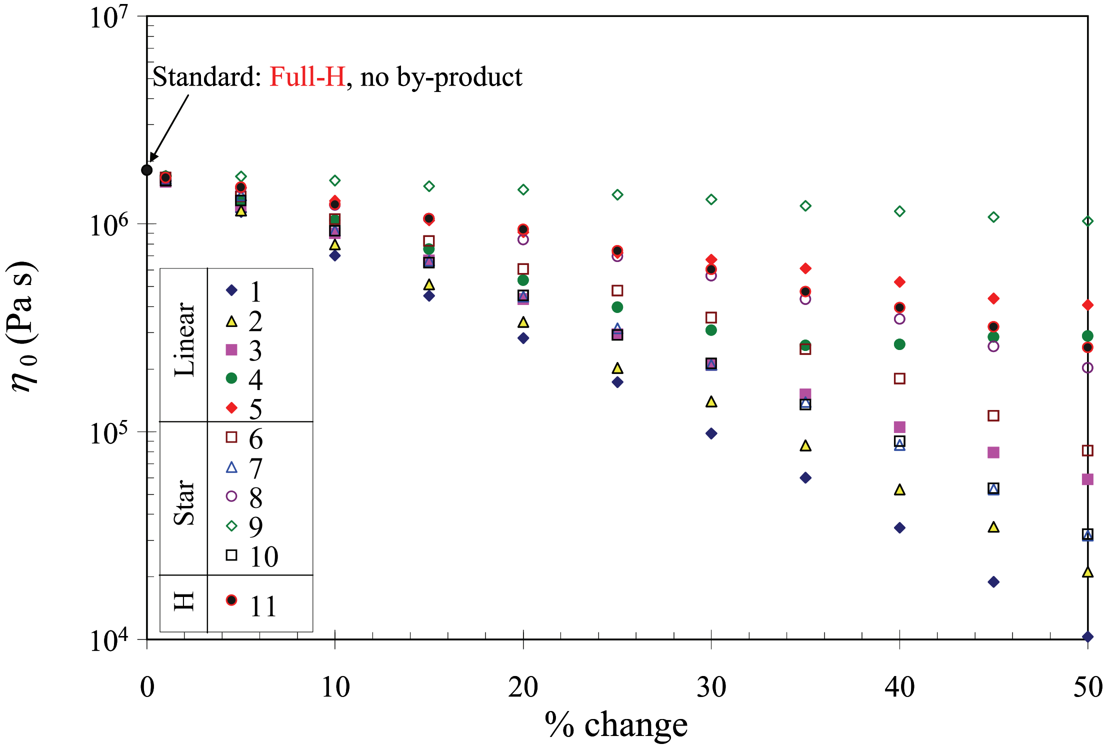

Figure 6.13 Sensitivity to low molecular weight by-products of η_0, as predicted by BoB

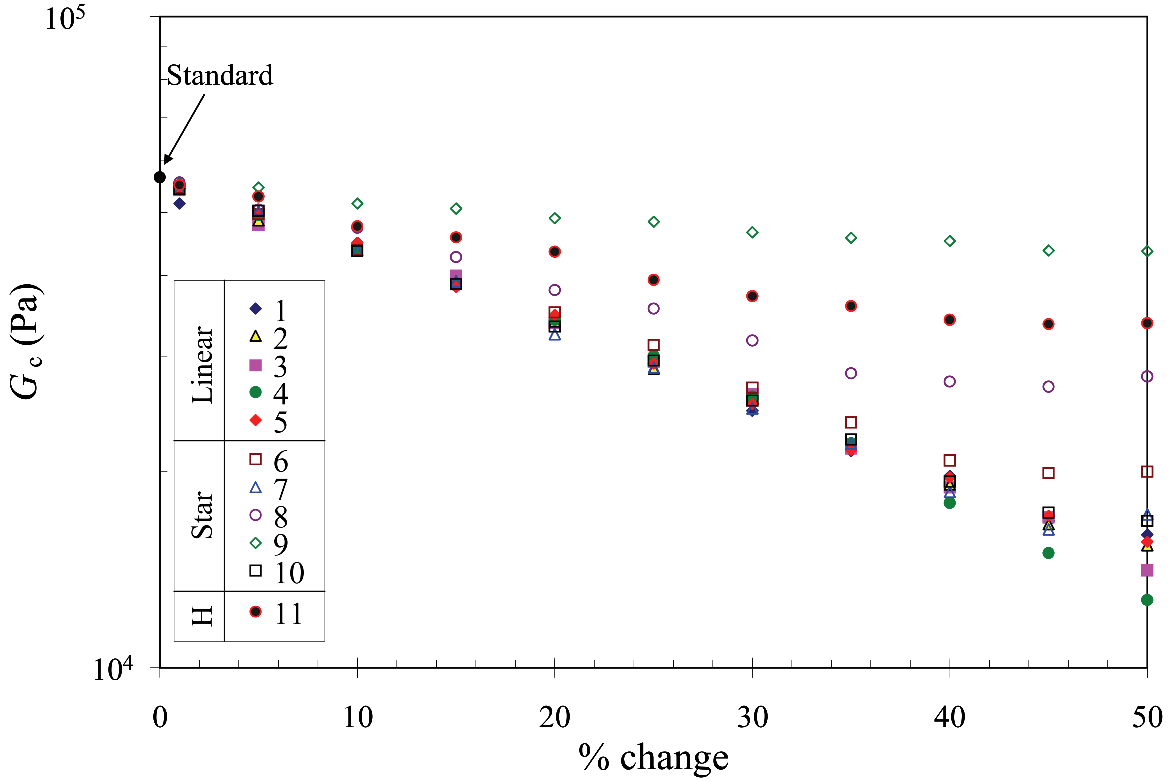

Figure 6.14 Sensitivity to low molecular weight by-products of G_c as predicted by BoB

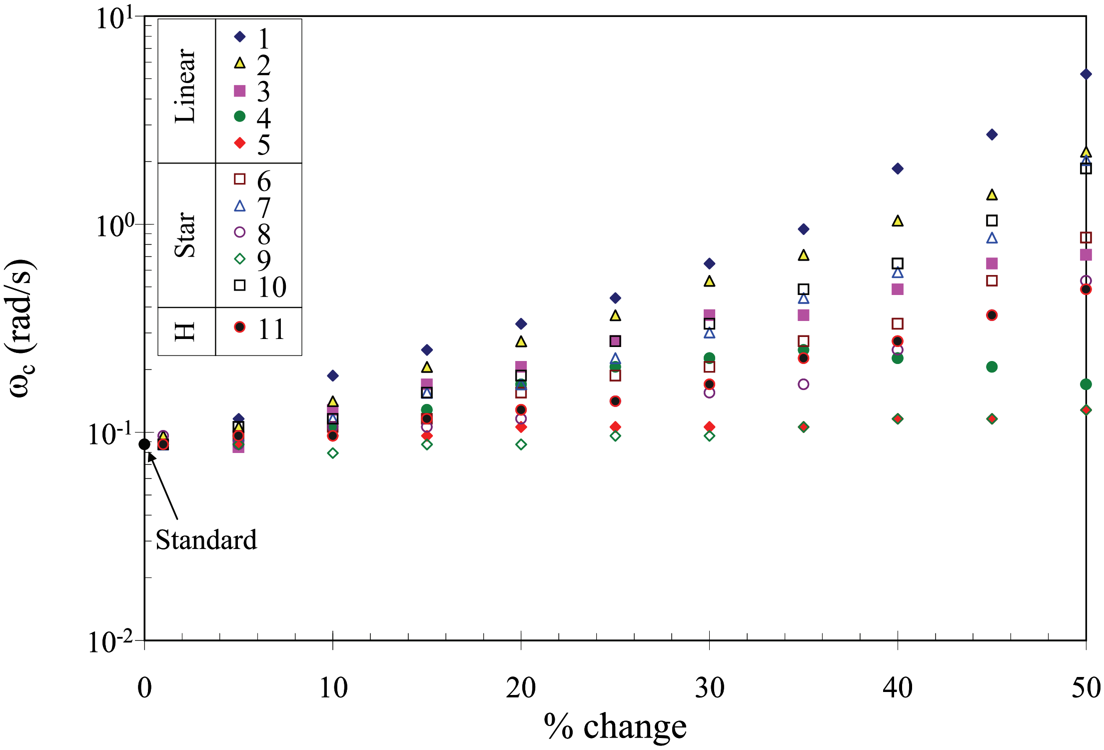

Figure 6.15 Sensitivity to low molecular weight by-products of ω_c as predicted by BoB

6.5.3 One-at-a-time (OAT) sensitivity analysis of the Hierachical-3.0 model

Ensembles used in Hierachical-3.0 throughout this chapter were generated by the BoB algorithm and converted to a format acceptable to Hierachical-3.0 by means of the program "ensemble_bob_to_hier.f" [66].

I. Sensitivity to G_N^0, τ_e, α and p^2

In Hierachical-3.0 the value of the dilution exponent α is pre-defined as either 1 or 4/3. Values other than these results in undefined values for other constants in the algorithm (line 246 to line 252 in Hierarchical_3.0). Therefore, sensitivity to α cannot be evaluated.

As shown in Figs. 6.16 to Fig. 6.18, τ_e and p^2 have relatively little effect when compared to G_N^0. A perturbation in τ_e result in one order of magnitude changes in ω_c and η_0 but only a 3% change in G_c. On the other hand, the maximum effect of varying p^2 was less than 2 %. As in the case of BoB, G_{N}^{0} is the most crucial variable among the three input variables. Changes in G_{N}^{0} result in as much as 10 orders of magnitude variation in η_0 and ω_c and about one order of magnitude in G_c. Therefore, the sensitivity of predictions to values of the input variables was in the order of G_{N}^{0} (most sensitive) $>> \tau_e > p^2$ (least sensitive).

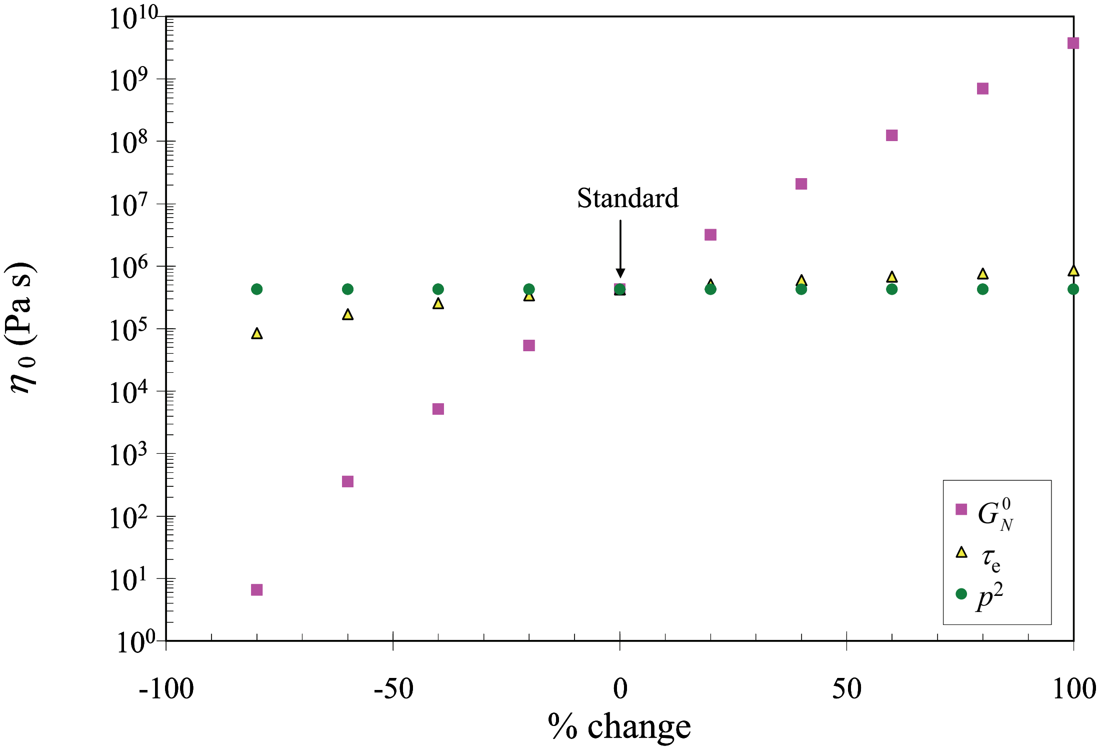

Figure 6.16 Sensitivity to G_{N}^{0}, τ_e and p^2 of η_0 predicted by Hierarchical-3.0

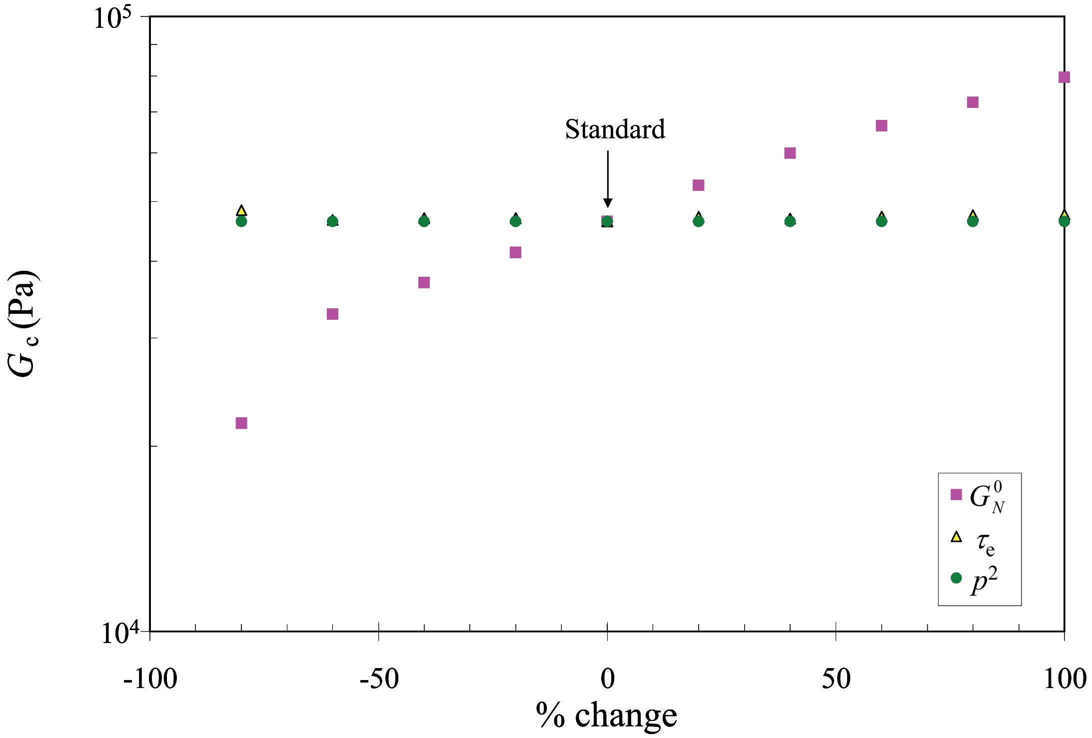

Figure 6.17 Sensitivity to G_N^0, τ_e and p^2 of G_c predicted by Hierarchical-3.0

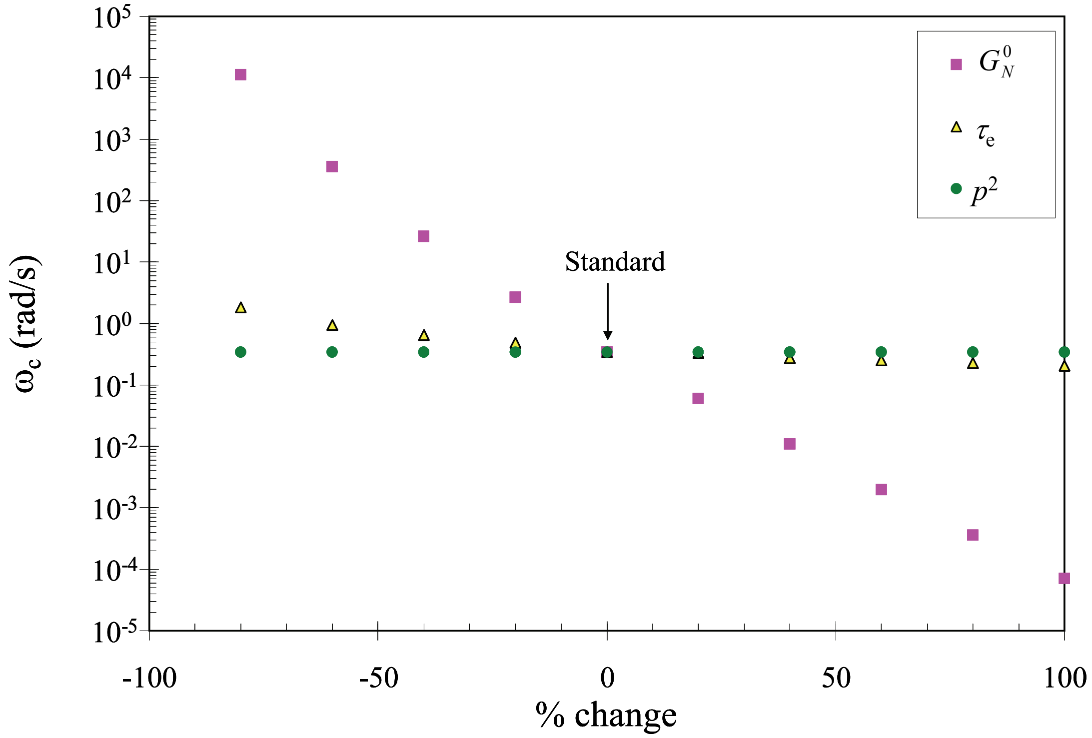

Figure 6.18 Sensitivity to G_N^0, τ_e and p^2 of ω_c predicted by Hierarchical-3.0

II. Sensitivity to $M_{\mathrm{w,cross\text{-}bar}}$, $M_{\mathrm{w,arm}}$, PDI$_{\mathrm{arm}}$ and PDI$_{\mathrm{cross\text{-}bar}}$

As in the case of BoB, $M_{\mathrm{w,cross\text{-}bar}}$ has a larger effect than $M_{\mathrm{w,arm}}$ on η_0 and ω_c, as shown in Figs. 6.19 and 6.20. Increases in $M_{\mathrm{w,cross\text{-}bar}}$ and $M_{\mathrm{w,arm}}$ causes an increase in η_0 and a decrease in ω_c. The effect of $M_{\mathrm{w,cross\text{-}bar}}$ on G_c is more complicated; as shown in Fig. 6.21 a positive deviation from the base value results in an increase in G_c. However, G_c has a local minimum at -20% in $M_{\mathrm{w,cross\text{-}bar}}$. It is noted that $M_{\mathrm{w,arm}}$ has a larger effect on G_c than $M_{\mathrm{w,cross\text{-}bar}}$, which is opposite to its effect on the BoB prediction.

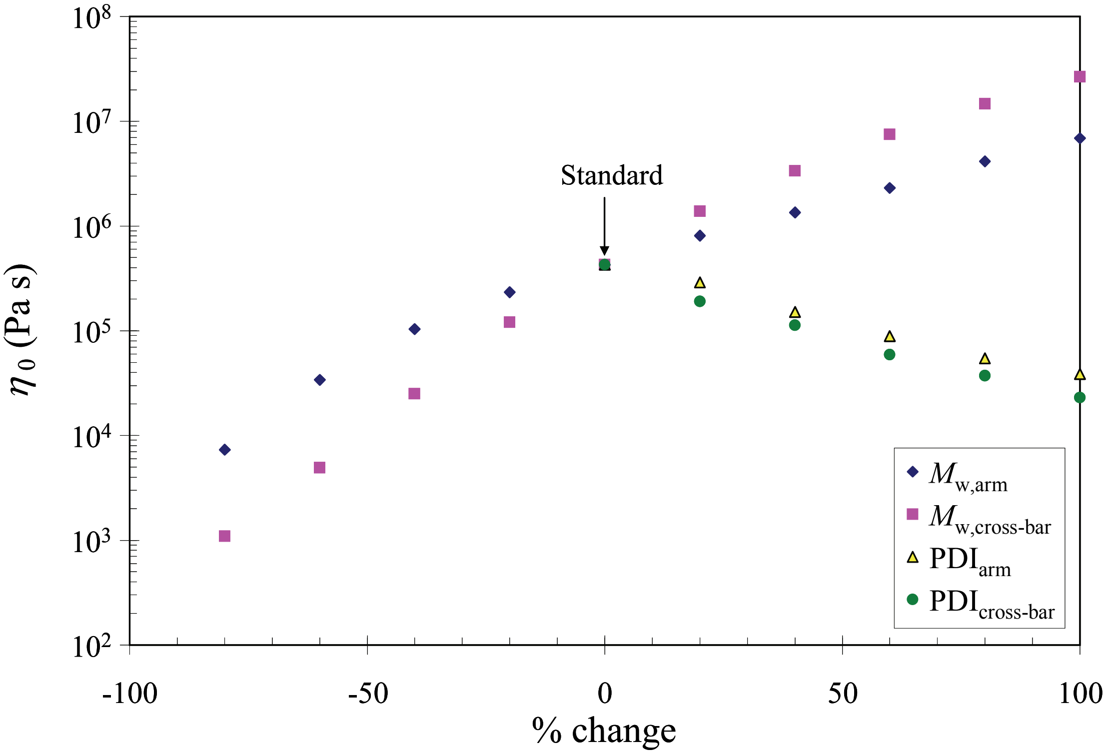

Figure 6.19 Sensitivity to molecular weight and distribution of η_0 as predicted by Hierarchical-3.0

In Hierachical-3.0, it was surprising that η_0 was slightly less sensitive to PDI$_{\mathrm{arm}}$ than to PDI$_{\mathrm{cross\text{-}bar}}$, which is opposite to what was found for the BoB model. However, both models predicted a decrease in η_0 with an increase in either PDI$_{\mathrm{arm}}$ or PDI$_{\mathrm{cross\text{-}bar}}$ when M_{w} and other parameters were fixed at their base values. Sensitivities to PDI$_{\mathrm{arm}}$ and

PDI$_{\text{cross-bar}}$ were almost the same for ω_c. On the other hand, PDI$_{\text{arm}}$ had a larger effect than PDI$_{\text{cross-bar}}$ on the predicted value of G_c.

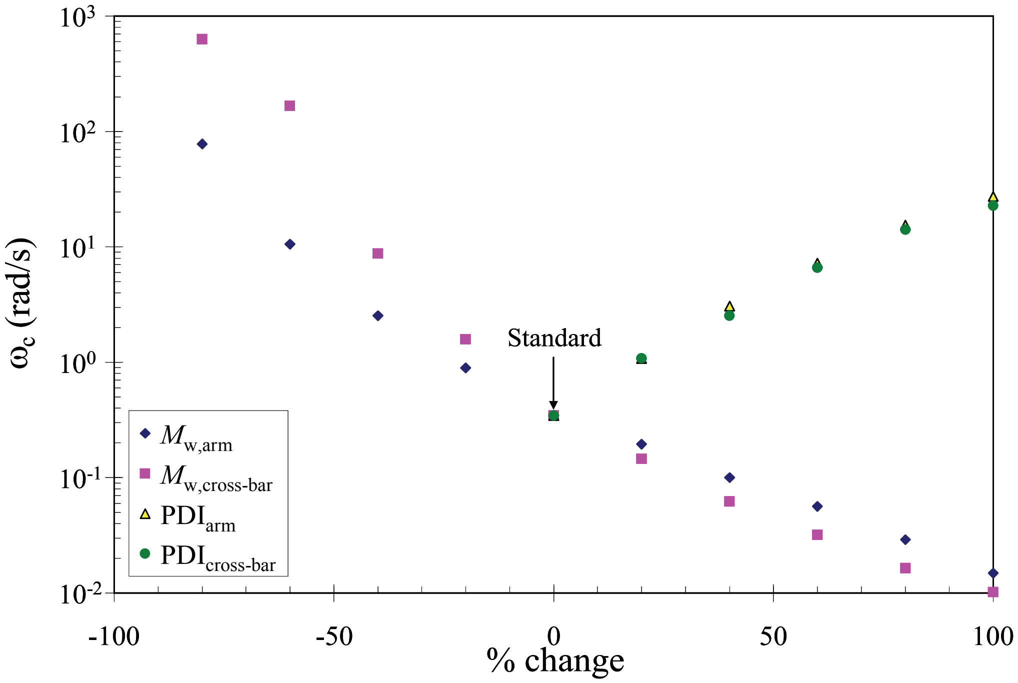

Figure 6.20 Sensitivity to molecular weights and distributions of ω_c as predicted by Hierarchical-3.0

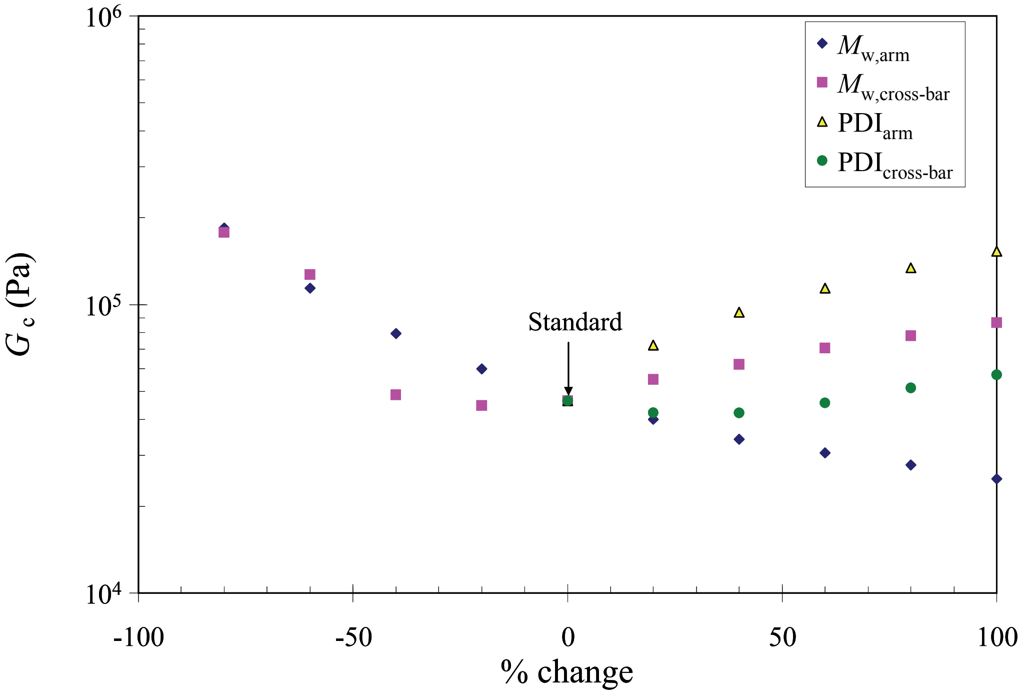

Figure 6.21 Sensitivity to molecular weights and distributions of G_c as predicted by Hierarchical-3.0

III. Sensitivity to the mode of the distribution

As shown in Fig. 6.22, the mode of distribution has negligible effect (1% maximum over the entire frequency range) on predictions when PDI is small.

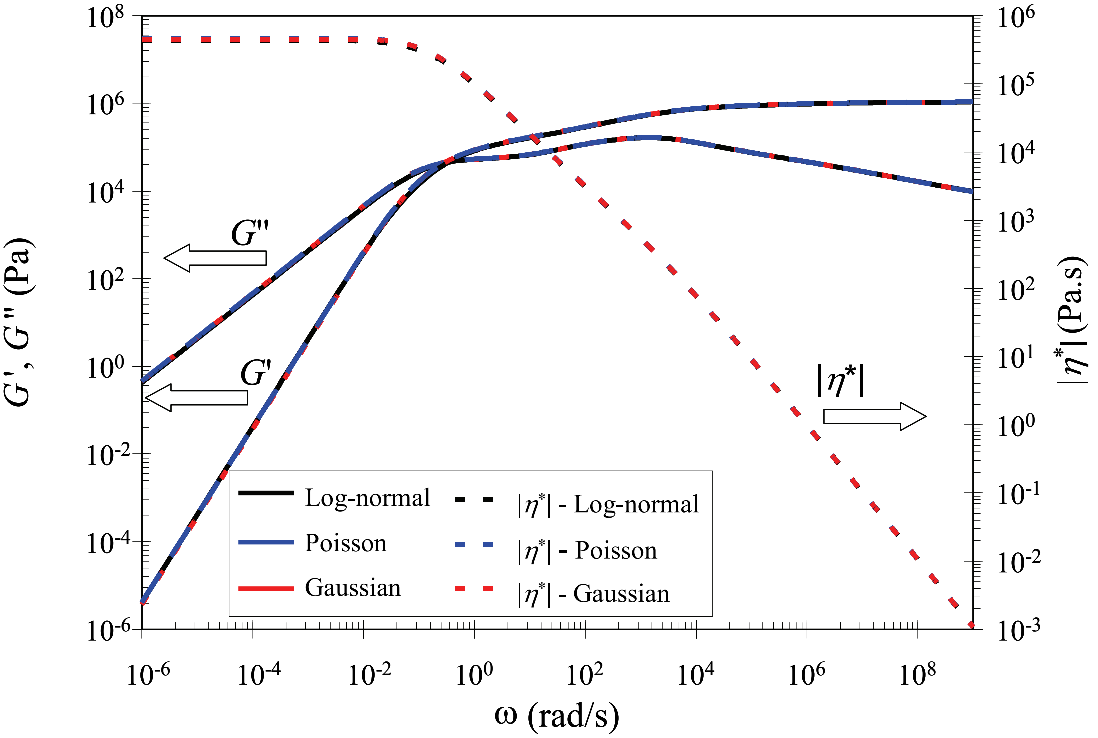

Figure 6.22 Sensitivity of moduli to mode of molecular weight distribution for a nearly monodisperse system; prediction of Hierarchical-3.0

Since a Poisson distribution is not appropriate for large PDI (e.g. PDI_{arm} and $\text{PDI}_{\text{cross-bar}}$ are both equal to 2), only the log-normal and Gaussian distributions were used to describe high PDIs of arms and cross-bars. As shown in Fig. 6.23, there was no effect of distribution on G_c but prominent effects on ω_c (30%) and η_0 (25%) when going from a log-normal to a Gaussian distribution.

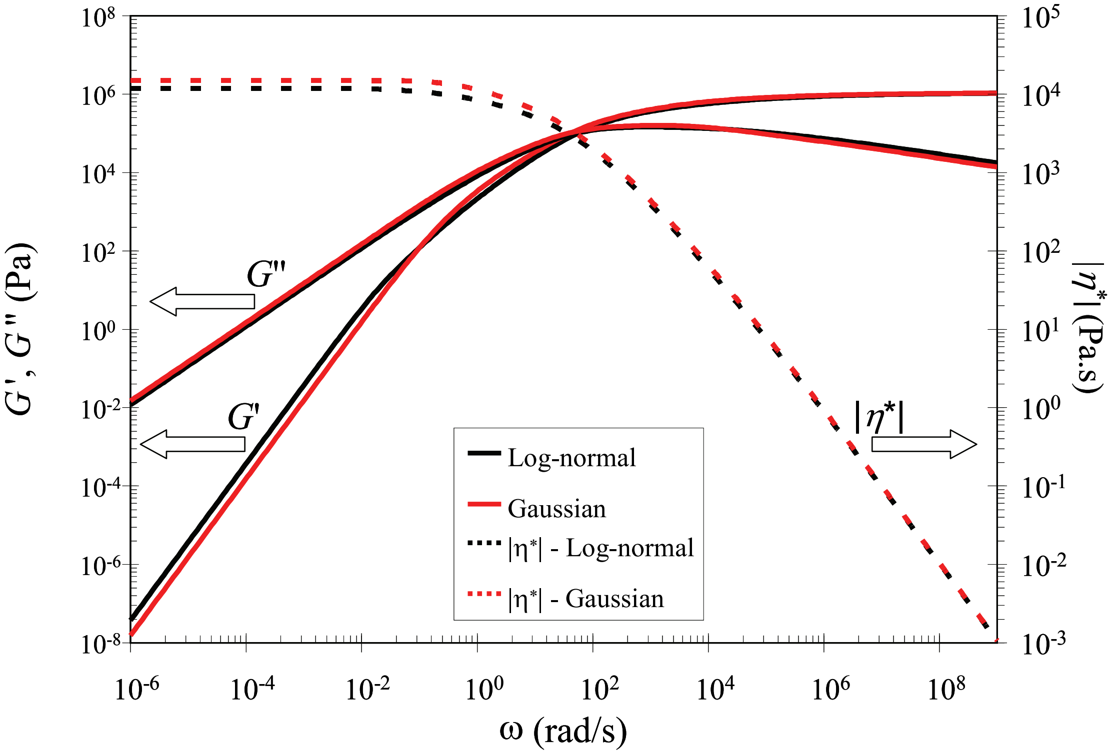

Figure 6.23 Sensitivity to mode of molecular weight distribution (polydisperse system) of moduli predicted by Hierarchical-3.0

IV. Sensitivity to number of ensembles

The number of ensembles used to represent the system was found to have negligible effect on predictions when it exceeded 10,000. Above 10,000, the effects on G_c and ω_c were 1% at most and on η_0 it was less than 5%. It is noted that 10,000 ensembles is the maximum allowed by the algorithm; predictions in Fig. 6.24 based on more than 10,000 ensembles were performed by a slight modification of the variable “maxm” in the hierarchical_3.f, a FORTRAN program written for use with Hierarchical-3.0.

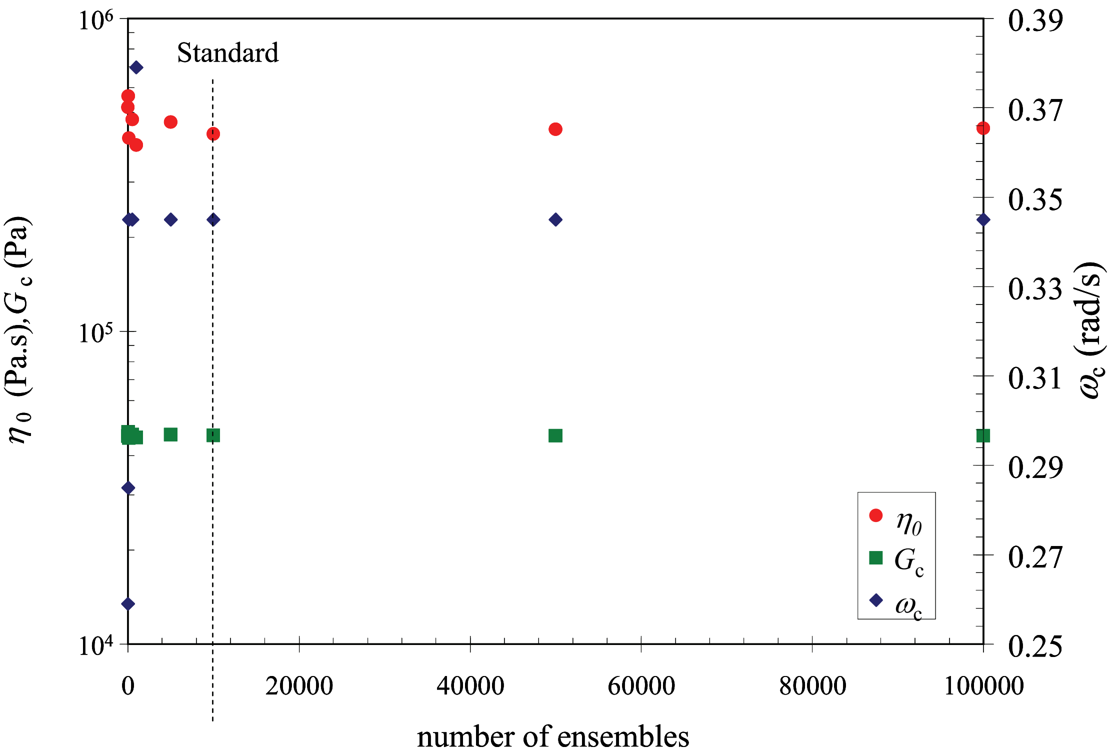

Figure 6.24 Sensitivity to number of ensembles of η_0, ω_c and G_c as predicted by the Hierarchical-3.0 model

V. Sensitivity to presence of reaction by-products

As in the case of the BoB model, the inclusion of any amount of by-product *except structure 8* resulted in a lower values of η_0 and G_c, but a higher ω_c as shown in Figs. 6.25 to Fig. 6.27. Again, inclusion of 1 wt% by-products of any structure, had negligible effect on η_0, G_c and ω_c. When including linear, star and H by-products in the simulation, the predictions of Hierachical-3.0 agreed well with those of BoB, with the following exceptions regarding G_c. First, the effect on G_c in hierachical-3.0 was more prominent than in BoB, in that G_c was unaffected up to 10 wt% linear by-products; regardless of chain length. Second, inclusion of asymmetric stars (*structure 8*) resulted in a local minimum in G_c at 20 wt%. Beyond 20wt%, G_c increased with increasing concentration of the by-product (*structure 8*). Lastly, inclusion of the H-shaped by-products (*structure 11*) had very little effect on G_c, which was less sensitive to this contaminant than in BoB predictions.

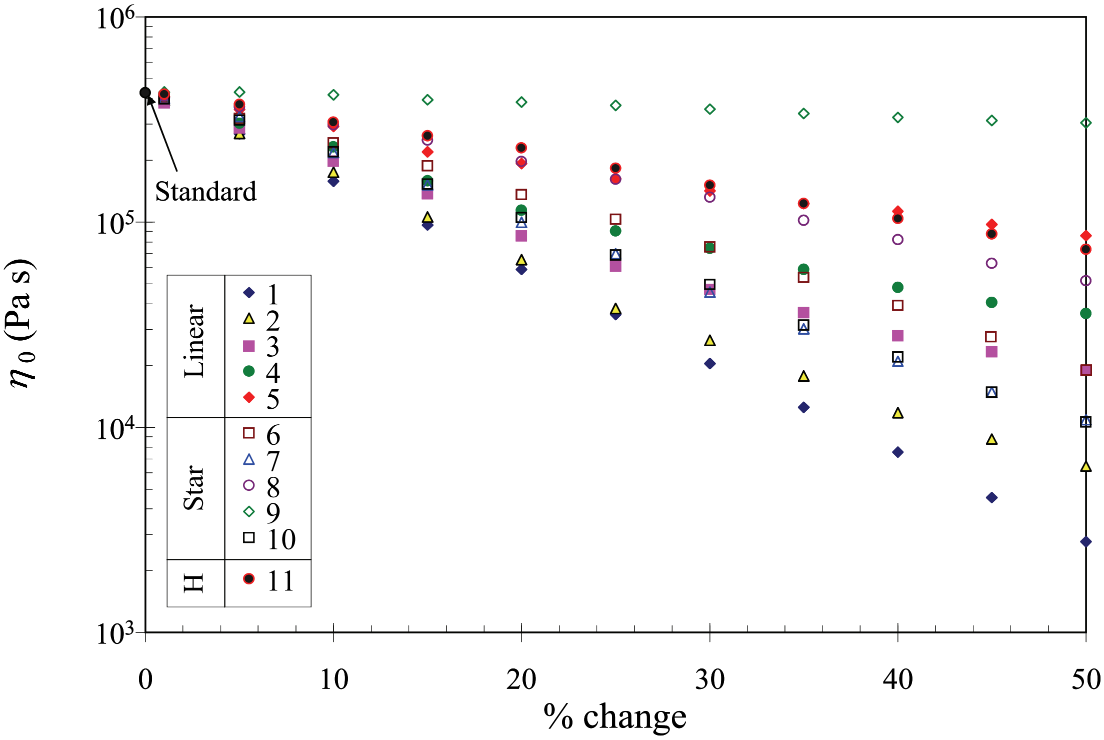

Figure 6.25 Sensitivity to low molecular weight by-products of η_0 predicted by hierarchical-3.0

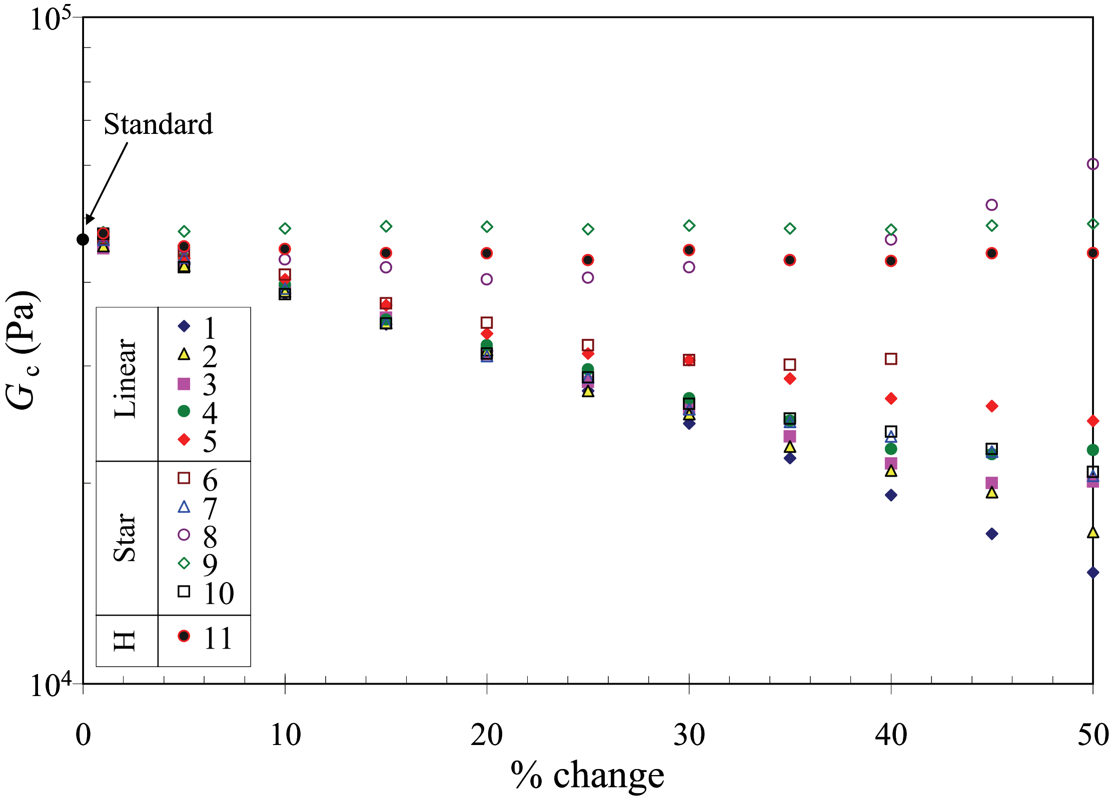

Figure 6.26 Sensitivity to low molecular weight by-products of G_c predicted by hierarchical-3.0

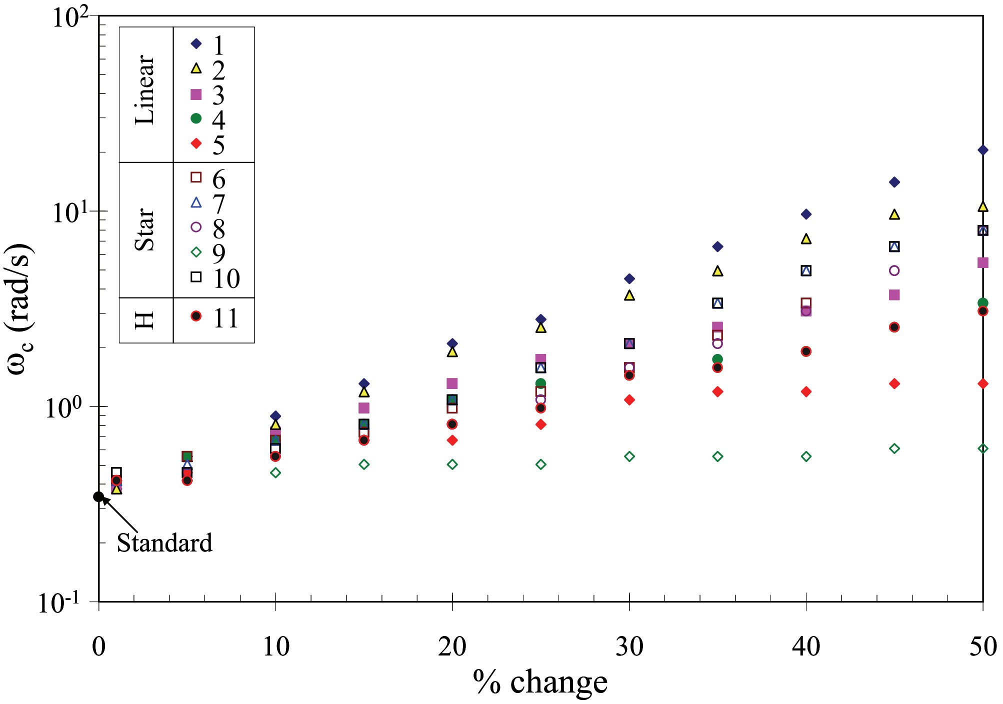

Figure 6.27 Sensitivity to low molecular weight by-products of ω_c predicted by hierarchical-3.0

6.5.4 Conclusions of OAT sensitivity analyses of the models

Based on the above sensitivity analysis of predictions for an H-shaped polymer, we note that τ_e has little effect on model predictions, and the mode of molecular weight distribution has negligible effect if the molecular weight distributions of arms and cross-bar are narrow, *e.g.* PDI$_{\text{cross-bar}}$ = 1.13. Predictions of both models are independent of the number of ensembles used to represent the system as long as it exceeds 10,000.

In response to a given variation G_N^0 has the largest effect on the predictions of both models, followed by the presence of short linear and symmetric-star by-products. However, the presence of asymmetric 3-arm stars that are equivalent to half-H molecules has the least effect of the by-products considered. The effects of α , p^2 , $M_{\text{w,cross-bar}}$, $M_{\text{w,arm}}$, PDI$_{\text{arm}}$, PDI$_{\text{cross-bar}}$ and the presence of other by-products are comparable for both models, although the sensitivity analysis was not applicable to α , and p^2 has a weak effect on hierachical-3.0 predictions. **Therefore, in doing simulations it is essential to know the detailed structure of the sample and to use an appropriate value of G_N^0 .**

6.6 Uncertainty analysis

An uncertainty analysis reveals the effects of lack of knowledge about the true values of model parameters and potential defects in the model. Both sensitivity and uncertainty analyses are required for the objective evaluation of a model by comparing its predictions with experimental of data. From the above sensitivity analysis, model predictions were found to be particularly sensitive to the value of G_N^0 and the presence of short linear and symmetric star by-products. In practice, the uncertainty in the experimental value of G_N^0 was ± 10% when it was determined as carefully as possible using the method described in Chapter 4. In other words, the value of G_N^0 that was identified with the minimum phase angle for H-polymer was found to be 1.05 ± 0.11 MPa, as shown in Chapter 4.

The TGIC data shown in Chapter 3 allow us to estimate the concentration of by-products in HA12B40. A small amount of material was fractionated by TGIC, and the molecular weight of each component was measured *in situ* by light scattering and a refractive index detectors. Refractive index signals were deconvoluted using Gaussian fitting to calculate the weight fraction of each component, and the results are shown in Table 6.3. At present, there is no explanation of peaks 7 to 9, which should correspond to higher molecular weight by-products. For reasons mentioned below, it was assumed that no high molecular weight by-products were present in HA12B40. First, peaks 6 and 7 were not completely separated. Second, the high molecular weight by-products observed by Perny *et al*. [104] were less likely to form in our case [110]. Third, neither model can deal with the structures hypothesized by Perny *et al*. [104]. And lastly, TGIC gives no information regarding the structures corresponding to these peaks.

The objective of this uncertainty analysis was to quantify the effect of uncertainty in the value of G_N^0 with a base value of 1.05MPa and the presence of the by-products listed in Table 6.3. Several cases were considered and are listed in Table 6.4. The standard case had the base values as shown in Table 6.2 except that G_N^0 was the experimentally determined value obtained as explained in Chapter 4 (1.05MPa for HA12B40). Cases I to

IV, involve the by-products listed in Table 6.3. As in the sensitivity analysis, values of η_0 , G_c and ω_c determined in the simulations were compared with experimental values.

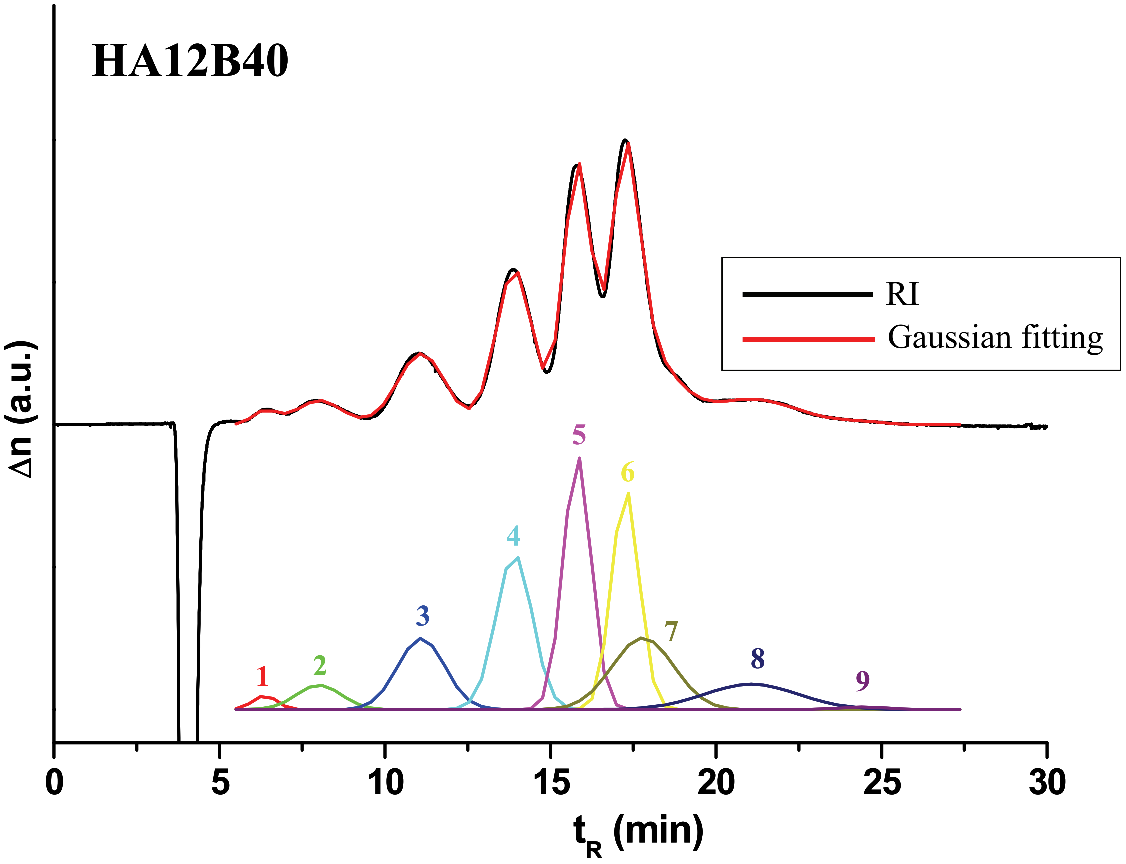

Figure 6.28 Refractive index signal of HA12B40 measured *in situ* during fractionation by TGIC

Table 6.3 Estimated by-products present in HA12B40

Peak	***M*w**	***M*n**	**wt%**	**Proposed structure**
1	29.3	28.8	1%	linear (structure 3)
2	57.3	56.4	5%	linear (structure 5)
3	43.4	43.1	14%	linear (structure 4) or star (structure 6)
4	55.3	55.1	24%	star (structure 8)
5	69.2	68.5	30%	star (structure 9)
6	79.6	79.1	26%	H

Table 6.4 Cases considered in the uncertainty analysis for HA12B40

	Input parameters	**Contains by-products?**
Base Case	Same as Table 6.2 except G_N^0 =1.05MPa	No
Case I	Same as Table 6.2 except G_N^0 =1.05MPa	Yes, peak 3 corresponds to a linear by-product
Case II	Same as Table 6.2 except G_N^0=1.05MPa	Yes, peak 3 corresponds to an asymmetric star by-product
Case III	Same as Table 6.2 except G_N^0 =1.16MPa (+10%)	Yes, peak 3 corresponds to a linear by-product
Case IV	Same as Table 6.2 except G_N^0=0.945MPa (-10%)	Yes, peak 3 corresponds to a linear by-product

6.6.1 Uncertainty analysis of BoB model predictions

Table 6.5 compares the BoB predictions for HA12B40 corresponding to the Cases listed in Table 6.4 with experimental data. Assuming that the material contains only H-molecules, and using the experimentally determined G_N^0 (the base case), the predicted terminal zone showed up much later than in the data, resulting in higher values of η_0 and G_c but a smaller ω_c.

Next, by-products at levels up to 75 wt% were added as shown in Table 6.4 for Cases I and II; this brought the predictions closer to the data, and agreement was further improved when the experimentally determined G_N^0 was reduced by 10%, which is Case IV. We note that changing the structure corresponding to peak 3 from a linear to an asymmetric star at the same total molecular weight had no effect on ω_c but caused variations of ~10% in G_c and ~20% in η_0 as shown by Cases I and II. However, significant changes in η_0 and G_c were observed when an uncertainty of ± 10% in G_N^0 was introduced along with the inclusion of the 75 wt% of the by-products listed in Table 6.3 and assuming peak 3 applies to a linear by-product (Cases III and IV). Case III shows that a 10% increase in G_N^0 above its base value of 1.05 MPa, keeping the same composition, increases η_0 ~150% and G_c ~10% and decreases ω_c ~50%. In Case IV, decreasing G_N^0 by 10% decreased η_0 by ~60% and increased G_c by ~7 % and ω_c by ~250%.

Table 6.5 Uncertainty analyses of BoB predictions for HA12B40

	Exp. Value	Base Case	Case I	Case II	Case III	Case IV
$G_c \times 10^{-4}$ (Pa)	3.49	5.56	2.43	2.64	2.7	2.59
$\eta_0 \times 10^{-5}$ (Pa.s)	0.834	18.1	3.25	3.96	8.28	1.24
ω_c (rad/s)	1.39	0.0795	0.206	0.206	0.106	0.712

Therefore, uncertainty in identifying by-product peak 3 as due to linear or star shaped molecules has little effect on predictions of the BoB model, whereas the presence of by-products and uncertainty in the value of G_N^0 have major effects on predictions. The inclusion of the by-products inferred from the MWD and the synthesis route gives the best agreement with experimental data that can be obtained without adjusting any parameters, as shown in Table 6.2.

6.6.2 Uncertainty analysis of Hierachical-3.0 model predictions

Table 6.6 shows the predictions for sample HA12B40 of Hierachical-3.0 using ensembles generated by the BoB algorithm. Again, assuming the sample contained only full H molecules (*i.e.* the base case) gave poor agreement with experimental data. The predicted terminal zone was shifted to a longer time (*i.e.* lower frequency), resulting in higher G_c and η_0 and lower ω_c than measured values.

Table 6.6 Uncertainty analyses of Hierarchical-3.0 predictions for HA12B40

	Exp. Value	Base Case	Case I	Case II	Case III	Case IV
$G_c \times 10^{-4}$ (Pa)	3.49	4.82	6.6	7.7	5.89	8.35
$\eta_0 \times 10^{-4}$ (Pa.s)	8.34	42.7	2.82	3.53	6.00	1.36
ω_c (rad/s)	1.39	0.442	14.1	15.5	5.98	44.1

Faster relaxation was predicted when 75 wt % by-products were included, *i.e.* Case I to Case IV as shown in Table 6.4. The effect of interpreting peak 3 as asymmetric stars rather than linear polymers, keeping the total molecular weight fixed, is revealed by comparing Cases I and II, where we see ~15% increase in G_c ,~20% increase in η_0 and 10% increase in ω_c. On the other hand, comparing Cases III and IV we see a 50% reduction in G_c and a 70% enhancement in η_0 when G_N^0 is increased by 10%. The effect on ω_c is dramatic as there is almost an order of magnitude decrease. We conclude that uncertainty in identifying the structure corresponding to peak 3 has similar effects on G_c, ω_c and η_0 for both models, while the uncertainty arising from the value of G_N^0 is less prominent for BoB than for Hierachical-3.0.

6.7 Corroboration

Corroboration is the process of comparing model predictions with experimental data, to evaluate the effectiveness of the model. For simulating polydisperse systems, a log-normal distribution was used to generate ensembles. Although the Poisson distribution is best for anionically synthesized polymer, it fails to generate ensembles that can represent polydisperse systems (*e.g*. PDI=2) for BoB simulations as shown by the sensitivity analysis. And when the system is fairly monodisperse, the prediction is insensitive to the distribution used.

Sensitivity analysis showed that the predictions of both models are very sensitive to the value of G_N^0, the presence of low molecular weight by-products, and the molecular weight distribution. Therefore, the evaluation of each model made use of several combinations of G_N^0 and molecular weight distribution. Parameter values were taken from previous work, and these are shown in Table 6.1 as the "suggested values" for both models, while "Exp. G_N^0" as shown in the legend of the following figures represents the experimental value of G_N^0 determined as described in Chapter 5. In this section, simulations performed for the monodisperse case were done using a total of 10,000 ensembles. For the polydisperse case, simulations were done using 10,000 ensembles for each indentified component.

The Hierachical-3.0 model does not include the fast Rouse motion that is the main relaxation mechanism at very short times or high frequencies, while the BoB model does not capture the frequency response for $\omega > 1/\tau_{\mathrm{e}}$, (*i.e.* $\omega > 10^6$ rad/s since $\tau_e = 2.75 \times 10^7 s$ for PBD). Thus, the maximum frequency considered for the evaluation of both models was ω=10^5 rad/s.

6.7.1 Linear PBDs

For linear PBDs, the molecular structures based on SEC/TALLS data were used for modeling. In both models, the molecular weight between entanglements M_e was related to G_{N}^0 by Eq. 6.1 except that the suggested value of G_{N}^0 was also used in a simulation based on Hierachical-3.0.

For PBD2, a binary blend of linear components, both models did equally well in predicting the linear rheological behavior, and the differences between suggested and experimental values of the parameters were small. As shown in Fig. 6.29, BoB gave the best prediction if it was assumed each component was monodisperse and if the suggested parameter values were used. On the other hand, Hierachical-3.0 gave the best prediction using the experimental G_{N}^0 and included the effect of polydispersity in molecular weight as seen in Fig. 6.30. The inclusion of the polydispersity in molecular weight of each component generally predicts a lower $|\eta^*|$ than in the monodisperse case. This is consistent with the result of the sensitivity analysis that a broader molecular weight distribution yields a lower value of η_0. For this linear blend, the two models give equally satisfactory predictions if the input information is allowed to vary according to the model

For PBD3, a blend of three linear polymers, BoB gave predictions similar to those for PBD2. A combination of assuming each component as monodisperse and using the suggested values gave the best BoB prediction as observed in Fig. 6.31. However, in contrast with the model's performance for PBD2, as shown in Fig. 6.32, the best prediction of Hierachical-3.0 is obtained by taking the polydispersity of each component into account and using the suggested values. Both models quantitatively predict the linear rheological behavior of the three-component blends, although neither can capture the shoulder in the $G'(\omega)$ curve.

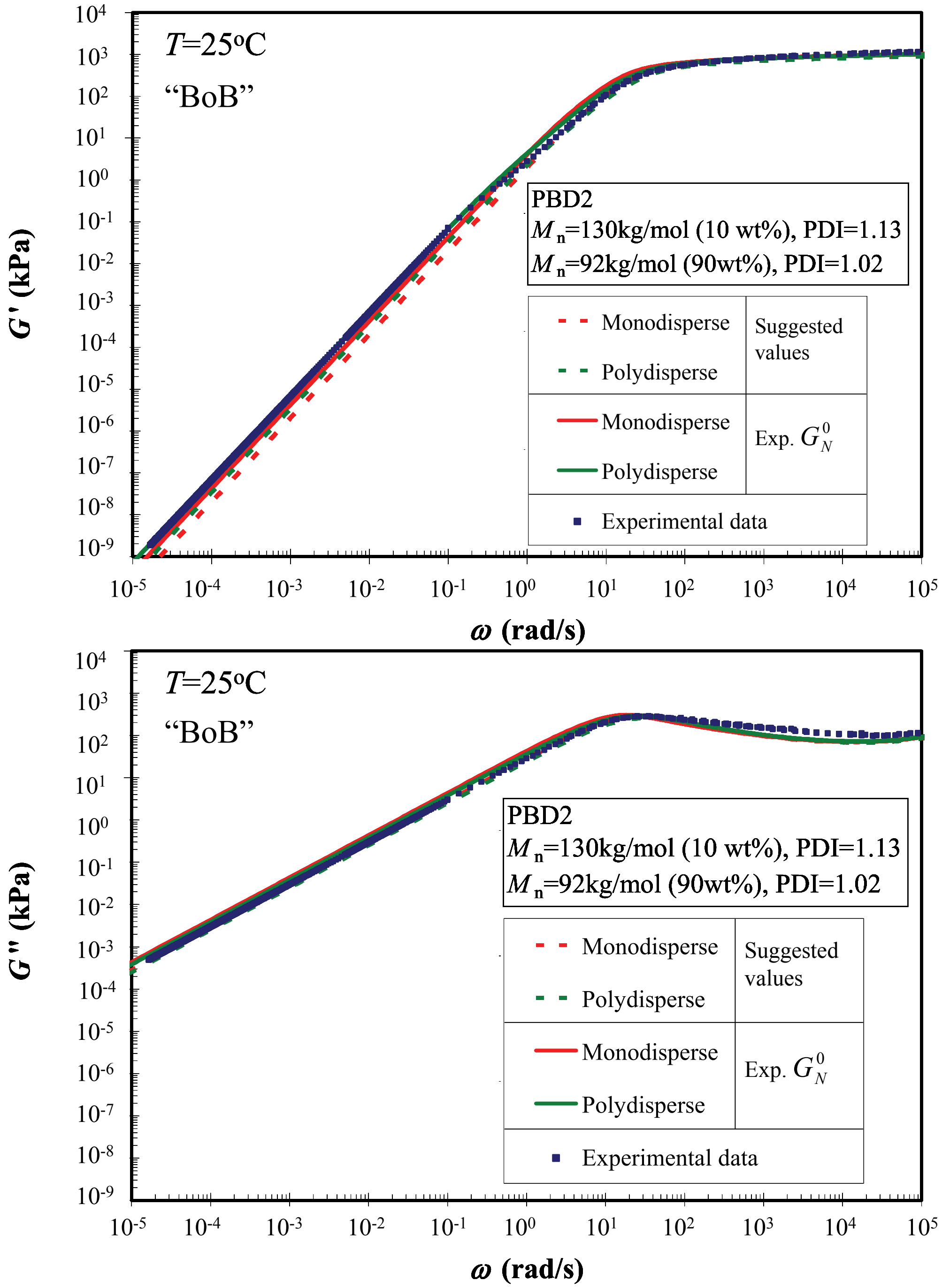

Figure 6.29 Comparison of storage and loss moduli predicted by BoB with experimental data for PBD2

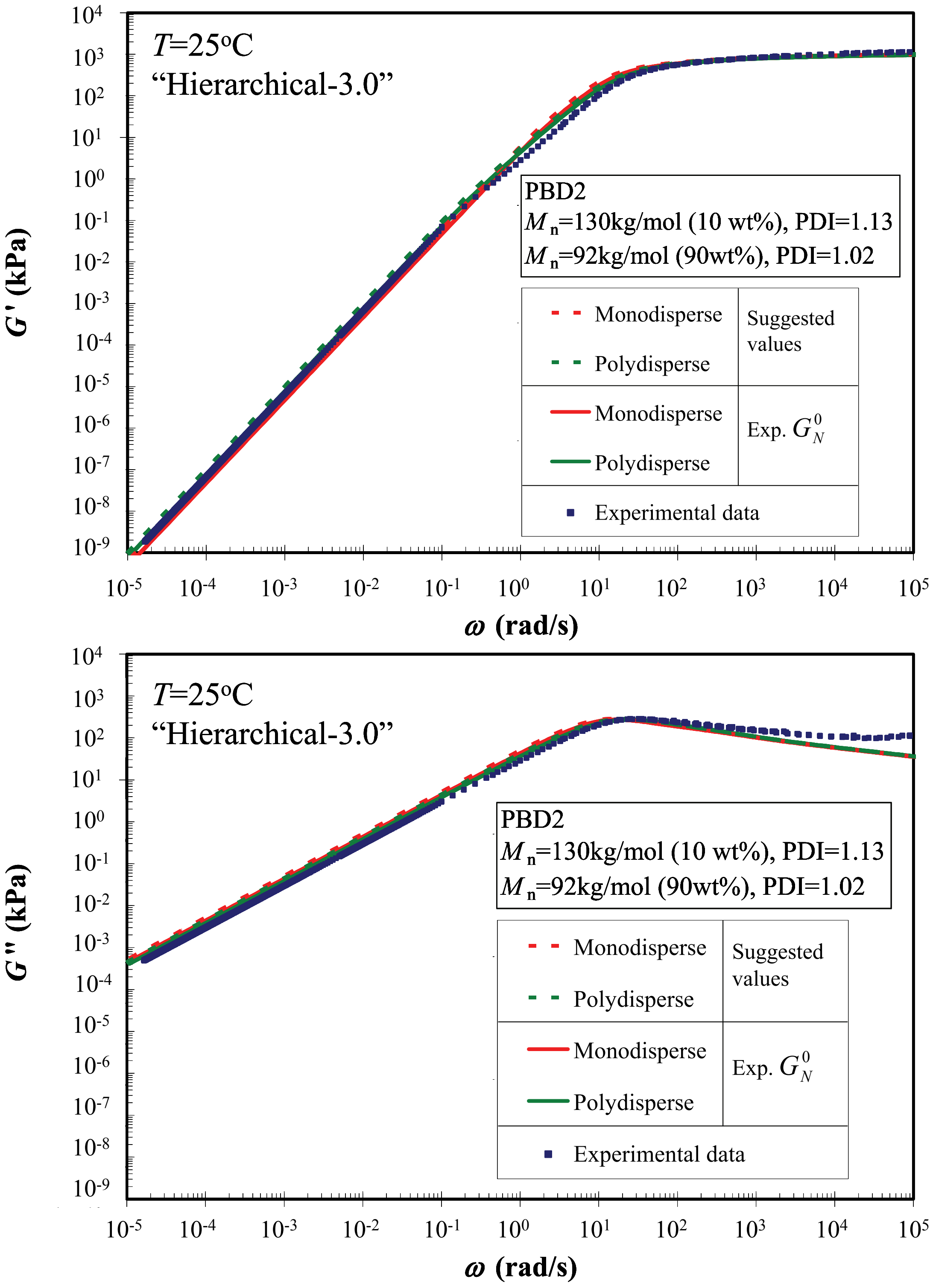

Figure 6.30 Comparison of storage and loss moduli predicted by Hierarchical-3.0 with experimental data for PBD2

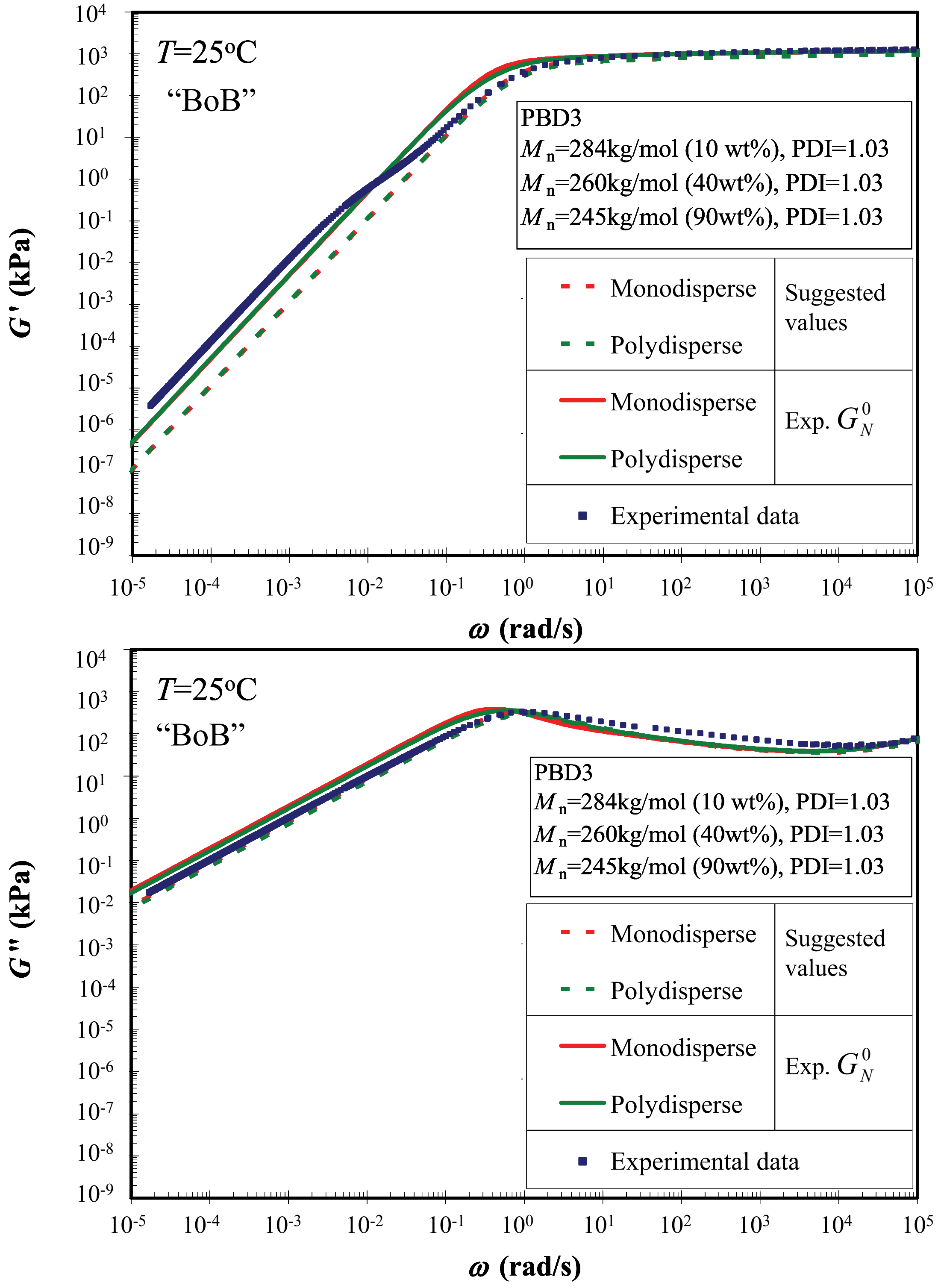

Figure 6.31 Comparison of storage and loss moduli predicted by BoB with experimental data for PBD3

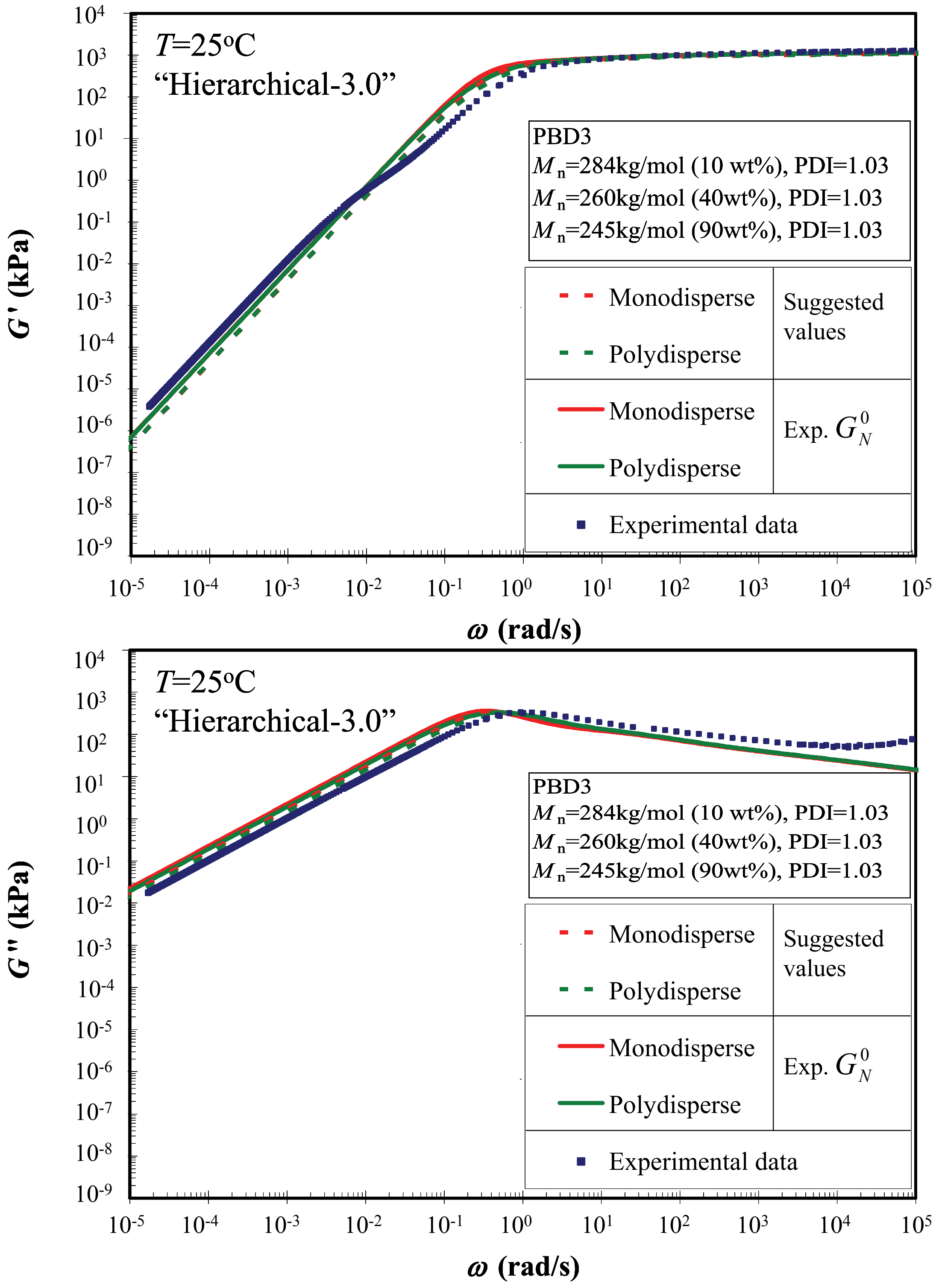

Figure 6.32 Comparison of storage and loss moduli predicted by Hierarchical-3.0 with experimental data for PBD3

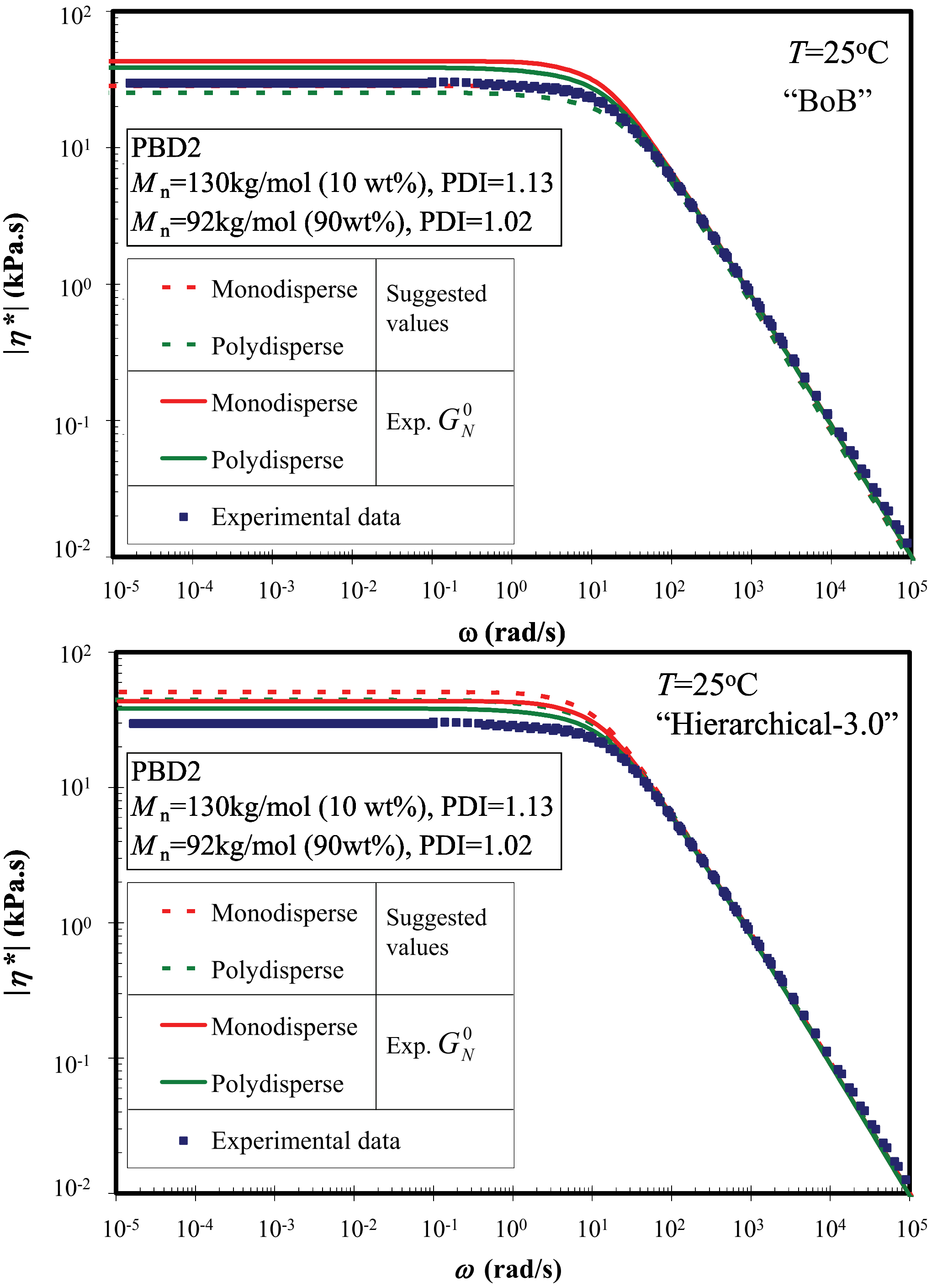

Figure 6.33 Comparison of the absolute value of the complex viscosity predicted by BoB and by Hierarchical-3.0 with experimental data for PBD2

We noted that considering only the absolute value of complex viscosity $|\eta^*|$ is not sufficient to compare models quantitatively. As shown in Fig. 6.33 at frequencies above

$\omega = 10^2$ rad/s for PBD2, predictions were essentially the same regardless of the combination of G_N^0 and PDI, and details shown in the dynamic moduli curves are smeared out. Therefore, to quantitatively compare the two models, we compared ω_c, G_c and η_0 obtained experimentally with predicted values. As shown in Tables 6.7 and 6.8, BoB generally works best with the suggested values and with PDI=1 for each component in the linear blends (highlighted in Grey in both Tables). However, Hierachical-3.0 generally works best with the inclusion of polydispersity for each component, while no definite conclusion can be made about the selection of the G_N^0 value (highlighted in Yellow in both Tables). Comparing the best predictions of each model, BoB gives a better prediction of η_0 than Hierachical-3.0, while both models do equally well in predicting ω_c and G_c. This is due to the fact that the value of the dilution exponent α =1 in BoB provides better predictions for the behavior of linear-linear binary blends than α = 4/3 in Hierachical-3.0 [63,158,176], and this is also true for three-component linear blends.

Table 6.7 Comparison of ω_c, G_c and η_0 predicted by both models with experimental data for PBD2

PBD2	ω_c (rad/s)		G_c (kPa)		η_0 (kPa.s)	
Experimental data	**25.2**		**284**		**29.8**	
	BoB	Hierachical-3.0	BoB	Hierachical-3.0	BoB	Hierachical-3.0
Suggested value + monodisperse	22	20.6	270	277	28.4	50.7
Suggested value + polydisperse	26.6	18.7	260	279	25.4	44.5
Exp. G_N^0 + monodisperse	15	18.7	297	274	43	43.4
Exp. G_N^0 + polydisperse	18.2	22.7	285	270	38.7	38.3

Table 6.8 Comparison of ω_c , G_c and η_0 predicted by both models with experimental data for PBD3

PBD3	ω_c (rad/s)		G_c (kPa)		η_0 (kPa.s)	
Experimental data	**0.89**		**307**		**1030**	
	BoB	Hierachical-3.0	BoB	Hierachical-3.0	BoB	Hierachical-3.0
Suggested value + monodisperse	0.7	0.5	312	330	838	1659
Suggested value + polydisperse	0.86	0.61	284	308	740	1436
Exp. G_N^0 + monodisperse	0.37	0.42	387	354	1955	2240
Exp. G_N^0 + polydisperse	0.49	0.5	354	332	1709	1917

6.7.2 H-shaped PBDs

For H-shaped PBDs, model predictions were preformed using the SEC/TALLS-based structural information provided by M.S. Rahman at the University of Tennessee. This is because this was the only molecular weight characterization that gave information about arms and half-H intermediates. Without assuming the molecular weights of arms or cross-bars, simulation could not be done using SEC data provided by Dow Chemical or Pohang University of Science and Technology. Since additional TGIC data were available for sample HA12B40, simulations based on these data are reported separately at the end of this section.

HA12B40– based on SEC/TALLS data

Use of the experimental G_N^0 for BoB simulations increased the relaxation time (Fig. 6.34) compared with results using the suggested value, and the opposite was observed for Hierachical-3.0 (Fig. 6.35). For both models, the inclusion of arm and cross-bar polydispersities decreased the relaxation time, but both models still over-estimated the relaxation time in all cases considered here. This is contrary to the observations of Wang *et al*. for an H-shaped polyisoprene [63], where both models under-estimated results using either set of input parameters.

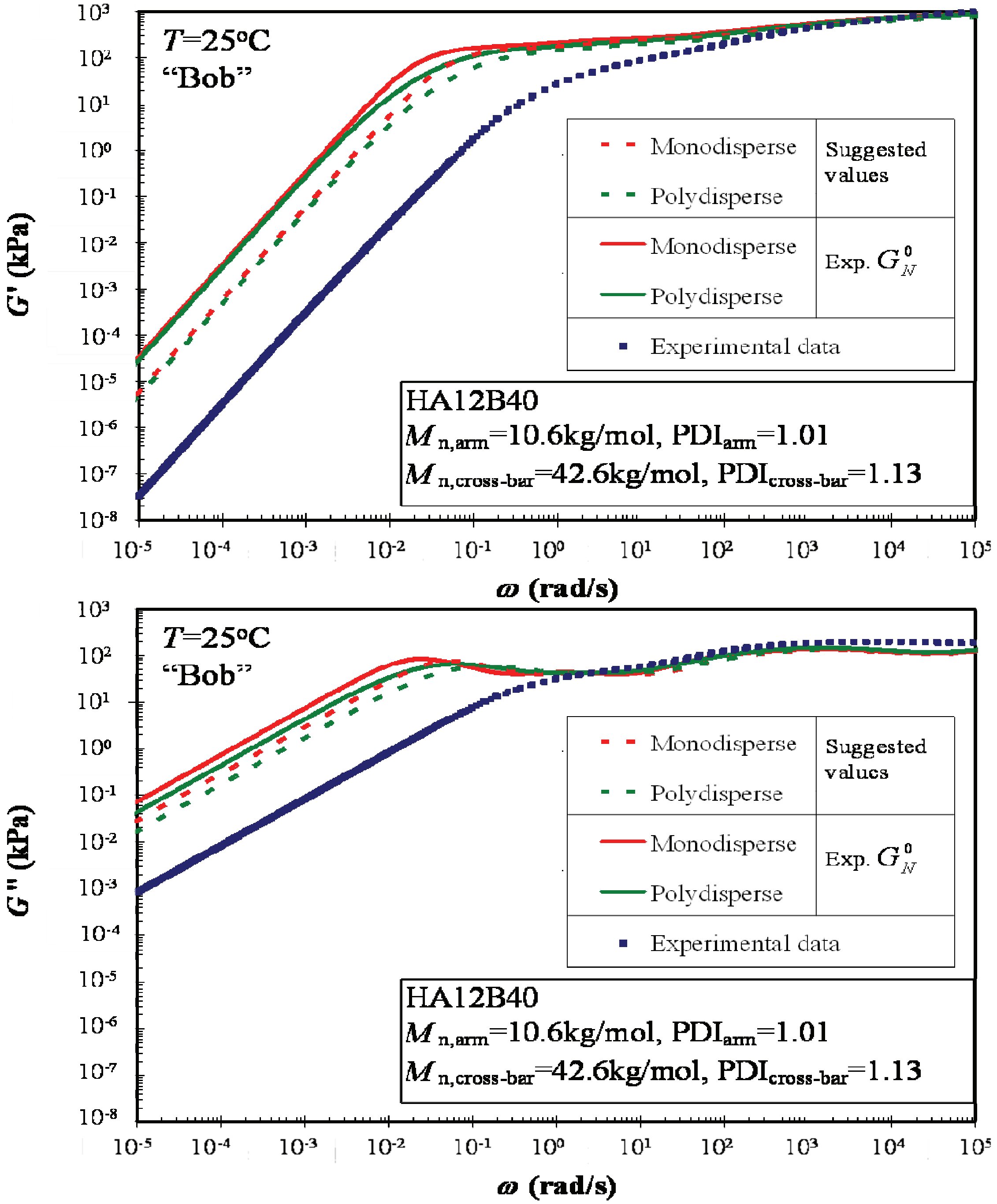

Figure 6.34 Comparison of storage and loss moduli predicted by BoB with experimental data for HA12B40 using molecular weight characterization based on SEC/TALLS data

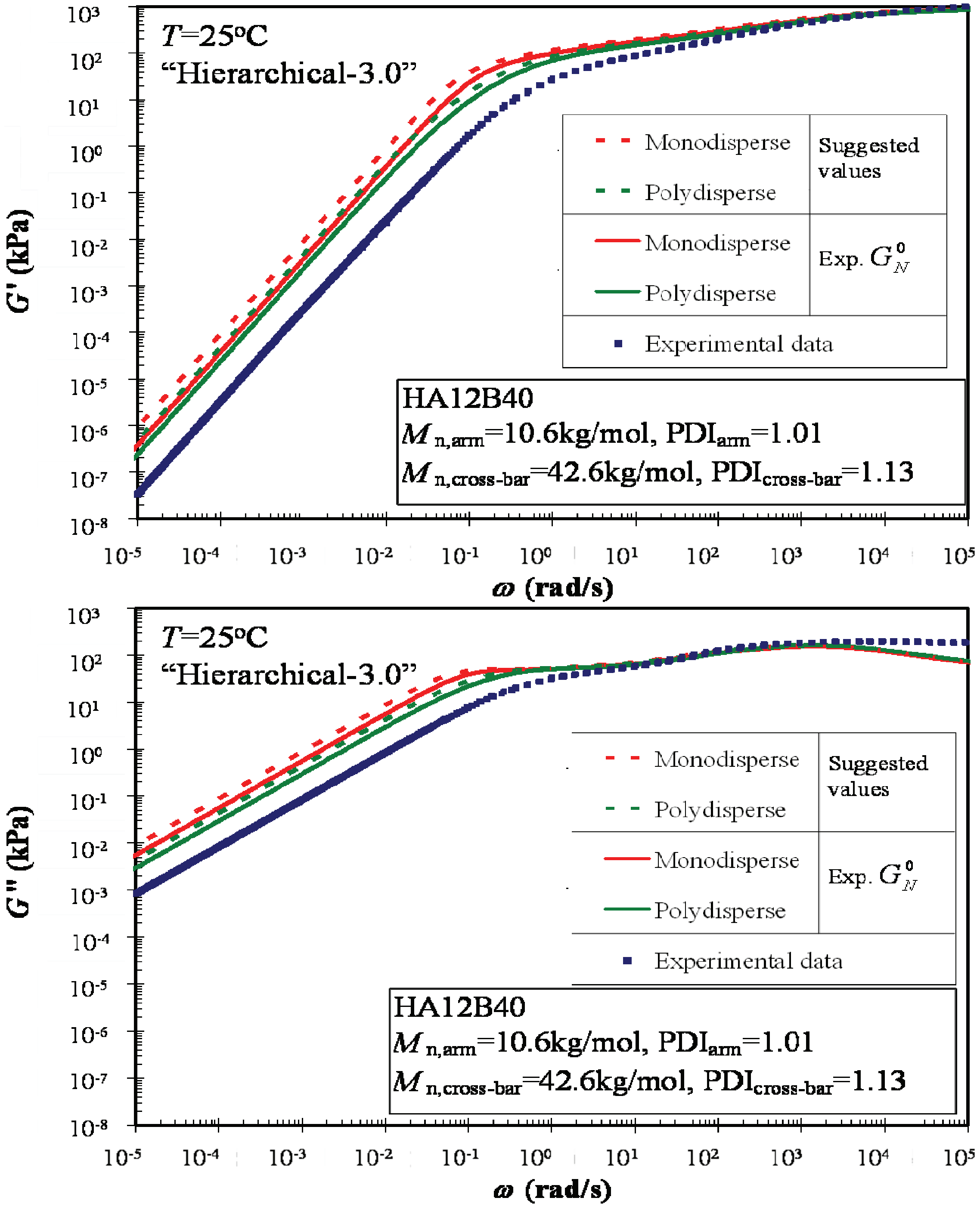

Figure 6.35 Comparison of storage and loss moduli predicted by Hierarchical-3.0 with experimental data for HA12B40 using molecular weight characterization based on SEC/TALLS data

As shown in Table 6.9, Hierarchical-3.0 generally gave a better prediction of ω_c, G_c and η_0 than BoB although ω_c from Hierachical-3.0 is still much lower than the experimental value. Das *et al*. [59] reported that for H-shaped polyisoprene a better fit was obtained by using an average cross-bar molecular weight that was larger than the experimentally determined one. However, this approach was not helpful in our case. An increase in cross-bar length would further increase the already over-estimated relaxation time. To obtain better agreement with experimental data without fitting any physical parameters, a lower molecular weight of the arms or cross-bars or the inclusion of lower molecular weight by-products could be considered. This is in accord with our assumption that there were no high-molecular weight by-products in our H-shaped PBDs.

Table 6.9 Comparison of ω_c, G_c and η_0 predicted by both models based on SEC/TALLS data with experimental data for HA12B40

HA12B40	ω_c (rad/s)		G_c (kPa)		η_0 (kPa.s)	
Experimental data	**1.93**		**40.5**		**83.4**	
	BoB	Hierachical-3.0	BoB	Hierachical-3.0	BoB	Hierachical-3.0
Suggested value + monodisperse	0.0049	0.13	69.7	48	297	88.2
Suggested value + polydisperse	0.087	0.31	55	45.2	174	43.9
Exp. G_N^0 + monodisperse	0.023	0.214	81.5	40.2	743	56.3
Exp. G_N^0 + polydisperse	0.041	0.554	56.7	50.2	440	29.8

HA12B60 – based on SEC/TALLS data

The results for HA12B60 were similar to those for HA12B40, except that the experimental G_{N}^{0} always gave a higher relaxation time than the suggested value, as shown in Figs. 6.36 and 6.37. Again, Hierachical-3.0 gives better predictions of ω_c, G_c and η_0 than BoB as shown in Table 6.10, although the predicted values of ω_c, and η_0 are still far from experimental data.

Table 6.10 Comparison of ω_c, G_c and η_0 predicted by both models based on SEC/TALLS data with experimental data for HA12B60

HA12B60	ω_c (rad/s)		G_c (kPa)		η_0 (kPa.s)	
Experimental data	**0.46**		**55.2**		**324**	
	BoB	Hierachical-3.0	BoB	Hierachical-3.0	BoB	Hierachical-3.0
Suggested value + monodisperse	9.76E-03	0.018	97.4	56.5	21700	7010
Suggested value + polydisperse	0.013	0.043	74.8	52.4	13700	3510
Exp G_{N}^{0} + monodisperse	1.60E-03	0.014	117	54.1	147000	10200
Exp. G_{N}^{0} + polydisperse	2.57E-03	0.032	90.3	48.6	86400	4980

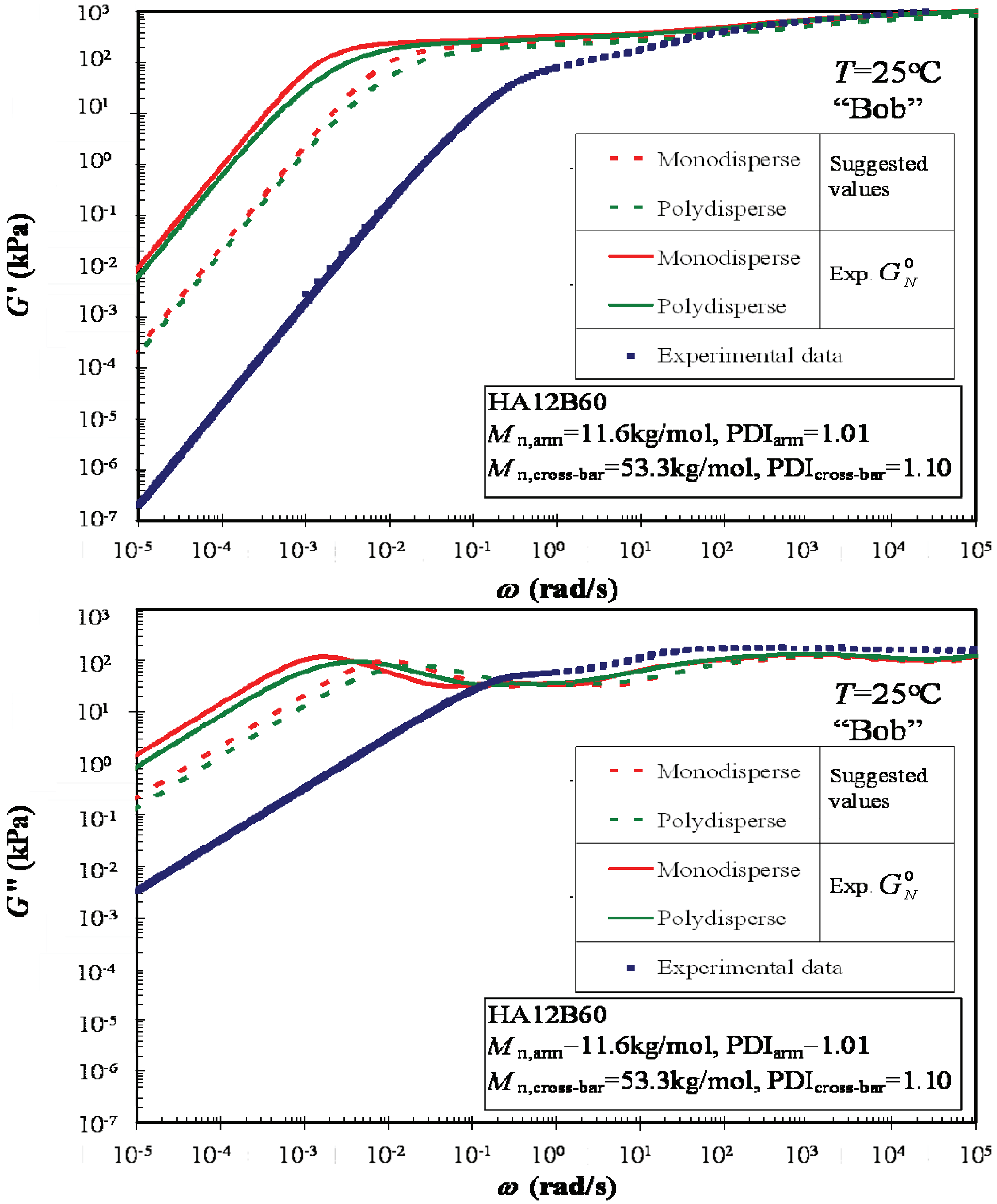

Figure 6.36 Comparison of storage and loss moduli predicted by BoB with experimental data for HA12B60 using molecular weight characterization based on SEC/TALLS data

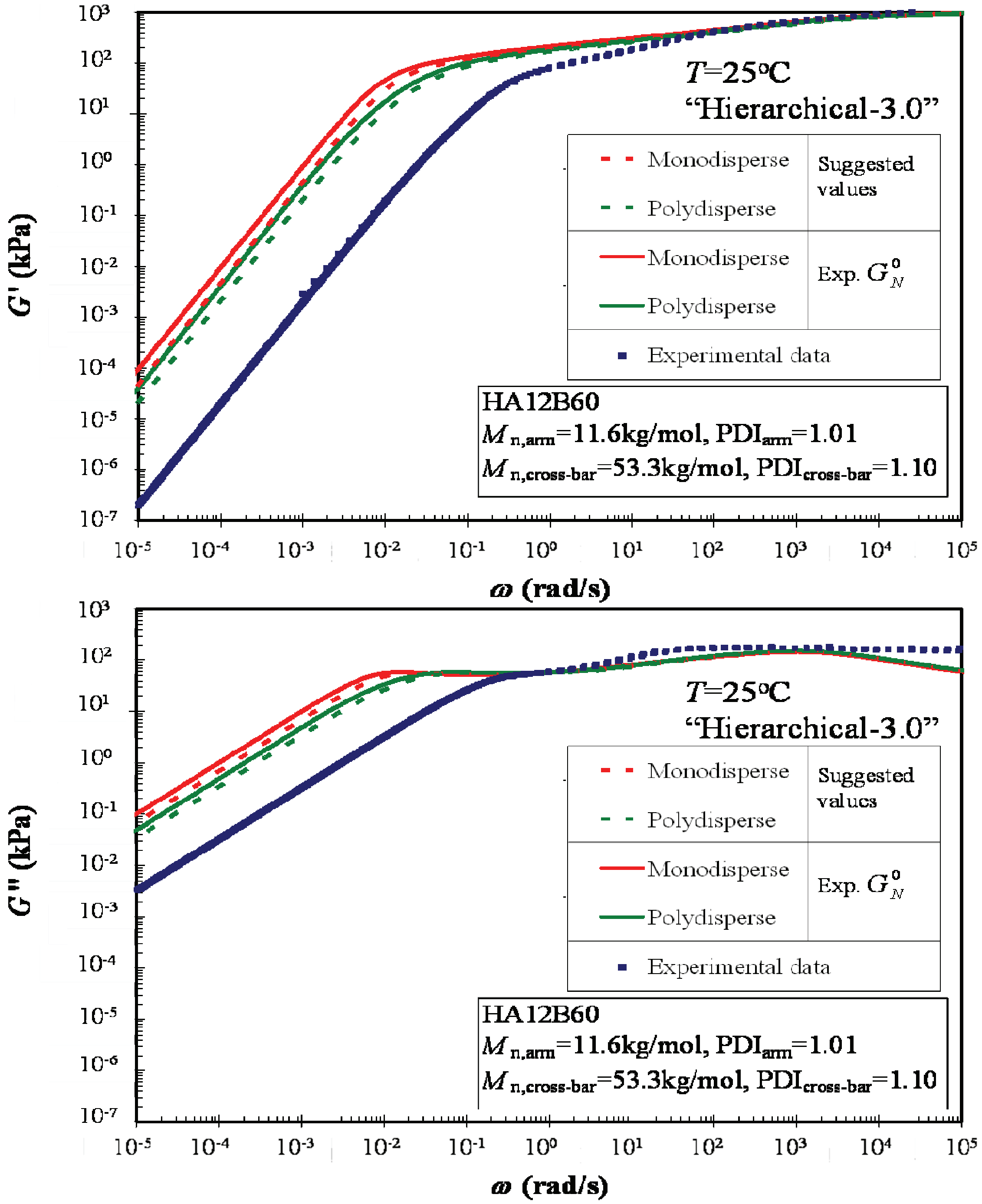

Figure 6.37 Comparison of storage and loss moduli predicted by Hierarchical-3.0 with experimental data for HA12B60 using molecular weight characterization based on SEC/TALLS data

HA12B100 – based on SEC/TALLS data

The experimental value of G_N^0 for HA12B100 happened to coincide with the suggested value for BoB. In BoB, the inclusion of polydispersity in the arms and cross-bars gave better agreement with experimental data, as shown in Fig. 6.38. However, the predictions were unable to capture the details in the shape of $G'(\omega)$. As in the cases of the above two polymers, predictions of BoB lay above the data, especially in the low frequency regime.

On the other hand, the use of the experimental G_N^0 in Hierarical-3.0 led to a modulus below the experimental data in the low frequency range, as shown in Fig. 6.39. When using the suggested values and including the polydispersity of arms and cross-bars, the prediction of Hierarachical-3.0 was in good agreement with the data, although some details in the shape $G'(\omega)$ were not predicted. Agreement for ω_c, G_c and η_0 were also good as highlighted in yellow in Table 6.11. Although a better prediction of G_c was obtained when the experimental value of G_N^0 was used in Hierachical-3.0, predictions of η_0 ω_c were worse.

Table 6.11 Comparison with experimental data of ω_c, G_c and η_0 predicted by both models based on SEC/TALLS data for HA12B100

HA12B100	ω_c (rad/s)		G_c (kPa)		η_0 (kPa.s)	
Experimental data	**2.2E-04**		**38.6**		**8.5E+05**	
	"BoB"	"Hierachical -3.0"	"BoB"	"Hierachical -3.0"	"BoB"	"Hierachical -3.0"
Suggested value + monodisperse	5.7E-05	8.8E-05	141	85.1	4.8E+06	2.4E+06
Suggested value + polydisperse	1.6E-04	3.7E-04	108	75.1	1.9E+06	7.0E+05
Exp. G_N^0 + monodisperse	5.7E-05	4.4E-04	141	73.7	4.8E+06	4.0E+05
Exp. G_N^0 + polydisperse	1.6E-04	1.5E-03	108	65.5	1.9E+06	1.3E+05

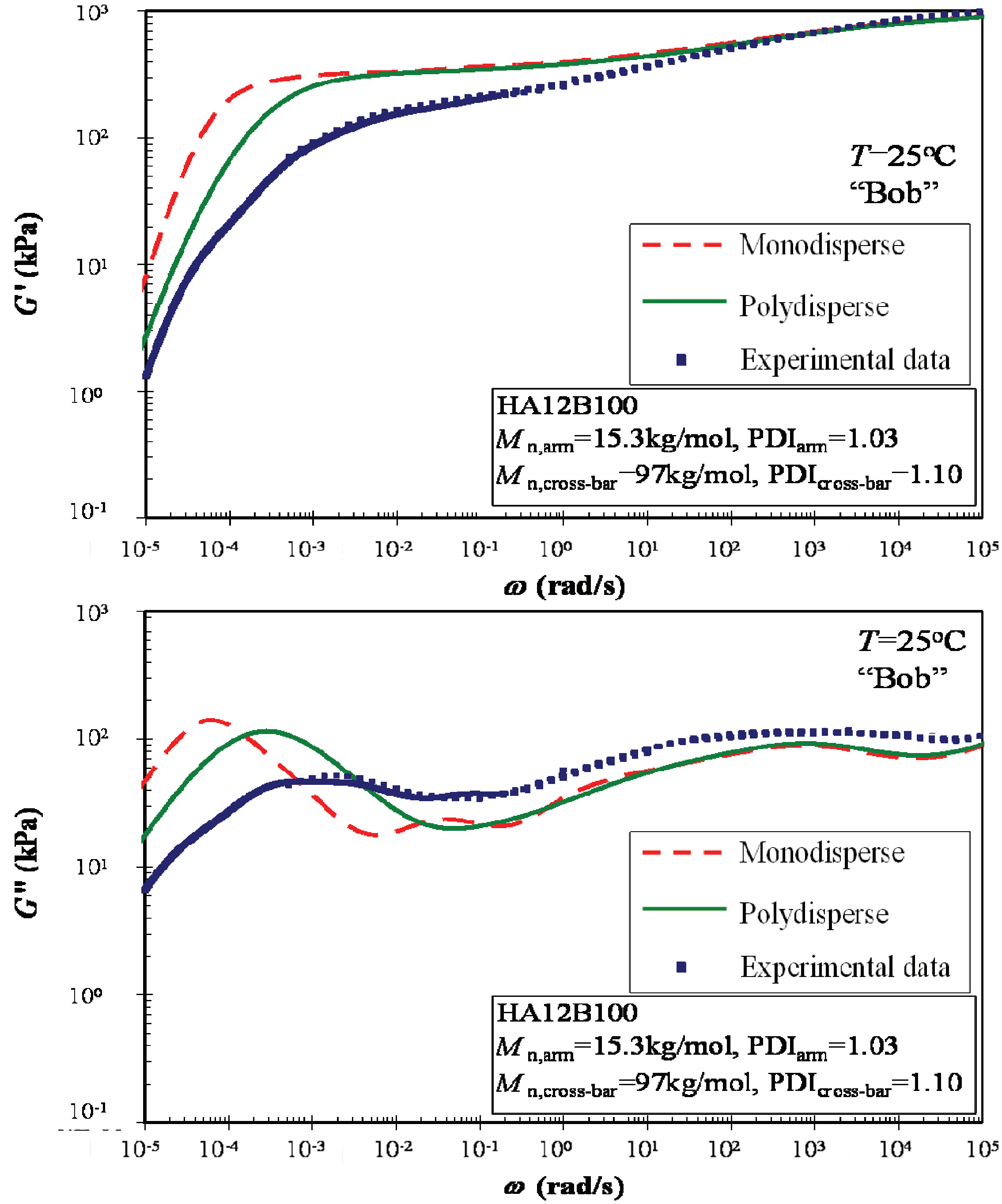

Figure 6.38 Comparison of storage and loss moduli predicted by BoB with experimental data for HA12B100 using molecular weight characterization based on SEC/TALLS data

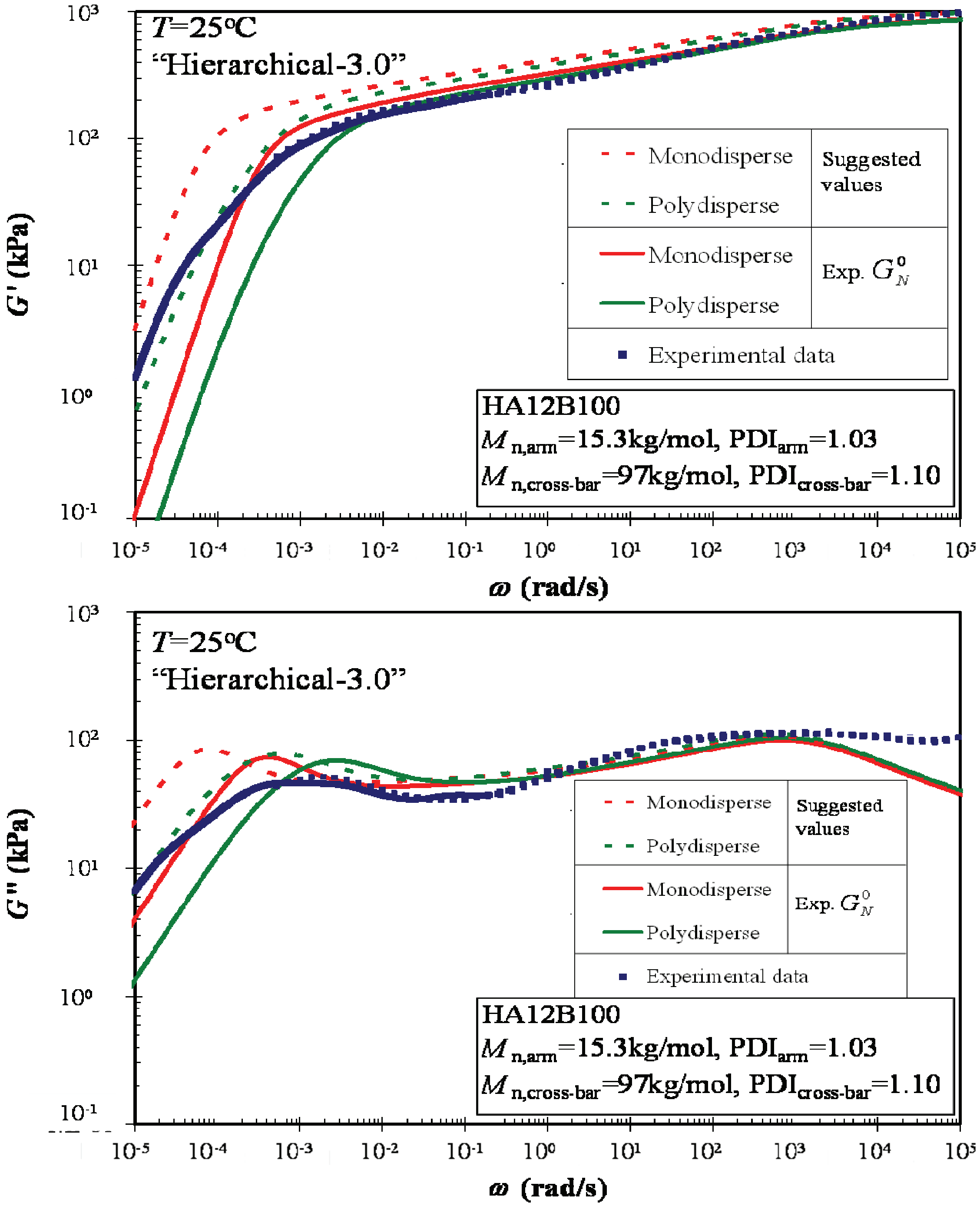

Figure 6.39 Comparison of dynamic modulus predicted from "Hierarchical-3.0" model and experimental data of HA12B100, molecular weight characterization based on SEC/TALLS data

HA30B40 – based on SEC/TALLS data

Figure 6.40 shows model predictions using BoB with the suggested parameter values and with the experimental value of G_N^0. In both situations, assuming monodisperse arms and cross-bars resulted in large disagreements with experimental data. Better agreement was obtained when polydispersities of arms and cross-bars were taken into account. For predictions obtained using suggested parameter values and including polydispersity, the predicted and experimental curves had similar curvatures. As in the case of Hierarchical-3.0, the inclusion of polydispersity of arms and cross-bars resulted in much better predictions. Since the experimental value of G_{N}^{0} =1.1MPa was close to the suggested value G_{N}^{0} =1.095MPa in Hierachical3.0, predictions obtained using these two values almost superposed, as shown in Fig. 6.41

When polydispersities of arms and cross-bars were not included in the simulation, predictions of loss and storage moduli obtained from both models did not show a cross-over point. Since terminal behavior was not reached experimentally in the frequency range studied, comparison of predicted and experimental values of η_0 was not possible. As shown in Table 6.12, using the experimental value of G_{N}^{0} and including polydispersity of arms and cross-bars in the simulation, Hierarchical-3.0 gave better agreement with experimental data than BoB, which was similar to the situation for HA12B100.

Table 6.12 Comparison of ω_c and G_c predicted by both models based on SEC/TALLS data with experimental data for HA12B100

HA30B40	ω_{c} (rad/s)		G_{c} (kPa)	
Experimental data	**1.8E-04**		**11.3**	
	BoB	Hierachical-3.0	BoB	Hierachical-3.0
Suggested value + monodisperse	N/A			
Suggested value + polydisperse	2.9E-05	8.6E-04	11.2	17.8
Exp. G_{N}^{0} + monodisperse	N/A			
Exp. G_{N}^{0} + polydisperse	N/A	8.4E-04	N/A	17.4

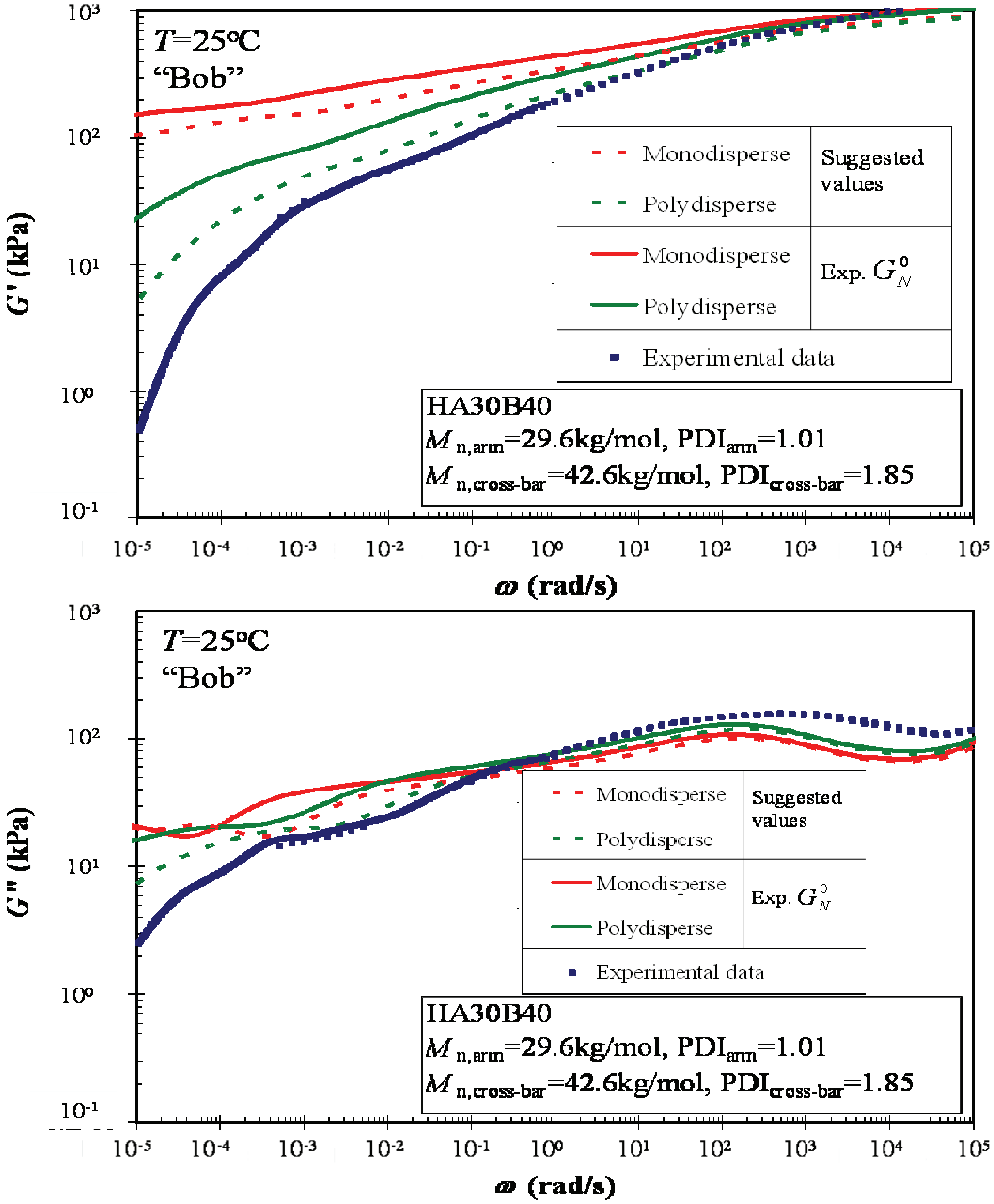

Figure 6.40 Comparison of dynamic modulus predicted from "BoB" model and experimental data of HA30B40, molecular weight characterization based on SEC/TALLS data

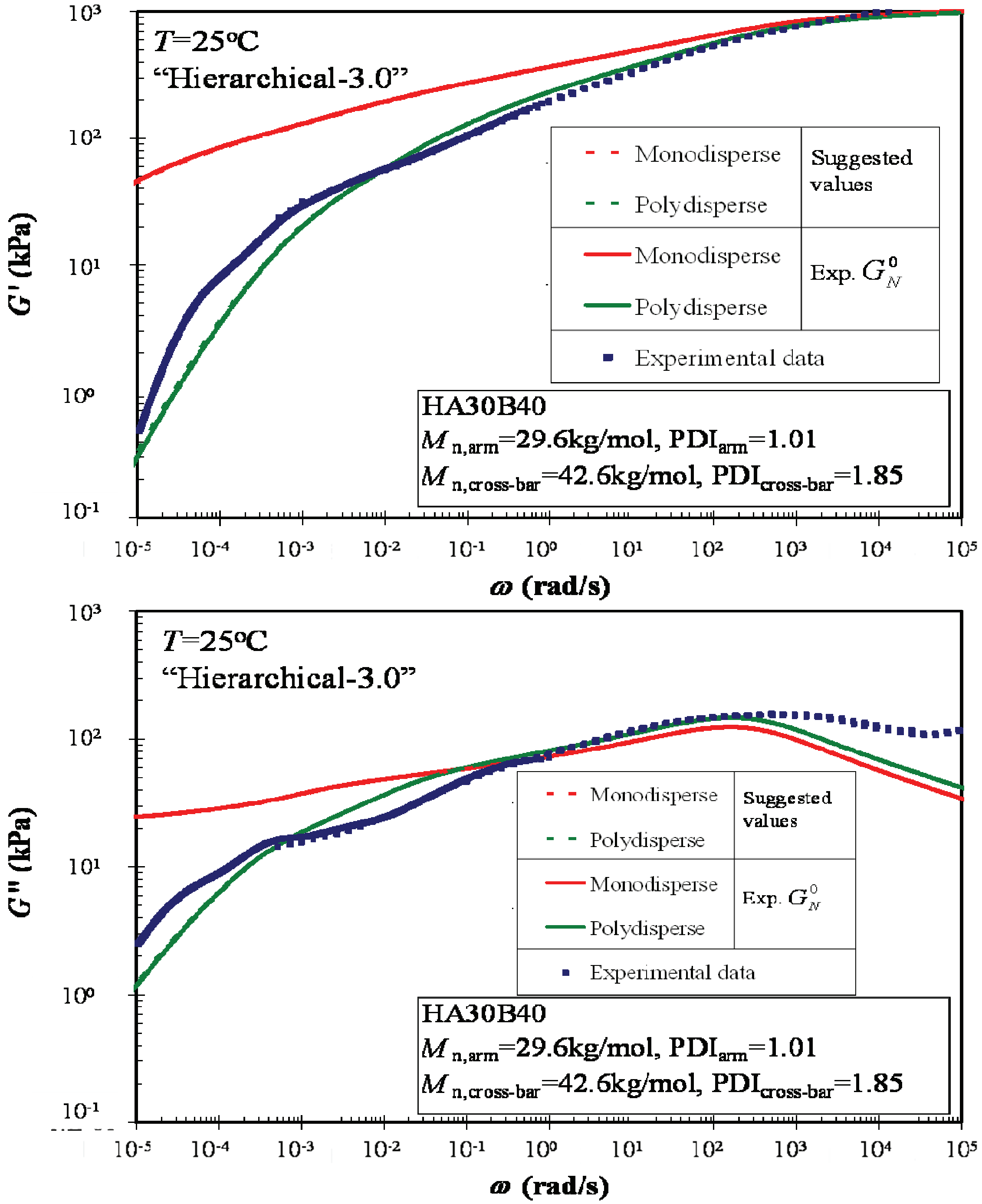

Figure 6.41 Comparison of dynamic modulus predicted from "Hierarchical-3.0" model and experimental data of HA30B40, molecular weight characterization based on SEC/TALLS data

HA40B40 – based on SEC/TALLS data

Again, the experimental G_N^0 (0.94MPa) of HA40B40 was very close to the suggested value (0.97MPa) for use in BoB, so predictions obtained using these two values were similar, as is shown in Fig. 6.42. In both cases, the predicted moduli were higher than the experimental data. As in the case of HA30B40, inclusion of polydispersity of arms and cross-bars resulted in faster relaxation and better agreement with experimental data. We note that regardless of assumptions made in the modeling of this sample, BoB was not able to make even qualitatively correct predictions.

As shown in Fig. 6.43 Hierarchical-3.0 also over-estimated the moduli except in one case, where the polydispersity of arms and cross-bars were included, and the experimental value of G_N^0 was used. Since the experimental G_N^0 of HA40B40 was about 10% lower than the suggested value in Hierarchical-3.0, and the model prediction was highly sensitive to the value of G_N^0, the use of the experimental value in this case did give a better prediction than the suggested value. However, as with the BoB model, Hierarchial-3.0 predictions did not capture details in curves of *G*'(ω) and *G*"(ω).

Since terminal behavior was seen in neither model predictions nor experimental data, and a cross-over point in loss and storage moduli curves was not observed in either model prediction on HA40B40, quantitative comparisons of predicted and measured values of ω_c, G_c and η_0 could not be made. Instead, we compared absolute values of complex viscosity $|\eta^*|$ predicted from the two models with experimental data, as shown in Fig. 6.44. We see that Hierarchical-3.0 gave better agreement with experimental data than BoB, which was similar to the case of HA12B100 and HA30B40. Predictions of Hierarchical-3.0 using the experimental value of G_N^0 and including polydispersity of arms and cross-bars resulted in a qualitatively good prediction of $|\eta^*|$ over a wide frequency range.

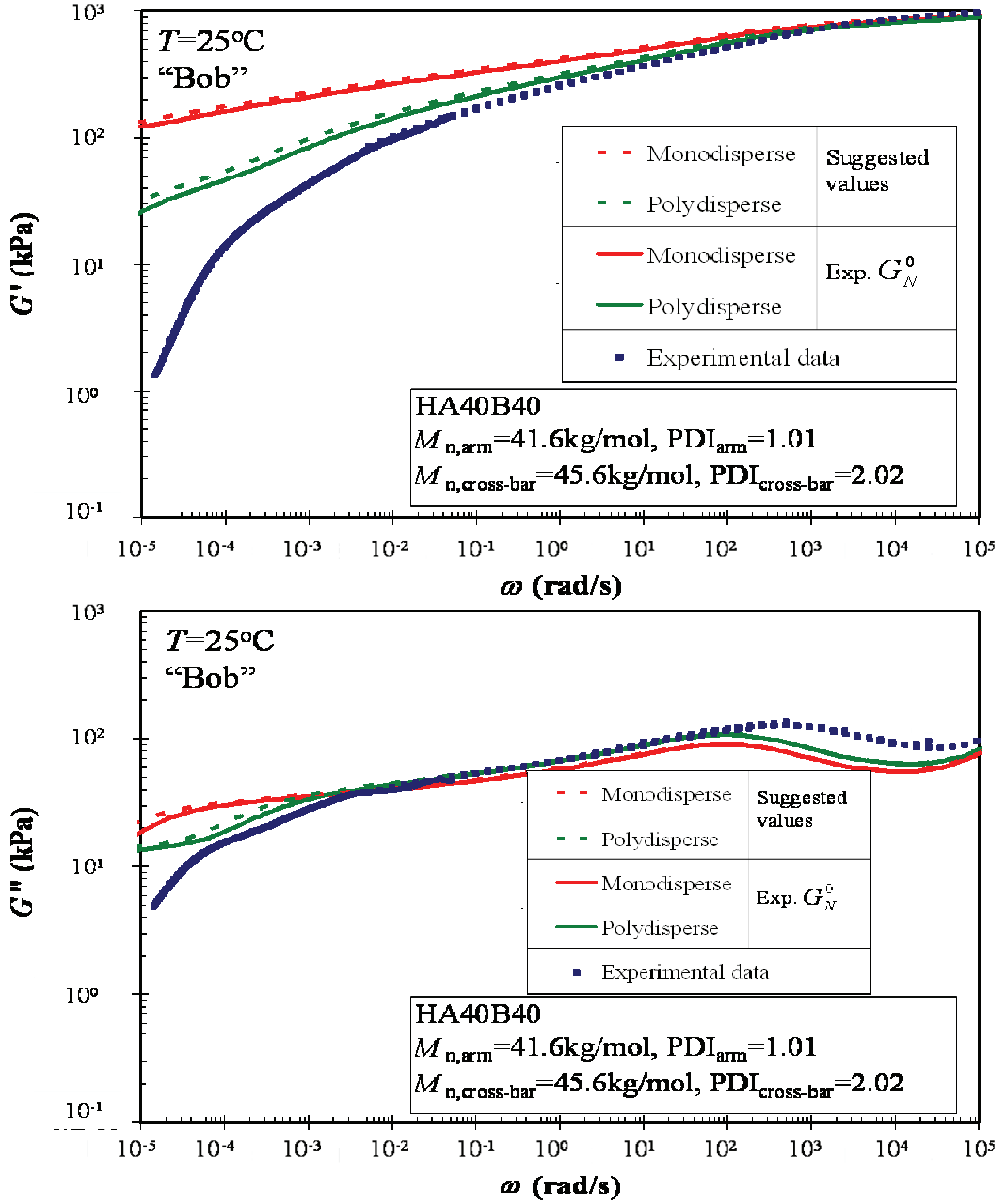

Figure 6.42 Comparison of dynamic modulus predicted from "BoB" model and experimental data of HA40B40, molecular weight characterization based on SEC/TALLS data

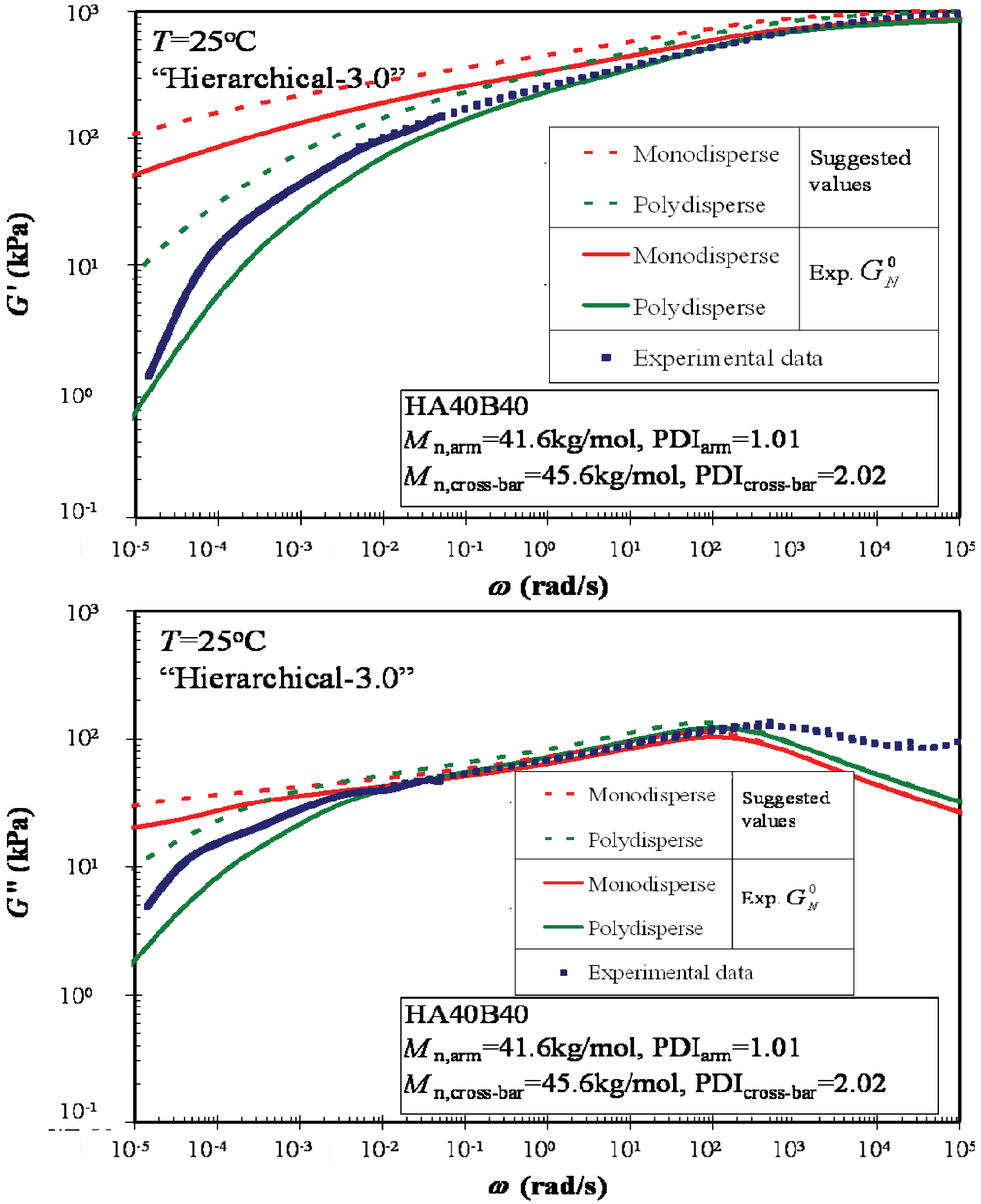

Figure 6.43 Comparison of dynamic modulus predicted from "Hierarchical-3.0" model and experimental data of HA40B40, molecular weight characterization based on SEC/TALLS data

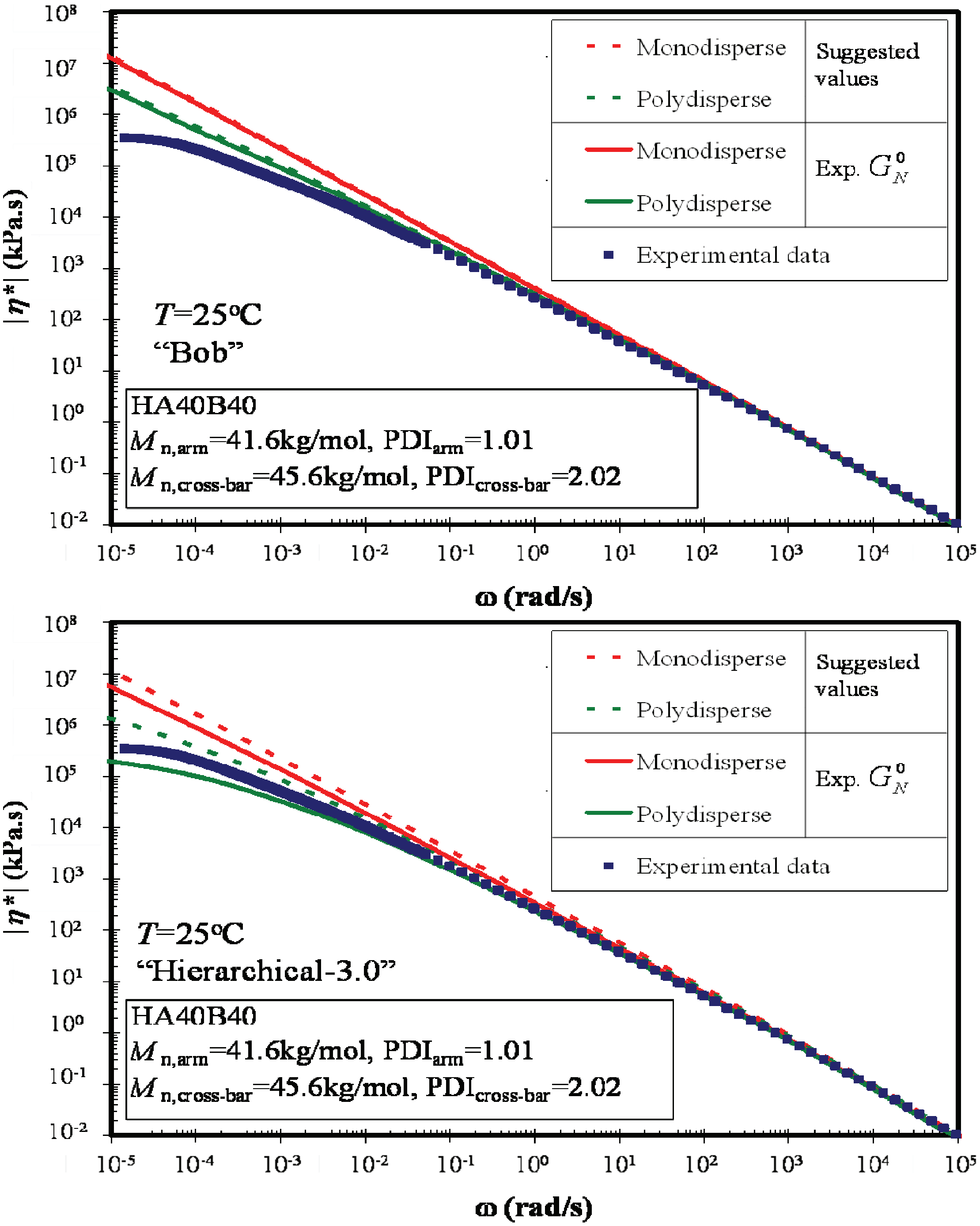

Figure 6.44 Comparison of complex viscosity predicted from "BoB" model and "Hierarchical-3.0" model and experimental data of HA40B40, molecular weight characterization based on SEC/TALLS data

HA1230B40

The original objective of including the blend in this study was to demonstrate the effect of polydispersity on LVE behavior in a controlled manner. However, all the H-shaped PBDs samples are now thought to be mixtures of linear, star and H-shaped polymers as revealed by TGIC. Moreover, the simulations of the behavior of both HA12B40 and HA30B40 using either model over-estimated the relaxation modulus. Therefore, we do not expect either model to be able to predict the behavior of this blend. Instead, simulations of HA12B40 behavior using TGIC data were used to compare the capabilities of the models in dealing with polydisperse systems.

HA12B40 – based on TGIC data

Shown in Figs. 6.45 and 6.46 are predictions of both models for HA12B40 that are based on structural details revealed by TGIC. As was shown by the uncertainty analysis, this sample can be considered to be a 6-component mixture of linear, asymmetric 3-arm stars and H-shaped molecules. Due to the inclusion of lower molecular weight by-products, the relaxation of this system was predicted to be much faster than that of a pure H system. Model predictions for the mixture are very close to experimental data, although BoB still over-predict the modulus, and hierachical-3.0 results are slightly under-predicted. The difference in the performance of the two models can be explained by the use of a longer reptation time in BoB and the difference in criteria for turning on constraint release-Rouse-motion. Despite the small departures from experimental data, both models are able to capture the detailed shapes of the curves of $G'(\omega)$ and $G''(\omega)$.

Table 6.13 compares the predictions of ω_c, G_c and η_0 by the two models with data, and one is surprised to note that the use of the suggested value of G_N^0 rather than the experimental value gave better agreement with experimental data for these rheological functions. We note that Hierarchical-3.0 gave a better prediction of experimental data than BoB for all the H-shaped PBDs. The fact that the suggested values gave the best fit to experimental data for both models suggests that these values are well suited to deal with all the structures considered here, provided that the test material is well characterized with respect to molecular structure, blend composition, polydispersity and molecular weights of arms, cross-bars of each component.

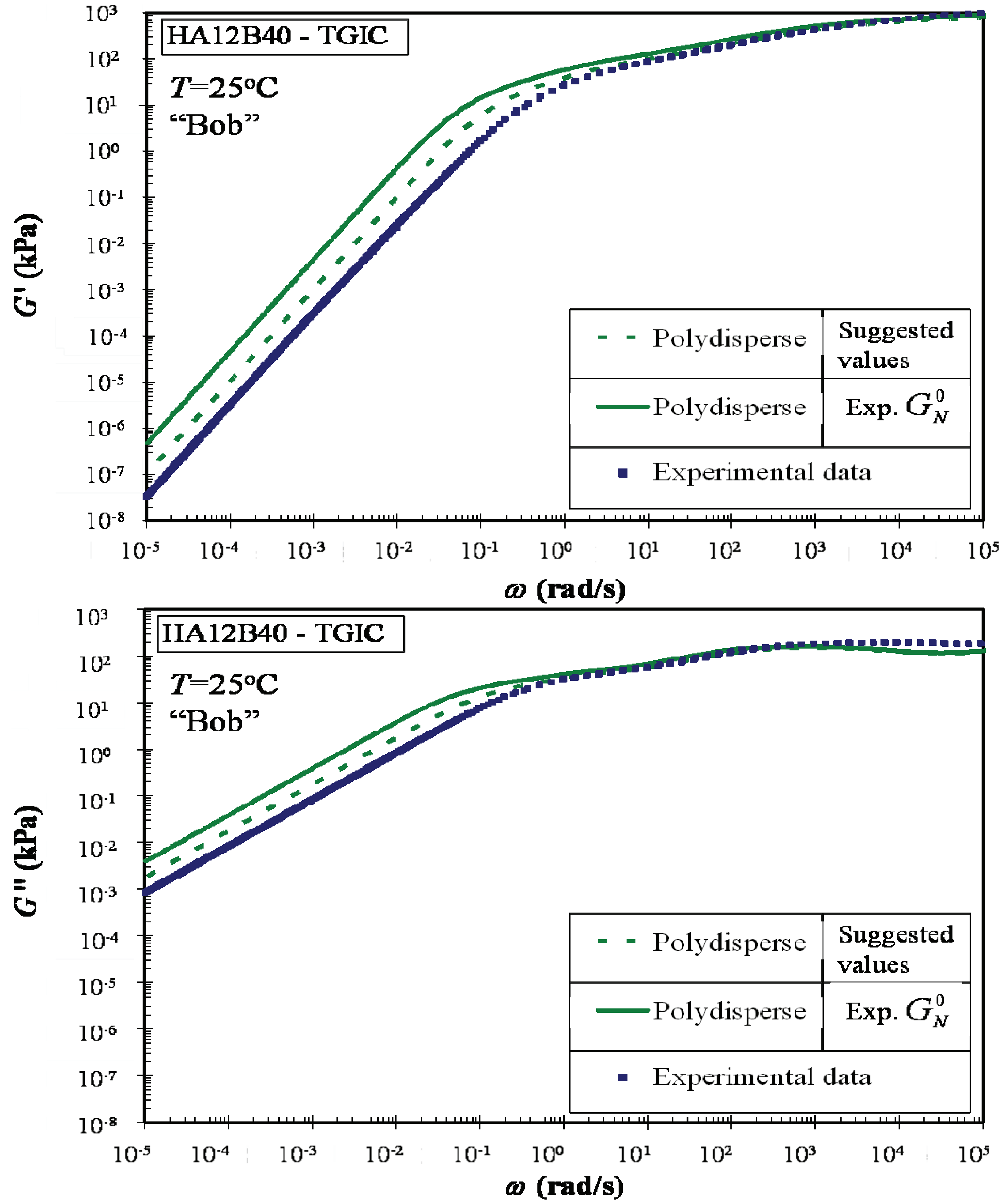

Figure 6.45 Comparison of storage and loss moduli predicted by BoB with experimental data for HA12B40 based on molecular weight data determined by TGIC

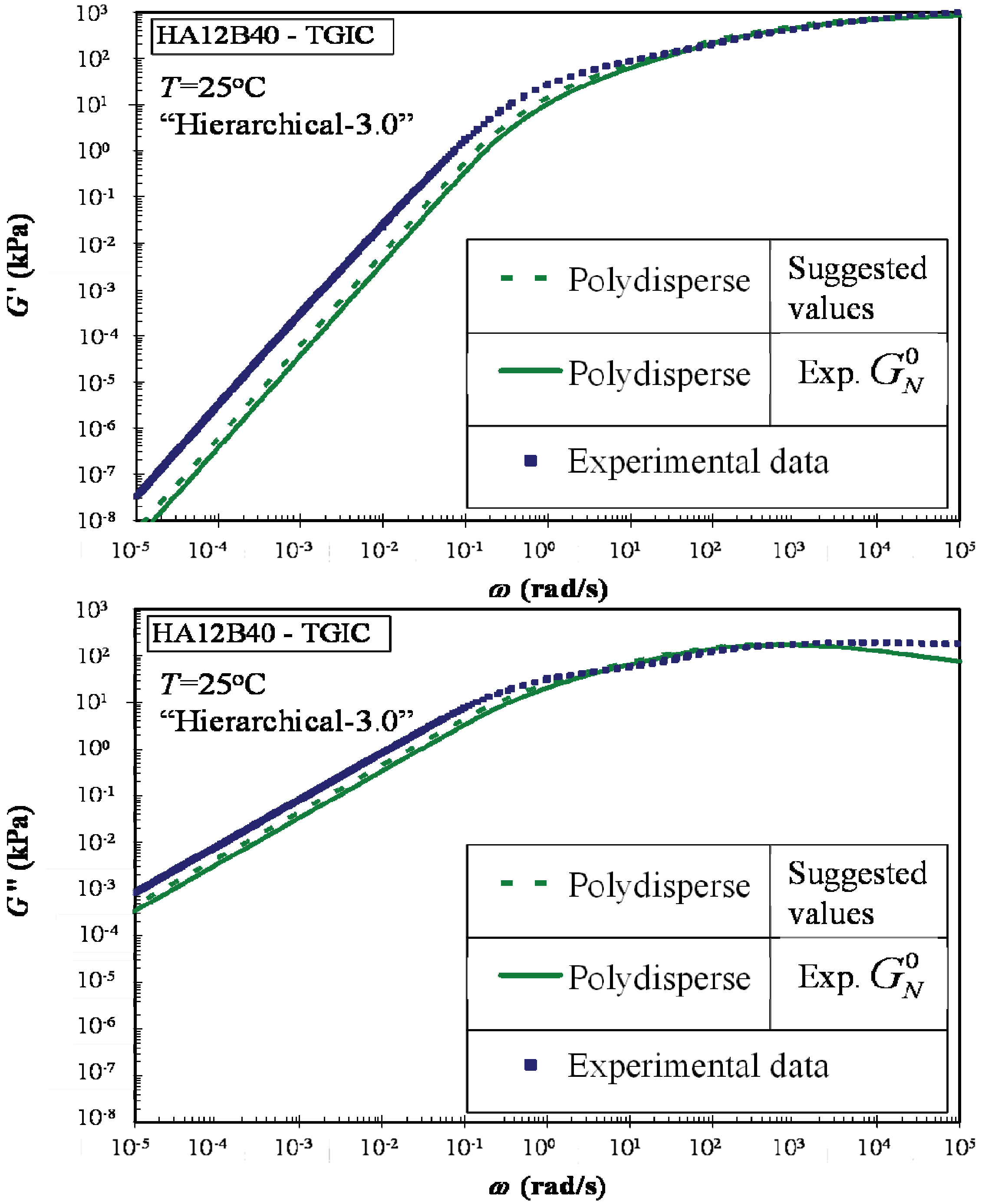

Figure 6.46 Comparison of storage and loss moduli predicted by hierarchical-3.0 with experimental data for HA12B40, based on molecular weight data from TGIC

Table 6.13 Comparison of ω_c , G_c and η_0 predicted by both models based on TGIC data with experimental data for HA12B40

HA12B40	ω_c (rad/s)		G_c (kPa)		η_0 (kPa.s)	
Experimental data	**1.9**		**40.5**		**83.4**	
	BoB	Hierachical-3.0	BoB	Hierachical-3.0	BoB	Hierachical-3.0
Suggested value + polydisperse	0.4	8.8	25.9	68.6	179	45.7
Exp. G_N^0 + polydisperse	0.3	11.6	28.0	68.5	389	34.2

6.8 Conclusions

As has been reported by others, both the Hierarchical-3.0 and BoB models are able to make good quantitative predictions of the LVE behavior of linear polymer blends. A sensitivity analysis revealed that predictions of both models are highly sensitive to the presence of low molecular weight by-products in linear and star systems and to the value of the plateau modulus used as an input parameter. It is essential to identify the source of uncertainty when comparing model predictions with data, such as uncertainties in the molecular structures of samples and the values of the input parameters. A list of the most probable by-product structures is proposed based on the synthesis mechanism, and this is used along with the TGIC data to infer the molecular structures present in a sample.

Without fitting any parameters, both models generally over-estimate the relaxation time of H-shaped PBDs, when the simulation is based on molecular weight information obtained by conventional SEC analysis *e.g.* SEC/TALLS. However, predictions of both models are greatly improved when the more detailed molecular weight information obtained by TGIC is used in the simulation, implying that the input parameters suggested in the literature are well suited for use with various molecular structures. In general Hierarchical-3.0 gives more accurate predictions than BoB for H-shaped PBDs, whether the simulation is based on SEC/TALLS data assuming the sample is pure H-shaped polymer or on TGIC data that indicate the material is a mixture of linear, star and H-shaped molecules. However, BoB gives better predictions for two- or three-component linear blends.

Chapter 7 Conclusions

1. Size exclusion chromatography (SEC) is an unreliable method to determine the structure of branched polymers that may be structurally polydisperse for the following reasons: First, SEC data on the final fractionated products from three reputable sources did not agree with each other; Second, this separation method is not sensitive to structural differences. Lastly, temperature gradient interaction chromatography (TGIC) analysis provides information that cannot be obtained by conventional SEC.
2. By combining knowledge of the synthesis mechanism with TGIC data for a functionally polydisperse branched sample (HA12B40), the molecular structure of each component can be inferred, where the components are mainly low molecular weight linear and three-arm stars resulting from an incomplete coupling reaction.
3. Both H-shaped PBDs and blends of linear PBDs are thermorheologically simple.
4. The plateau modulus G_{N}^{0} is 1.12 ± 0.06 MPa for linear PBDs blends and 1.05 $\pm\, 0.12$ MPa for H-shaped PBDs; these are consistent with literature values for linear PBD.
5. The presence of long-chain branching enhances η_0 dramatically for a given total molecular weight.
6. With a longer cross-bar, the low frequency peak in $G''(\omega)$ resulting from cross-bar relaxation shifts to a lower frequency but has a higher magnitude and a better defined peak.
7. With a longer arm, the prominent “shoulder” seen in $G''(\omega)$, which results from arm relaxation, becomes wider.
8. A sensitivity analysis reveals that predictions of the Hierarchical-3.0 and BoB models are very sensitive to the presence of low molecular weight by-products and to the value of G_{N}^{0} used as an input parameter.
9. Both of the tube-based models are able to predict quantitatively the linear viscoelastic behavior of linear PBD blends. The BoB model provides slightly better predictions than Hierarchical-3.0.

10. Both models over-estimate the relaxation time of H-shaped PBDs when the simulation is based on SEC/TALLS structural data.
11. When the simulation is based on TGIC data with structural polydispersity taken into account the predictions of both models are greatly improved.
12. Hierarchical-3.0 gives the more accurate predictions than BoB for H-shaped PBDs, whether the simulation is based on SEC/TALLS or TGIC data.

Chapter 8 Original Contributions to Knowledge

1. Obtained broad frequency range rheological data of a series of H-shaped PBDs at 25°C.
2. Proposed criteria and demonstrated the use of a hierarchical model to optimize the structures of branched samples, which are used in the preparation for synthesis.
3. Demonstrated that conventional SEC analysis is an unreliable method for determining the structure of branched polymers that may be structurally polydisperse.
4. Showed that both of the tube-based models evaluated can quantitatively predict the linear viscoelastic behavior of polydisperse linear blends without fitting any parameters.
5. Showed that TGIC analysis along with knowledge of the synthesis method is a reliable way to infer the molecular structure of structurally polydisperse H-shaped PBD.
6. Demonstrated that both of the tube-based models evaluated can predict the LVE behavior of polydisperse linear, star, and H-shaped polymers without fitting any parameters, provided that structures inferred from TGIC data are used in the simulation.

Bibliography

1. Kaminsky, Walter, "*Trends in polyolefin chemistry*", Macromolecular Chemistry and Physics, **209**, 459-466 (2008)

2. Chum, P.S. and Swogger, K.W., "*Olefin polymer technologies - History and recent progress at The Dow Chemical Company*", Progress in Polymer Science, **33** (8), 797-819 (2008)

3. Lohse, David. J, Garcia-Franco, Cesar, and Hadjichristidis, Nikos, "*Synthesis and use of well-defined, highly-branched saturated hydrocarbon polymers*" United states patent application publication, Pub. No.: US 2007/0135583 A1 (2007)

4. Jordan, E.A., Donald, A.M., Fetters, L.J., and Klein, J., "*Transition from linear to star-branched diffusion in entangled polymer melts*", Polymer preprints (ACS, divison of polymer chemistry), **30** (1), 63-64 (1989)

5. Gell, C.B., Graessley, W.W., Efstratiadis, V., Pitsikalis, M., and Hadjichristidis, N., "*Viscoelasticity and self diffusion in metls of entangled asymmetric star polymers*", Journal of Polymer Science, Part B: Polymer Physics, **35** (12), 1943-1954 (1997)

6. Usami, T., Gotoh, Y., Takayama, S., Ohtani, H., and Tsuge, S., "*Branching structures in high-pressure low-density polyethylene as a function of molecular weight determined by 13C nuclear magnetic resonance and pyrolysis-hydrogenation gas chromatography*", Macromolecules, **20** (7), 1557-1561 (1987)

7. Janzen, J. and Colby, R.E., "*Diagnosing long-chain branching in Polyethylenes*", J.Mol.Struct., **486**, 569-584 (1999)

8. Wood-Adams, P.M., Dealy, J.M., deGroot, A.W., and Redwing, O.D., "*Effect of molecular structure on the linear viscoelastic behavior of polyethylene*", Macromolecules, **33** (20), 7489-7499 (2000)

9. Vega, J., Aguilar, M., Peon, J., Pastor, D., and Salazar, J.M., "*Review: effect of long chain branching on linear viscoelastic melt properties of polyolefins*", E-polymers, **46**, 1-35 (2002)

10. Adams, P.M.W. and Dealy, J.M., "*Effect of molecular structure on the linear viscoelastic behavior of polyethylene*", Macromolecules, **33**, 7489-7499 (2000)

11. Gabriel, C., Kaschta, J., and Munstedt, H., "*Influence of molecular structure on rheological proeprties of polyethylene*", Rheol Acta, **37**, 7-20 (1998)

12. Gabriel, C., Kokka, E., Lofgren, B., Seppala, J., and Munstedt, H., "*Analytical and rheological characterization of long-chain branched metallocene-catalyzed ethylene homopolymers*", Polymer, **43**, 6383-6390 (2002)

13. Kurzbeck, S., Oster, F., Munstedt, H., Nguyen, T.Q., and Gensler, R., "*Rheological properties of two polypropylenes with different molecular structure*", Journal of Rheology, **43** (2), 359-374 (1999)

14. Graessley, W.W. and Roovers, J., "*Melt rheology of four-arm and six-arm star polystyrenes*", Macromolecules, **12** (5), 959-965 (1979)

15. Hsieh, H. L. and Quirk, R. P., "*Anionic Polymerization*", New York, Marcel Dekker (1996)

16. "*Advances in controlled/living radical polymerization*", Washington, D.C., American Chemical Society (2003)

17. Patten, T.E. and Matyjaszewski, K., "*Atom transfer radical polymerization and the synthesis of polymeric materials*", Advanced Materials, **10** (12), 901-915 (1999)

18. Fetters, L.J., Kiss, A.D., Pearson, D.S., Quack, G.F., and Jerome Vitus, F., "*Rheological behavior of star-shaped polymers*", Macromolecules, **26** (4), 647-654 (1993)

19. Carella, J.M., Gotro, J.T., and Graessley, W.W., "*Thermorheological effects of long-chain branching in entangled polymer melts*", Macromolecules, **19**, 659-667 (1986)

20. Roovers, J., "*Melt rheology of H-shaped polystyrenes*", Macromolecules, **17** (6), 1196-1200 (1984)

21. McLeish, T.C.B., Allgaier, J., Bick, D.K., Bishko, G., Biswas, P., Blackwell, R., Blottiere, B., Clarke, N., Gibbs, B., Groves, D.J., Hakiki, A., Heenan, R.K., Johnson, J.M., Kant, R., Read, D.J., and Young, R.N., "*Dynamics of entangled H-polymers: Theory, rheology, and neutron-scattering*", Macromolecules, **32** (20), 6734-6758 (1999)

22. McLeish, T.C.B., "*Moelcular rheology of H-polymers*", Macromolecules, **21** (4), 1062-1070 (1988)

23. Hakiki, A., Young, R.N., and McLeish, T.C.B., "*Synthesis and characterization of H-shaped Polyisoprene*", Macromolecules, **29** (10), 3639-3641 (1996)

24. McLeish, T.C.B. and Larson, R.G., "*Molecular constitutive equations for a class of branched polymers: The pom-pom polymer*", Journal of Rheology, **42** (1), 81-110 (1998)

25. Archer, L.A. and Juliani, "*Linear and Nonlinear Viscoelasticity of Entangled Multiarm (Pom-Pom) Polymer Liquids*", Macromolecules, **37** (3), 1076-1088 (2004)

26. Islam, M.T., Juliani, Archer, L.A., and Varshney, S.K., "*Linear Rheology of Entangled Six-Arm and Eight-Arm Polybutadienes*", Macromolecules, **34** (18), 6439-6449 (2001)

27. Kirkwood, Keith M., Leal, L. Gary, Vlassopoulos, Dimitris, Driva, Paraskevi, and Hadjichristidis, Nikos, "*Stress Relaxation of Comb Polymers with Short Branches*", Macromolecules (Washington, DC, U.S.), **42** (24), 9592-9608 (2009)

28. Inkson, N. J., Graham, R. S., McLeish, T. C. B., Groves, D. J., and Fernyhough, C. M., "*Viscoelasticity of Monodisperse Comb Polymer Melts*", Macromolecules, **39** (12), 4217-4227 (2006)

29. Daniels, D.R., McLeish, T.C.B., Crosby, B.J., Young, R.N., and Fernyhough, C.M., "*Molecular rheology of comb polymer melts. 1. Linear viscoelastic response*", Macromolecules, **34** (20), 7025-7033 (2001)

30. Fernyhough, C.M. and Young, R.N., "*The synthesis and characterization of Polybutadiene and Poly(ethylene-1-butene) Combs*", Macromolecules, **34** (20), 7034-7041 (2001)

31. Roovers, J. and Graessley, W.W., "*Melt rheology of some model comb polystyrenes*", Macromolecules, **14** (3), 766-773 (1981)

32. Fujimoto, T., Narukawa, H., and Nagasawa, M., "*Viscoelastic properties of comb-shaped polystyrenes*", Macromolecules, **3** (1), 57-64 (1970)

33. Kapnistos, M., Vlassopoulos, D., Roovers, J., and Leal, L. G., "*Linear Rheology of Architecturally Complex Macromolecules: Comb Polymers with Linear Backbones*", Macromolecules, **38** (18), 7852-7862 (2005)

34. Chambon, Pierre, Fernyhough, Christine M., Im, Kyuhyun, Chang, Taihyun, Das, Chinmay, Embery, John, McLeish, Tom C. B., and Read, Daniel J., "*Synthesis, Temperature Gradient Interaction Chromatography, and Rheology of Entangled Styrene Comb Polymers*", Macromolecules (Washington, DC, U.S.), **41** (15), 5869-5875 (2008)

35. van Ruymbeke, E., Orfanou, K., Kapnistos, M., Iatrou, H., Pitsikalis, M., Hadjichristidis, N., Lohse, D.J., and Vlassopoulos, D., "*Entangled dendritic polymers and beyond: rheology of symmetic cayley-tree polymers and macromolecular self-assemblies*", Macromolecules, **40** (16), 5941-5952 (2007)

36. Marrucci, G., "*Advances in transport processes*", New York, Wiley (1984)

37. Abdel-Goad, M., Pyckhout-Hintzen, W., Kahle, S., Allgaier, J., Richter, D., and Fetters, L.J., "*Rheological Properties of 1,4-Polyisoprene over a Large Molecular Weight Range*", Macromolecules, **37** (21), 8135-8144 (2004)

38. Kharchenko, S.B., Kannan, R.M., Cernohous, J.J., and Venkataramani, S., "*Role of Architecture on the Conformation, Rheology, and Orientation Behavior of Linear, Star, and Hyperbranched Polymer Melts. 1. Synthesis and Molecular Characterization*", Macromolecules, **36** (2), 399-406 (2003)

39. Archer, L.A. and Varshney, S.K., "*Synthesis and Relaxation Dynamics of Multiarm Polybutadiene Melts*", Macromolecules, **31** (18), 6348-6355 (1998)

40. Adams, C.H., Hutchings, L.R., Klein, P.G., McLeish, T.C.B., and Richards, R.W., "*Synthesis and Dynamic Rheological Behavior of Polybutadiene Star Polymers*", Macromolecules, **29** (17), 5717-5722 (1996)

41. Heinrich, M., Pyckhout-Hintzen, W., Allgaier, J., Richter, D., Straube, E., McLeish, T.C.B., Wiedenmann, A., Blackwell, R.J., and Read, D.J., "*Small-Angle Neutron Scattering Study of the Relaxation of a Melt of Polybutadiene H-Polymers Following a Large Step Strain*", Macromolecules, **37** (13), 5054-5064 (2004)

42. Fetters, L. J., Lohse, D. J., and Colby, R. H., "*Chain dimensions and entanglement spacings. In Physical properties of polymers handbook*", New York, Springer (2006)

43. Kraft, M., Meissner, J., and Kaschta, J., "*Linear viscoelastic characterization of polymer melts with long relaxation times*", Macromolecules, **32**, 751-757 (1999)

44. Meissner, J., "*Experimental problems and recent results in polymer melt rheometry*", Makromolekulare Chemie, Macromolecular Symposia, **56**, 25-42 (1992)

45. Meissner, J., "*Combined constant strain rate and stress relaxation test for linear viscoelastic studies*", J.Polym.Sci: Polymer Physics Edition, **16**, 915-919 (1978)

46. Liu, C.Y., He, J., van Ruymbeke, E., Keunings, R., and Bailly, C., "*Evaluation of different methods for the determination of the plateau modulus and the entanglement molecular weight*", Polymer, **47**, 4461-4479 (2006)

47. Liu, G., Park, C.B., and Lefas, J.A., "*Production of low-density LLDPE foams in rotational molding*", Polymer Engineering & Science, **38** (12), 1997-2009 (1998)

48. Graessley, W.W. and Raju, V.R., "*Some rheological properties of solutions and blends of hydrogenated polybutadiene*", Journal of Polymer Science, Polymer Symposia, **71**, 77-93 (1984)

49. Roovers, J., "*Properties of the plateau zone of star-branched polybutadienes and polystyrenes*", Polymer, **26**, 1091-1095 (1985)

50. Larson, R.G., Zhou, Q., Shanbhag, S., and Park, S.J., "*Advances in modeling of polymer melt rheology*", AIChE, **53** (3), 542-548 (2007)

51. Edwards, S.F., "*Statistical mechanics of polymerized material*", Proceedings of the physical society, **92** (1), 9-16 (1967)

52. deGennes, P.G., "*Reptation of a polymer chain in thepresence of fixed obstacles*", J.Chem.Phys., **55**, 572-579 (1971)

53. Doi, M. and Edwards, S. F., "*The theory of polymer dynamics*", New York, Oxford University Press (1986)

54. Doi, M. and Edwards, S.F., "*Dynamics of Concentrated Polymer Systems: Part I. - Brownian Motion in the Equilibrium State*", Journal of the Chemical Society, Faraday Transactions 2: Molecular and Chemical Physics, **74** (10), 1789-1801 (1978)

55. Doi, Masao and Edwards, S. F., "*Dynamics of concentrated polymer systems. Part 3. The constitutive equation*", J.Chem.Soc., Faraday Trans.2, **74** (10), 1818-1832 (1978)

56. Doi, Masao and Edwards, S. F., "*Dynamics of concentrated polymer systems. Part 2. Molecular motion under flow*", J.Chem.Soc., Faraday Trans.2, **74** (10), 1802-1817 (1978)

57. van Ruymbeke, E., Keunings, R., Stephenne, V., Hagenaars, A., and Bailly, C., "*Evaluation of reptation models for predicting the linear viscoelastic properties of entnagled polymers*", Macromolecules, **35** (7), 2689-2699 (2002)

58. van Ruymbeke, E., Keunings, R., and Bailly, C., "*Prediction of linear viscoelastic properties for polydisperse mixtures of entangled star and linear polymers: Modified tube-based model and comparison with experimental results*", J.Non-Newtonian Fluid Mech., **128**, 7-22 (2005)

59. Das, C., Inkson, N.J., Read, D.J., Kelmanson, M.A., and McLeish, T.C.B., "*Computational linear rheology of general branch-on-branch polymers*", Journal of Rheology, **50** (2), 207-234 (2006)

60. Park, S.J., Shanbhag, S., and Larson, R.G., "*A hierarchical algorithm for predicting the linear viscoelastic properties of polymer melts with long-chain branching*", Rheol Acta, **44**, 319-330 (2005)

61. Larson, R.G., "*Combinatorial rheology of branched polymer melts*", Macromolecules, **34** (13), 4556-4571 (2001)

62. Bonchev, D. and Rouvray, D.H., "*Chemical topology: introduction and fundamentals*", Amsterdam, Gordon & Breach; Abingdon: Marston (1999)

63. Wang, Z.W., Chen, X., and Larson, R.G., "*Comparing tube models for predicting the linear rheology of branched polymer melts*", Journal of Rheology, **(in print)** (2009)

64. van Ruymbeke, E., Keunings, R., and Bailly, C., "*Prediction of linear viscoelastic properties for polydisperse mixtures of entangled star and linear polymers: Modified tube-based model and comparison with experimental results*", J.Non-Newtonian Fluid Mech., **128**, 7-22 (2005)

65. van Ruymbeke, E., Bailly, C., Keunings, R., and Vlassopoulos, D., "*A general methodology to predict the linear rheology of branched polymers*", Macromolecules, **39**, 6248-6259 (2006)

66. Wang, Z.W. and Larson, R.G., "*The hierarchical-3.0 codes and input files*", http://www.engin.umich.edu/dept/cheme/people/larson.html (2009)

67. Szwarc, M., Levy, M., and Milkovich, R., "*Polymerization initiated by electron transfer to monomer.A new method of formation of block copolymers*", J.Am Chem Soc, **78**, 2656-2657 (1956)

68. Szwarc, M., "*Living" polymers*", Nature, **176**, 1168-1169 (1956)

69. Hadjichristidis, N., Iatrou, H., Pitsikalis, M., and Mays, J., "*Macromolecular architectures by living and controlled/living polymerizations*", Progress in Polymer Science, **31** (12), 1068-1132 (2006)

70. Hadjichristidis, N., Iatrou, H., Pitsikalis, M., and Mays, J., "*Macromolecular architectures by living and controlled/living polymerizations*", Progress in Polymer Science, **31** (12), 1068-1132 (2006)

71. Hadjichristidis, N., Pitsikalis, M., Pispas, S., and Iatrou, H., "*Polymers with complex architecture by living anionic polymerization*", Chem.Rev., **101**, 3747-3792 (2001)

72. Rempp, P., Franta, E., and Herz, J., "*Anionic polymerization: kinetics, mechanisms, and synthesis*", Washington, D.C., American Chemical Society (1981)

73. Szwarc, M., "*Carbanions, living polymers and electron transfer processes*", New York, Inter science (1968)

74. Quirk, R.P. and Lee, B., "*Experimental Criteria for Living Polymerizations*", Polymer International, **27** (4), 359-367 (1992)

75. Szwarc, M., "*Living polymers. Their discovery, characterization, and properties*", J.of Polymer Science Part A: Polymer Chemistry, **36** (1), ix-xv (1998)

76. Szwarc, M., "*Comments on "Living Polymerization: Rationale for Uniform Terminology" by Darling et al.*", J.of Polymer Science Part A: Polymer Chemistry, **38** (10), 1710-1752 (2000)

77. Morton, M., "*Anionic Polymerization: Principles and Practice*", New York, Academic Press (1983)

78. Flory, P.J., "*Molecular size distribution in ethylene oxide polymers*", J.Am.Chem.Soc., **62** (6), 1561-1565 (1940)

79. Fetters, L. J., "*Encyclopedia of polymer science and engineering*", New York, Wiley-Interscience (1987)

80. Hsieh, H.L. and McKinney, O.F., "*Relationship between the heterogeneity index and the kinetic ratio of anionically polymerized polymers*", Journal of polymer science, Part B: Polymer Letters, **4** (11), 843-847 (1966)

81. Trepka, W. J., "*Lithium: Current applications in science, medicine and technology*", New York, John Wiley (1985)

82. Chang, C.C., Miller, J.W.Jr., and Schorr, G.R., "*Fundamental modeling in anionic polymerization processes*", J.Appl.Polym.Sci., **39** (11-12), 2395-2417 (1990)

83. Koo, C.M., Wu, L., Lim, L.S., Mahanthappa, M.K., Hillmyer, M.A., and Bates, F.S., "*Microstructure and mechanical properties of semicrystalline-rubber-semicrystalline triblock copolymers*", Macromolecules, **38**, 6090-6098 (2005)

84. Pryke, A., Blackwell, R.J., McLeish, T.C.B., and Young, R.N., "*Synthesis, hydrogenation, and rheology of 1,2-polybutadiene star polymers*", Macromolecules, **35**, 467-472 (2002)

85. Lee, J.S., Quirk, R.P., and Foster, M.D., "*Synthesis and characterization of well-defined, regularly branched polystyrenes utilizing multifunctional initiators*", Macromolecules, **38**, 5391-5392 (2005)

86. Quirk, R.P., Yin, J., Guo, S.H., Hu, X.W., Summers, G., Kim, J., Zhu, L.F., and Schock, L.E., " *Anionic synthesis of chain-end functionalized polymers*", Makromolekulare Chemie, Macromolecular Symposia, **32**, 47-59 (1990)

87. Schulz, D.N., Sanda, J.C., and Willoughby, B.G., "*Functionally terminal polymers via anionic methods*", ACS symposium series, **166** (Anionic polym.), 427-440 (1981)

88. Hadjichristidis, N., Iatrou, H., Pispas, S., and Pitsikalis, M., "*Anionic polymerization: High vacuum techniques*", Journal of Polymer Scienc: Part A: Polymer Chemistry, **38**, 3211-3234 (2000)

89. Uhrig, D. and Mays, J.W., "*Experimental techniques in high-vacuum anionic polymerization*", J.of Polymer Science: Part A: Polymer Chemistry, **43**, 6179-6222 (2005)

90. Coyne, G.S. and Cobb, C.L., "*Efficient, inexpensive, and useful techniques for low vacuum leak detection with a Tesla coil*", Journal of chemical education, **68** (6), 526-528 (1991)

91. Suffert, J., "*Simple direct titration of organolithium reagents using N-pivaloyl-o-toluidine and/or N-pivaloyl-o-benzylaniline*", Journal of organic chemistry, **54** (2), 509-510 (1989)

92. Gilman, H. and Cartledge, F.K., "*The analysis of organolithium compounds*", Journal of organometallic chemistry, **2**, 447-454 (1964)

93. Watson, S.C. and Eastham, J.F., "*Colored indicators for simple direct titration of magnesium and lithium reagents*", Journal of organometallic chemistry, **9** (1), 165-168 (1967)

94. Pangborn, A.B., Giardello, M.A., Grubbs, R.H., Posen, R.K., and Timmers, F.J., "*Safe and convenient procedure for solvent purification*", Organometallics, **15**, 1518-1520 (1996)

95. Kurata, M. and Tsunashima, Y., "*Polymer Handbook*", New York, Wiley (1989)

96. Kanaoka, S., Sawamoto, M., and Higashimura, T., "*Star-shaped polymers by living cationic polymerization. 1. Synthesis of star-shaped polymers of alkyl and vinyl ethers*", Macromolecules, **24** (9), 2309-2313 (1991)

97. Mayadunne, R.T.A., Jeffery, J., Moad, G., and Rizzardo, E., "*Living Free Radical Polymerization with Reversible Addition-Fragmentation Chain Transfer (RAFT Polymerization): Approaches to Star Polymers*", Macromolecules, **36** (5), 1505-1513 (2003)

98. Jacob, S., Majoros, I., and Kennedy, J.P., "*New Stars: Eight Polyisobutylene Arms Emanating from a Calixarene Core*", Macromolecules, **29** (27), 8631-8641 (1996)

99. Alward, D.B., Kinning, D.J., Abdel-Goad, M., Thomas, E.L., and Fetters, L.J., "*Effect of arm number and arm molecular weight on the solid-state morphology of poly(styrene-isoprene) star block copolymers*", Macromolecules, **19** (1), 215-224 (1986)

100. Lee, J.S., Quirk, R.P., and Foster, M.D., "*Effect of Butadiene End-Capping of Arms in a Star Polystyrene on Solution Properties, Bulk Dynamics, and Bulk Thermodynamic Interactions in Binary Blends*", Macromolecules, **37** (26), 10199-10204 (2004)

101. Uhrig, D. and Mays, J., "*Synthesis of combs, centipedes, and barbwires: poly(isoprene-graft-styrene) regular multigraft copolymers with trifunctional, tetrafunctional, and hexafunctional branch points*", Macromolecules, **35** (19), 7182-7190 (2002)

102. Roovers, J. and Toporowski, P.M., "*Preparation and characterization of H-shaped polystyrene*", Macromolecules, **14** (5), 1174-1178 (1981)

103. Hild, G., Kohler, A., and Rempp, P., "*Synthesis of ring-shaped macromolecules*", European polymer journal, **16** (6), 525-527 (1980)

104. Perny, S., Allgaier, J., Cho, D., Lee, W., and Chang, T., "*Synthesis and structural analysis of an H-shaped polybtuadiene*", Macromolecules, **34**, 5408-5415 (2001)

105. Ikker, A. and Moller, M., "*Coupling of polystyryllithium with divinyl compounds*", New polymeric materials, **4**, 35-51 (1993)

106. Yu, Y.S., Dubois, Ph., Jerome, R., and Teyssie, Ph., "*Difunctional initiators based on 1,3-diisopropenylbenzene. 3. Synthesis of a pure dilithium adduct and its use as difunctional anionic polymerization initiator*", Macromolecules, **29**, 2738-2745 (1996)

107. Lee, H.C. and Chang, T., "*Polymer molecular weight characterization by temperature gradient high performance liquid chromatography*", Polymer, **37** (25), 5747-5749 (1996)

108. Lee, H.C., Chang, T., Harville, S., and Mays, J., "*Characterization of Linear and Star Polystyrene by Temperature-Gradient Interaction Chromatography with a Light-Scattering Detector*", Macromolecules, **31** (3), 690-694 (1998)

109. Lee, H.C., Lee, W., Chen, T.H., Yoon, J.S., Frater, D.J., and Mays, J., "*Linking Reaction Kinetics of Star Shaped Polystyrene by Temperature Gradient Interaction Chromatography*", Macromolecules, **31** (13), 4114-4119 (1998)

110. Rahman, M.S., Aggarwal, R., Larson, R.G., Dealy, J.M., and Mays, J., "*Synthesis and Dilute Solution Properties of Well-Defined H-Shaped Polybutadienes*", Macromolecules, **41** (21), 8225-8230 (2008)

111. Mavroudis, A. and Hadjichristidis, N., "*Synthesis of Well-Defined 4-Miktoarm Star Quarterpolymers (4m-SIDV) with Four Incompatible Arms: Polystyrene (S), Polyisoprene-1,4 (I), Poly(dimethylsiloxane) (D), and Poly(2-vinylpyridine) (V)*", Macromolecules, **39** (2), 535-540 (2006)

112. Orfanou, K., Iatrou, H., Lohse, D.J., and Hadjichristidis, N., " *Synthesis of Well-Defined Second (G-2) and Third (G-3) Generation Dendritic Polybutadienes*", Macromolecules, **39** (13), 4361-4365 (2006)

113. Maric, M. and Macosko, C.W., "*Improving polymer blend dispersions in mini-mixers*", Polymer Engineering & Science, **41** (1), 118-130 (2001)

114. Nicholson, J. W., "*The chemistry of polymers*", Cambridge, UK, The Royal Society of Chemistry (2006)

115. Daniels, D.R., McLeish, T.C.B., Kant, R., Crosby, B.J., Young, R.N., Pryke, A., Allgaier, J., Groves, D.J., and Hawkins, R.J., "*Linear rheology of diluted linear, star and model long chain branched polymer melts*", Rheol Acta, **40**, 403-415 (2001)

116. Heinrich, M., Pyckhout-Hintzen, W., Allgaier, J., Richter, D., Straube, E., Read, D.J., McLeish, T.C.B., Groves, D.J., Blackwell, R.J., and Wiedenmann, A., "*Arm relaxation in deformed H-polymers in elongational flow by SANS*", Macromolecules, **35**, 6650-6664 (2002)

117. Heinrich, M., Pyckhout-Hintzen, W., Richter, D., Straube, E., and Wiedenmann, A., "*Relaxation of entangled model H-shaped polymers: a SANS investigation*", Appl.Phys.A: Materials science and processing, **74 [Suppl]**, S380-S382 (2002)

118. McLeish, T.C.B. and Milner, S.T., "*Entangled dynamics and melt flow of branched polymers*", Advances in Polymer Science, **143**, 195-256 (1999)

119. Chang, T., "*Polymer characterization by interaction chromatography*", Journal of polymer Science: Part B: Polymer Physics, **43**, 1591-1607 (2005)

120. Chang, T., "*Recent advances in liquid chromatography analysis of synthetic polymers*", Adv.Polym.Sci., **163**, 1-60 (2003)

121. Glockner, G., "*Gradient HPLC of copolymers and chromatographic cross-fractionation*", Berlin, Springer Verlag (1992)

122. Lee, W., Lee, H.C., Chang, T., and Kim, S.B., "*Characterization of Poly(methyl methacrylate) by Temperature Gradient Interaction Chromatography with On-Line Light Scattering Detection*", Macromolecules, **31**, 344-348 (1998)

123. Lee, W., Lee, H., Cha, J., Chang, T., Hanley, K.J., and Lodge, T.P., "*Molecular Weight Distribution of Polystyrene Made by Anionic Polymerization*", Macromolecules, **33** (14), 5111-5115 (2000)

124. Santee, E.R., Chang, R., and Morton, M., "*300 MHz proton NMR of polybutadiene: measurement of cis-trans isomeric content*", J.Polymer Science: Polymer Letters Edition, **11** (7), 449-452 (1973)

125. Bywater, S., Firat, Y., and Black, P.E., "*Microstructures of polybutadienes prepared by anionic polymerization in polar solvents. Ion-pair and solvent effects*", J.of Polymer Science: Polymer Chemistry Edition, **22**, 669-672 (1984)

126. Schwarzl, F. and Staverman, A.J., "*Time-Temperature Dependence of Linear Viscoelastic Behavior*", J.appl.phys., **23** (8), 838-843 (1952)

127. Williams, M.L., Landel, R.F., and Ferry, J.D., "*The Temperature Dependence of Relaxation Mechanisms in Amorphous Polymers and Other Glass-forming Liquids*", J.Am.Chem.Soc., **77** (14), 3701-3707 (1955)

128. Wood-Adams, P.M. and Costeux, S., "*Thermorheological behavior of polyethylene: effects of microstrucre and long chain branching*", Macromolecules, **34**, 6281-6290 (2001)

129. He, C.X., Wood-Adams, P.M., and Dealy, J.M., "*Broad frequency range characterization of molten polymers*", Journal of Rheology, **48** (4), 711-724 (2004)

130. Eckstein, A., Suhm, J., Friedrich, C., Maier, R.D., Sassmannshausen, J., Bochmann, M., and M haupt, R., "*Determination of Plateau Moduli and Entanglement Molecular Weights of Isotactic, Syndiotactic, and Atactic Polypropylenes Synthesized with Metallocene Catalysts*", Macromolecules, **31,** 1335-1340 (1998)

131. Friedrich, C., Honerkamp, J., and Weese, J., "*New ill-posed problems in rheology*", Rheological Acta, **35,** 186-193 (1996)

132. Weese, J., "*A regularization method for non-linear ill-posed problems*", Comput.Phys.Commun., **77**, 429-440 (1993)

133. Baumgaertel, M. and Winter, H.H., "*Determination of discrete relaxation and retardation spectra from dynamic mechanical data*", Rheological Acta, **28**, 511-519 (1989)

134. Tschoegl, N. W., "*The phenomenological theory of linear viscoelastic behavior : an introduction*", New York, Springer-Verlag (1989)

135. Ferry, J. D., "*Viscoelastic properties of polymers*", New York, Wiley (1980)

136. Gabriel, C. and Kaschta, J., "*Comparison of different shear rheometers with regard to creep and creep recovery measurements*", Rheological Acta, **37**, 358-364 (1998)

137. Franck, A.J.P., "*A rheometer for characterizing polymer melts and suspensions in shear creep and recovery experiments*", J.of Rheology, **29** (6), 833-850 (1985)

138. Lomellini, P., "*Effect of chain length on the network modulus and entanglement*", Polymer, **33** (6), 1255-1260 (1992)

139. Kraus, G. and Rollmann, K.W., "*The entanglement plateau in the dynamic modulus of rubbery styrene-diene block copolymers. Significance to pressure-sensitive adhesive formulations*", J.Applied Poly.Sci., **21**, 2311-3318 (1977)

140. Carella, J.M., Graessley, W.W., and Fetters, L.J., "*Effects of chain microstructure on the viscoelastic properties of linear polymer melts: polybutadienes and hydrogenated polybutadienes*", Macromolecules, **17** (12), 2775-2786 (1984)

141. Zoller, P. and Walsh, D. J., "*Standard pressure-volume-temperature data for polymers*", Lancaster, PA, Technomic Pub. Co. (1995)

142. Wood-Adams, P.M. and Costeux, S., "*Thermorheological behavior of polyethylene:effects of microstructure and long chain branching*", Macromolecules, **34** (18), 6281-6290 (2001)

143. Dealy, J. and Plazek, D., "*Time-temperature superposition - a users guide*", Rheology Bulletin, **78** (2), 16-31 (2009)

144. Van Gurp, M. and Plamen, J., "*Time temperature superposition for polymeric blends*", Rheol Bull, **67**, 5-8 (1998)

145. Park, H.E., Dealy, J., and Munstedt, H., "*Influence of long-chain branching on time-pressure and time-temperature shift factors for polystyrene and polyethylene*", Rheological Acta, **46**, 153-159 (2006)

146. Valentine, R.H., Ferry, J.D., Homma, T., and Ninomiya, K., "*Viscoelastic properties of polybutadienes-linear and lightly crosslinked near the gel point*", J.of Poly.Sci.: Part A-2, **6**, 479-492 (1968)

147. Colby, R.H., Fetters, L.J., and Graessley, W.W., "*The melt viscosity-molecular weight relationship for linear polymers*", Macromolecules, **20** (9), 2226-2237 (1987)

148. Honerkamp, J. and Weese, J., "*A nonlinear regularization method for the calculation of relaxation spectra*", Rheological Acta, **32**, 65-73 (1999)

149. Kaschta, J. and Schwarzl, F., "*Calculation of discrete retardation spectra from creep data - I. Method*", Rheol Acta, **33**, 517-529 (1994)

150. Fetters, L. J., Lohse, D. J., and Colby, R. H., "*Physical properties of polymers handbook*", New York, Springer (2007)

151. Robles-Vasquez, O., Gonzalez-Alvarez, A., Puig, J.E., and Manero, O., "*A composition rule to predict the linear viscoelastic properties of Polybutadienes*

with varying microstructure", Rubber Chemistry and Technology, **79** (5), 859-869 (2006)

152. Fetters, L.J., Lohse, D.J., and Graessley, W.W., "*Chain dimensions and entanglement spacings in dense macromolecular systems",* J.Polym.Sci.B, **37**, 1023-1033 (1999)

153. Wu, S., "*Chain structure and entanglement",* Journal of Polymer Science, Part B: Polymer Physics, **27**, 723-741 (1989)

154. Graessley, W.W., "*The entanglement concept in polymer rheology",* Advances in Polymer Science, **16**, 1-179 (1974)

155. Doi, Masao and Edwards, S. F., "*Dynamics of concentrated polymer systems. Part 1. Brownian motion in the equilibrium state",* J.Chem.Soc., Faraday Trans.2, **74** (10), 1789-1801 (1978)

156. United States Environmental Protections: The council for regulatory environmental modeling, "*Draft guidance on the development, evaluation, and application of regulatory environmental models*", http://www.epa.gov/crem/library/cred_guidance-0309.pdf (2009)

157. Milner, S.T. and McLeish, T.C.B., "*Parameter-free theory for stress relaxation in star polymer melts",* Macromolecules, **30**, 2157-2166 (1997)

158. Milner, S.T. and McLeish, T.C.B., "*Reptation and contour-lentgh fluctuations in melts of linear polymers",* Phys.Rev.Lett, **81,** 725-728 (1998)

159. Blottiere, B., McLeish, T.C.B., Hakiki, A., Young, R.N., and Milner, S.T., "*The rheology of bimodal blends of star polymer melts",* Macromolecules, **31**, 9295-9304 (1998)

160. Milner, S.T., McLeish, T.C.B., Young, R.N., Hakiki, A., and Johnson, J.M., "*Dynamic dilution, constraint-release, and star-linear blends",* Macromolecules, **31**, 9345-9353 (1998)

161. Ball, R.C. and McLeish, T.C.B., "*Dynamic dilution and the viscosity of star polymer melts",* Macromolecules, **22,** 1911-1913 (1989)

162. Marrucci, G., "Re*laxation by reptation and tube enlargement: a model for polydisperse polymers",* J.Polym.Sci., Polym.Phys.Ed., **23** (1), 159-177 (1985)

163. Viovy, J.L., Rubinstein, M., and Colby, R.H., " *Constraint release in polymer melts: tube reorganization versus tube dilation",* Macromolecules, **24** (12), 3587-3596 (1991)

164. Fetters, L.J., Lohse, D.J., Richter, D., Witten, T.A., and Zirkel, A., "*Connection between Polymer Molecular Weight, Density, Chain Dimensions, and Melt Viscoelastic Properties*", Macromolecules, **27** (17), 4639-4647 (1994)

165. Pearson, D.S., Mueller, L.J., Fetters, L.J., and Hadjichristidis, N.J., "*Comparison of the rheological properties of linear and star-branched polyisoprenes in shear and elongational flow*", Polym.Sci.Polym.Phys.Ed., **21**, 2287-2298 (1983)

166. Frischknecht, A.L., Milner, S.T., Pryke, A., Young, R.N., Hawkins, R., and McLeish, T.C.B., "*Rheology of three-arm asymmetric star polymer melts*", Macromolecules, **35** (12), 4801-4820 (2002)

167. Lee, J.H., Fetters, L.J., Archer, L.A., and Halasa, A.F., "*Tube dynamics in binary polymer blends*", Macromolecules, **38**, 3917-3932 (2005)

168. Dealy, J. M. and Larson, R. G.; *Structure and rheology of molten polymers: From structure to flow behavior and back again (2*006) Munich, Carl Hanser Verlag

169. Struglinski, M.J. and Graessley, W.W., "*Effects of polydispersity on the linear viscoelastic properties of entangled polymers. 3. Experimental observations on binary mixtures of linear and star polybutadienes*", Macromolecules, **21**, 783-789 (1988)

170. Struglinski, M.J. and Graessley, W.W., "*Effects of polydispersity on the linear viscoelastic properties of entangled polymers. 1. Experimental observations for binary mixtures of linear polybutadiene*", Macromolecules, **18** (12), 2630-2643 (1985)

171. Park, S.J. and Larson, R.G., "*Dilution exponent in the dynamic dilution theory for polymer melts*", Journal of Rheology, **47** (1), 199-211 (2003)

172. Saltelli, A., Tarantola, S., Campolongo, F., and Ratto, M., "*Sensitivity analysis in practice: a guide to assessing scientific models*",Chichester ; Hoboken, NJ, Wiley (2004)

173. Stadler, F.J., Piel, C., Kaschta, J., Rulhoff, S., Kaminsky, W., and Munstedt, H., "*Dependence of the zero shear-rate viscosity and the viscosity function of linear high-density polyethylenes on the mass-average molar mass and polydispersity*", Rheol Acta, **45**, 755-764 (2006)

174. Gabriel, C. and Munstedt, H., "*Influence of long-chain branches in polyethylenes on liner viscoelastic flow properties in shear*", Rheol.Acta., **41**, 232-244 (2002)

175. Das, C., "*Manual of Bob-2.3",* http://sourceforge.net/projects/bob-rheology (2008)

176. Park, S.J. and Larson, R.G., "*Tube dilation and reptation in binary blends of monodisperse linear polymers*", Macromolecules, **37**, 597-604 (2004)

177. Fetters, L.J., Lohse, D.J., Milner, S.T., and Graessley, W.W., "*Packing length influence in linear polymer melts on the entanglement, critical, and reptation molecular weights*", Macromolecules, **32** (20), 6847-6851 (1999)

178. Trinkle, S. and Friedrich, C., "*Van Gurp-Palmen-plot: a way to characterize polydispersity of linear polymers*", Rheological Acta, **40**, 322-328 (2001)

179. Trinkle, S., Walter, P., and Friedrich, C., "*Van Gurp-Palmen Plot II - classification of long chain branched polymers by their topology*", Rheological Acta, **41**, 103-113 (2002)

180. Davies, A.R. and Anderssen, R.S., "*Sampling localization in determining the relaxation spectrum*", J.Non-Newtonian Fluid Mech., **73**, 163-179 (1997)

181. Masuda, T., Ohta, Y., and Onogi, S., "*Rheological properties of anionic polystyrenes. III. Characterization and rheological properties of four-branch polystyrenes*", Macromolecules, **4** (6), 763-768 (1971)

182. Raju, V.R., Menezes, E.V., Marin, G., Graessley, W.W., and Fetters, L.J., "*Concentration and molecular weight dependence of viscoelastic properties in linear and star polymers*", Macromolecules, **14** (6), 1668-1676 (1981)

183. Doi, M. and Kuzuu, N., "*Rheology of star polymers in concentrated solutions and melts*", Journal of polymer science, polymer letters edition, **18** (12), 775-780 (1980)

Appendix A

Determine Molarity of *n*-BuLi by Watson-Eastham Method

I. Experimental details

1. Rinse two 125 ml volumetric flask with methyl chloride and dry with N_2 gas
2. Add Teflon coated stir bar and 0.003 g indicator (2,2 biquinoline) to one of the above flask and cover with rubber septum. (flask A)
3. Put flask A on top of a balance and transfer ~ 50ml or ~ 25g of hexane by double tipped cannula with N_2 bubbling to the hexane bottle. This is to create a pressure difference between the hexane bottle and flask A, such that hexane can be transferred under an inert atmosphere.
4. Fill the other flask with N_2 for syringe rinse. To prevent the septum from popping out, use a plastic tie to tighten the flask opening.
5. Prepare needle syringe, rinse the needles with MeCl and blow dry with N2. Repeat the rinse for several times with the N_2 filled flask.
6. Suck in ~ 1ml initiator and weight.
7. Add initiator to flask A slowly, and weight again. Record the difference which will be the amount of initiator used. (Solution should turn to yellow while adding initiator)
8. Rinse new syringe with needle.
9. Use it to suck ~2ml 2-butanol and record the weight.
10. Titrate with flask A until the yellow color changed to colorless.
11. Weight the syringe and record down the difference, which is the amount of 2-butanol used for the titration.

II. Sample calculations

Since number of mole of *n*-BuLi toBuOH is 1:1, therefore:

$$\text{Molarity of } n\text{-BuLi} = \frac{\text{mass of BuOH}}{\text{mass of } n\text{ - BuLi}} \times \frac{\rho_{\text{n-BuLi}}}{M_{w,\text{BuOH}}} \times 1000 \ \text{(M)}$$

where $\rho_{\text{n-BuLi}} = 0.693$ g/cm^3 and $M_{w,\text{BuOH}}$ = 74g/mol.

Appendix B

Molecular Weights Characterization

I. Molecular weights characterization by University of Tennessee

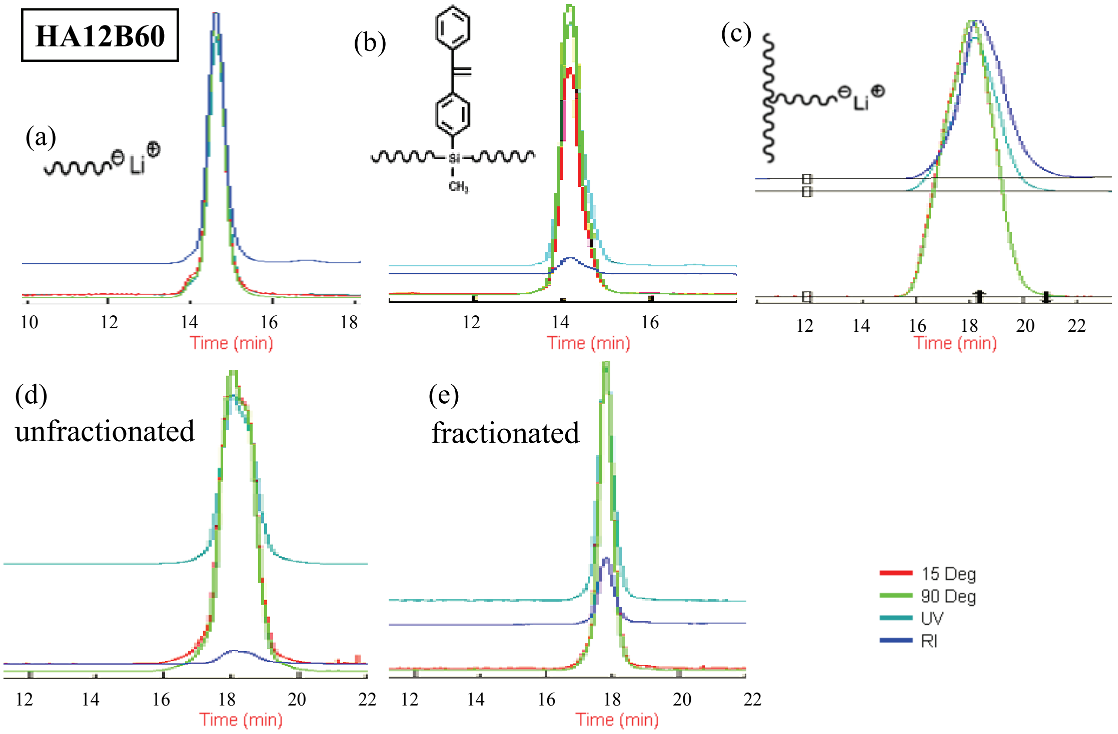

Figure B1 SEC elution profiles of precursors and final product of HA12B60: (a) living PBD arm, (b) coupled PBD arms, (c) living half H, (d) unfractionated final product, and (e) fractionated final product

HA12B100

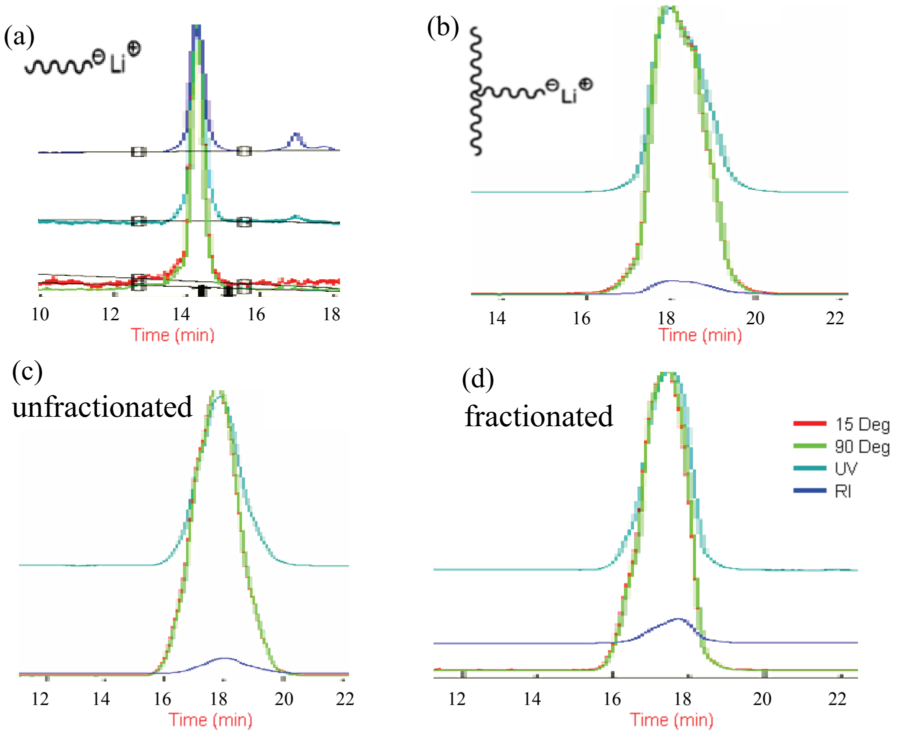

Figure B2 SEC elution profiles of precursors and final product of HA12B100: (a) living PBD arm, (b) living half H, (c) unfractionated final product, and (d) fractionated final product

HA30B40

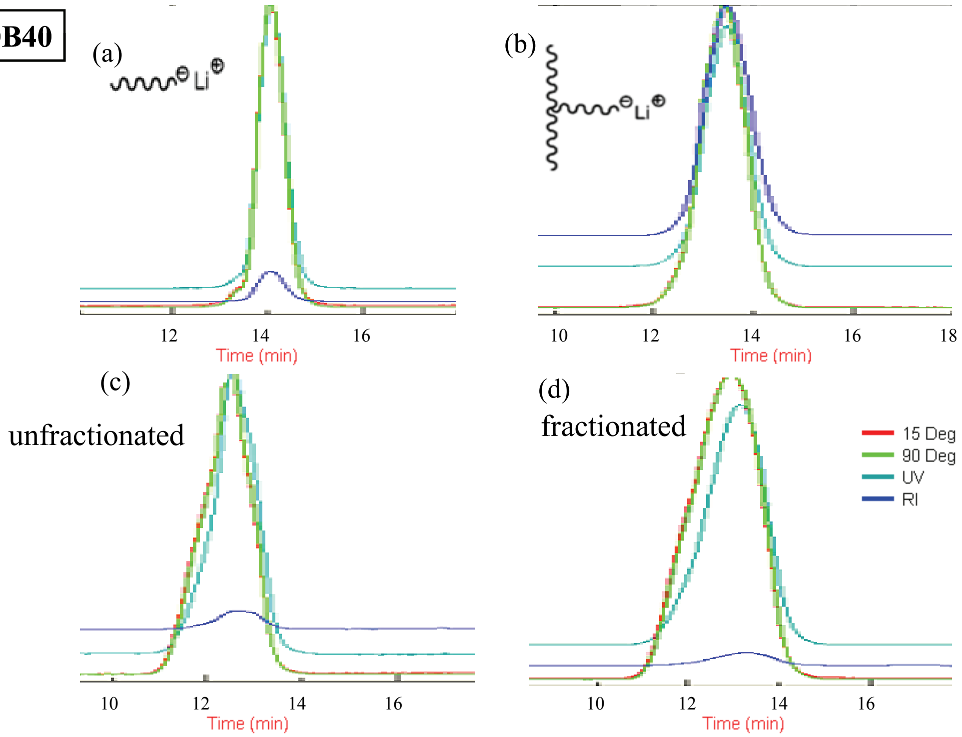

Figure B3 SEC elution profiles of precursors and final product of HA30B40: (a) living PBD arm, (b) living half H, (c) unfractionated final product, and (d) fractionated final product

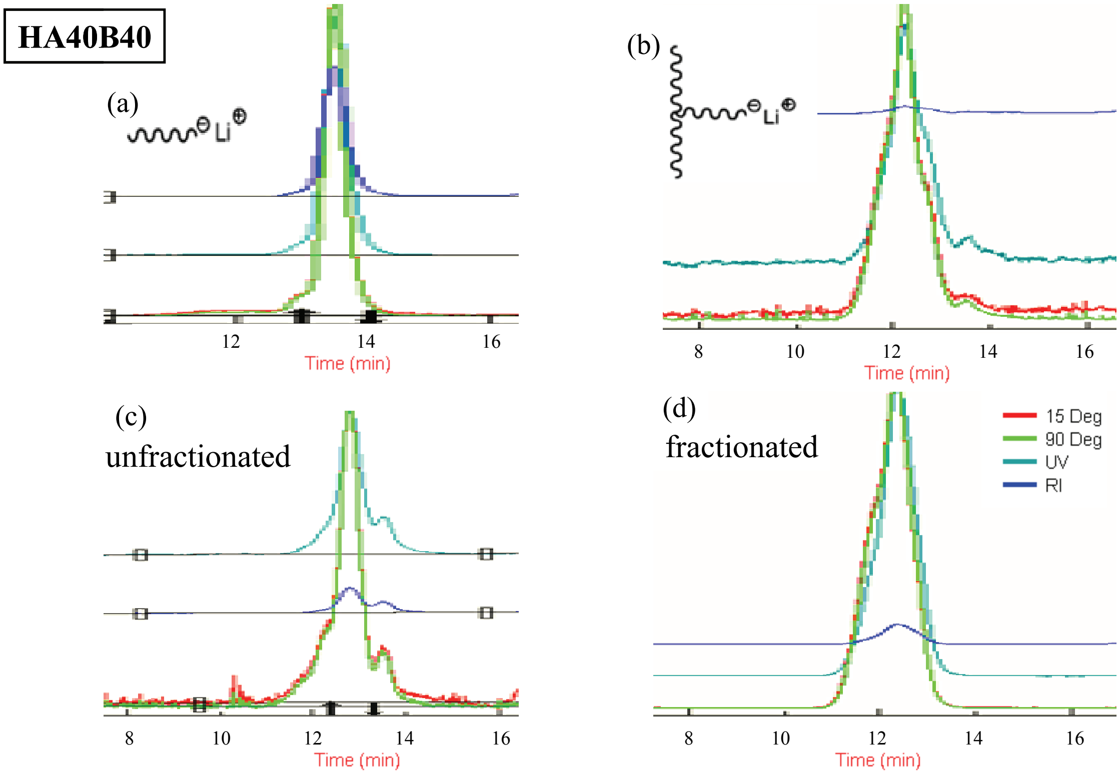

Figure B4 SEC elution profiles of precursors and final product of HA40B40: (a) living PBD arm, (b) living half H, (c) unfractionated final product, and (d) fractionated final product

Appendix C

^{1}H NMR Spectra of PBDs

Characteristic peaks of each configuration are listed in Table C1 [124] while the corresponding resonance groupings are illustrated in Fig. C1. Sample calculation on the concentration of vinyl, *cis* and *trans* configuration on PBD2 is illustrated below. The NMR spectra on the two linear PBDs and five H-shaped PBDs used for rheological characterization are shown in Figs. C2 to C8.

Table C1 Chemical shifts of resonance peaks representing *cis*, *trans* and vinyl isomer in polybutadiens

Resonance groupings	**Chemical shift (ppm)**
1,2 alphatic	1.3
1,2 terminal olefinic	4.8
1,2 non-terminal olefinic	5.6
1,4 alphatic trans	1.98
1,4 alphatic cis	2.03
1,4 olefinic trans	5.32
1,4 olefinic cis	5.37

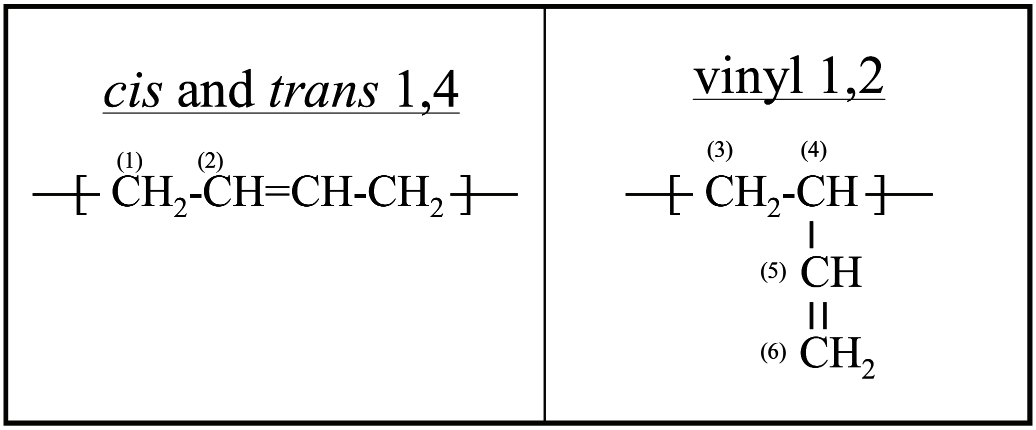

Figure C1 Resonance groupings of polybutadienes

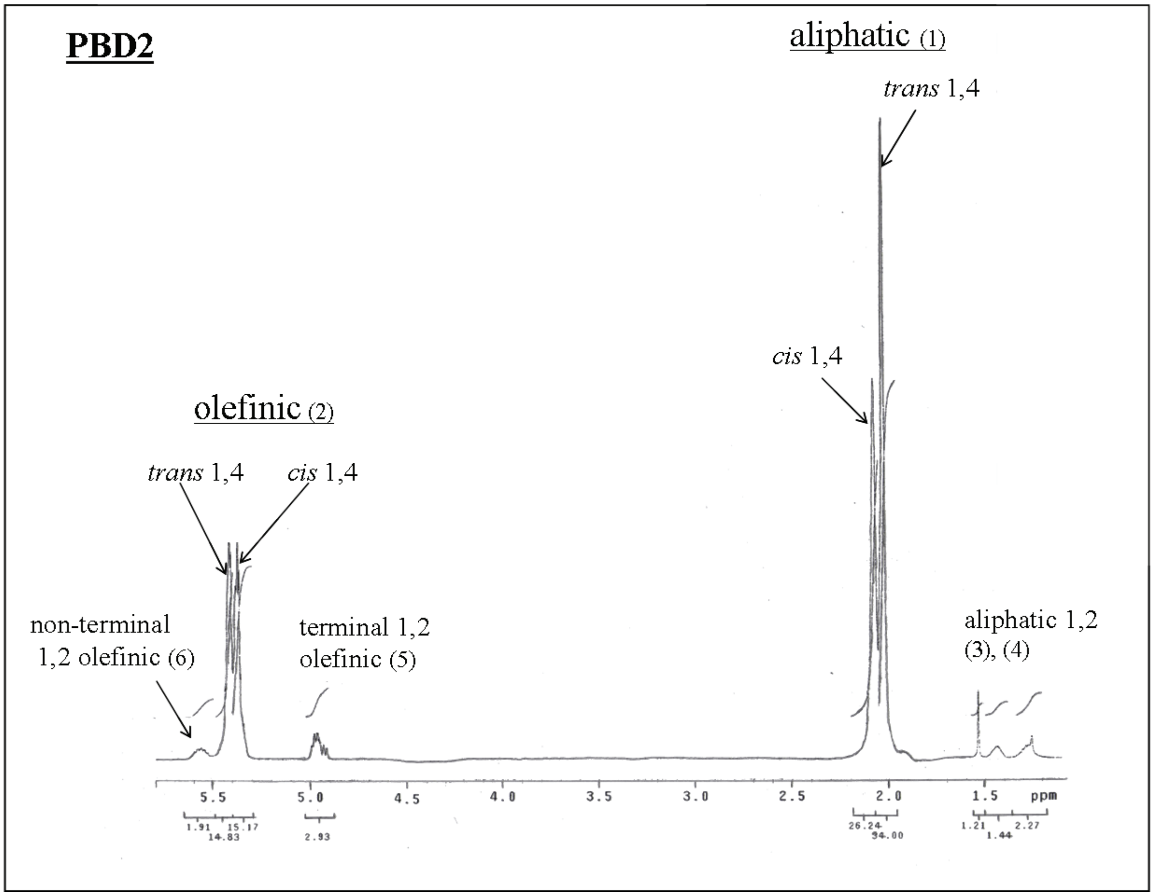

Figure C2 ^{1}H NMR spectrum of PBD2

Sample calculation on PBD2

Sum of 1,2 addition = 1,2 alphatic + 1,2 terminal olefinic + 1,2 non-terminal olefinic

$= (1.21 + 1.44 + 2.27) + 2.93 + 1.91 = 9.76$

Sum of *cis* 1,4 addition = aliphatic *cis* 1,4 + olefinic *cis* 1,4

$= 26.24 + 15.17 = 41.41$

Sum of trans 1,4 addition = aliphatic *trans* 1,4 + olefinic *trans* 1,4

$= 34.00 + 14.83 = 48.83$

Total = 9.76 + 41.41 + 48.83 = 100

% of 1,2 vinyl addition = 9.76/100 =9.76%

% of *cis* 1,4 addition = 41.41/100 = 41.41%

% of *trans* 1,4 addition = 48.83/100 = 48.83%

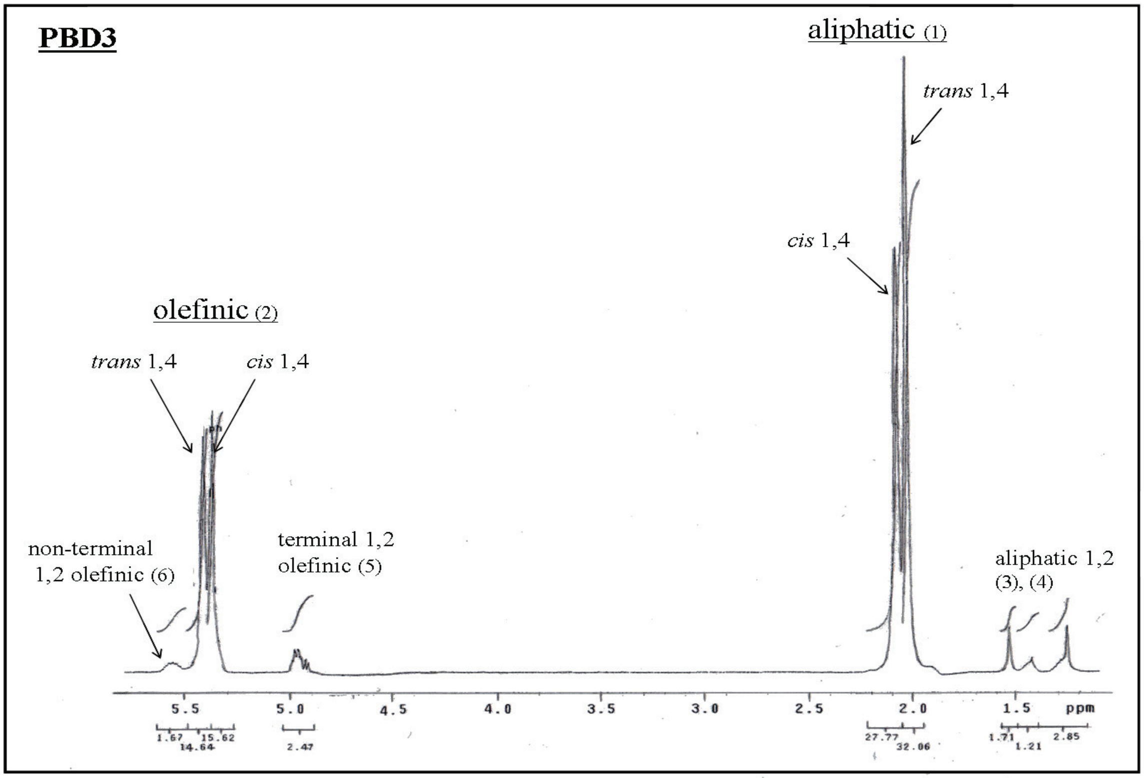

Figure C3 ^{1}H NMR spectrum of PBD3

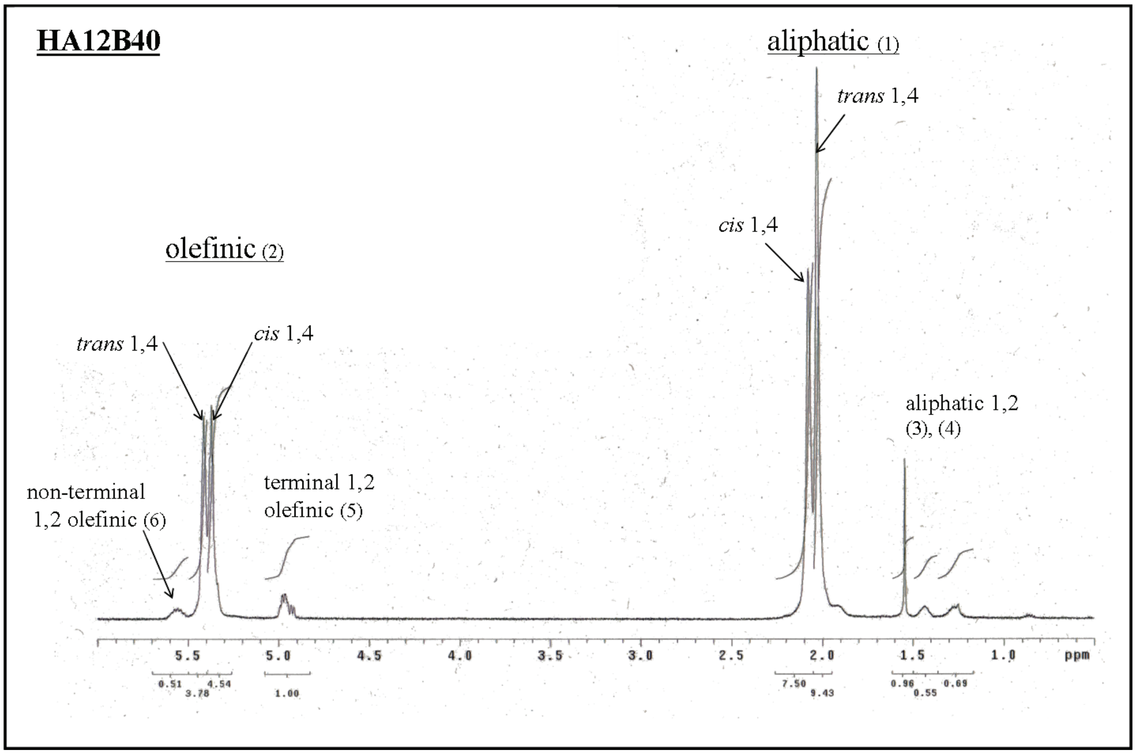

Figure C4 ^{1}H NMR spectrum of HA12B40

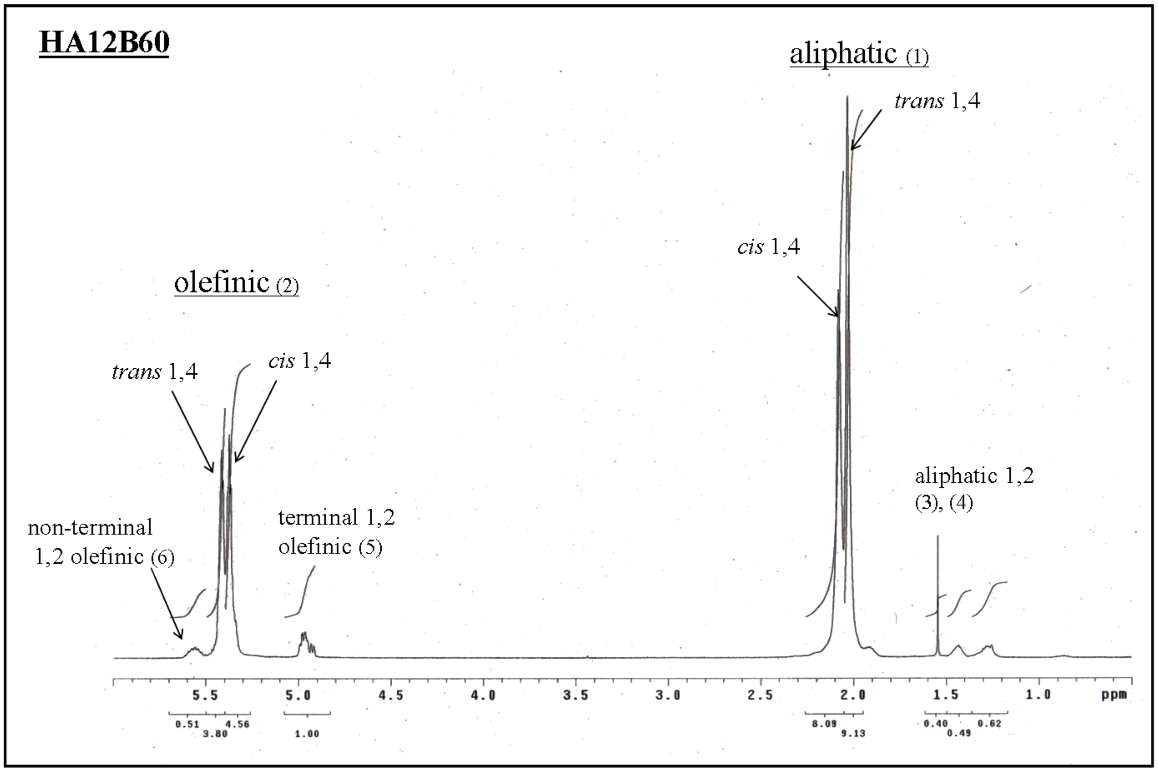

Figure C5 ^{1}H NMR spectrum of HA12B60

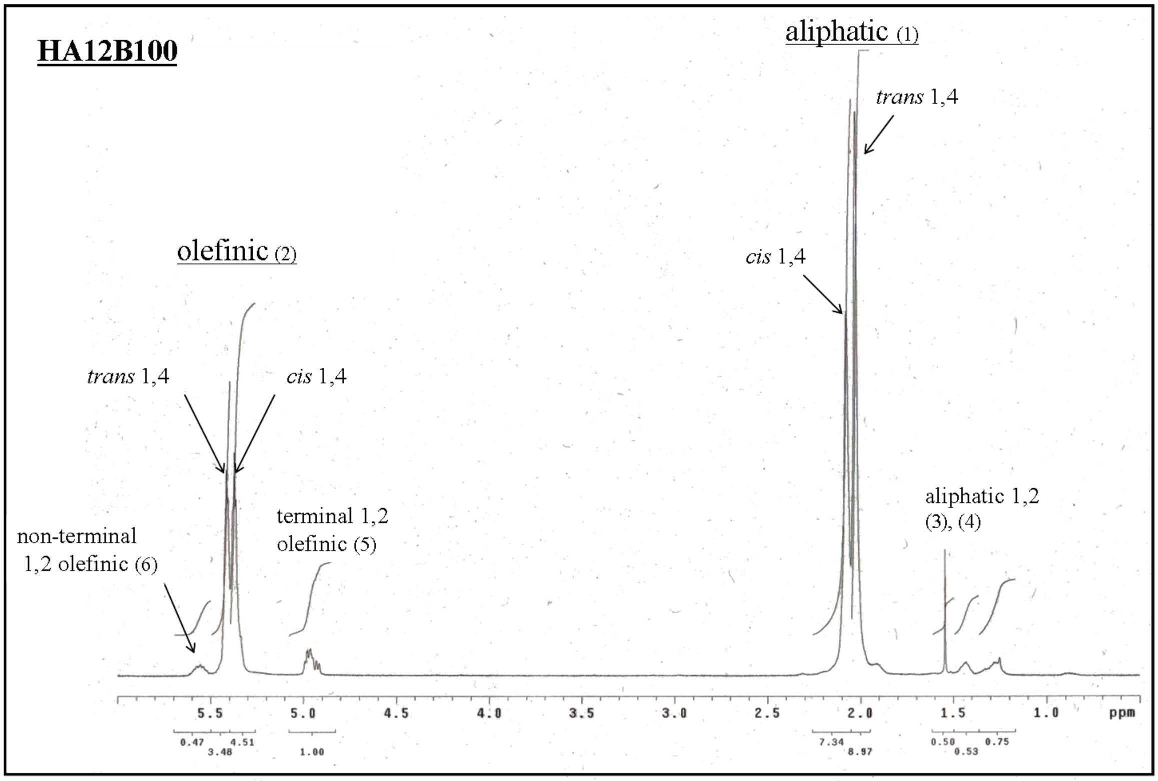

Figure C6 ^{1}H NMR spectrum of HA12B100

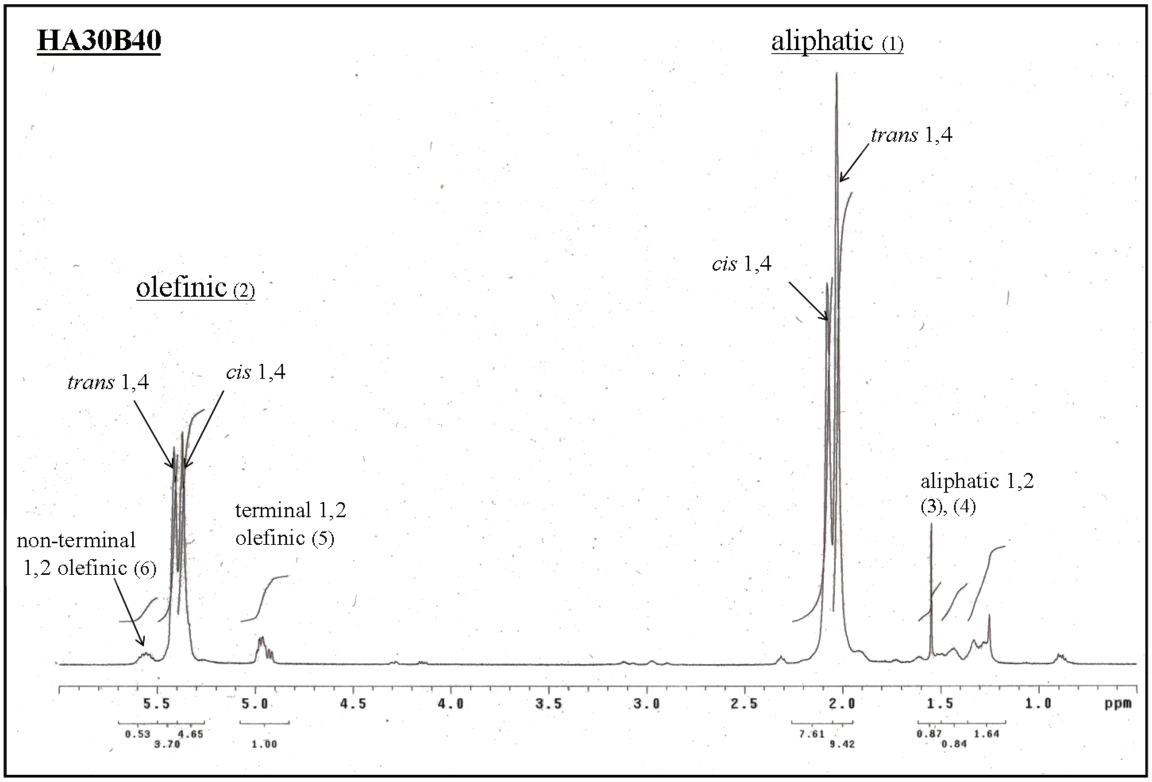

Figure C7 ^{1}H NMR spectrum of HA30B40

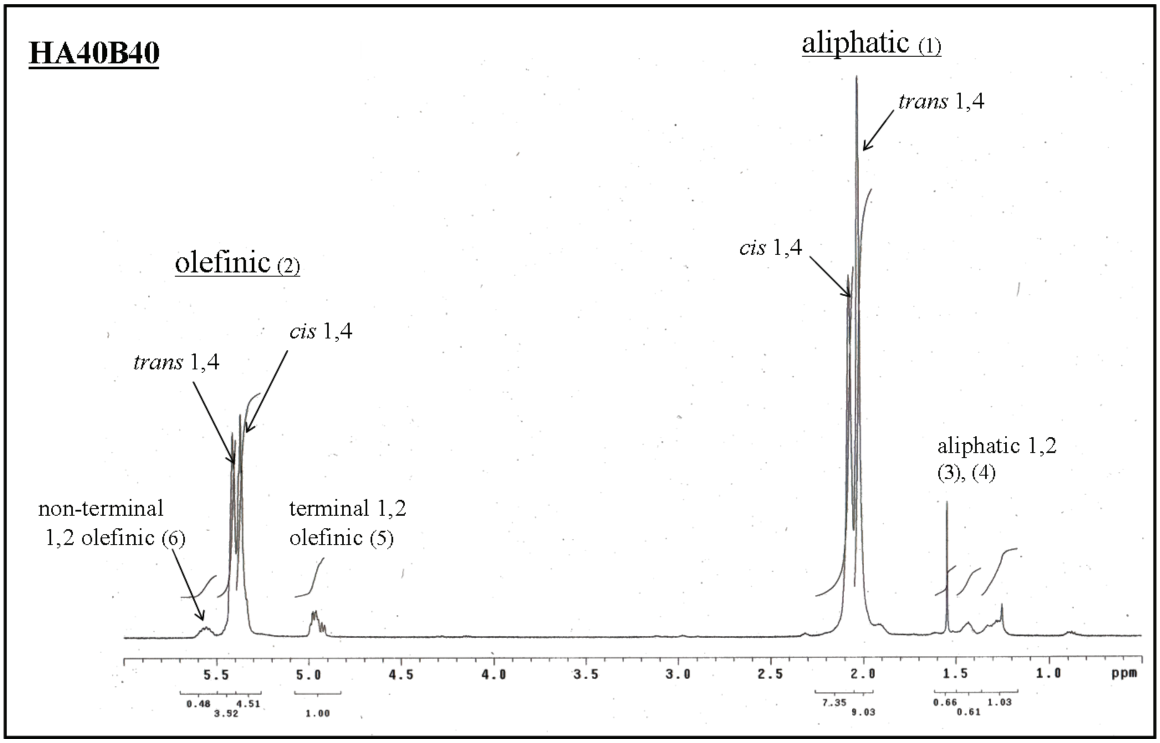

Figure C8 ^{1}H NMR spectrum of HA40B40

Appendix D Supplementary Result of Chapter 4

I. Dynamic strain sweep test

Tables D1 to D7 shown the linear regime of strain for dynamic frequency sweet test. Experimental details can be found in section 4.5.2.2

Table D1 Strain (%) used for dynamic frequency sweep experiment of PBD2

Temperature (°C)	Frequency Range (rad/s)			
	500-100	100-10	10-1	1-0.1
25	0.5	1	3	21
0	0.5	1	1.5	4
-25	1	1.5	1.5	2
-50	0.5	1	1	1.2
-75	0.2	0.5	0.5	0.7

Table D2 Strain (%) used for dynamic frequency sweep experiment of PBD3

Temperature (°C)	Frequency Range (rad/s)				
	500-100	100-10	10-1	1-0.1	0.1-0.01
25	0.5	0.7	1	2	--
0	0.5	0.7	1	1.5	2
-25	0.5	0.7	1	1.5	2
-50	0.5	0.7	1	1.3	1.5
-75	--	0.3	0.5	0.8	1

Table D3 Strain (%) used for dynamic frequency sweep experiment of HA12B40

Temperature (°C)	Frequency Range (rad/s)				
	500-100	100-10	10-1	1-0.1	0.1-0.01
25	1	1.5	2	5	10
0	0.5	1	2	4	4
-25	0.5	0.7	1	2	2
-50	0.5	0.7	0.9	1.5	1.5
-75	1	1.3	0.5	1	1

Table D4 Strain (%) used for dynamic frequency sweep experiment of HA12B60

Temperature (^oC)	Frequency Range (rad/s)				
	500-100	100-10	10-1	1-0.1	0.1-0.01
25	0.7	0.9	1	1.5	3
0	0.7	0.9	1	1.2	2
-25	1.1	0.7	0.9	1.2	1.2
-50	1.2	0.5	0.7	0.9	0.9
-75	1.3	0.9	0.7	0.9	0.9

Table D5 Strain (%) used for dynamic frequency sweep experiment of HA12B100

Temperature (^oC)	Frequency Range (rad/s)				
	500-100	100-10	10-1	1-0.1	0.1-0.01
25	2	1.5	1.7	2	2.5
0	1.2	1	1	1	1.5
-25	0.8	0.8	0.8	1	1.5
-50	1	1	1	1.5	2.5
-75	0.5	0.5	1	1	1.5

Table D6 Strain (%) used for dynamic frequency sweep experiment of HA30B40

Temperature (^oC)	Frequency Range (rad/s)				
	500-100	100-10	10-1	1-0.1	0.1-0.01
25	0.5	1	1	1.5	1.5
0	0.5	0.7	1	1.3	1.3
-25	0.5	0.7	1	1.3	1.3
-50	0.5	0.7	1	1	1
-75	0.9	0.7	0.5	0.7	0.7

Table D7 Strain (%) used for dynamic frequency sweep experiment of HA40B40

Temperature (^oC)	Frequency Range (rad/s)				
	500-100	100-10	10-1	1-0.1	0.1-0.01
25	0.7	0.5	0.8	1	1.3
0	0.8	0.8	1	1.3	1.3
-25	0.9	1	1	1.2	1.2
-50	0.9	0.7	0.9	0.9	0.9
-75	1.3	1.1	0.9	0.9	1.1

II. Dynamic frequency sweep test

Figs. D1 to D7 shown the dynamic modulus measured by dynamic frequency sweep test at various test temperatures. Experimental details can be found in section 4.5.2.3.

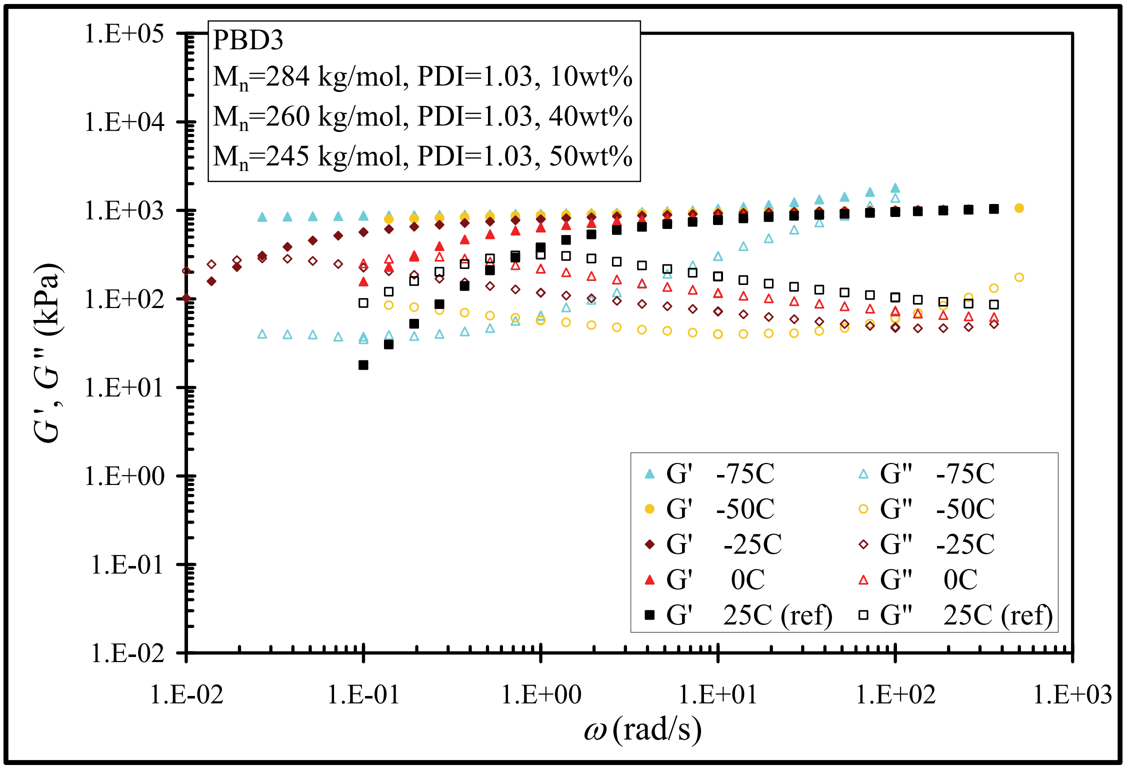

Figure D1 Storage and loss moduli of PBD3 measured at temperature between 25°C and 75°C

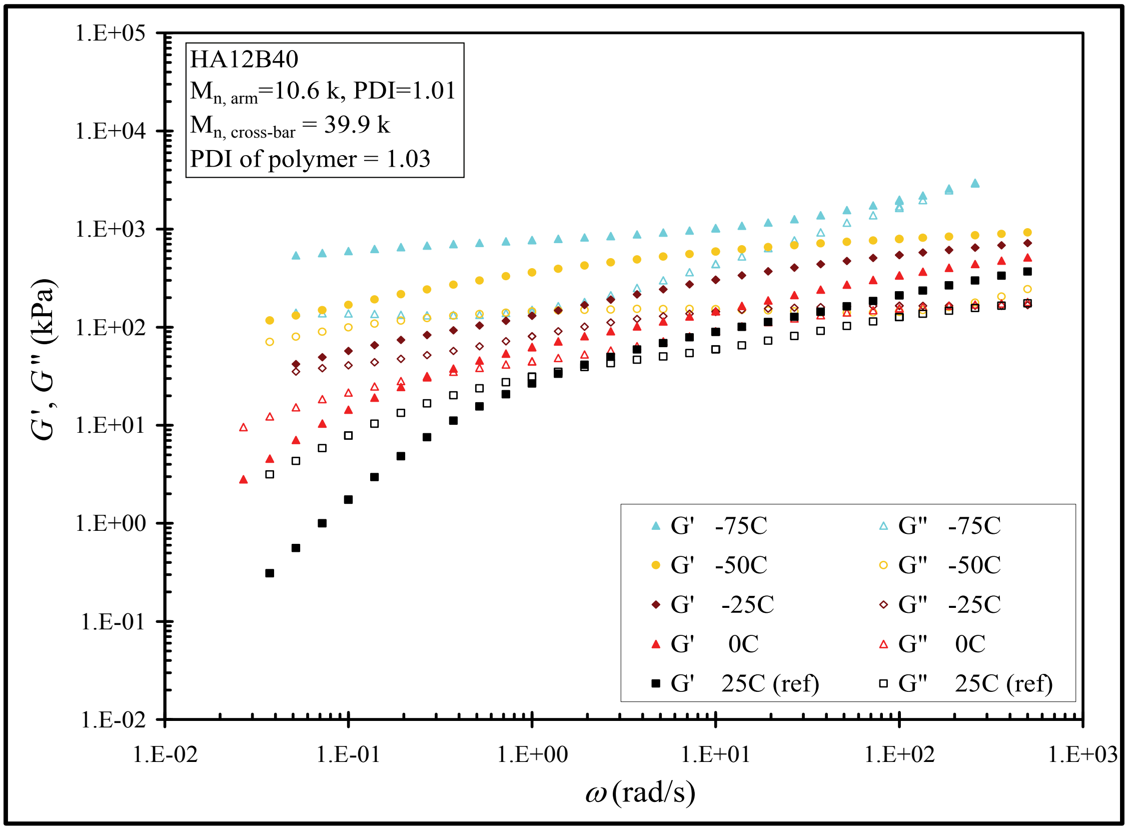

Figure D2 Storage and loss moduli of HA12B40 measured at temperatures between 25°C and 75°C

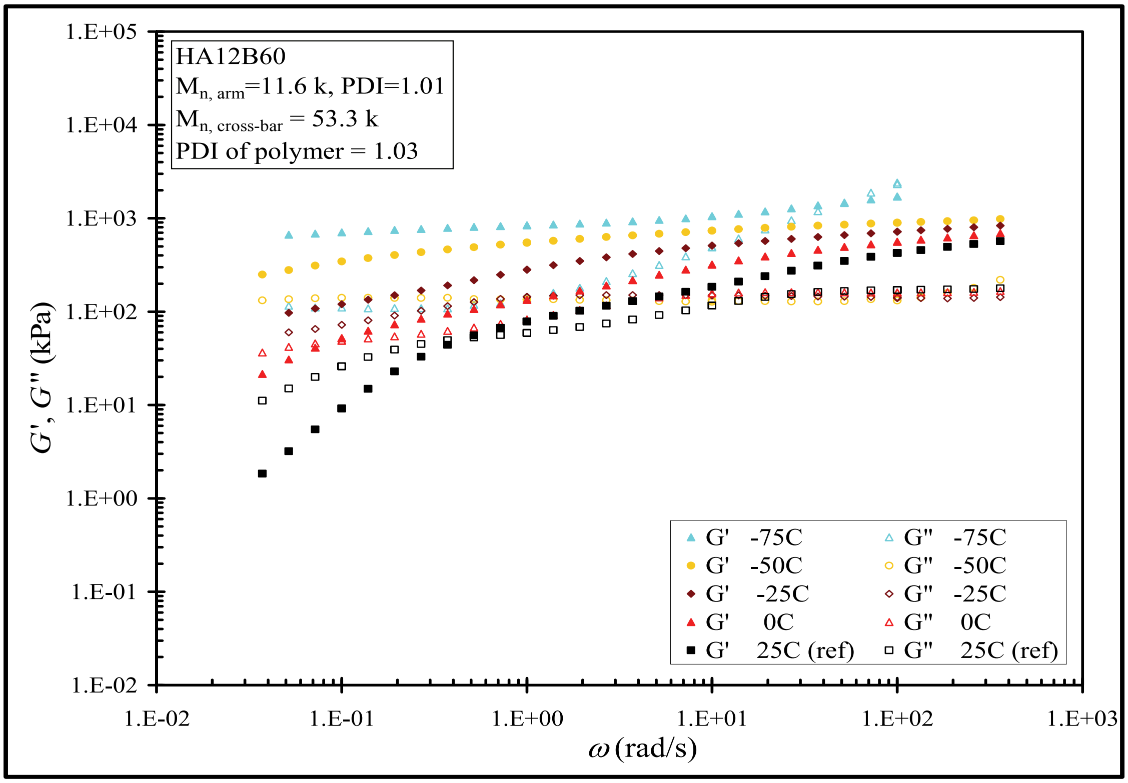

Figure D3 Storage and loss moduli of HA12B60 measured at temperatures between 25°C and 75°C

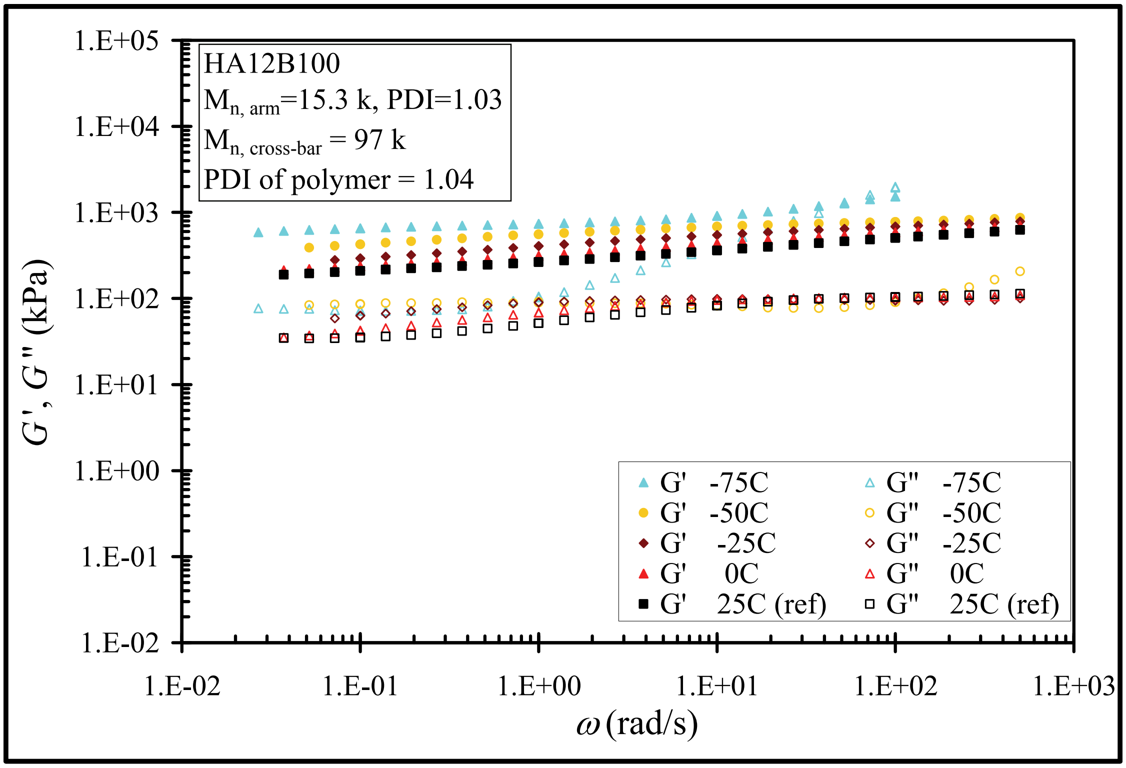

Figure D4 Storage and loss moduli of HA12B100 measured at temperatures between 25°C and 75°C

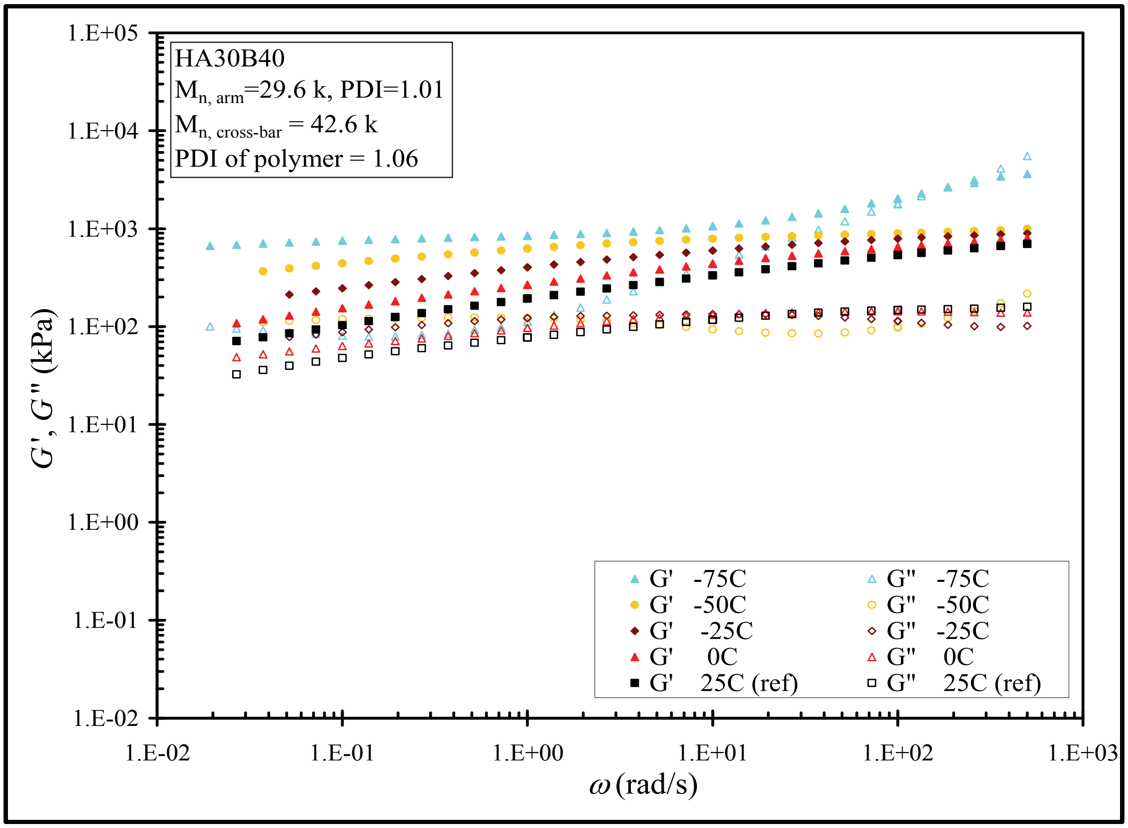

Figure D5 Storage and loss moduli of HA30B40 measured at temperatures between 25°C to -75°C

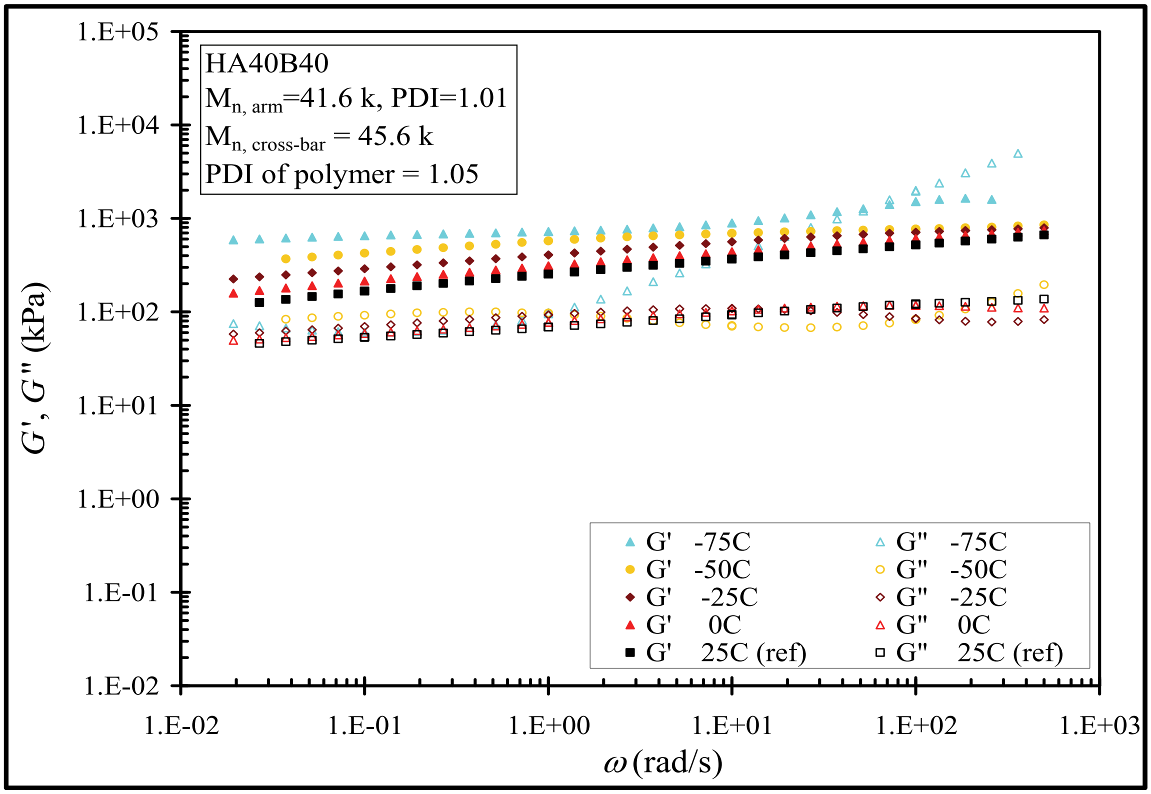

Figure D6 Storage and loss moduli of HA40B40 measured at temperatures between 25°C and 75°C

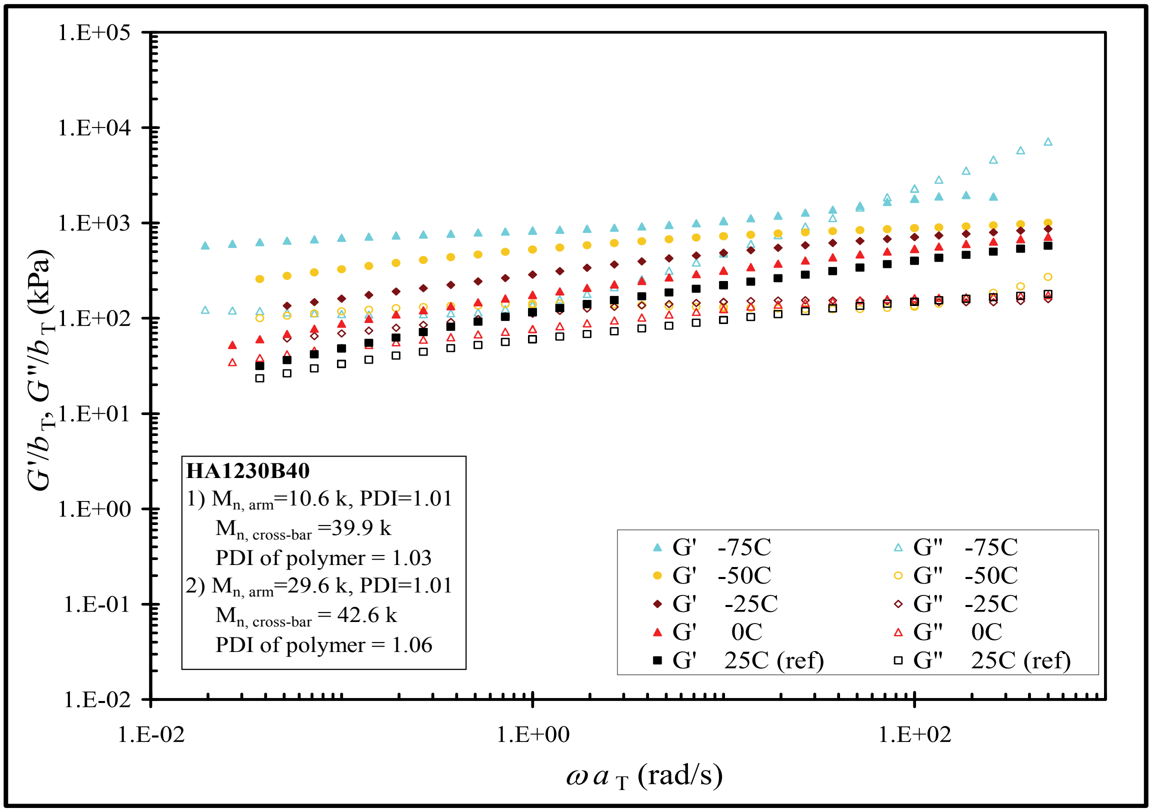

Figure D7 Storage and loss moduli of HA1230B40 measured at temperatures between 25°C and 75°C

III. Linearity of applied stress on creep compliance

Preliminary creep tests on various applied stresses and creep time were performed in order to identify the optimum stress and creep time that are still within LVE region. For creep recovery experiment, this linearity response is shown in Figs. D8 to D14.

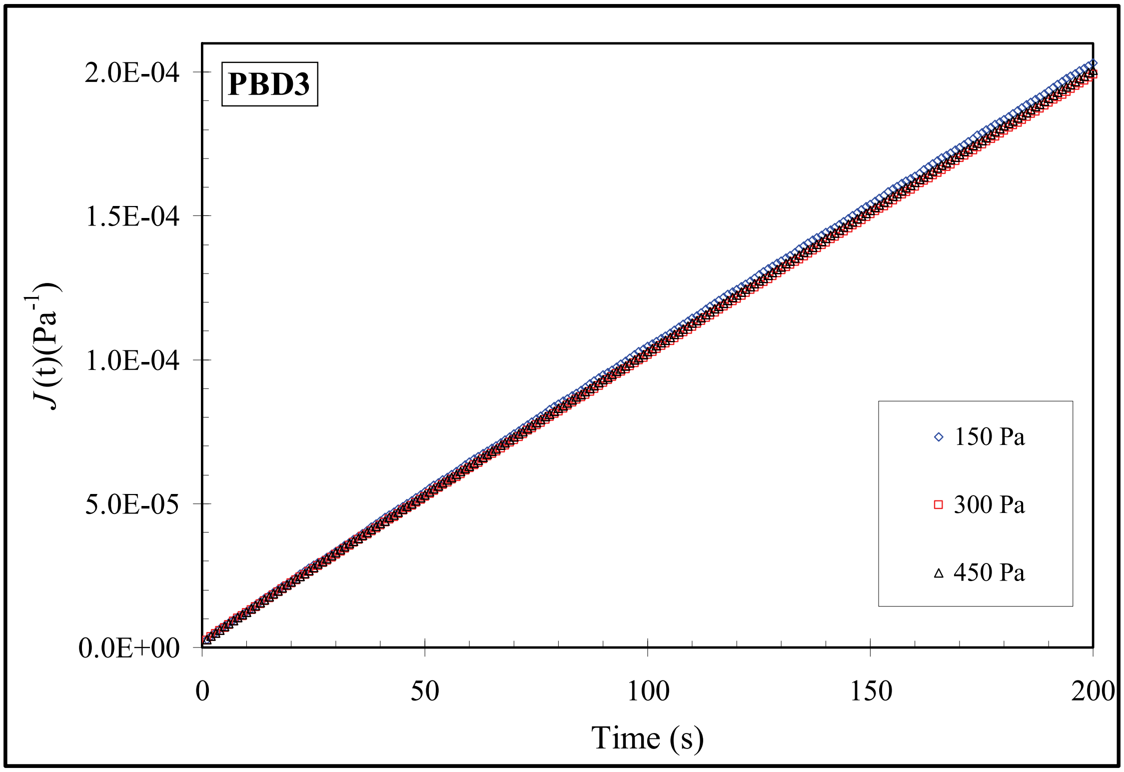

Figure D8 Creep compliance of PBD3 at various applied stresses in 200s creep time (25^{o}C)

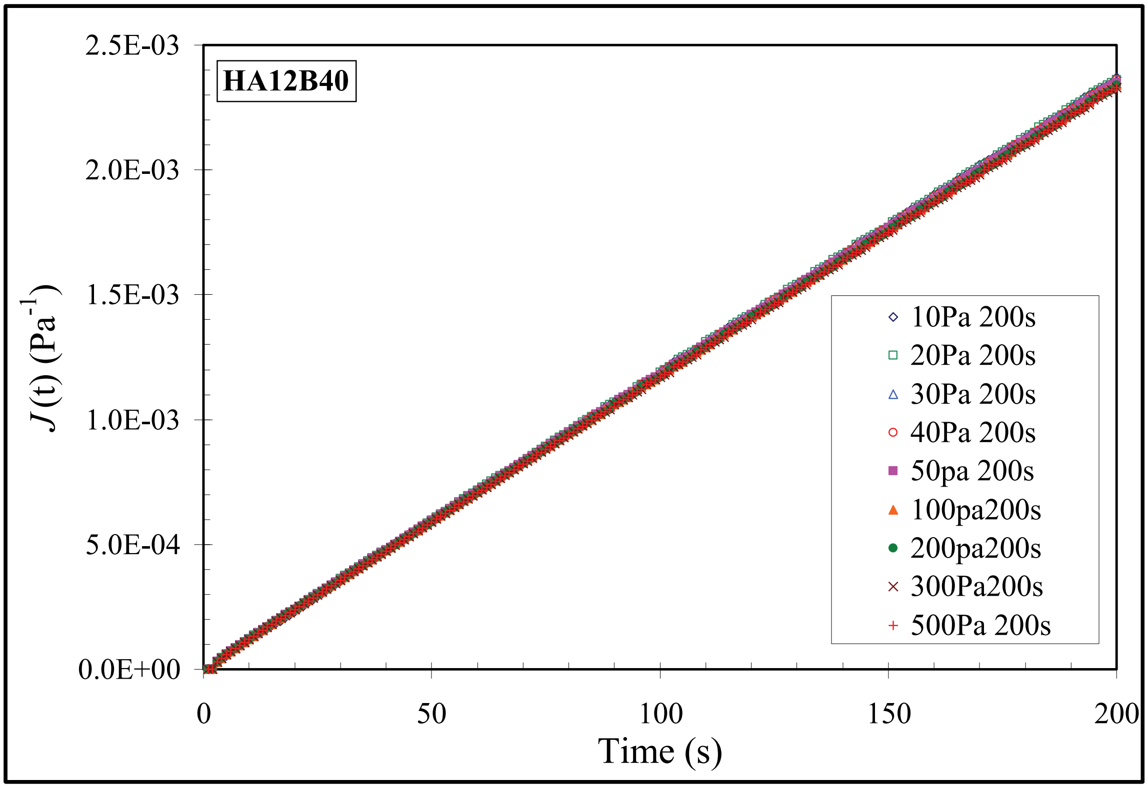

Figure D9 Creep compliance of HA12B40 at various applied stresses in 200s creep time (25^{o}C)

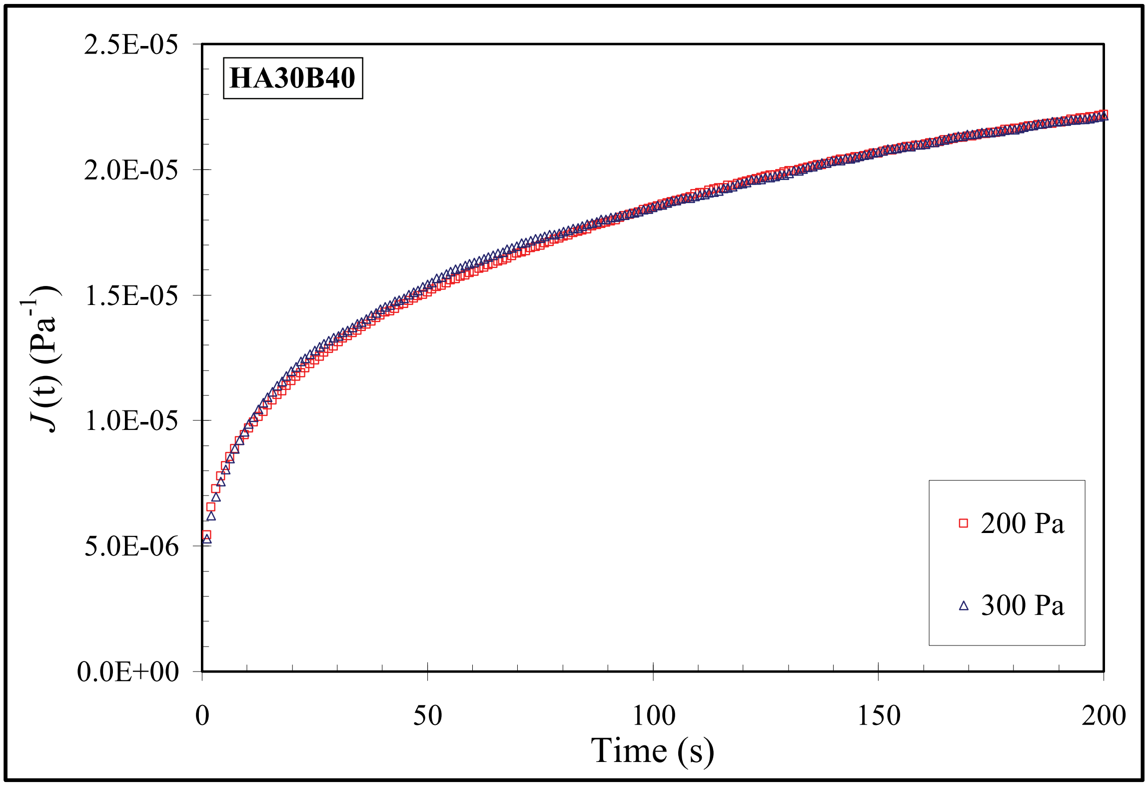

Figure D10 Creep compliance of HA30B40 at various applied stresses in 200s creep time (25^{o}C)

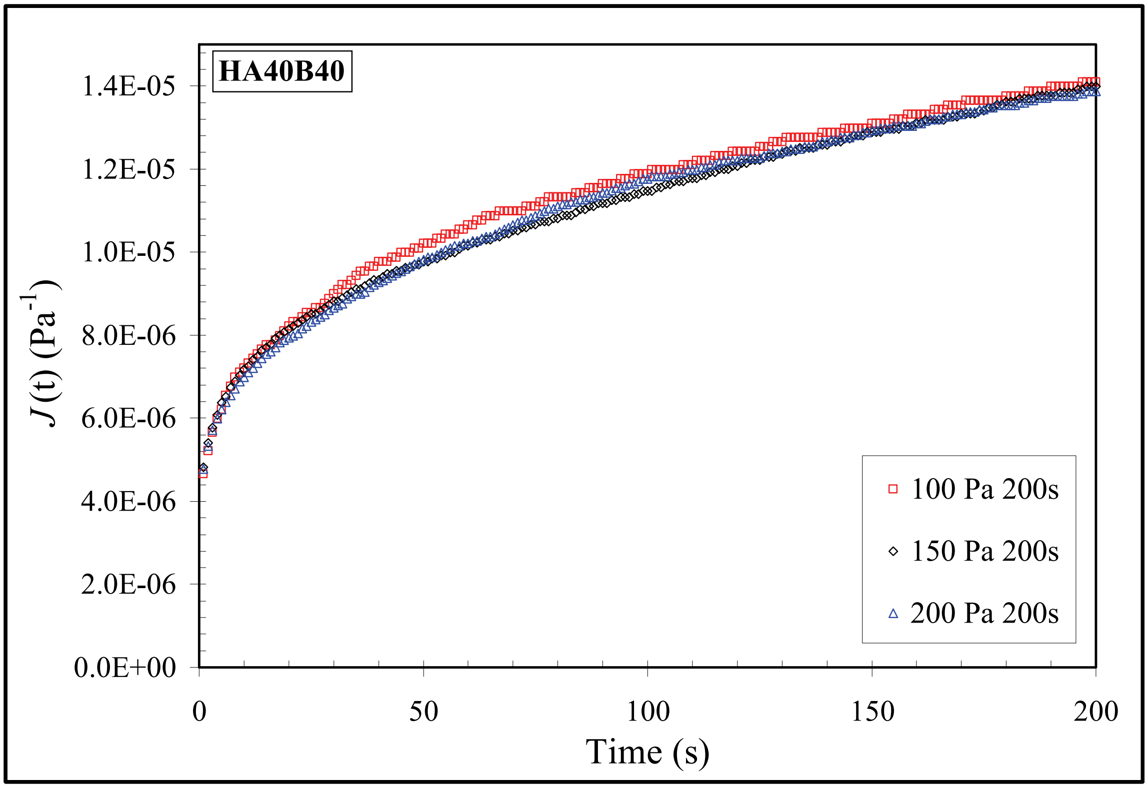

Figure D11 Creep compliance of HA40B40 at various applied stresses in 200s creep time (25^{o}C)

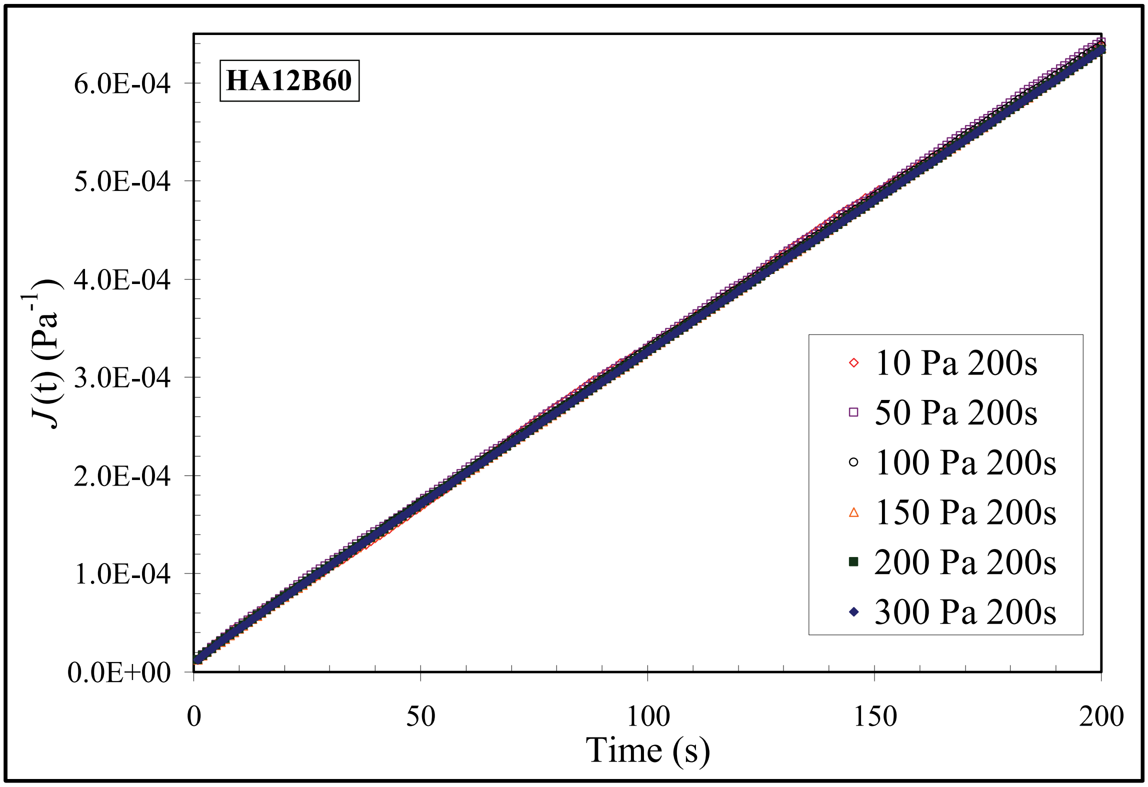

Figure D12 Creep compliance of HA12B60 at various applied stresses in 200s creep time (25^{o}C)

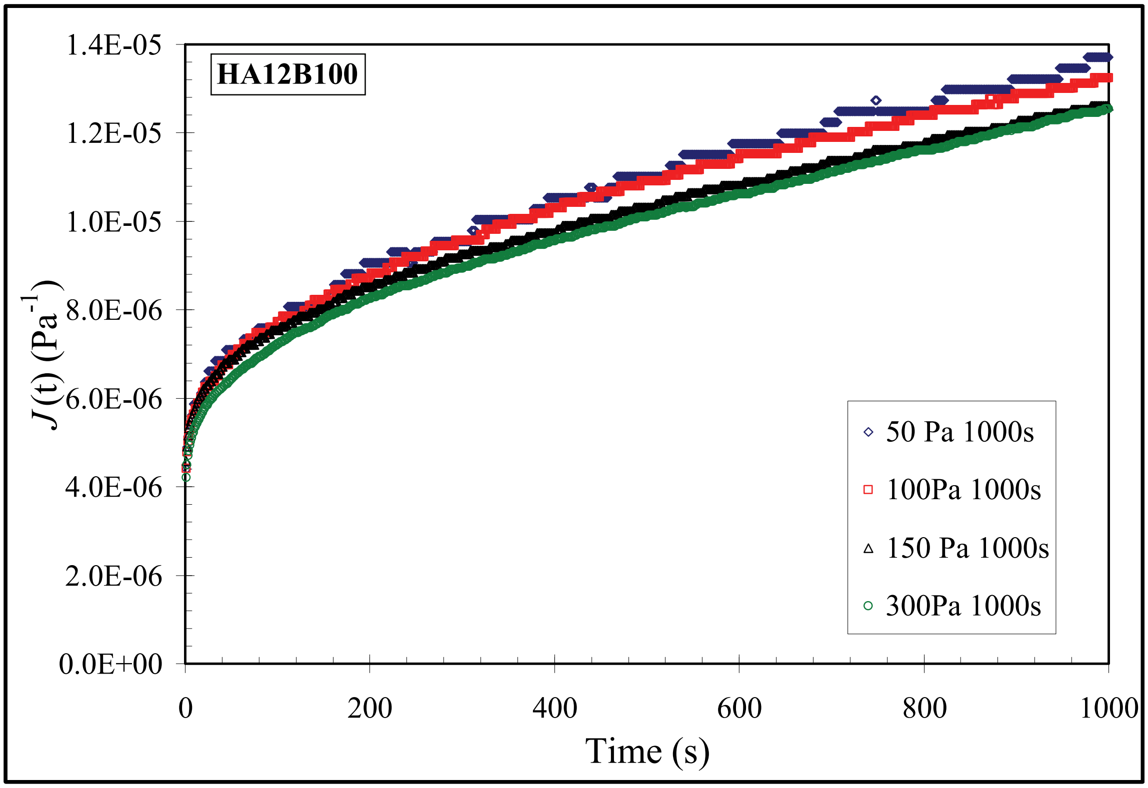

Figure D13 Creep compliance of HA12B100 at various applied stresses in 1000s creep time (25^{o}C)

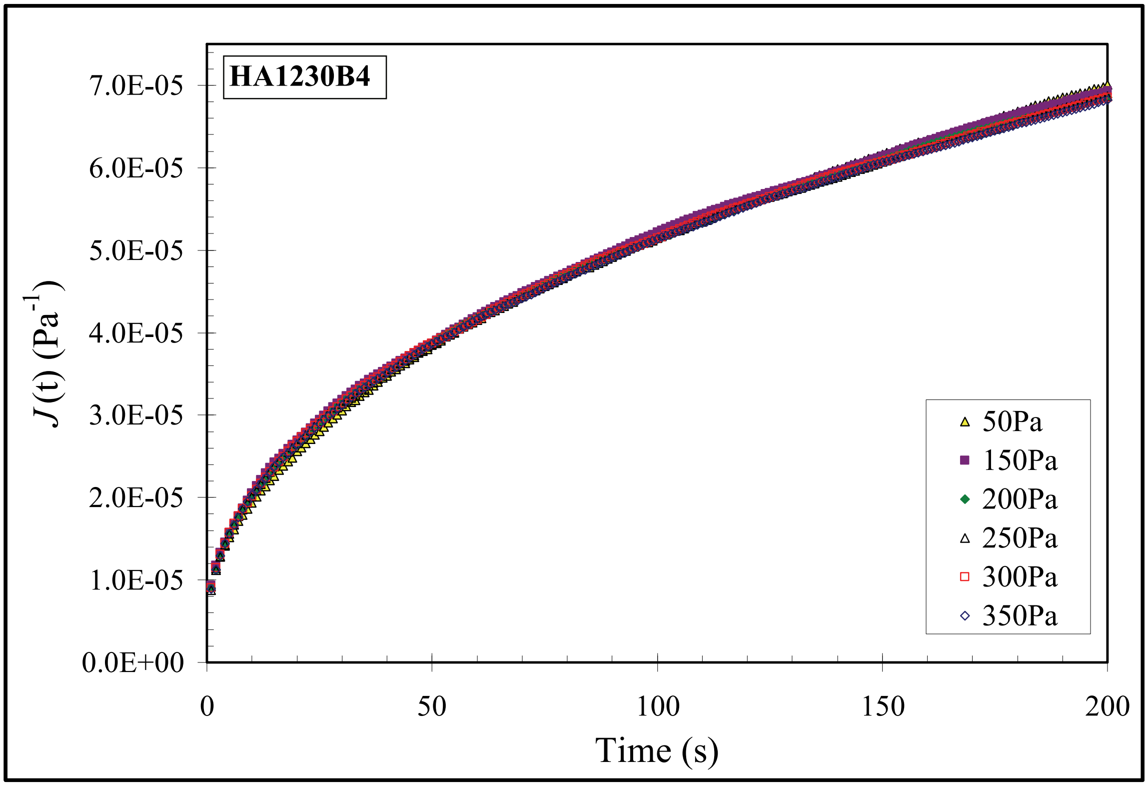

Figure D14 Creep compliance of HA1230B100 at various applied stresses in 1000s creep time (25^{o}C)

Similar studies were done on HA12B40 and HA40B40 to identify the optimum stress and creep time for creep only experiment. Results are shown in Figs. D15 and D16.

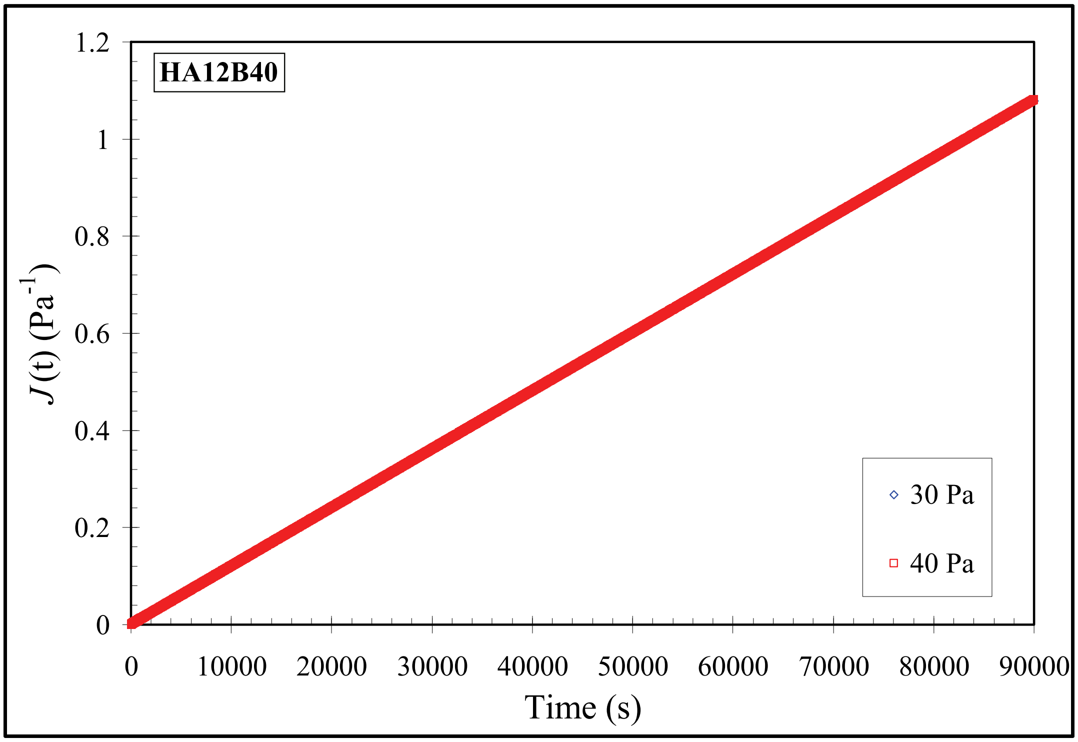

Figure D15 Creep compliance of HA12B40 at various applied stresses in 25 hrs creep time (25^{o}C)

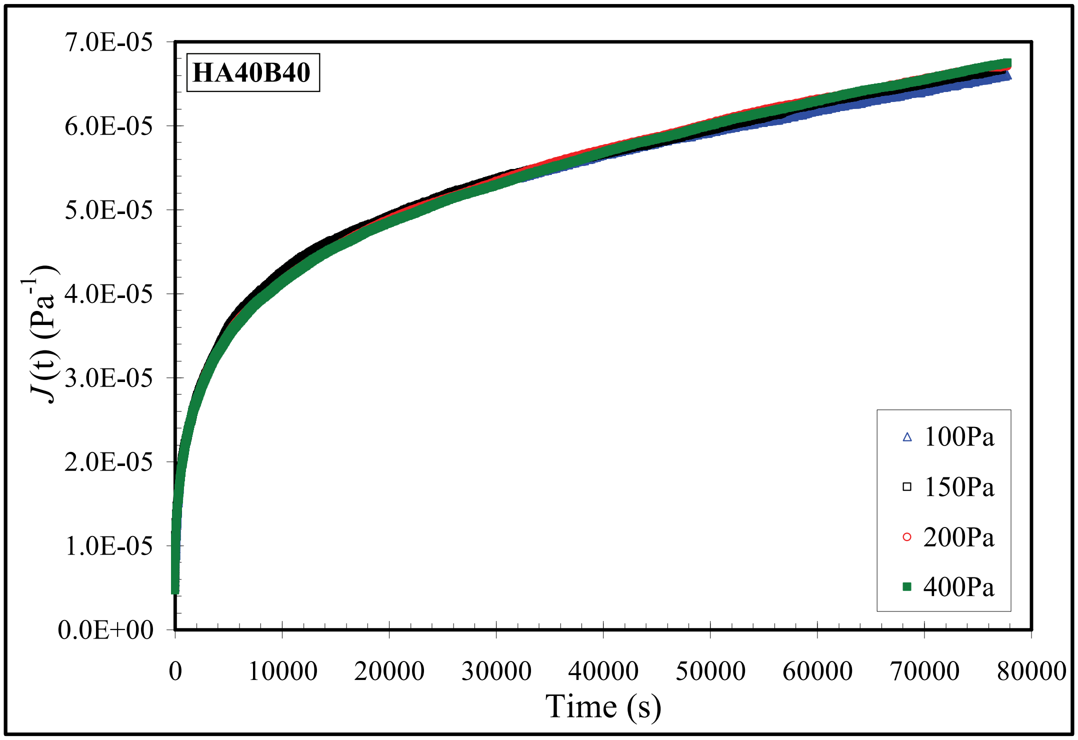

Figure D16 Creep compliance of HA40B40 at various applied stresses in 22 hrs creep time (25^{o}C)

IV. Strain and creep compliance curves from creep/recovery experiment

Figures D17 to D23 are the strain and composite creep compliance curves measured in a creep/recovery experiment. Experimental details can be found in section 4.4.3.2.

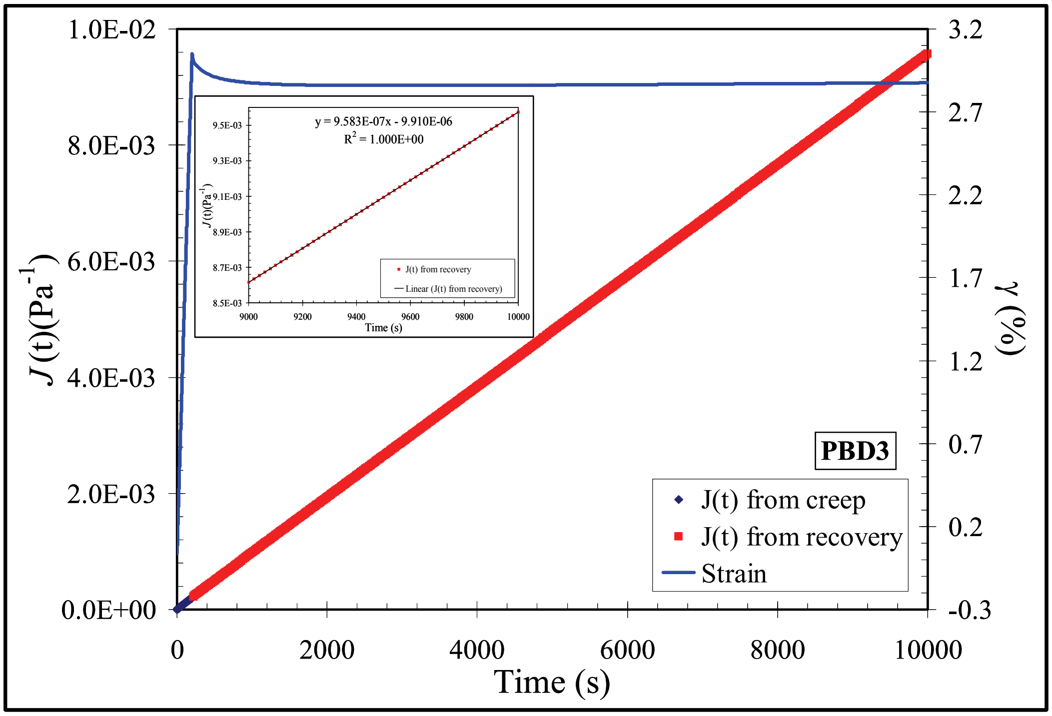

Figure D17 Strain and creep compliance as a function of time for PBD3 at 150 Pa, 25°C.

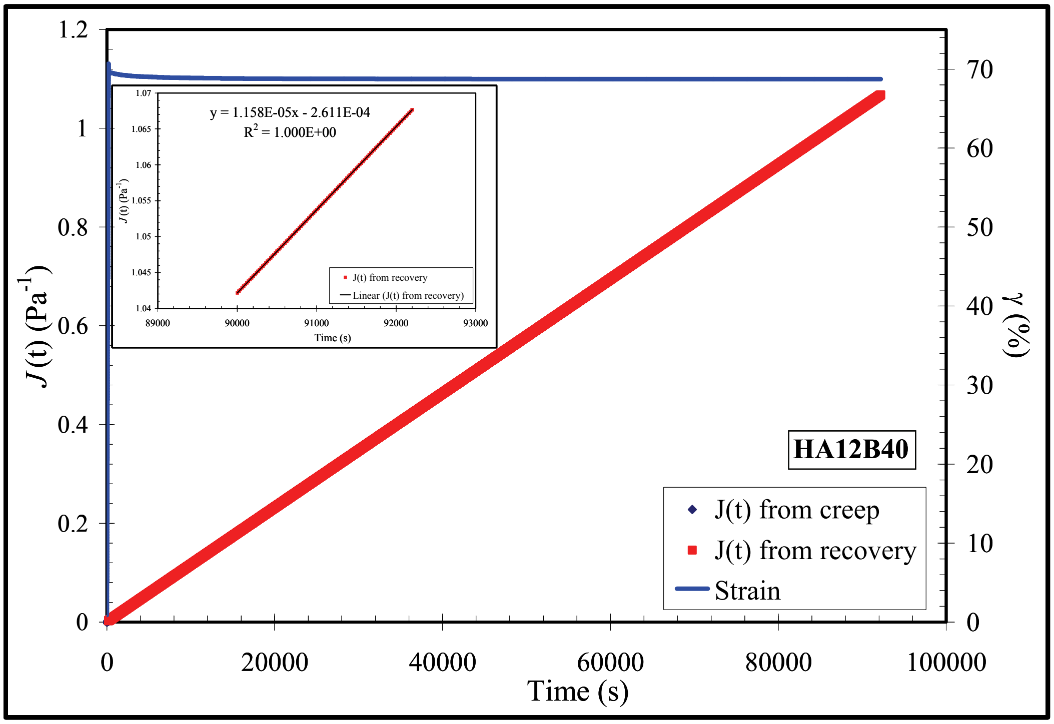

Figure D18 Strain and creep compliance as a function of time for HA12B40 at 300 Pa, 25°C.

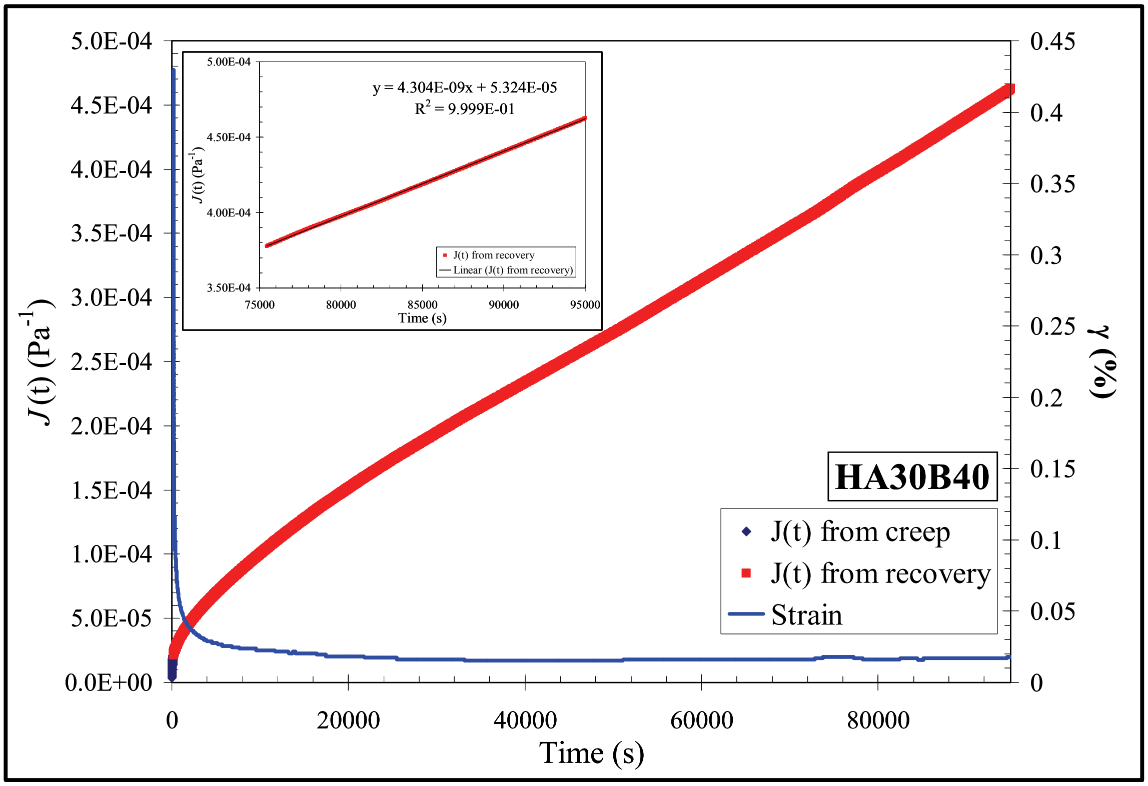

Figure D19 Strain and creep compliance as a function of time for HA30B40 at 200 Pa, 25°C.

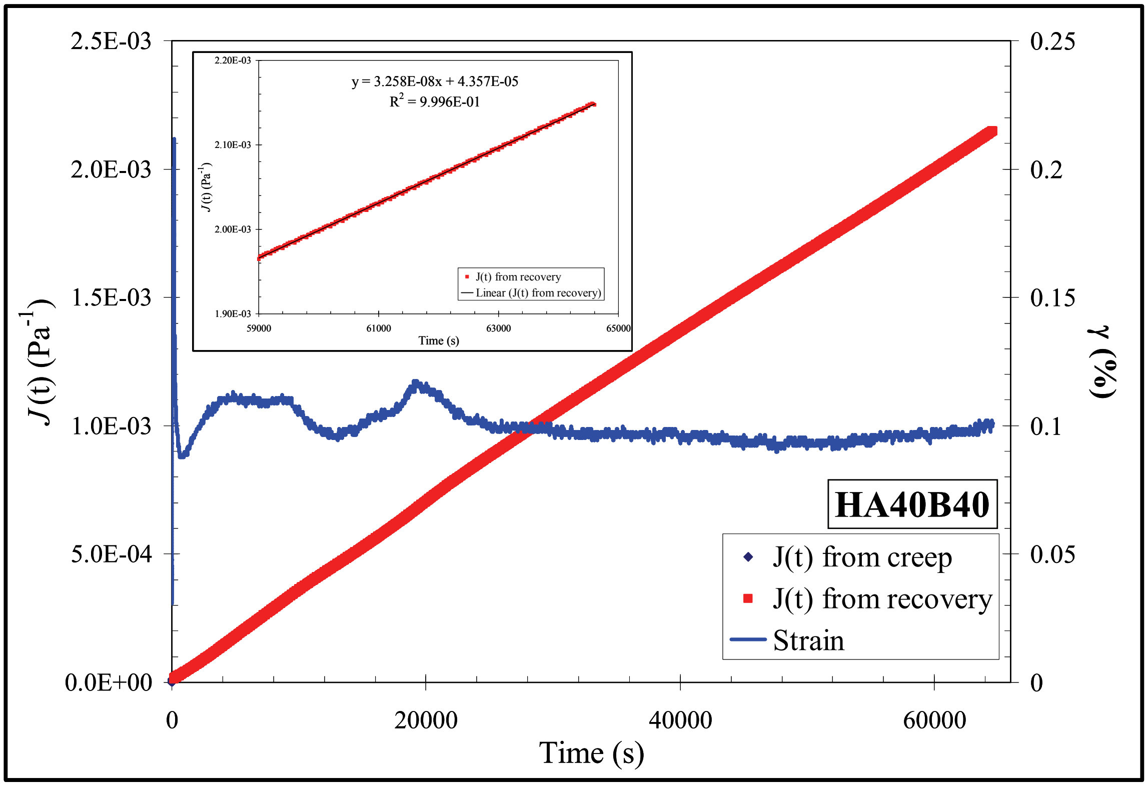

Figure D20 Strain and creep compliance as a function of time for HA40B40 at 150 Pa, 25°C.

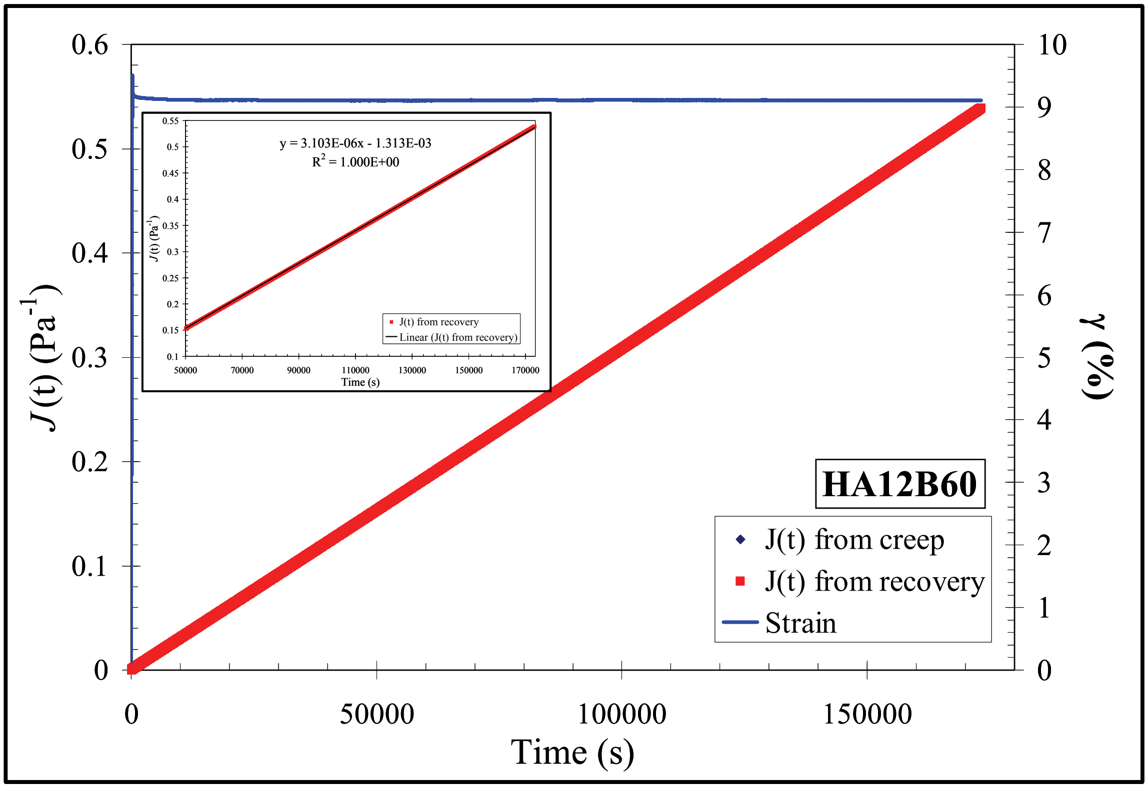

Figure D21 Strain and creep compliance as a function of time for HA12B60 at 150 Pa, 25°C.

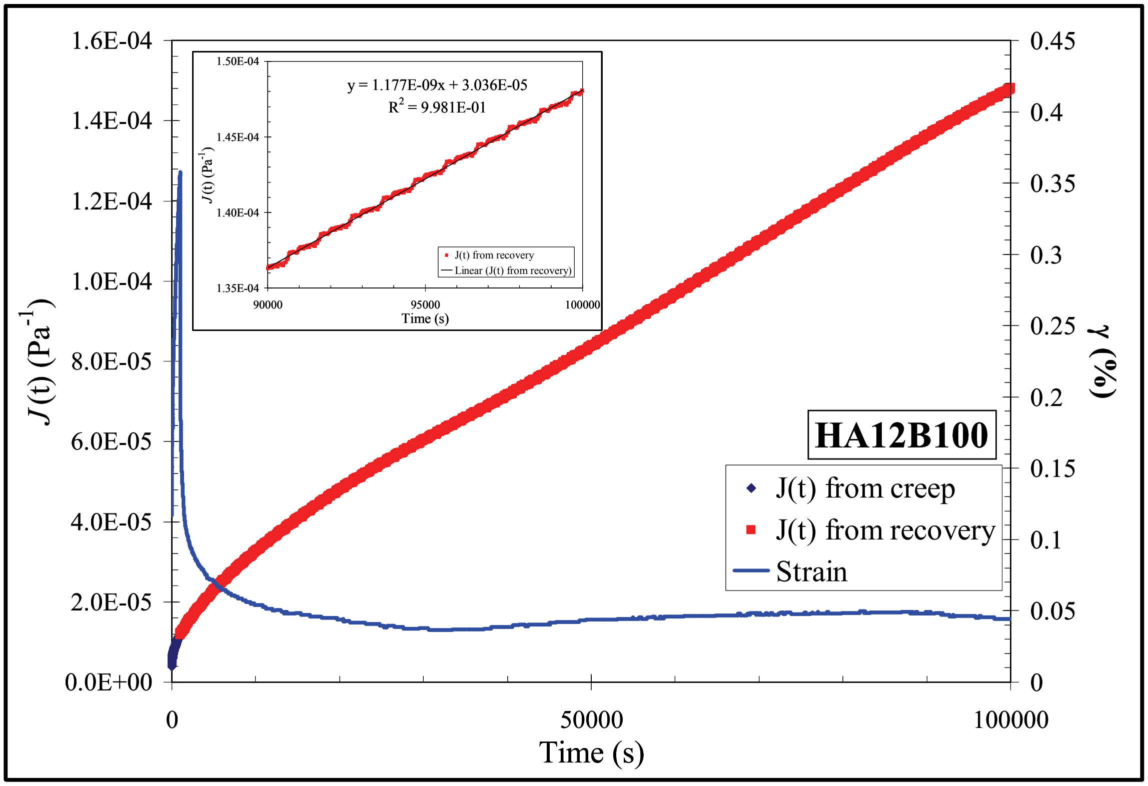

Figure D22 Strain and creep compliance as a function of time for HA12B100 at 300 Pa, 25°C.

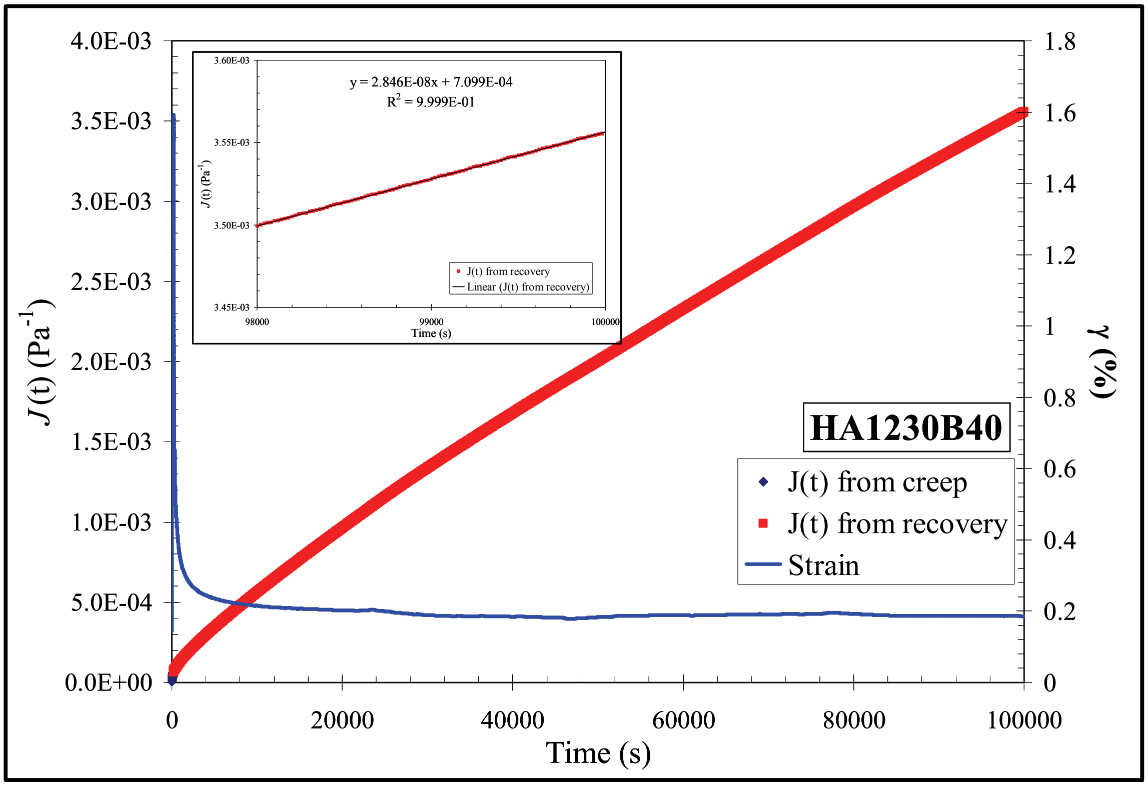

Figure D23 Strain and creep compliance as a function of time for HA1230B40 at 250 Pa, 25°C.

V. Recoverable compliance curve from creep recovery experiment

Figures D24 to D29 are the recoverable compliance curves measured in a creep recovery experiment. Experimental details can be found in section 4.4.3.3.

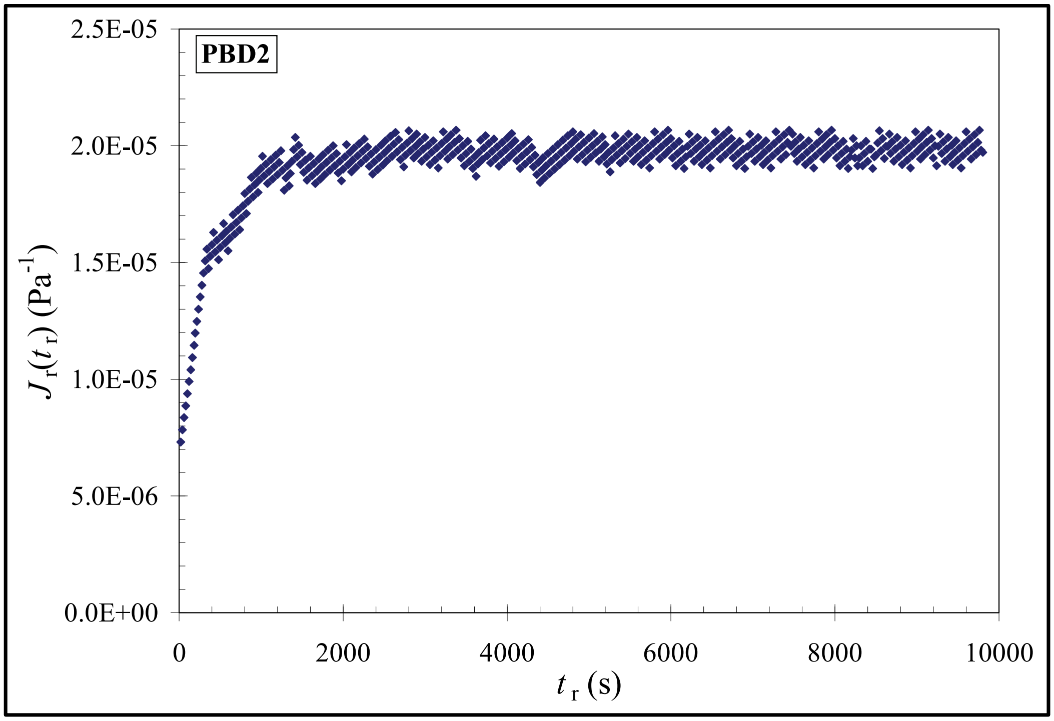

Figure D24 Recoverable compliance of PBD2

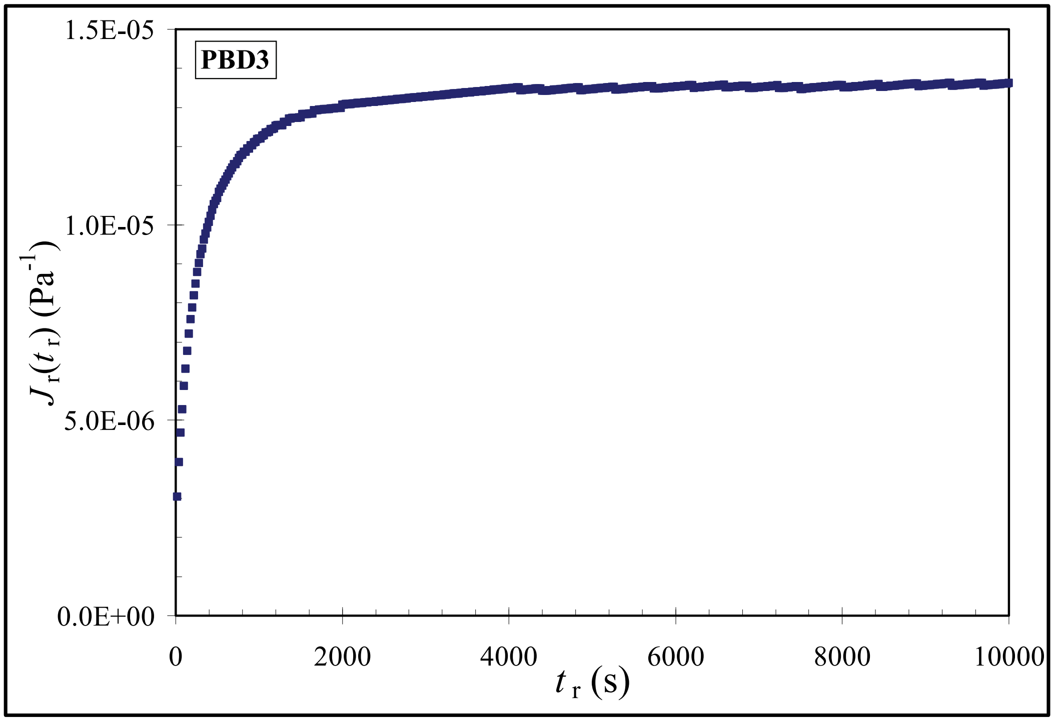

Figure D25 Recoverable compliance of PBD3

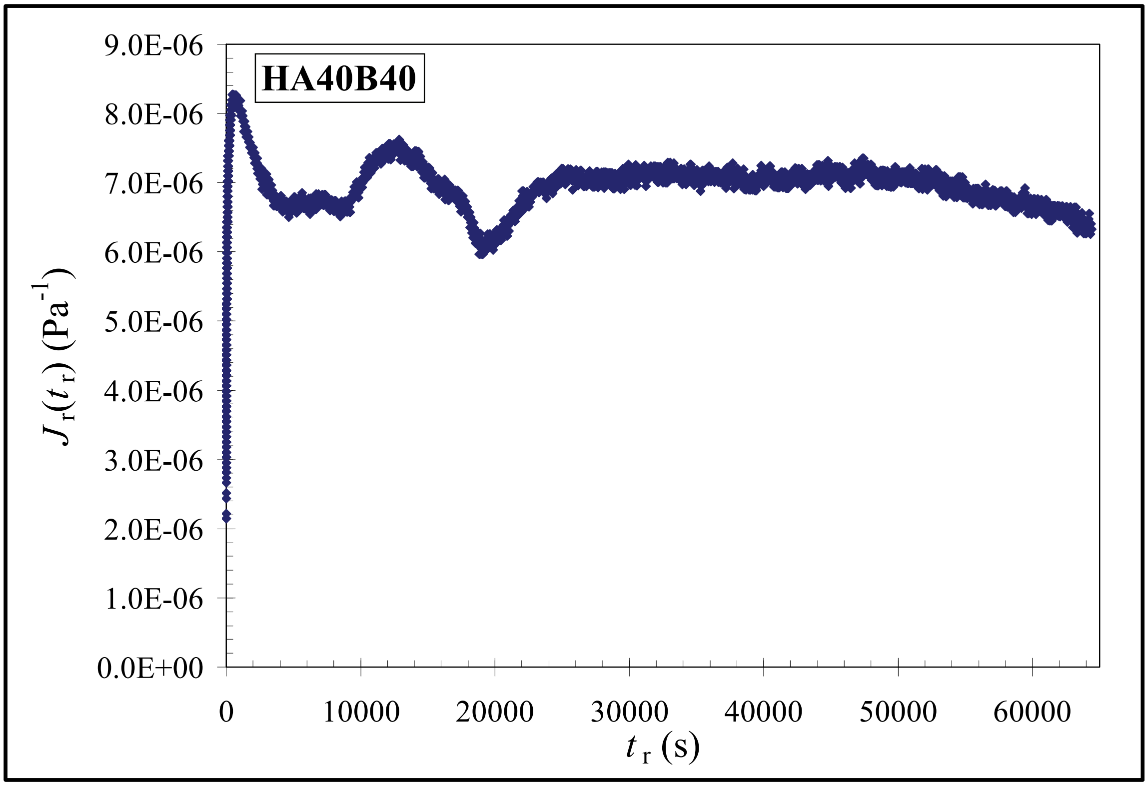

Figure D26 Recoverable compliance of HA40B40

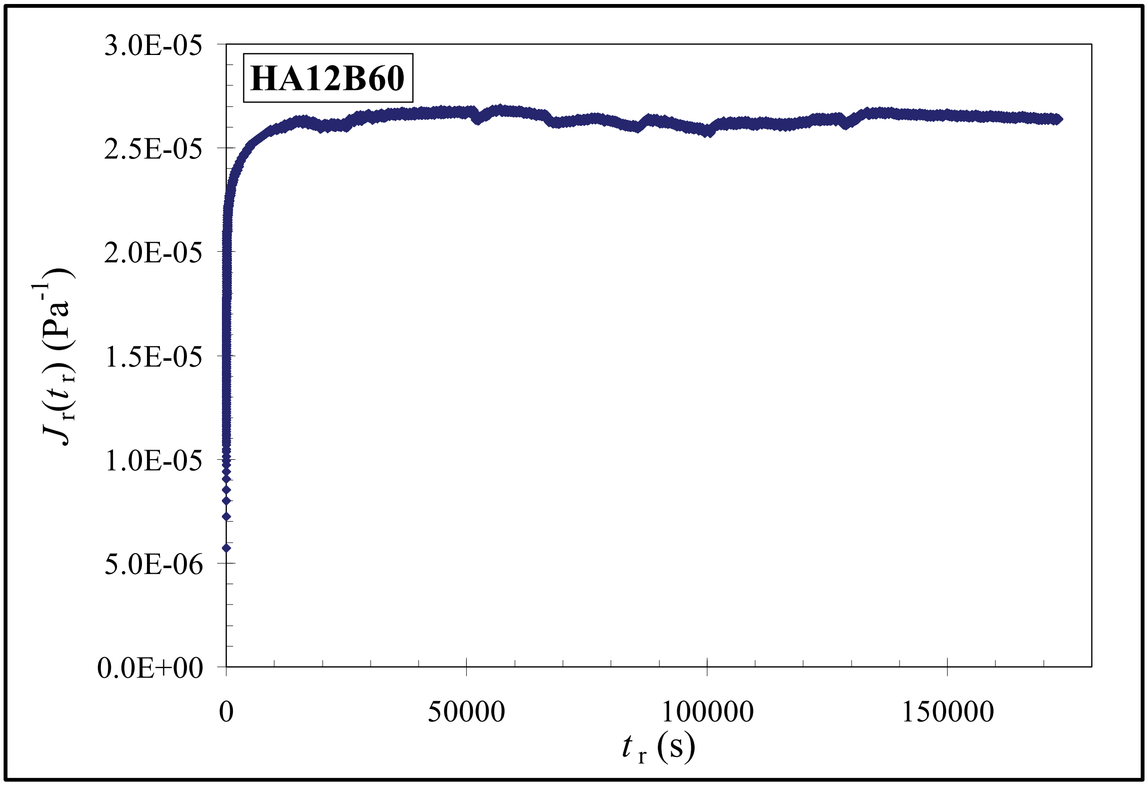

Figure D27 Recoverable compliance of HA12B60

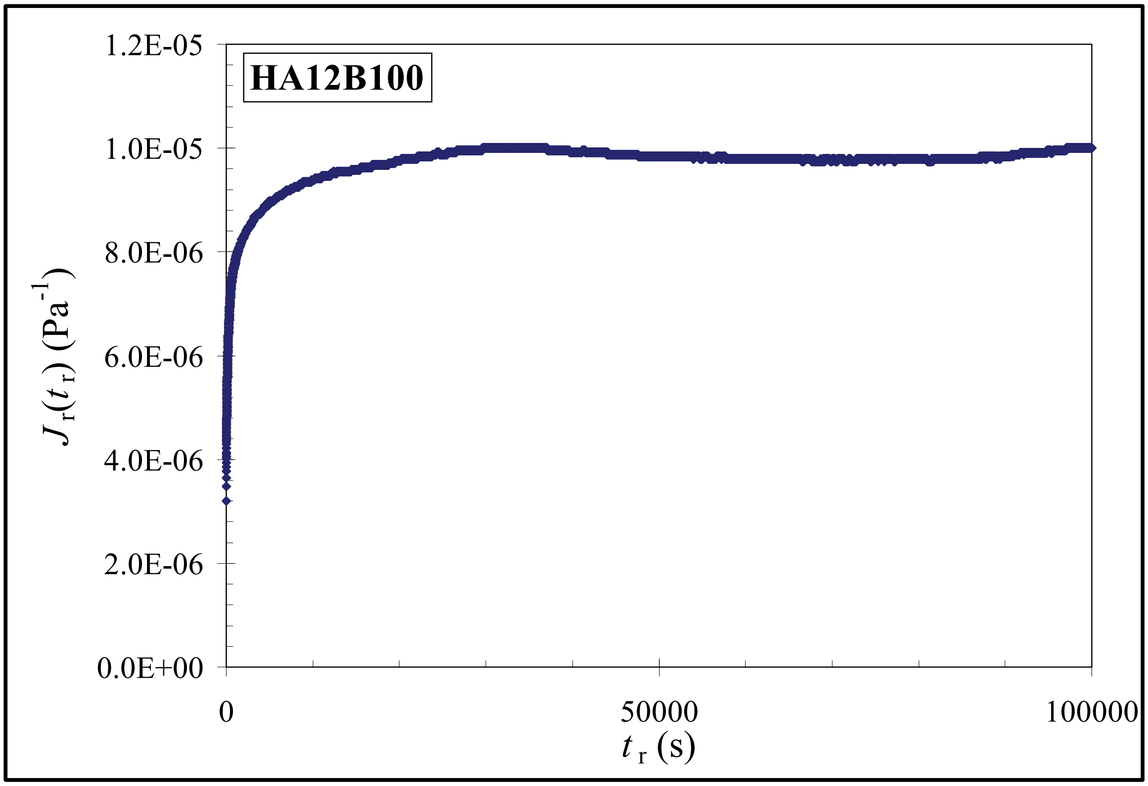

Figure D28 Recoverable compliance of HA12B100

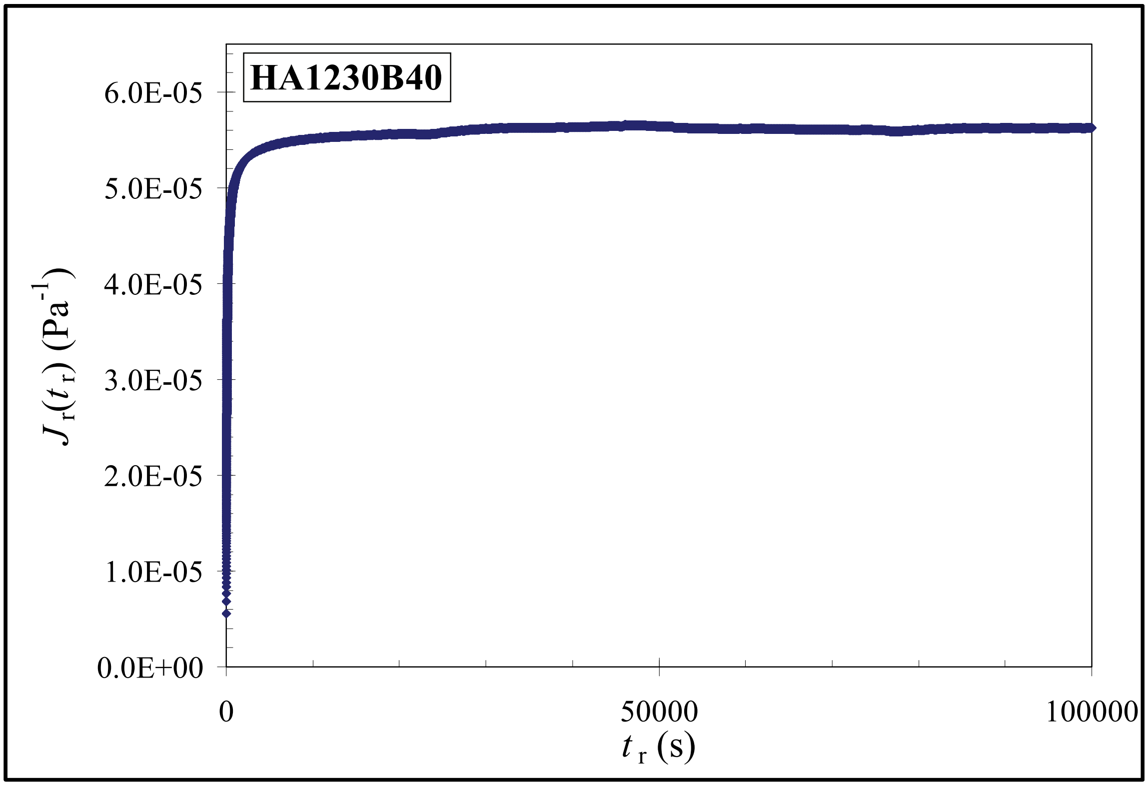

Figure D29 Recoverable compliance of HA1230B40

Appendix E Time Temperature Superposition of Dynamic Data

I. Dynamic modulus shifted to $T_{\mathrm{ref}}=25^{\mathrm{o}}\mathrm{C}$ in log-log scale

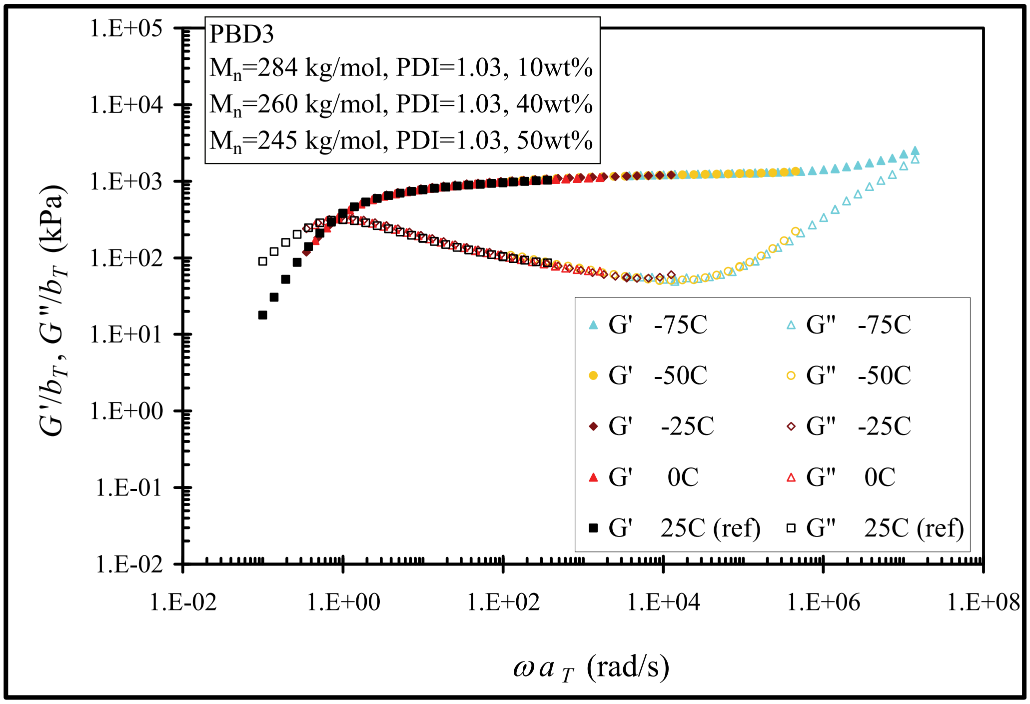

Figure E1 Master curves of storage and loss moduli of PBD3 shifted to $T_{\mathrm{ref}}=25^{\mathrm{o}}\mathrm{C}$

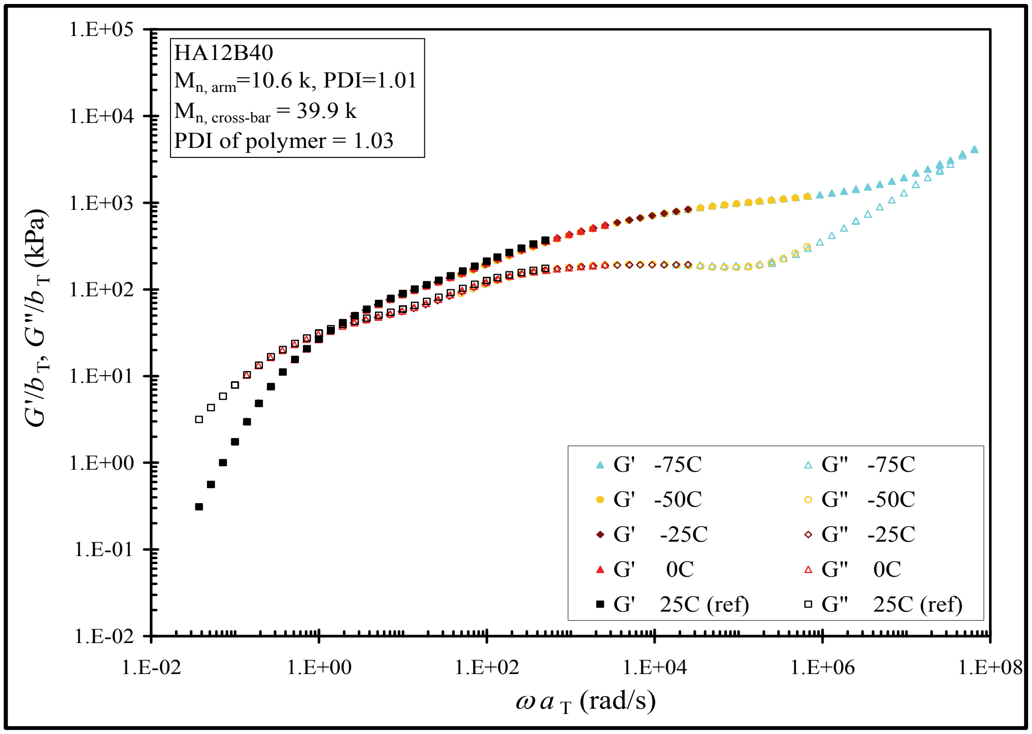

Figure E2 Master curves of storage and loss moduli of HA12B40 shifted to $T_{\mathrm{ref}}=25^{\mathrm{o}}\mathrm{C}$

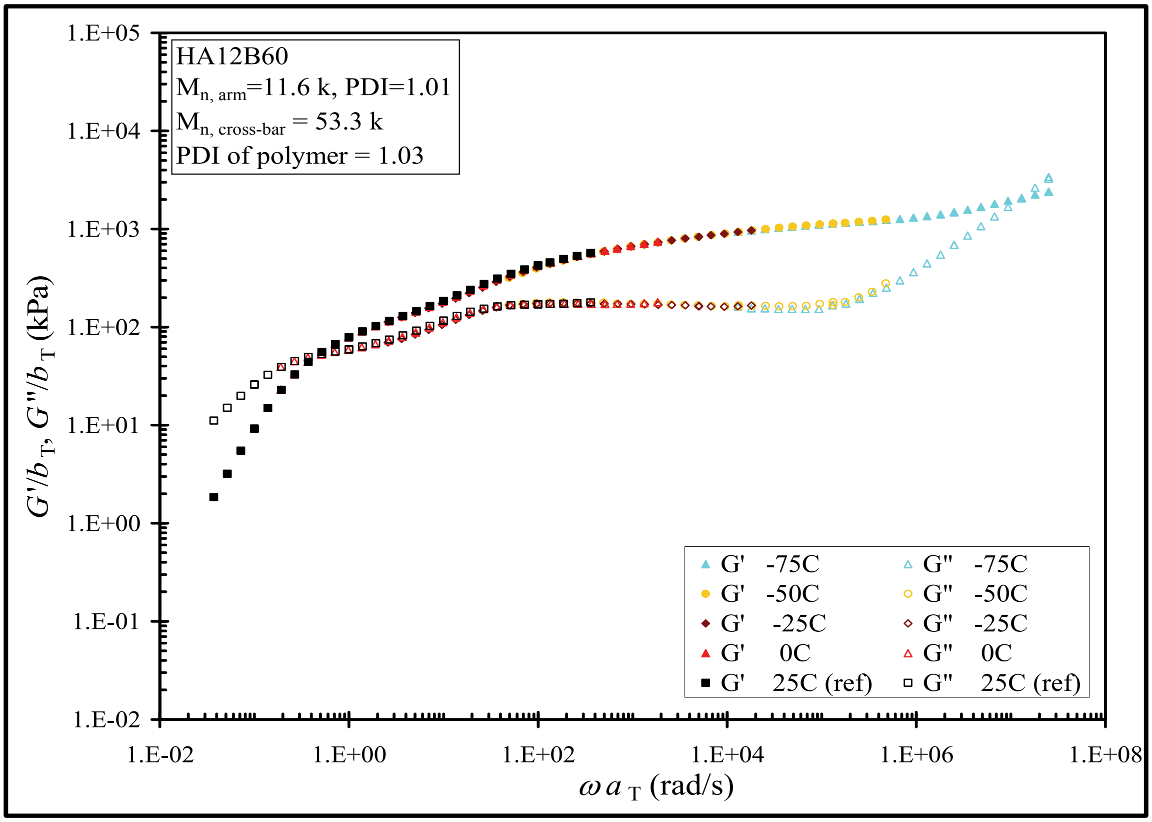

Figure E3 Master curves of storage and loss moduli of HA12B60 shifted to T_{ref}=25^{o}C

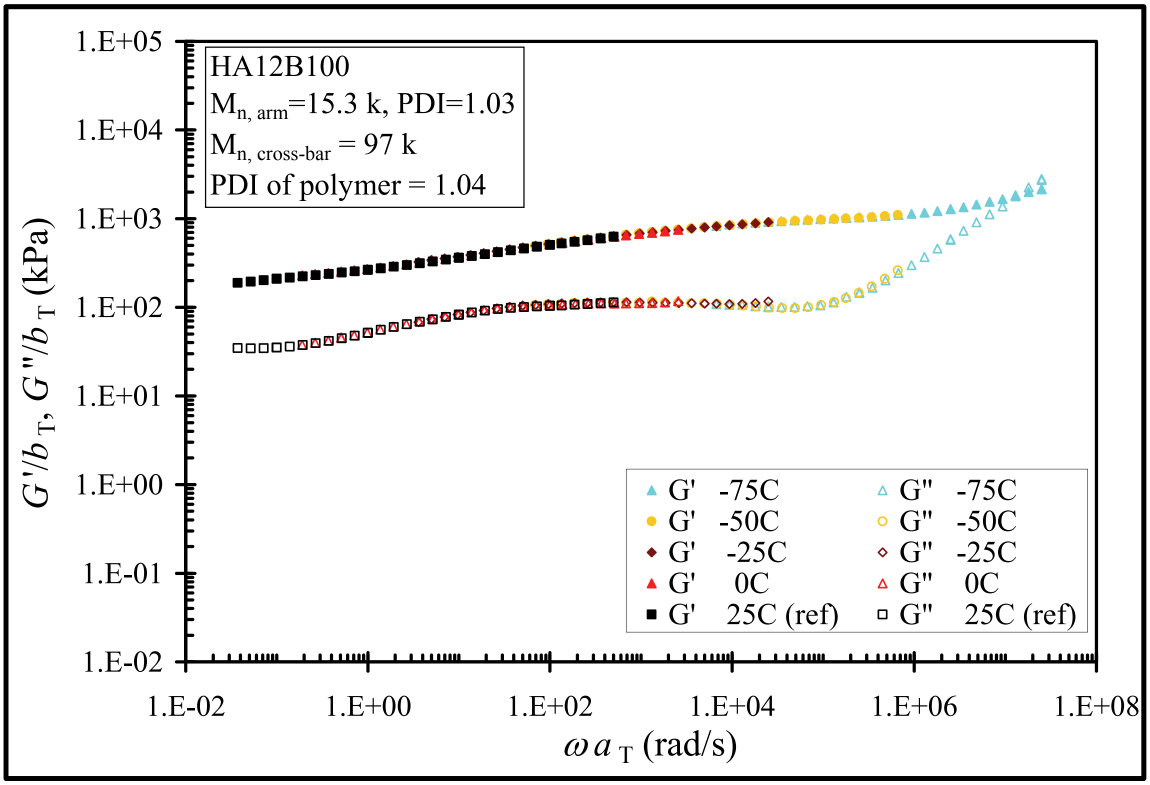

Figure E4 Master curves of storage and loss moduli of HA12B100 shifted to T_{ref}=25^{o}C

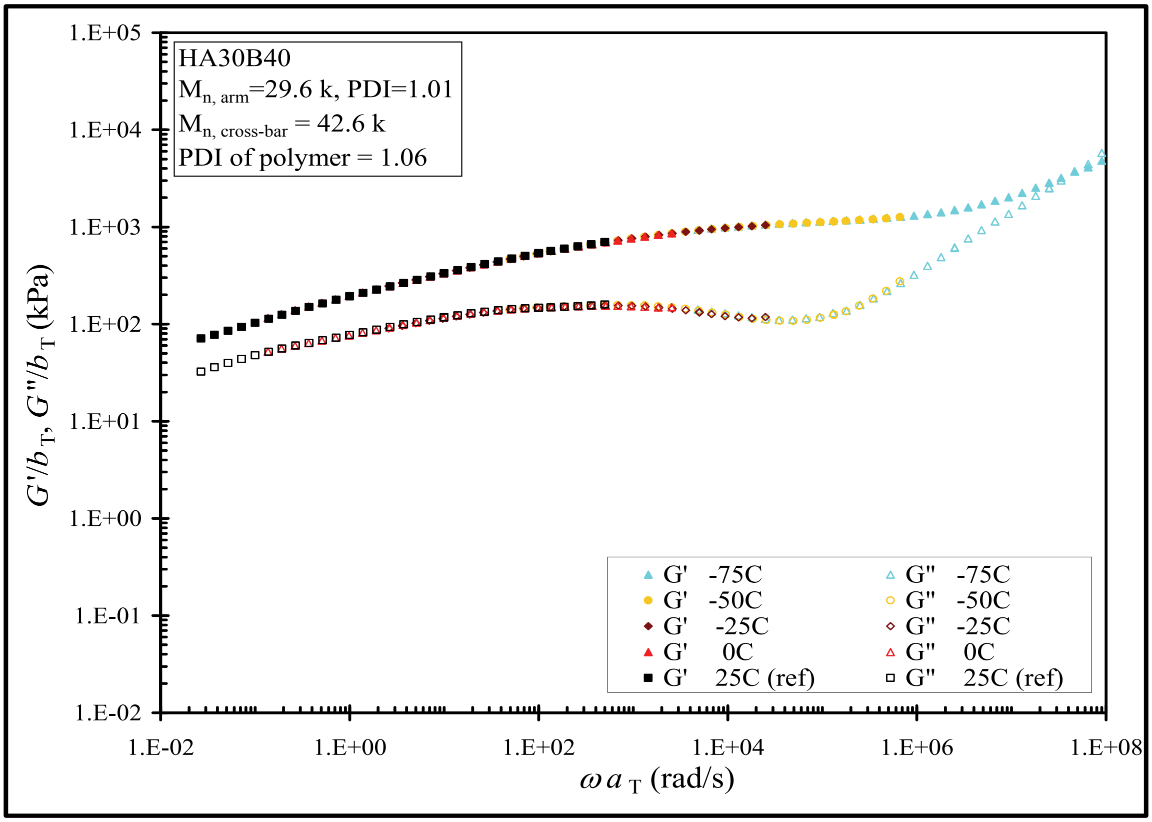

Figure E5 Master curves of storage and loss moduli of HA30B40 shifted to T_{ref}=25^{o}C

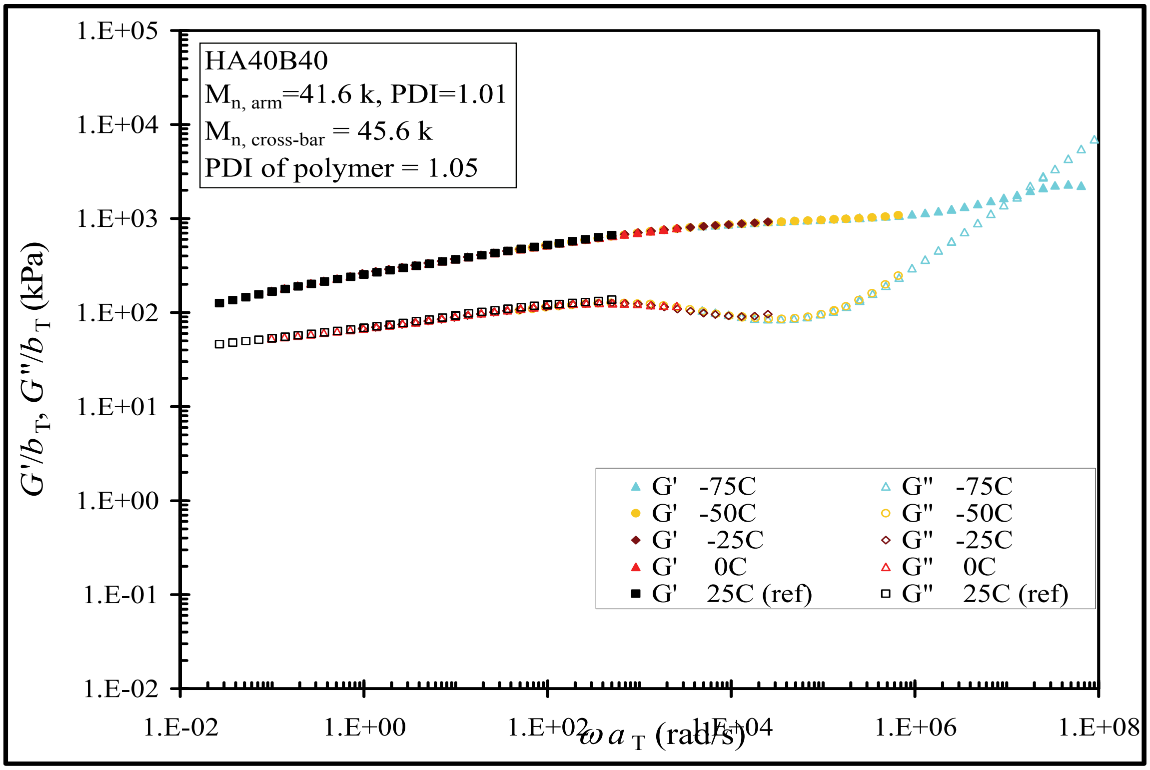

Figure E6 Master curves of storage and loss moduli of HA40B40 shifted to T_{ref}=25^{o}C

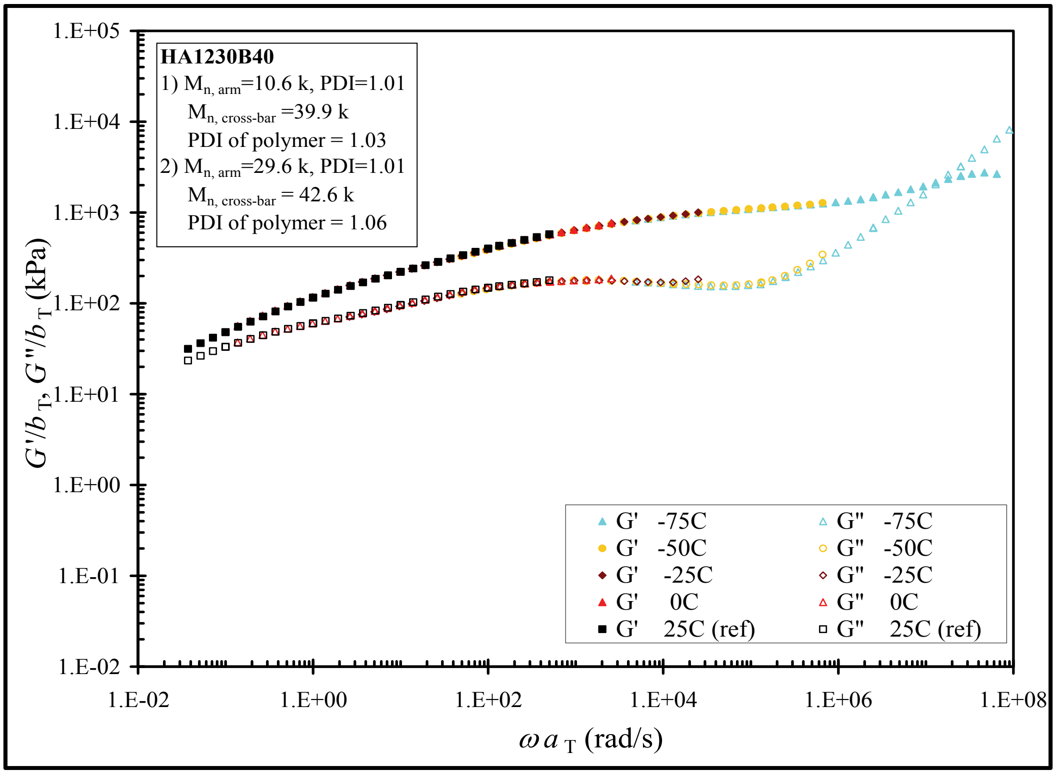

Figure E7 Master curves of storage and loss moduli of HA1230B40 shifted to T_{ref}=25°C

II. Complex viscosity shifted to T_{ref}=25°C

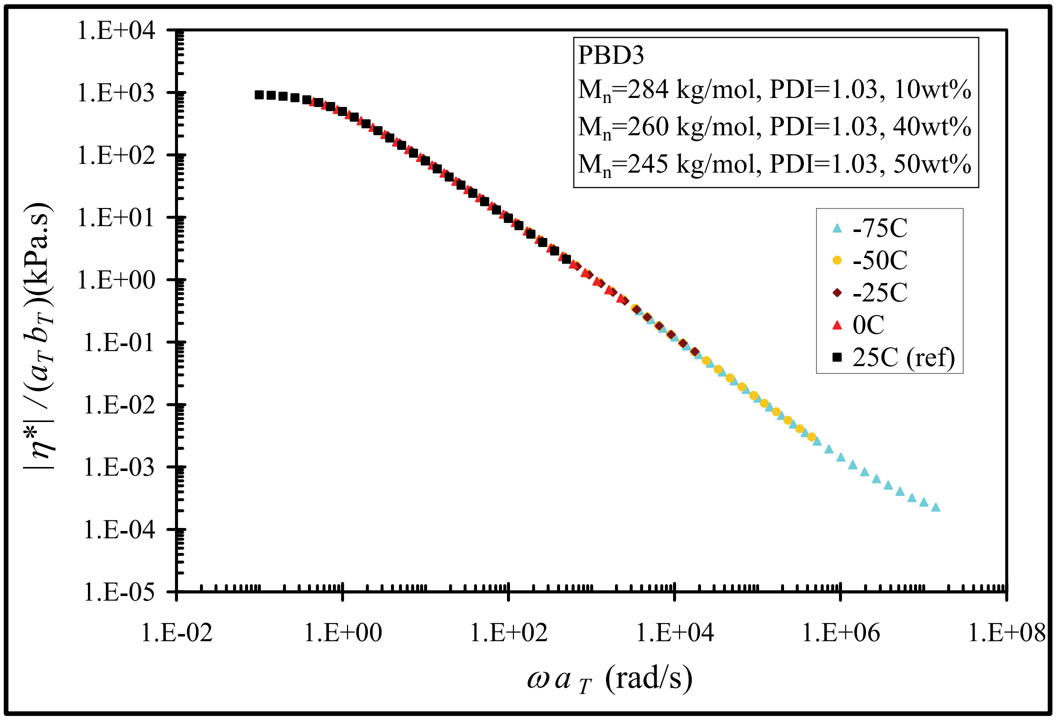

Figure E8 Complex viscosity of PBD3 shifted to T_{ref}=25°C

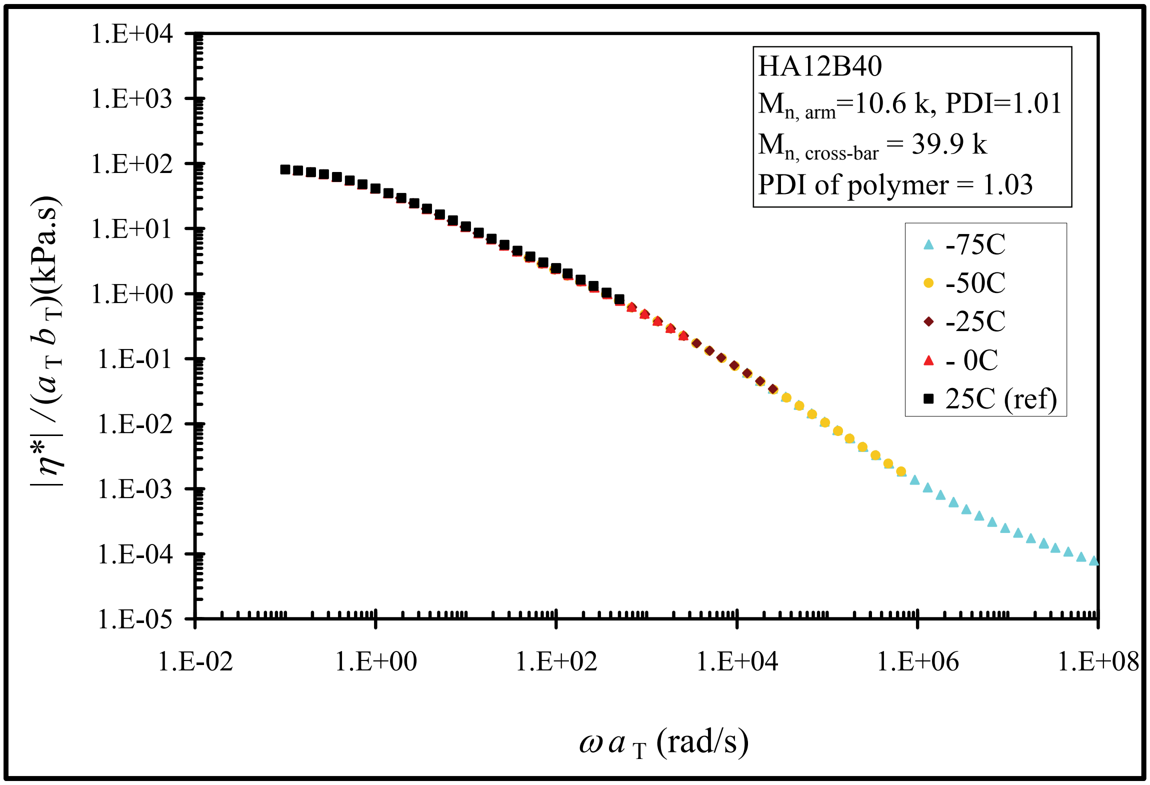

Figure E9 Complex viscosity of HA12B40 shifted to T_{ref}=25°C

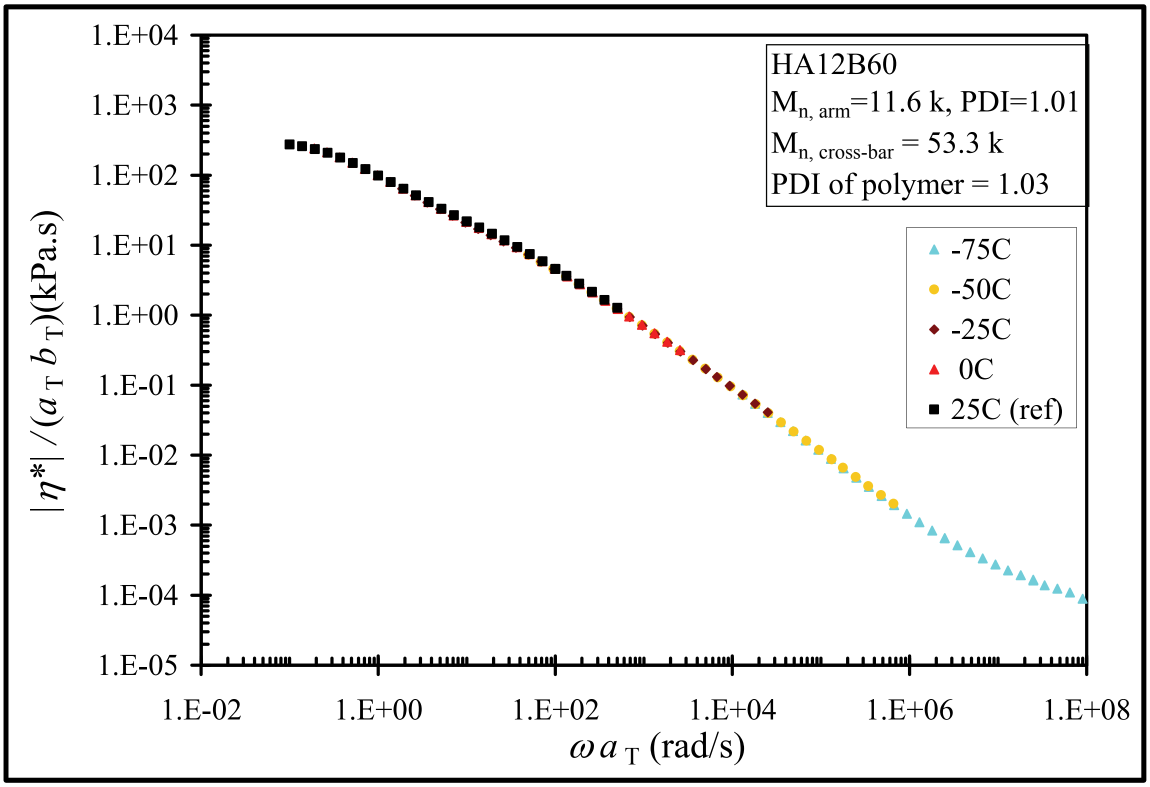

Figure E10 Complex viscosity of HA12B60 shifted to T_{ref}=25°C

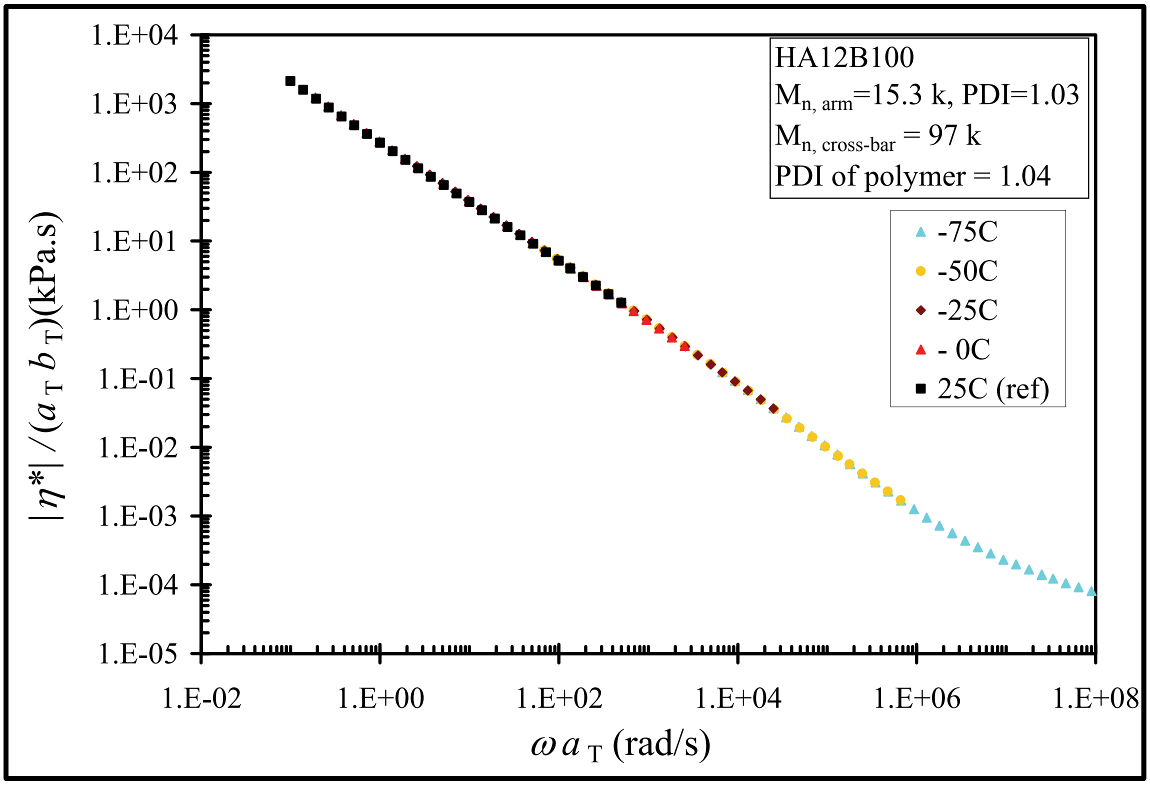

Figure E11 Complex viscosity of HA12B100 shifted to T_{ref}=25°C

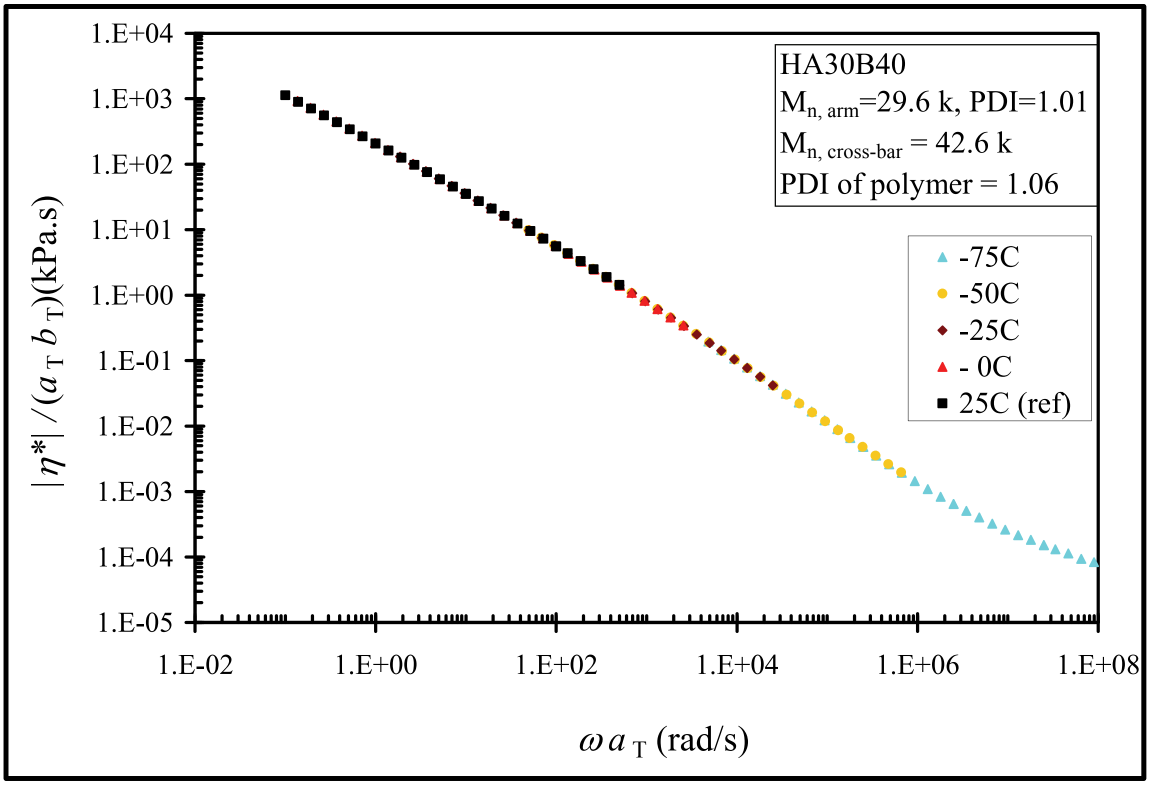

Figure E12 Complex viscosity of HA30B40 shifted to T_{ref}=25°C

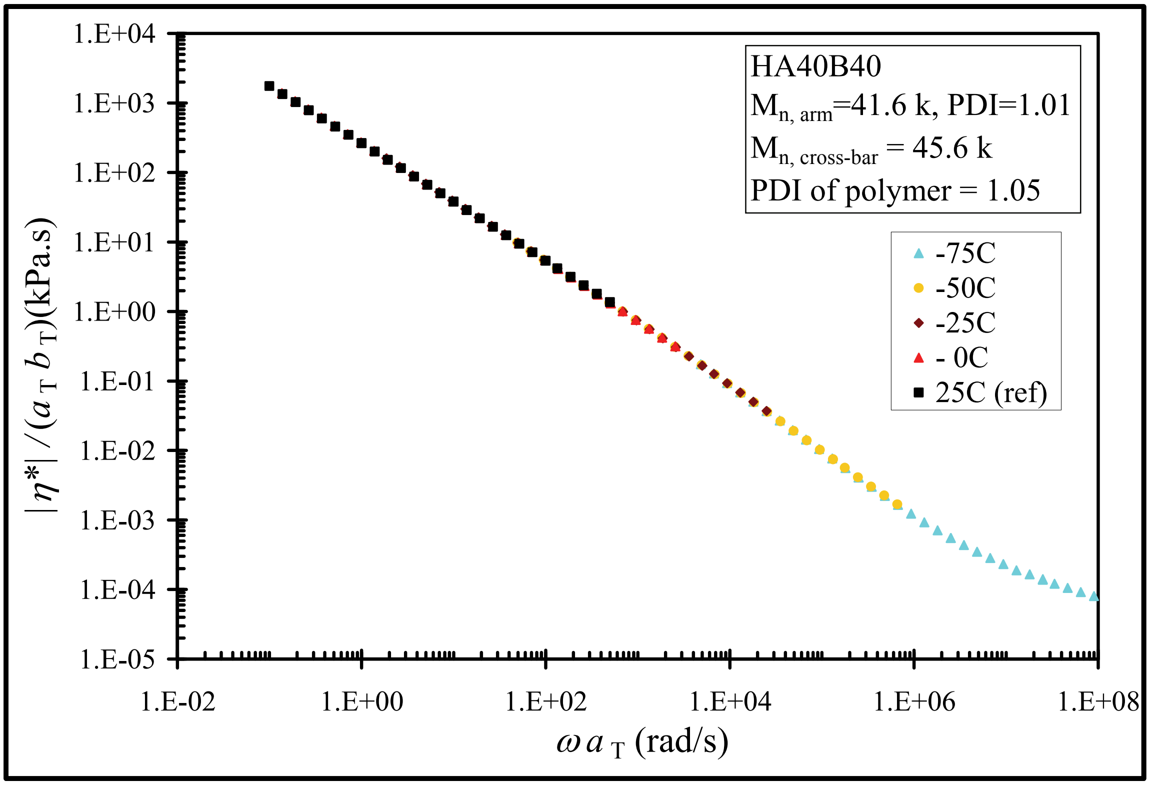

Figure E13 Complex viscosity of HA40B40 shifted to T_{ref}=25°C

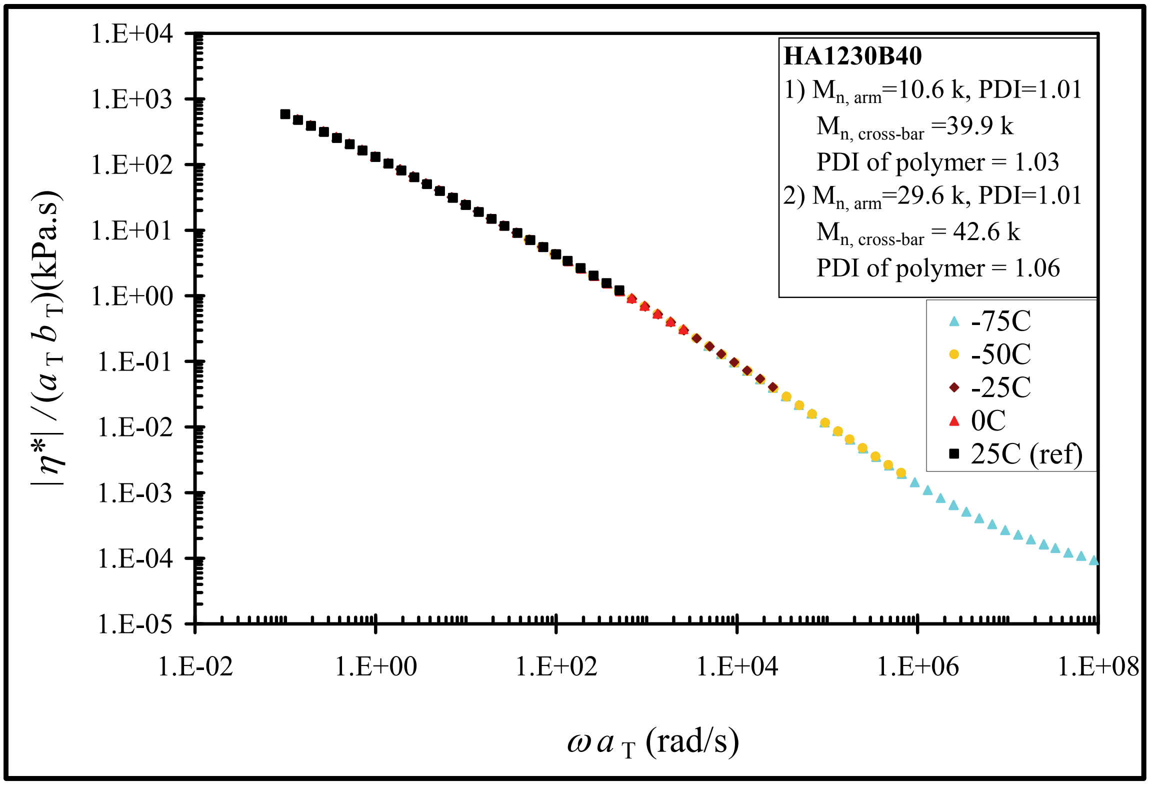

Figure E14 Complex viscosity of HA1230B40 shifted to T_{ref}=25°C

III. Plot of loss tangent versus reduced frequency

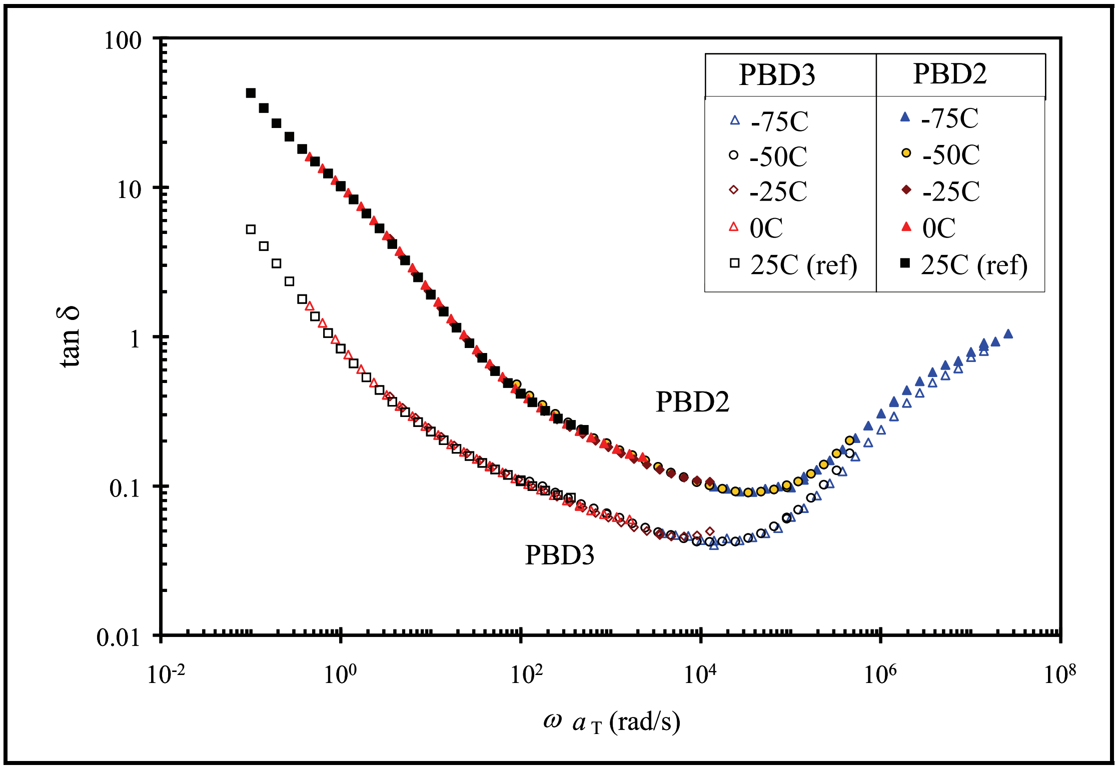

Figure E15 Comparison of loss tangent of PBD2 and PBD3 at 25°C

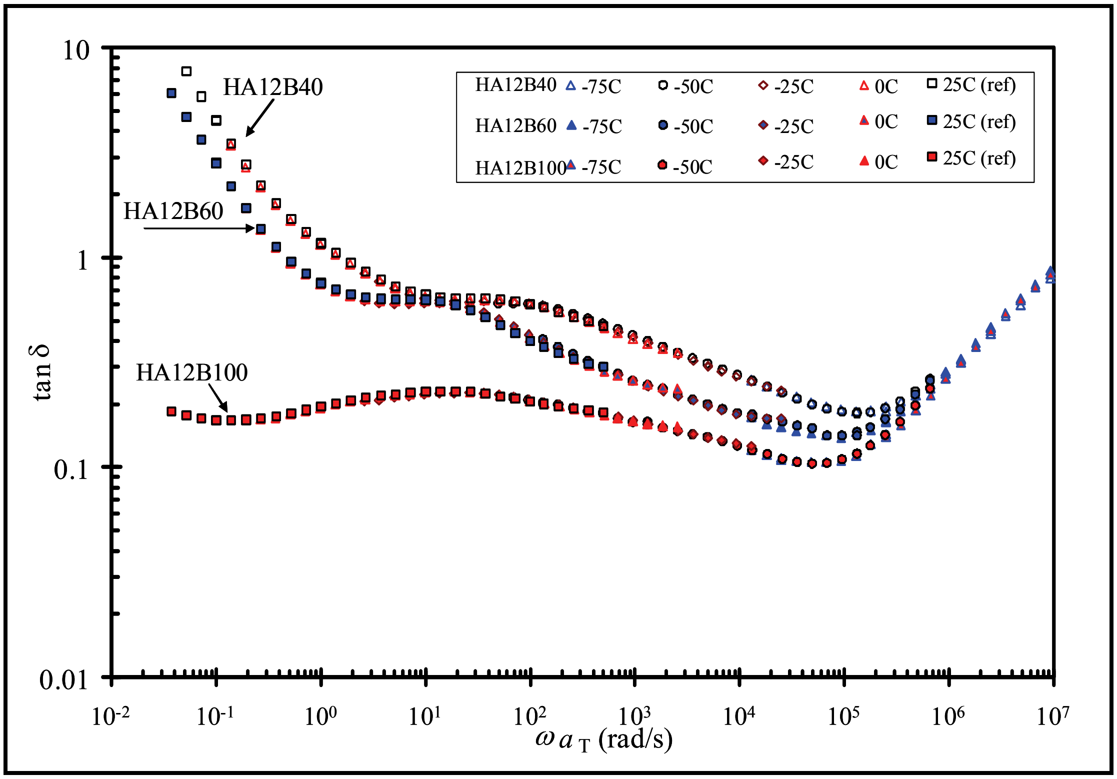

Figure E16 Comparison of loss tangent of H-shaped PBDs with equal arm length at 25°C

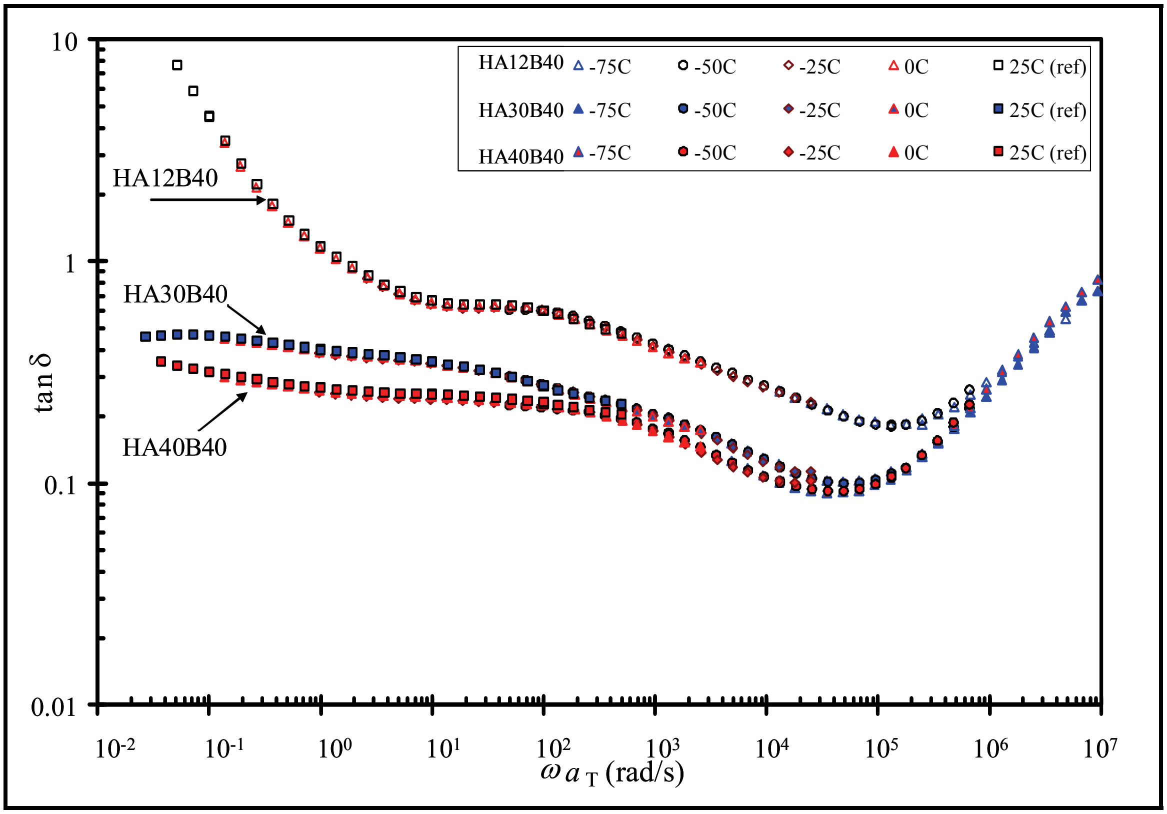

Figure E17 Comparison of loss tangent of H-shaped PBDs with equal cross-bar length at 25^{o}C

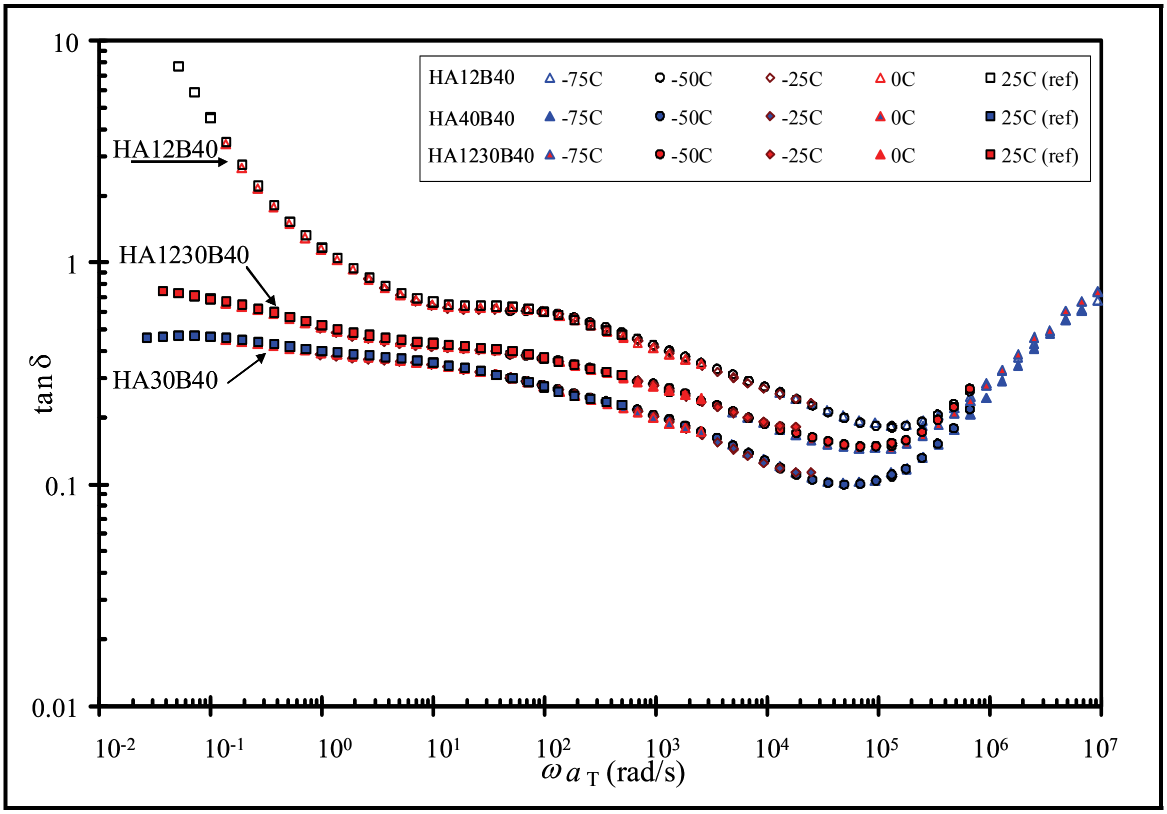

Figure E18 Comparison of loss tangent of HA12B40, HA30B40 and their blend at 25^{o}C

Appendix F Calculation of Viscoelastic Properties

This appendix serves as a supplement to Chapter 5 by comparing various methods in estimating G_{N}^{0} and J_s^0.

I. Estimation of the plateau modulus G_{N}^{0}

Method P1: Composition rule

A composition rule proposed by Robles-Vasquez *et al.* [151] relates G_{N}^{0} of narrow molecular weight distribution PBDs with various vinyl contents in the melt state. The general equation for PBDs melt is shown below:

$$G_{\mathrm{N}}^{o}\left(x_{12},1\right)=G_{N}^{o}\left(0,1\right)10^{B_1 x_{12}} \qquad \text{Eq. F1}$$

Where x_{12} = vinyl weight fraction of PBD

$G_{\mathrm{N}}^{o}\left(0,1\right)$ = plateau modulus of PBD with zero vinyl fraction in melt state

= 1.22×10^{6} ($\pm 2.3\times10^{3}$) Pa

B_1 = best fit constant = -0.363 ($\pm$ 0.03)

Such correlation work best in the range of 10% to 50% vinyl content since PBD with 100% vinyl content has not been obtained. The value of $G_{\mathrm{N}}^{o}\left(0,1\right)$ is an extrapolation of data in the literature of PBDs with various vinyl contents.

Method P2: Packing length

Packing length p is a length parameter that correlates rheological properties with the degree of entanglement. It is defined as the ratio of the occupied volume of a chain to the mean-square end-to-end distance. An empirical relationship regarding packing length proposed by Fetters *et al.* is shown in Eq. F2 [152].

$$M_e = 218\, p^3 N_A \rho \qquad \text{Eq. F2}$$

Where N_A is the Avogadro's number = $6.0221415\times10^{23}\ \mathrm{mol}^{-1}$

ρ is the density of 1,4 polybutadienes = $0.89\ \mathrm{g/cm}^3$ [150,177]

p is the packing length of cis polybutadienes = 2.44 $\overset{\circ}{A}$ [150]

The entanglement molecular weight (M_e) calculated from the above equation is 1700g/mol, which corresponds to $G_{\mathrm{N}}^{0} = 1.04\mathrm{MPa}$ by Eq. 1.11.

Method P3: Crossover modulus

Wu[153] proposed an empirical equation relating the entanglement behavior to chain structure: it describes the entanglement junction as a pseudo-topological model. The relationship as shown in Eq. F3 has been verified for a series of linear polymers with a wide variety of skeletal and pendant structures with polydispersity ratio $p = {M_w}/{M_n} < 3$.

$$\log\left(\frac{G_N^0}{G_c}\right) = 0.380 + \frac{2.63(\log p)}{1 + 2.45(\log p)} \qquad \text{Eq. F3}$$

Where the crossover modulus G_c means $G'(\omega) = G''(\omega)$

It is noted that Eq. F3 gives the lowest plateau modulus among the methods evaluated here and does not apply to structures with long chain branching.

Method P4: Minimum phase angle (details in Chapter 4)

$$G_{\mathrm{N}}^{0} = G'(\omega)|_{\delta=\min} \qquad \text{Eq. 4.13}$$

Method P5: Van Gurp-Palmen plot [144]

The van Gurp-Palmen plot is a chart where the phase angles δ is plotted against the absolute values of the complex shear modulus $|G^*|$ from a rheological experiment. For time temperature superposition to be valid, the isothermal frequency curves will merge into a common line. The minimum in the vGP plot is associated with the experimental plateau modulus $G_{N,\exp}^{0}$ which is another way to express Eq. 4.13. Trinkle and Friedrich suggested that the lower the minimum of δ is, the more accurate is Eq. F4 [178] since δ never goes to zero experimentally.

$$G_N^0 = \lim_{\delta \to 0} |G^*(\delta)| \qquad \text{Eq. F4}$$

Method P6: Integration of loss modulus

Plateau modulus of linear polymers can be obtained by integration over the terminal loss peak alone as shown in Eq. F5 when the terminal and transition responses are well resolved [135].

$$G_N^0 = \frac{2}{\pi}\int_{-\infty}^{\infty} G''(\omega)\, d\ln\omega \qquad \text{Eq. F5}$$

To correctly separate the terminal zone from the usually overlapped high-frequency Rouse motion, samples should be highly entangled with a degree of entanglement = 50. In most cases, the terminal zone has to be extrapolated at high frequencies and extrapolation should not exceed four decades of the whole frequency range[46]. However, the maximum degree of entanglement of our samples was less than 50 and some samples contained LCB, thus this method was not used in this project to obtain G_N^0 .

Table.F1 Plateau modulus of linear PBD blends and H-shaped PBDs determined by various methods, with unit MPa

Method		Sample								Average of Linear PBDs	Average of H-PBDs
		PBD2	PBD3	HA12B40	HA30B40	HA40B40	HA12B60	HA12B100	HA1230B40		
P1	Composition rule (Eq. F1)	1.12	1.12	1.1	1.07	1.09	1.12	1.11	N/A	1.12 ± 0.01	1.10 ± 0.03
P2	Packing length (Eq. F2 and Eq. 1.11)	1.04		N/A						1.04	N/A
P3	Crossover modulus (Eq. F3)	0.96	0.86	N/A						0.91 ± 0.05	N/A
P4	Minimum phase angle (Eq. 4.13)	1.06	1.17	1.05	1.1	0.94	1.13	0.97	1.08	1.12 ± 0.06	1.05 ± 0.11
P5	van Gurp-Palmen-Plot (Eq. F4)	1.09	1.18	1.07	1.07	0.91	1.09	0.95	1.08	1.14 ± 0.05	1.03 ± 0.12

For linear PBDs, as shown in Table F1, G_N^0 determined from method P1, P4 and P5 agree well with each other within an uncertainty of 5%. Values determined by method P2 and P3 are generally underestimated due to the empirical nature of the relationship. Van Gurp-Palmen plot for linear samples is uniquely characterized by one minimum and one inflection point as shown in Fig. F1. The location of these points and the shape of the curve can be correlated to G_N^0, molecular weight and polydispersity. The phase angle δ passes a minimum and rises again moving from high to low modulus, then moves through an inflection point before approaching its limiting value at $\delta = 90^o$ which is equivalent to the terminal flow range in the master curves and indicates viscous behavior. This characteristic curvature is found only for amorphous polymers but not on crystalline polymers as crystallization occurs at the low temperatures that are necessary to reach the minimum region. Results shown in Fig. F1 for linear PBDs agree well with the observation of Trinkle and Friedrich [178] that a high molecular mass sample (PBD3) passes the minimum at a lower phase angle than that of a low molecular mass sample (PBD2).

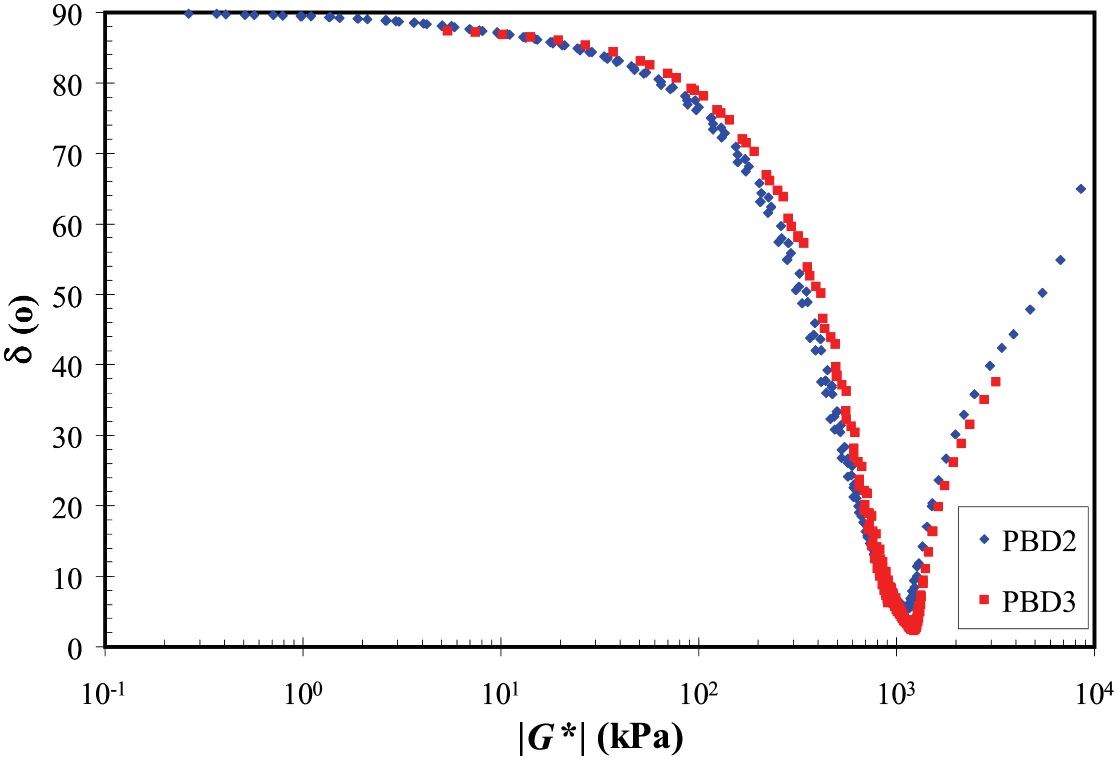

Figure F.1 Van Gurp-Palmen plot for linear PBDs blends at 25°C

For H-PBDs, method P2 and P3 were not applicable because the equations are purely empirical and have been tested on linear PBDs only. Although method P1 is semi-quantitative regardless of the polymer structure and is based solely on the microstructure content, it generally overestimated G_N^0 for H-PBDs. In the Van Gurp-Palmen plot of H-shaped samples that contain LCB, bumps are observed between the minimum in δ and the 90° plateau as shown in Fig. F2. Trinkle *et al.* [179]quantitatively described the bumps by a characteristic point and related it with the topology of the polymers.

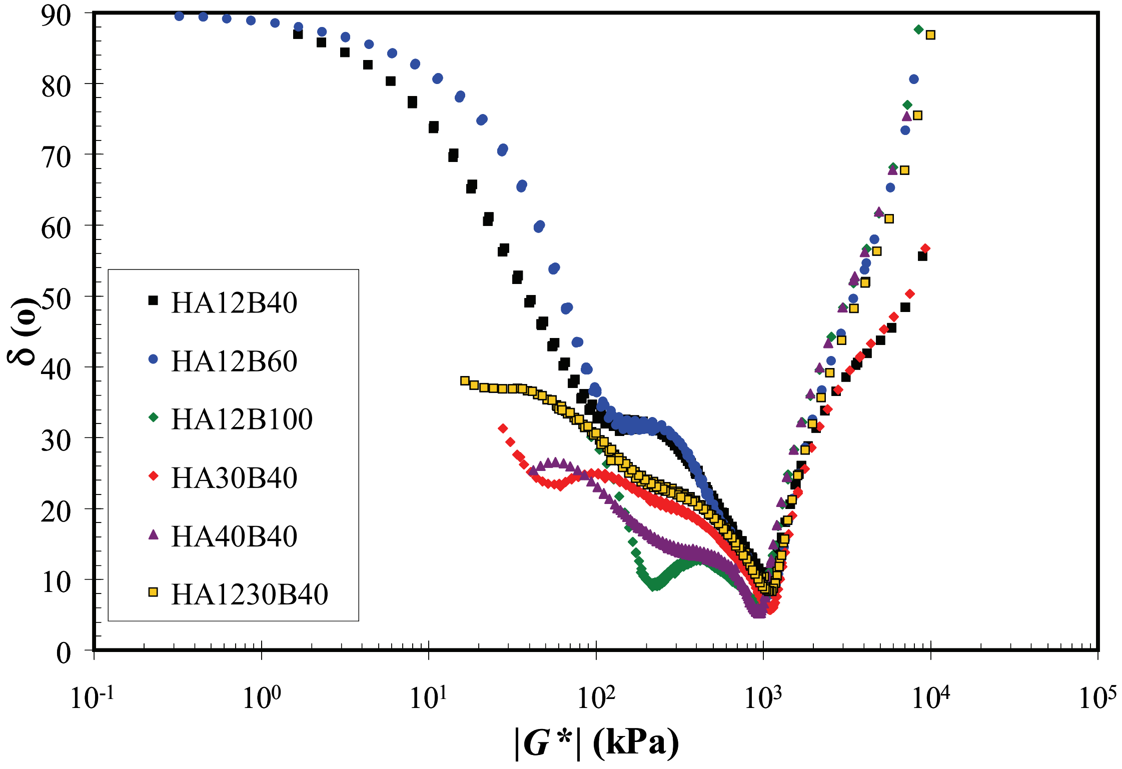

Figure F.2 Van Gurp-Palmen plots for H-shaped PBDs at 25°C

II. Estimation of steady state compliance J_s^0

Method S1: Composite creep compliance *J*(t) from creep (or creep/recovery)

As shown in Eq. 1.10, the intersection on *J*(*t*) extrapolated from long time is equal to J_s^0 which are shown in the insert of Fig. 4.11 and those in Appendix D.

Due to the significant effect of residual torque on the recovery process as shown in Figs. 4.12 and D17, J_s^0 of HA12B40 and HA40B40 were calculated from the intersection of *J*(t) obtained from creep only experiment as shown in the insert of Figs. 4.14 and 4.15.

Method S2: Limit of storage modulus

Similar to η_0, it is possible to determine J_s^0 from the limiting value of the ratio of storage modulus $G'(\omega)$to frequency ω when frequency approaches zero as shown in Eq. F6.

$$J_s^0 = \frac{1}{\eta_0^2} \lim_{\omega \to 0} \frac{G'(\omega)}{\omega^2} \qquad \text{Eq. F6}$$

Method S3: Limit of storage to loss modulus ratio

Another limiting value that can determine J_s^0 is shown in Eq. F7 which is valid when ω approaches zero.

$$J_s^0 = \lim_{\omega \to 0} \left(\frac{G'}{G''^2} \right) \qquad \text{Eq. F7}$$

Method S4: $J_s^0 = \int_{-\infty}^{\infty} L(\tau)\, d\ln\tau + J_g$, $L(\tau)$ inferred from oscillatory shear only

Steady state creep compliance can be obtained from the integration of retardation spectrum $L(\tau)$over the entire retardation time τ . For viscoelastic melt, the instantaneous recovery, J_g , is negligible because of its minute magnitude [43]. Since the dynamic oscillatory shear data are obtained over a limited frequency range instead of over the entire frequency range from 0 to ∞, it limits the times range in which a relaxation spectrum and thus the retardation spectrum can be determined. Davies and Anderssen

[180] proposed that the valid time range of a relaxation spectrum inferred from oscillatory shear data have the following limits:

$$t_{\min} = \frac{e^{\pi/2}}{\omega_{\max}} \qquad \text{Eq. F8}$$

$$t_{\max} = \frac{e^{-\pi/2}}{\omega_{\min}} \qquad \text{Eq. F9}$$

Using a nonlinear regression with regularization program (NLREG) (Freiburg Materials Research Center, version 2929, January 2, 2008) [132,148,149] as mentioned in section 4.1.2., a relaxation spectrum with the above time limit was inferred from the oscillatory shear data shifted to T_{ref}=25°C. From this relaxation spectrum, a retardation spectrum was inferred.

Method S5: $J_s^0 = \int_{-\infty}^{\infty} L(\tau)\, d\ln\tau + J_g$ **,** $L(\tau)$ **inferred from creep compliance only**

For simplification, creep compliance obtained from creep only experiment were used in the following calculation on HA12B40 and HA40B40, while the composite creep compliance from creep and recovery experiment were used on the rest of the samples. Using the software NLREG, a retardation spectrum was inferred from the creep compliance for HA12B40 and HA40B40 (composite creep compliance for the rest of the samples) at T_{ref}=25°C.

Method S6: $J_s^0 = \int_{-\infty}^{\infty} L(\tau)\, d\ln\tau + J_g$ **,** $L(\tau)$ **inferred from the whole range of dynamic modulus**

Similar to method S5, instead of using oscillatory shear data that is shifted to T_{ref}=25°C, the combined dynamic modulus obtained from oscillatory shear tests and creep (or creep and recovery) test are used in calculating a relaxation spectrum that is then used to calculate a retardation spectrum to determine J_s^0. Again, the valid time range of a relaxation spectrum is governed by Eq. F8 and Eq. F9.

J_s^0 as determined by method S1-S6 are summarized in Table F2. In principle, the various J_s^0 estimated from these methods should agree with each other; but this agreement is subject to very broad assumptions, and each method has its own sources of error.

Comparing among various methods, method S1 is a less preferable method to estimate J_s^0 since it is very sensitive to the attainment of steady state at long time and is prone to extrapolation error. The accuracy of methods S2 and S3 depends on the limiting value of loss and storage modulus in the terminal region. Thus, these two methods were used only when samples had reached the terminal zone within our experimental frequency range. Meanwhile, method S4, S5 and S6 strongly depend on the shape of retardation spectrum at long retardation time. Method S4 generally underestimates the value of J_s^0 since the retardation spectrum was inferred only from behavior at high frequency (short time) where the terminal behavior was not included in calculation. Similarly, the retardation spectrum involved in method S5 accounts mainly for the terminal behavior and neglects the intermediate and high frequency behavior. It is only method S6 capable to include terminal, intermediate and high frequencies behavior in the retardation spectrum. Therefore, for linear PBDs blends that reached terminal behavior, the average value of method S2, S3 and S6 is considered to be the closest approximation of J_s^0. The values of J_s^0 determined from these three methods agree well with each other, having ~4% difference. Averages the values from these three methods (S2, S3 and S6) give $< J_s^0 >= 7.46 \times 10^{-6} Pa^{-1}$ for PBD2 and $< J_s^0 >= 1.23 \times 10^{-5} Pa^{-1}$ for PBD3.

For a linear monodisperse polymer, J_s^0 increase linearly with molecular weight (*M*) when *M* is less than a critical molecular weight $M_c^{'}$. J_s^0 becomes independent of *M* when *M* is above $M_c^{'}$. For polydisperse polymers, J_s^0 is very sensitive to molecular weight distribution, especially to the high molecular weight tail in the distribution. When comparing the average values of J_s^0 of PBD2 and that of PBD3, we observed a significant increase of ~65% moving from a binary linear PBD blend to a three component blend of linear PBD. Comparing with the literature value of a nearly monodisperse linear PBD with $\mathrm{PDI} < 1.1$ and with a comparable microstructure content,

J_s^0 ranges from $2\times10^{-6}\,Pa^{-1}$ to $6\times10^{-6}\,Pa^{-1}$[26,169] at 25°C : it is much less than those of PBD2 and PBD3, suggesting PBD2 and PBD3 have a much broader overall molecular weight distribution , $\mathrm{PDI}>1.1$.

Similarly, J_s^0 of H-shaped PBDs is best estimated by methods S2, S3 and S6 when terminal behavior is observed. J_s^0 of HA12B40 and HA12B60 estimated by methods S2, S3 and S6 agree well with each other within ~6% difference. For the rest of the H-shaped PBDs, methods S2 and S3 did not agree well with method S6. This discrepancy is probably due to the fact that these samples did not reach terminal behavior within our experimental range of frequency; the lowest frequencies used in method S2 and S3 were not low enough to reach the limiting response that happened in the terminal region. J_s^0 estimated by method S6 is generally smaller than it ought to be for those samples that did not show terminal behavior. Since low frequency dynamic data correspond to long relaxation times in a relaxation spectrum, which is responsible to the long retardation time τ in the retardation spectrum $L(\tau)$. Missing this range of information would significantly lower the value of J_s^0 as determined by method S6. Therefore, for samples in which terminal behavior was not observed in our experimental frequency range (i.e. .HA30B40, HA40B40, HA12B100 and HA1230B40), J_s^0 is best approximated by averaging the values attained by method S2 and S3 only.

J_s^0 of H-shaped PBDs are higher than that of the linear PBD blends even though the H-shaped PBDs show narrow molecular weight distribution as characterized by the same method (SEC-TALLS). In other words, the enhancement of J_s^0 resulting from the presence of LCB is greater than that from a broad molecular weight distribution. When comparing PBD2 with HA12B40, both are highly entangled and have comparable total molecular weight. J_s^0 of HA12B40 is 6 times greater than that of PBD2, despite the fact that it has a narrow molecular weight distribution as revealed in SEC/TALLS. Similar enhancement effect on J_s^0 in the presence of LCB was observed also in four-arm stars[181], comb-shaped [32] and pom-pom[26] structure polymer.

As suggested by Roovers [20] on a study of H-shaped polystyrene with arm length equal to cross-bar length and degree of entanglement of arm/cross-bar ranges from 6 to 37, an increase of J_s^0 as much as a factor of 10 in molecular weight was observed among the samples. The dependence of J_s^0 that Roovers observed was linear but started to depart at high molecular weight samples. A similar observation was found for stars polymers [14,182] but a linear dependence on molecular weight was always present, as first discussed by Doi and Kuzuu [183]. For Roovers' H-polymers, the volume fraction of arms was constant since arm length was equal to cross bar length. Thus, the increase of J_s^0 on Roovers' H-polymers was solely due to an increase in total molecular weight.

However, the H-PBDs studied in this project have the same arm length but different cross-bar length. Increasing the cross-bar length only is essentially reducing the volume fraction of arms (*i.e.* LCB), and thus its contribution to J_s^0. Therefore, increasing the cross-bar at fixed arm length is a combinatory effect of: (i) J_s^0 enhancement due to increase in total molecular weight and (ii) J_s^0 reduction due to decrease in volume fraction of arms. When comparing HA12B40, HA12B60 and HA12B100, the changes of J_s^0 were not as prominent as observed by Roover, an initial drop followed by an increase of J_s^0 was observed with a longer cross-bar length. It is also interesting to note that J_s^0 of HA1230B40 was found to be 6 times more than that of 100 wt% HA30B40 and this was the highest J_s^0 among all the H-PBDs that was studied in this project. Such enhancement is a combined effect by changes in molecular weight distribution, total molecular weight and volume fraction of arms. Changes in J_s^0 contributed from the broad molecular weight distribution is enough to compensate for the reduction caused by a decrease in total molecular weight and volume fraction of arms, which illustrates once again the sensitivity of J_s^0 to polydispersity.

Table F.2 Steady state compliance of linear and H-PBDs determined by various methods at 25^{o}C, with unit Pa^{-1}

Method			Sample							
			PBD2	**PBD3**	**HA12B40**	**HA30B40**	**HA40B40**	**HA12B60**	**HA12B100**	**HA1230B40**
SAOs	S4	Integration of *L*(τ), *L*(τ) inferred from SAOS	4.65E-06	2.79E-06	3.38E-05	1.56E-05	1.16E-05	2.25E-05	5.73E-06	2.14E-05
Creep and recovery experiment*	S1	Composite *J*(t) (Eq. 4.11)	-6.12E-03	-9.91E-06	-5.83E-04	5.32E-05	4.78E-05	-1.31E-03	3.04E-05	7.10E-04
	S2	Limit of storage modulus (Eq. F6)	7.50E-06	1.22E-05	4.61E-05	8.16E-05	4.06E-05	1.82E-05	1.32E-05	5.49E-04
	S3	Limit of storage to loss modulus ratio (Eq. F7)	7.58E-06	1.24E-05	4.60E-05	7.80E-05	5.49E-05	1.79E-05	2.97E-05	4.31E-04
	S5	Integration of *L*(τ), *L*(τ) inferred from *J*(t)	5.60E-06	9.74E-06	3.36E-05	7.15E-05	3.23E-05	1.49E-05	1.96E-05	5.70E-04
	S6	Integration of *L*(τ), *L*(τ) inferred from overall *G*'(*ω*), *G*"(*ω*)	7.31E-06	1.22E-05	4.83E-05	4.40E-05	2.30E-05	1.87E-05	1.08E-05	1.62E-04
Average			7.46E-06	1.23E-05	4.68E-05	7.98E-05	4.78E-05	1.83E-05	2.15E-05	4.90E-04

*For sample HA12B40 and HA40B40, steady state compliance were determined from experimental data obtained by creep only experiment

Nomenclature

Roman Letters

a	Power law index
a_T	Horizontal shift factor
A	Empirical constant
b_T	Vertical shift factor
B	Empirical constant
B_1	Best fit constant
BoB	Branch-on-branch model
E_a	Activation energy
f	Functionality of initiator
$\lvert G^*\rvert$	Complex modulus
$G'(\omega)$	Storage modulus
$G''(\omega)$	Loss modulus
G_c	Crossover modulus
G_r	Reduced modulus
G_N^0	Plateau modulus
$G(T)$	Modulus at temperature T
GPC	Gel permeation chromatography
$J(t)$	Creep compliance
$J'(\omega)$	Storage compliance
$J''(\omega)$	Loss compliance
J_g	Instantaneous compliance
$J_r(t)$	Recoverable creep compliance
J_s^0	Steady state compliance
$<J_s^0>$	Average value of steady state compliance
$L(\tau)$	Retardation spectrum
LCB	Long chain branching
LVE	Linear viscoelastic
M_c	Critical molecular weight for entanglement

$M_c^{'}$	Critical molecular weight for steady state compliance
M_e	Entanglement molecular weight
M_n	Number average molecular weight
$M_\mathrm{n,arm}$	Number average molecular weight of arm
$M_\mathrm{n,crossbar}$	Number average molecular weight of crossbar
M_o	Molar mass of monomer
M_p	Peak molecular weight
M_w	Weight average molecular weight
$M_\mathrm{w,arm}$	Weight average molecular weight of arm
$M_\mathrm{w,crossbar}$	Weight average molecular weight of crossbar
MWD	Molecular weight distribution
N	Number of molecules used in modeling, number of ensembles
N_A	Avogadro's number
N_e	Number of monomers in an entanglement length
NMR	Nuclear magnetic resonance
OAT	One-at-a-time (sensitivity analysis)
p	Packing length
P^2	Frictional constant
PDI	Polydispersity index
$\mathrm{PDI}_\mathrm{arm}$	Polydispersity index of arm
$\mathrm{PDI}_\mathrm{crossbar}$	Polydispersity index of crossbar
R	Gas constant
RI	Refractive index detector
SEC	Size exclusion chromatography
t_r	Recovery time
T	Temperature
T_0, T_ref	Reference temperature
TALLS	Two-angle laser light scattering
TGIC	Temperature gradient interaction chromatography
VI	Viscometer detector
x_{12}	Vinyl weight fraction of PBD

Greek Letters

α	Dilution exponent
α'	Correction factor for gap change due to temperature
δ	Phase angle
$\dot{\gamma}$	Shear rate
γ_r	Recoil or recovered strain
η_0	Zero shear viscosity
$\|\eta^*\|$	(Absolute magnitude) complex viscosity
ρ	Density
ρ_0	Density at reference temperature
σ	Shear stress
τ	Retardation time
τ_e	Entanglement time
τ_{late}	Late time arm retraction
ω	Frequency
ω_c	Crossover frequency
ω_r	Reduced frequency